

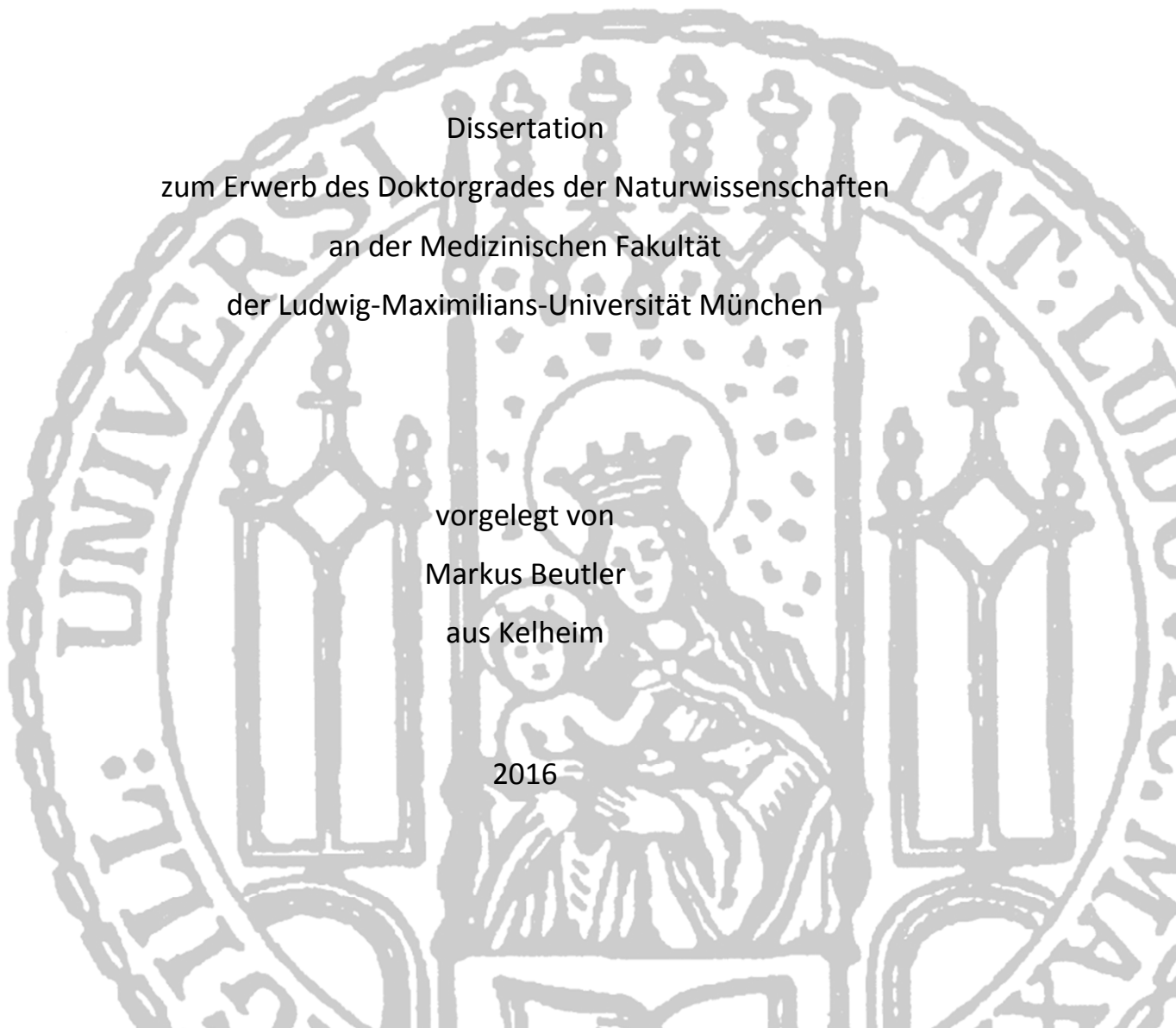
Aus dem Max von Pettenkofer-Institut
für Hygiene und Medizinische Mikrobiologie
der Ludwig-Maximilians-Universität München
Lehrstuhl: Bakteriologie
Vorstand: Prof. Dr. med. Sebastian Suerbaum

**Elucidating the mechanisms of dysbiosis and inflammation-
induced ‘blooms’ of *Salmonella enterica* serovar
Typhimurium and other enteric pathogens using a novel
gnotobiotic mouse model**

Dissertation
zum Erwerb des Doktorgrades der Naturwissenschaften
an der Medizinischen Fakultät
der Ludwig-Maximilians-Universität München

vorgelegt von
Markus Beutler
aus Kelheim

2016



Gedruckt mit Genehmigung der Medizinischen Fakultät
der Ludwig-Maximilians-Universität München

Betreuerin:	Prof. Dr. Barbara Stecher-Letsch
Zweitgutachterin:	Prof. Dr. Gabriele Rieder
Dekan:	Prof. Dr. med. dent. Reinhard Hickel
Tag der mündlichen Prüfung:	21.03.2017

Eidesstattliche Erklärung

Ich, Markus Beutler, erkläre hiermit an Eides statt, dass ich die vorliegende Dissertation mit dem Thema:

‘Elucidating the mechanisms of dysbiosis and inflammation-induced ‘blooms’ of *Salmonella enterica* serovar Typhimurium and other enteric pathogens using a novel gnotobiotic mouse model’

selbständig verfasst, mich außer der angegebenen keiner weiteren Hilfsmittel bedient und alle Erkenntnisse, die aus dem Schrifttum ganz oder annähernd übernommen sind, als solche kenntlich gemacht und nach ihrer Herkunft unter Bezeichnung der Fundstelle einzeln nachgewiesen habe.

Ich erkläre des Weiteren, dass die hier vorgelegte Dissertation nicht in gleicher oder in ähnlicher Form bei einer anderen Stelle zur Erlangung eines akademischen Grades eingereicht wurde.

München, den ..21.3.2017

Markus Beutler

Schatzinger ☺

Table of contents

Table of contents

List of abbreviations	xiii
List of publications.....	xvi
Summary.....	xvii
Zusammenfassung.....	xx
1. Introduction	1
1.1 Elucidation of gut microbiota functions using gnotobiotic mouse models	1
1.1.1 General functions of a healthy gut microbiota	1
1.1.2 Composition of the gut microbiota: from health to dysbiosis and disease	2
1.1.3 Analysis tools.....	2
1.1.4 Defined microbial consortia for gnotobiotic mouse models	3
1.1.5 The Oligo-Mouse-Microbiota	3
1.2 <i>Salmonella enterica</i> serovar Typhimurium pathogenesis and disease	5
1.2.1 Pathogenesis of <i>Salmonella enterica</i> serovar Typhimurium is dependent on type 3 secretion systems.....	5
1.2.2 <i>S. Tm</i> invades the gut ecosystem and induces inflammation	6
1.2.3 <i>S. Tm</i> profits from an inflammatory gut milieu and outcompetes the indigenous microbiota	7
1.3 Interactions of other enteric pathogens and the gut microbiota	9
1.3.1 <i>Citrobacter rodentium</i> , a model for human enteropathogenic <i>Escherichia coli</i> infection.....	9
1.3.2 <i>Clostridium difficile</i> , a leading cause of antibiotic associated diarrhea (AAD)	10
1.4 Dysbiosis and inflammatory bowel diseases.....	11
1.5 Common changes in microbiota composition upon enteric infection and inflammatory bowel diseases	12
1.6 Aims of the study	14
2. Material and Methods	16
2.1 Strains and plasmids.....	16
2.1.1 Strains.....	16
2.1.2 Plasmids.....	17

Table of contents

2.2 Buffers, media and Oligonucleotides	19
2.2.1 Buffers and media	19
2.2.2 Oligonucleotides.....	26
2.3 Chemicals, antibodies and devices.....	30
2.3.1 Chemicals.....	30
2.3.2 Antibodies.....	34
2.3.3 Devises and specific materials.....	34
2.4 Microbiological methods.....	36
2.4.1 Preparation of bacterial cryo-stocks (<i>S. Tm</i> and <i>E. coli</i> strains)	36
2.4.2 Bacterial culture for <i>in vivo</i> experiments	36
2.4.3 <i>In vitro</i> growth assay of <i>S. Tm</i> strains.....	37
2.4.4 <i>In vitro</i> competition assay	37
2.4.5 Preparation of starter inocula for growth assays of Oligo-MM ¹² strains.....	38
2.4.6 <i>In vitro</i> growth assay of Oligo-MM ¹² strains.....	38
2.4.7 Chromazurol S (CAS) agar assay for siderophore production	39
2.4.8 Generation of chemo-competent cells.....	39
2.4.9 Generation of electro-competent cells	39
2.5 Molecular biological and biochemical methods.....	40
2.5.1 Agarose gel electrophoresis	40
2.5.2 Lipocalin-2 (LCN-2) ELISA (mouse lipocalin-2/NGAL detection kit (R&D, DY1857))	40
2.5.3 Cloning of 16S rRNA full length sequences into pJET1.2 cloning vector	40
2.5.4 Transformation chemo-competent cells	41
2.5.5 Total DNA extraction of fecal and cecal microbiota.....	41
2.5.6 DNA extraction from bacterial cell pellets harvested from <i>in vitro</i> cultures	42
2.5.7 Colorimetric quantification of nitrite concentrations	42
2.5.8 Hydrolysis probe based quantitative real-time PCR (qPCR)	43
2.5.8.1 Design of specific primers and hydrolysis probes	43
2.5.8.2 Preparation of plasmid DNA for standards curves.....	43

Table of contents

2.5.8.3 Determination of 16S rRNA gene copy numbers	44
2.5.8.4 qPCR reaction conditions	44
2.5.8.5 Titration of primers and probes as well as template DNA concentrations.....	44
2.5.8.6 Evaluation of qPCR efficiency and establishment of a duplex qPCR assay	45
2.5.8.7 Validation of specificity and determination of the limit of detection	45
2.5.9 Generation of gene deletion mutants in <i>S. Tm</i> by λ red recombination	46
2.5.9.1 Generation of PCR fragments	46
2.5.9.2 Electroporation of electro-competent <i>S. Tm</i> harboring pKD46.....	46
2.5.9.3 P22 transduction	47
2.5.9.4 Deletion of antibiotic-resistance markers using the Flp-recombinase	48
2.5.9.5 Construction of <i>S. Tm</i> mutants.....	49
2.5.10 Immuno-fluorescence staining.....	50
2.6 Animal experiments	50
2.6.1 Ethics	50
2.6.2 Generation of gnotobiotic Oligo-MM ¹² mice	50
2.6.3 High fat diet and oleic acid supplementation	51
2.6.4 Infection of gnotobiotic Oligo-MM ¹² mice with <i>S. Tm</i> and <i>C. rodentium</i>	51
2.6.5 Infection of CD18 ^{-/-} mice with <i>S. Tm</i>	51
2.6.6 Infection of Oligo-MM ¹² mice with <i>C. difficile</i>	52
2.6.7 Reversible colitis model: <i>H. typhlonius</i> infection and CD45RB ^{hi} T-cell transfer	52
2.6.8 Antibody mediated depletion of neutrophils	52
2.6.9 Monitoring depletion of neutrophils by FACS.....	52
2.6.10 Collection of mouse tissues.....	53
2.6.11 Hematoxylin eosin (HE) staining and histopathology	53
2.7 Bioinformatics and statistics	54
2.7.1 RAST automated gene annotation	54
2.7.2 Statistics	54
3. Results.....	55

Table of contents

3.1 Establishment of a qPCR assay for specific detection and quantification of bacterial strains....	55
3.1.1 General considerations: SYBR green versus hydrolysis probe based qPCR	55
3.1.2 Design of strain-specific primers and hydrolysis probes	55
3.1.3 Optimization of primer and hydrolysis probe concentrations	56
3.1.4 Multiplexing and qPCR performance.....	58
3.2 Composition and characteristics of the Oligo-MM ¹²	61
3.2.1 Selection of strains constituting the Oligo-Mouse-Microbiota (Oligo-MM ¹²).....	61
3.2.2 The Oligo-MM ¹² matures and stably colonizes germfree mice.....	62
3.2.3 The Oligo-MM ¹² is vertically transmitted and remains stable over 6 filial generations.....	66
3.2.4 The composition of the Oligo-MM ¹² is comparable between different animal facilities.....	69
3.2.5 High-fat diet as well as oleic acid supplementation shift Oligo-MM ¹² composition	72
3.3 The Oligo-MM ¹² is a tool to study inflammation induced dysbiosis	75
3.3.1 Infection with wild type <i>S. Typhimurium</i> causes severe colitis and dysbiosis	75
3.3.2. Performance of individual Oligo-MM ¹² strains during <i>S. Tm</i> ^{WT} induced colitis.....	81
3.4 Towards understanding the mechanisms causing shifts in microbiota composition	89
3.4.1 Influence of Type 3 secretion systems (T3SS) 1 and 2.....	89
3.4.1.1 Both T3SSs are necessary to cause colitis and dysbiosis.....	89
3.4.1.2 The Oligo-MM ¹² is resilient to infection with <i>S. Tm</i> ^{SPI-2}	96
3.4.2 Influence of altered environmental conditions during colitis on the microbiota	99
3.4.2.1 <i>In vitro</i> testing of <i>Salmonella</i> strains deficient in anaerobic respiration, siderophore production and ethanolamine utilization.....	99
3.4.2.1.1 <i>S. Tm</i> ^{Ni} ($\Delta narZ$; $narG::cat$; $napA::aphT$) is incapable of nitrate respiration	99
3.4.2.1.2 <i>S. Tm</i> ^{Ni + Te} ($\Delta narZ$; $narG::cat$; $napA::aphT$; $ttrS::tet$) shows impaired growth in anaerobic tetrathionate broth	101
3.4.2.1.3 <i>S. Tm</i> ^{EntA} ($entA::cat$) is impaired in siderophore secretion	102
3.4.2.1.4 <i>S. Tm</i> ^{EA} ($eutC::aphT$) exhibits reduced growth on ethanolamine under anaerobic conditions in the presence of tetrathionate	103
3.4.2.2 Dysbiosis following <i>Salmonella</i> ‘blooms’ is fueled by anaerobic respiration.....	104

Table of contents

3.4.2.3 The performance of single Oligo-MM ¹² strains during inflammation correlates with the presence of fitness genes	113
3.4.3 Influence of innate immune system on microbiota composition during colitis	118
3.4.3.1 Depletion of neutrophils does not prevent dysbiosis and <i>Salmonella</i> ‘blooming’	118
3.5 Comparing the influence of infections with other enteric pathogens and T-cell-induced colitis on Oligo-MM ¹² composition.....	125
3.5.1 <i>Citrobacter rodentium</i> infection does not lead to dysbiosis in Oligo-MM ¹² mice	125
3.5.2 <i>Clostridium difficile</i> infection shifts Oligo-MM ¹² composition at day 3 p.i.	128
3.5.3 Reversible, T-cell-induced colitis in RAG1 ^{-/-} mice associated with the Oligo-MM ¹² and <i>Helicobacter typhlonius</i> induced mild microbiota shifts.....	131
3.5.4 Comparison of the impact of infections with <i>S. Tm</i> , <i>C. rodentium</i> and <i>C. difficile</i> as well as T-cell-induced colitis on the Oligo-MM ¹² composition	134
4. Discussion.....	139
4.1 The Oligo-MM ¹² , a novel consortium of gut commensals applicable for studies of host-microbe interactions	139
4.1.1 Strain-specific quantitative real-time PCR enables reliable, fast and affordable quantification of individual Oligo-MM ¹² strains.....	140
4.1.2 The Oligo-MM ¹² as a tool to study kinetics of microbiota maturation as well as shifts in microbial composition and phenotypes upon changes in diet	141
4.1.3 The Oligo-MM ¹² that is stable over several generations and between animal facilities is a robust model microbiota for the research community	143
4.2 The influence of <i>Salmonella</i> -induced gut inflammation on the indigenous microbiota in the Oligo-MM ¹² model	144
4.2.1 Profiling the performance of Oligo-MM ¹² strains in the presence of <i>Salmonella</i> -induced gut inflammation during ecosystem invasion	147
4.2.2 Performance of Oligo-MM ¹² strains in a colitic environment correlates with the presence fitness genes.....	151
4.2.3 Investigating the contribution of anaerobic respiration, ethanolamine utilization and iron acquisition via siderophores to <i>Salmonella</i> ‘blooming’ and concomitant dysbiosis	153
4.2.4 ‘Nutrient-’ versus ‘killing-hypothesis’, the role of infiltrating neutrophils for <i>Salmonella</i> ‘blooming’ and dysbiosis.....	155

Table of contents

4.3 Parallels between dysbiosis induced by enteric pathogens and chronic gut inflammation	158
5. Appendix	161
Danksagung	188
Curriculum Vitae	189

List of abbreviations

List of abbreviations

AAM	<i>Akkermansia</i> medium
ABTS	2,2'-Azino-di-(3-ethylbenzthiazolin-6-sulfonsäure)
AGR2	Anterior gradient homolog 2
ANOVA	Analysis of variance
ASF	Altered Schaedler Flora
BFP	Bundle forming pilus
BHQ1	Black whole quencher 1
bp	Base pairs
BSA	Bovine serum albumin
°C	Degrees Celsius
CAS	Chromazurol S
CD	Crohn`s disease
CDT	<i>C. difficile</i> toxin
CFU	Colony forming units
CMF	Clean mouse facility
Cq	Quantification cycle
CR	Colonization resistance
DAPI	4',6-diamidino-2-phenylindole
ddH ₂ O	Double-distilled water (Ampuwa)
dH ₂ O	Distilled water
Diam.	Diameter
DMSO	Dimethyl S-oxide
DNA	Deoxyribonucleic acid
ds	Double-stranded
DSMZ	Deutsche Sammlung von Mikroorganismen und Zellkulturen
DTL	Limit of detection
DTPA	Diethylenetriamine pentaacetic acid
EA	Ethanolamine
EDTA	Ethylenediaminetetraacetic acid
EGTA	Ethylene glycol tetraacetic acid
ELISA	Enzyme-linked immunosorbent assay
EPEC	<i>Enteropathogenic Escherichia coli</i>
ETHZ	Eidgenössische Technische Hochschule Zürich

List of abbreviations

F	Filial
FACS	Fluorescence-activated cell sorting
FAM	6-carboxyfluoresceine
FCS	Fetal calf serum
FISH	Fluorescence <i>in situ</i> hybridization
FRT	Flippase recognition target (FRT) sites
dDNA	Genomic DNA
GF	Germfree
H&E	Hematoxylin and eosin
HEX	6-carboxyhexafluoresceine
HPLC	High-performance liquid chromatography
HRP	Horseradish peroxidase
IBD	Inflammatory bowel disease
ID	Identity
IgA	Immunoglobulin A
IL	Interleukin
iNOS	Inducible nitric oxide synthase
IVC	Individually ventilated cage
LB	Luria-Bertani
LCN-2	Lipocalin-2
MGB	Minor groove binder
mLN	Mesenteric lymphnode
MvP	Max von Pettenkofer-Institut
NGAS	Next generation amplicon sequencing
Ni.	Nitrate
n.s.	Not significant
nt	Nucleotide
Oligo-MM	Oligo-Mouse-Microbiota
o/n	Overnight
OD ₆₀₀	Optical density of 600 nm
P	Parental
p.a.	Pro analysis
PBS	Phosphate buffered saline
PCoA	Principal Coordinate Analysis
PCR	Polymerase chain reaction

List of abbreviations

PFA	Paraformaldehyde
PHOX	Phagocyte oxidase
PMN	Polymorphonuclear neutrophil
QIIME	Quantitative Insights Into Microbial Ecology
qPCR	Quantitative real-time polymerase chain reaction
RAST	Rapid Annotations using Subsystems Technology
RNA	Ribonucleic acid
RNAseq	RNA sequencing
rpm	Revolutions per minute
RT	Room temperature
SCFA	Short chain fatty acids
SCV	<i>Salmonella</i> -containing vacuole
SD	Standard deviation
SDS	Sodium dodecyl sulfate
SPF	Specific pathogen-free
SPI	<i>Salmonella</i> pathogenicity island
spp.	Species
<i>S. Tm</i>	<i>Salmonella enterica</i> serovar Typhimurium
Strep	Streptomycin
Te.	Tetrathionate
Tir	Translocated intimin receptor
T3SS	Type three secretion system
T3SS-1	T3SS encoded by SPI-1
T3SS-2	T3SS encoded by SPI-2
T6SS	Type six secretion system
UC	Ulcerative colitis
WHO	World Health Organization
WT	Wildtype

List of publications

List of publications

Work conducted during the course of this thesis that is published:

Studer, N., L. Desharnais, **M. Beutler**, S. Brugiroux, M. A. Terrazos, L. Menin, C. M. Schürch, K. D. McCoy, S. A. Kuehne and N. P. Minton (2016). "Functional Intestinal Bile Acid 7 α -Dehydroxylation by *Clostridium scindens* Associated with Protection from *Clostridium difficile* Infection in a Gnotobiotic Mouse Model." Frontiers in Cellular and Infection Microbiology **6**.

Brugiroux, S., **M. Beutler**, C. Pfann, D. Garzetti, H. Ruscheweyh, M. Diehl, D. Ring, Y. Lötscher, S. Hussain, R. Pukall, D. H. Huson, P. C. Münch, A. C. McHardy, K. D. McCoy, A. J. Macpherson, A. Loy, T. Clavel, D. Berry and B. Stecher. "Genome-guided modular design of a novel defined mouse microbiota that confers colonization resistance against *Salmonella enterica* serovar Typhimurium." Nature Microbiology **2**: 16215.

Spriewald, S., J. Glaser, **M. Beutler**, M. B. Koepfel and B. Stecher (2015). "Reporters for Single-Cell Analysis of Colicin Ib Expression in *Salmonella enterica* Serovar Typhimurium." PloS one **10**(12): e0144647.

Other publications:

Pla, D., O. K. Paiva, L. Sanz, **M. Beutler**, C. E. Wright, J. J. Calvete, D. J. Williams and J. M. Gutiérrez (2014). "Preclinical efficacy of Australian antivenoms against the venom of the small-eyed snake, *Micropechis ikaheka*, from Papua New Guinea: An antivenomics and neutralization study." Journal of proteomics **110**: 198-208.

Paiva, O., D. Pla, C. E. Wright, **M. Beutler**, L. Sanz, J. M. Gutiérrez, D. J. Williams and J. J. Calvete (2014). "Combined venom gland cDNA sequencing and venomomics of the New Guinea small-eyed snake, *Micropechis ikaheka*." Journal of proteomics **110**: 209-229.

Hupfeld, T., B. Chapuy, V. Schrader, **M. Beutler**, C. Veltkamp, R. Koch, S. Cameron, T. Aung, D. Haase and P. LaRosee (2013). "Tyrosinekinase inhibition facilitates cooperation of transcription factor SALL4 and ABC transporter A3 towards intrinsic CML cell drug resistance." British journal of haematology **161**(2): 204-213.

Summary

Summary

The indigenous gut microbiota exerts many beneficial tasks for the host including nutrient degradation, development of a functional immune system as well as protection from enteric infections and is therefore indispensable for health. Upon disturbances such as antibiotic intake, fluctuations in microbial diversity and density (dysbiosis) can occur, which renders the host more susceptible to infections with enteric pathogens like *Salmonella enterica* serovar Typhimurium (*S. Tm*). *S. Tm* induces severe gut inflammation which is accompanied by pathogen overgrowth ('blooming') and massive dysbiosis. Dysbiosis observed in human patients which is also a hallmark of inflammatory bowel diseases is generally characterized by Enterobacteriaceae overgrowth. Recently, first insights into the underlying mechanisms have been obtained: On the one hand, anaerobic electron acceptors, ethanolamine and iron selectively foster pathogen growth. On the other hand, the microbiota can experience collateral damage by the antimicrobial defense reaction, e.g. neutrophils which infiltrate the gut lumen in response to *Salmonella*-induced inflammation. Yet, it is still unclear which of these mechanisms is more important for the induction of dysbiosis and pathogen 'blooming': the altered nutritional environment or differential killing by the inflammatory immune response. Furthermore, it has remained elusive, how the environment of an inflamed gut impacts on individual species of a normal microbiota. Due to the high complexity of the gut microbiota, it is difficult to address functions of individual bacteria in host-pathogen-microbiota interactions. Therefore, gnotobiotic mouse models with reduced microbial complexity are needed. Thus, our group has established a novel gnotobiotic mouse model termed the Oligo-Mouse-Microbiota (Oligo-MM¹²) which is based on 12 murine bacterial isolates. Interestingly, the Oligo-MM¹² consortium covers 5 eubacterial main phyla (Firmicutes, Bacteroidetes, Actinobacteria, Verrucomicrobia and Proteobacteria) and was able to confer colonization resistance against an avirulent *Salmonella* strain. Preliminary work that was conducted before I joined the group included isolation and characterization of the Oligo-MM¹² strains, the establishment of strain-specific fluorescence *in situ* hybridization (FISH) probes as well as stable association of germfree C57BL/6J mice with the Oligo-MM¹² consortium.

One major aim of my doctoral thesis was to establish strain-specific quantitative real-time PCR (qPCR) assays that allow for quantification of individual Oligo-MM¹² bacteria as well as pathogens and other gut commensals. In addition, the course of wildtype *Salmonella* infection in the Oligo-MM¹² model as well as the influence of nutrients provided by an inflammatory milieu on *Salmonella* 'blooming' and concomitant microbiota shifts (dysbiosis) should be investigated. Furthermore, the importance of infiltrating neutrophils during *Salmonella*-induced dysbiosis should be assessed. In addition, it was aimed to compare the effect of infections with *S. Tm*, *Clostridium difficile* (*C. difficile*),

Summary

Citrobacter rodentium (*C. rodentium*) and T-cell-induced colitis on individual microbiota species using the Oligo-MM¹² model.

Using qPCR assays, I could show that the Oligo-MM¹² once administered orally, colonized the gut of germfree mice and was additionally vertically transmitted across filial generations which enables breeding of mice stably associated with the Oligo-MM¹². Furthermore community composition across animal facilities was similar, which is a pre-requisite for comparable host-microbe interaction studies.

Remarkably, wildtype *S. Tm* (*S. Tm*^{WT}) infection induced severe colitis at day 4 post infection in Oligo-MM¹² mice. Colitis was accompanied by *Salmonella* 'blooming' and drastic dysbiosis. Interestingly, the Oligo-MM¹² strains showed different abundance upon *S. Tm* induced colitis. Individual members of the phyla Bacteroidetes, Verrucomicrobia and Proteobacteria were drastically reduced, whereas Firmicutes strains were less affected by *S. Tm* induced inflammation and some strains even seemed to benefit from colitis. Especially *Enterococcus faecalis* KB1 thrived in the inflamed gut. The performance of Oligo-MM¹² strains positively correlated with the presence of genes for sporulation, iron acquisition, anaerobic respiration and ethanolamine utilization in their genome sequences. Infection experiments with *S. Tm* mutants deficient in siderophore production, anaerobic nitrate and tetrathionate respiration as well as ethanolamine utilization underlined a particular importance of anaerobic respiration and ethanolamine utilization for *S. Tm* overgrowth and concomitant microbiota shifts. Antibody mediated depletion of neutrophils favored dysbiosis. This suggests that neutrophils may not play a role in inducing dysbiosis and *Salmonella* 'blooming'.

We additionally compared other colitis models with *S. Tm*-induced colitis. Interestingly in contrast to *S. Tm* infection, infection with *C. rodentium* and T-cell-induced colitis only caused mild inflammation and no or just moderate changes in Oligo-MM¹² composition. However, after infection with *C. difficile* dysbiosis and pathogen 'blooming' was apparent. Remarkably, *C. difficile*-induced inflammation caused similar shifts in Oligo-MM¹² composition compared to *S. Tm*.

In conclusion, these data suggest that the Oligo-MM¹² is not damaged by neutrophils but outcompeted by *S. Tm* which profits from an inflammatory milieu and its associated nutritional environment – especially, from anaerobic electron acceptors and ethanolamine. Furthermore, individual Oligo-MM¹² species behaved differently in the presence of severe colitis. Genes involved in sporulation, anaerobic respiration, ethanolamine utilization and iron acquisition might contribute to survival during harsh conditions present in the inflamed gut. Interestingly, upon infection with different enteric pathogens and T-cell-induced colitis, there were parallels between microbiota shifts, indicating a conserved pattern of dysbiosis during gut inflammation. These findings could contribute

Summary

to the identification of general biomarkers for dysbiosis and the development of novel therapeutic concepts for Salmonellosis and inflammation-induced dysbiosis.

Zusammenfassung

Zusammenfassung

Die indigene Darm-Mikrobiota ist für die Gesundheit von großer Bedeutung: Sie unterstützt die Verdauung, trägt zur Entwicklung eines funktionalen Immunsystems bei und schützt vor Darminfektionen. Antibiotikatherapien oder andere exogene Störungen verändern die Diversität und Dichte der Darmbakterienzusammensetzung substanziell (Dysbiose). Infolgedessen wird der Organismus anfälliger für Infektionen mit darmpathogenen Erregern wie zum Beispiel *Salmonella enterica* serovar Typhimurium (S. Tm). S. Tm verursacht eine schwere Darmentzündung, die mit einem übermäßigen Salmonellenwachstum ('blooming') und Dysbiose einhergeht. Dysbiose, die in Patienten auftritt und auch ein Kennzeichen für chronisch-entzündliche Darmerkrankungen darstellt, ist hauptsächlich charakterisiert durch ein Überhandnehmen von Bakterien der Familie Enterobacteriaceae. Es konnte bisher gezeigt werden, dass einerseits Mechanismen wie die anaerobe Atmung, die Verwertung von Ethanolamin, sowie Eisenaufnahme ein sogenanntes *Salmonella*-‘blooming’ begünstigen. Andererseits könnte die Darm-Mikrobiota von neutrophilen Granulozyten, die während einer *Salmonellen*-vermittelten Darmentzündung in das Darmlumen emigrieren, stark geschädigt werden. Bis heute ist nicht abschließend geklärt, was für das Überhandnehmen eines Erregers und die damit verbundene Dysbiose entscheidender ist: Nährstoffe, die gehäuft in einem Entzündungsmilieu vorkommen und das selektive Wachstum von Erregern begünstigen oder das Töten von kommensalen Darmbakterien, welches von Effektoren des Immunsystems vermittelt wird.

Außerdem ist bis heute wenig darüber bekannt, wie sich eine Darmentzündung auf einzelne Arten einer gesunden Darm-Mikrobiota auswirkt. Aufgrund der hohen Komplexität der Darmbakterienzusammensetzung ist es äußerst schwierig, genaue Erkenntnisse über die Interaktionen der einzelnen Bakterien mit ihrem Wirt und einem Erreger zu gewinnen. Aus diesem Grund werden sogenannte gnotobiotische Tiermodelle verwendet, die eine definierte und weniger komplexe Darmbakterienzusammensetzung aufweisen. Unsere Arbeitsgruppe hat daher die Oligo-Mouse-Microbiota (Oligo-MM¹²) etabliert. Dieses neue gnotobiotische Mausmodell basiert auf 12 Bakterien, die aus Mäusen isoliert wurden. Bemerkenswerterweise repräsentieren die Oligo-MM¹² Stämme 5 eubakterielle Hauptphyla (Firmicutes, Bacteroidetes, Actinobacteria, Verrucomicrobia und Proteobacteria). Es konnte gezeigt werden, dass die Oligo-MM¹² eine Kolonisierungsresistenz gegenüber einem avirulenten Salmonellenstamm vermittelt. Zu Beginn meiner Arbeit waren die Oligo-MM¹² Stämme bereits isoliert und charakterisiert, spezifische Sonden für die Fluoreszenz *in situ* Hybridisierung (FISH) etabliert, sowie keimfreie C57BL/6J Mäuse mit dem Oligo-MM¹² Konsortium assoziiert.

Zusammenfassung

Ziel meiner Doktorarbeit war es, ein auf quantitativer real-time PCR (qPCR) basierendes Verfahren zur Detektion einzelner Oligo-MM¹² Stämme, anderer Erreger und weiterer kommensalen Darmbakterien zu etablieren. Des Weiteren sollte untersucht werden, wie sich eine Infektion mit *S. Tm* auf die Oligo-MM¹² auswirkt und welchen Einfluss Nährstoffe, die während einer Darmentzündung vorherrschen, auf *Salmonella*-‘blooming’ und Dysbiose haben. Auch der Beitrag von neutrophilen Granulozyten zur *Salmonella*-induzierten Dysbiose sollte erforscht werden. Ein weiteres Ziel der Arbeit war es, die Auswirkung von Infektionen mit *S. Tm*, *Clostridium difficile* (*C. difficile*), *Citrobacter rodentium* (*C. rodentium*) und T-Zell induzierter Kolitis auf einzelne Arten der Oligo-MM¹² zu untersuchen.

Ich konnte zeigen, dass die Oligo-MM¹² nach einmaliger Verabreichung den Darm von keimfreien Mäusen besiedelt und nach erfolgreicher Besiedlung vertikal über viele Filialgenerationen übertragen wird, was die Zucht von stabil kolonisierten Oligo-MM¹² Mäusen ermöglicht. Außerdem war die Oligo-MM¹² Zusammensetzung in verschiedenen Tierhaltungen sehr ähnlich, was eine Voraussetzung für die Vergleichbarkeit verschiedener Studien ist.

Die Infektion von Oligo-MM¹² Mäusen mit einem Wildtyp Salmonellenstamm führte an Tag 4 nach der Infektion zu einer schweren Darmentzündung. Bemerkenswerterweise, war dafür keine Antibiotikavorbereitung, die eine mögliche darmbakterienvermittelte Kolonisierungsresistenz brechen könnte, erforderlich. Die Kolitis wurde von einem drastischen Überwachsen von *Salmonella* und Dysbiose begleitet, wobei Oligo-MM¹² Stämme, die zu den Phyla Bacteroidetes, Verrucomicrobia und Proteobacteria gehören, stark abnahmen, Firmicutes hingegen weniger beeinträchtigt waren und Stämme wie *Enterococcus faecalis* von der Entzündung sogar profitierten. Des Weiteren fanden wir heraus, dass das Überleben einzelner Oligo-MM¹² Stämme mit dem Vorhandensein von Fitnessgenen korreliert, welche zur Sporulation, anaeroben Atmung und Ethanolaminverwertung beitragen. Infektionsexperimente mit Salmonellenstämmen, die außerstande waren Siderophore zu bilden, Nitrat und Tetrathionat zu veratmen oder Ethanolamin zu verwerten, brachten die Erkenntnis, dass gerade anaerobe Atmung und Ethanolamin essentiell für *Salmonella*-‘blooming’ und die Induktion der Dysbiose sind. Außerdem, begünstigt die Antikörper-basierte Depletion von neutrophilen Granulozyten die Entstehung von Dysbiose, was darauf schließen lässt, dass neutrophile Granulozyten eher vor *Salmonella*-induzierter Dysbiose schützen.

Zudem haben wir andere Kolitis-Modelle mit *Salmonella*-induzierter Kolitis verglichen. Im Gegensatz zur *S. Tm*-Infektion, verursachte eine, durch die Infektion mit *C. rodentium* und T-Zell-induzierte Kolitis in Oligo-MM¹² Mäusen eine milde Darmentzündung, welche nur zu einer geringen Abweichung der Darmbakterienzusammensetzung führte. Eine durch eine *C. difficile*-Infektion

Zusammenfassung

verursachte Kolitis rief dagegen ähnliche Veränderungen wie *Salmonella* in der Oligo-MM¹² Zusammensetzung hervor.

Auf Basis meiner Arbeit konnte festgestellt werden, dass kommensale Darmbakterien während einer *S. Tm*-induzierten Kolitis von neutrophilen Granulozyten nicht direkt getötet werden. Vielmehr wird die Darm-Mikrobiota von *S. Tm* aus dem Feld geschlagen, da *S. Tm* besonders von Stoffen wie Nitrat, Tetrathionat und Ethanolamin, die in einem Entzündungsmilieu vorkommen, profitiert und die Mikrobiota überwächst. Gene, die in kommensalen Bakterien vorkommen und wichtig für Sporulation, anaerobe Atmung, Ethanolaminverwertung und Eisenaufnahme sind, begünstigen möglicherweise das Überleben der Darmbakterien im entzündeten Darm. Interessanterweise konnten Parallelen zwischen Veränderungen in der Darmbakterienzusammensetzung aufgrund von Infektionen mit verschiedenen darmpathogenen Erregern und einer T-Zell-induzierten Kolitis festgestellt werden, was auf ein konserviertes Muster von Dysbiose während einer Darmentzündung schließen lässt. Diese Erkenntnisse könnten dazu beitragen generelle Biomarker für Dysbiose zu finden und neue Therapiekonzepte für die Behandlung der Salmonellose und Dysbiose zu entwickeln.

1. Introduction

1.1 Elucidation of gut microbiota functions using gnotobiotic mouse models

1.1.1 General functions of a healthy gut microbiota

The intestinal tract of humans and other mammals is colonized by a highly diverse and complex bacterial community, the microbiota. The bacteria increase in diversity and abundance along the digestive tract (Hooper and Macpherson 2010) and reach an enormously amount of 10^{12} cells per gram of large intestinal content (Marchesi and Shanahan 2007). Several thousands of years of co-evolution and symbiosis attributed the gut microbes special tasks that are essential for human health and wellbeing. Besides influencing gut motility as well as shaping the gut architecture by reducing cecal size and supporting microvilli formation (Falk *et al.* 1998), the gut microbiota contributes to the development of a functional immune system (Hooper *et al.* 2012). For example, commensals trigger production of secretory immunoglobulin A (Macpherson and Uhr 2004) and antimicrobial peptides via activation of Paneth cells (Vaishnavi *et al.* 2008), induction of regulatory T-cells (Atarashi *et al.* 2013) and differentiation of T_H17 cells (Atarashi *et al.* 2008). Furthermore, commensal bacteria protect against food allergen sensitization (Stefka *et al.* 2014). A disturbed microbiota was associated with allergic diseases and obesity (Baothman *et al.* 2016, Simonyte *et al.* 2016).

In addition to the educative effects on the immune system, the metabolic activity of the gut microbiota contributes to nutrition of the host (Nicholson *et al.* 2012). Microbiota produces metabolites such as vitamins (Said 2011), amino acids (Zheng *et al.* 2011) and carbohydrates (Flint *et al.* 2012). Moreover, the microbiota catabolizes complex, nutrient derived fibers and long-chained sugars into simple sugars as well as short-chain fatty acids (SCFAs) like butyrate (Donohoe *et al.* 2014), acetate and propionate (Caspari and Macy 1983). Butyrate has been shown to be the primary energy source of colonocytes (Donohoe *et al.* 2012). Consumption of butyrate by colonocytes renders the epithelium hypoxic, which strengthens barrier function (Kelly *et al.* 2015) as well as favors growth of obligate anaerobic bacteria such as *Clostridia* (Rivera-Chávez *et al.* 2016). The microbiota also provides protection against bacterial infection (Buffie and Pamer 2013, Stecher *et al.* 2013). This protective effect is termed colonization resistance (CR) and is on the one hand mediated by occupation of vacant niches, competition for nutrients or by production of inhibitory and toxic substances as well as immune stimulation. Taken together, the microbiota fulfills essential and highly versatile tasks including the protection from pathogens. However, under certain circumstances pathogens manage to break CR and induce disease.

Introduction

1.1.2 Composition of the gut microbiota: from health to dysbiosis and disease

A balanced microbial community in the healthy gut is basically characterized by domination of anaerobic bacteria such as members of the phyla Bacteroidetes and Firmicutes, whereas Proteobacteria, Actinobacteria and Verrucomicrobia are less abundant (Eckburg *et al.* 2005, Ley *et al.* 2005). Interestingly, the microbial composition between man and mice is similar at the phylum level. However, there are differences at the genus level: humans are preferentially colonized by *Prevotella*, *Faecalibacterium* and *Ruminococcus*, whereas the microbiota of mice is enriched in *Lactobacillus*, *Alistipes*, *Turicibacter* and *Mucispirillum* (Krych *et al.* 2013, Nguyen *et al.* 2015).

Exogenic factors like antibiotics (Maurice *et al.* 2013) as well as changes in diet (Agus *et al.* 2016) can disturb this equilibrium and induce shifts in microbial composition termed dysbiosis which are paralleled by reduction of bacterial diversity (Dethlefsen *et al.* 2008) and are associated with increased susceptibility to infections with enteric pathogens (Ubeda and Pamer 2012). In addition, chronic inflammation as well as acute infections could be also linked to dysbiosis. Interestingly, dysbiosis observed in irritable bowel syndrome (Kerckhoffs *et al.* 2011, Carroll *et al.* 2012) and IBD (Crohn's disease and Ulcerative colitis) (Baumgart *et al.* 2007, Frank *et al.* 2007) as well as after antibiotic treatment (Spees *et al.* 2013), chemically induced colitis (Lupp *et al.* 2007) or infection with enteric pathogens (Stecher *et al.* 2007, Barman *et al.* 2008) was commonly characterized by a drastic increase of Proteobacteria ('blooming'), whereas abundance of Bacteroidetes and Firmicutes was decreased (Winter and Bäuml 2014).

1.1.3 Analysis tools

Dysbiosis associated with diseases is primarily discovered in cohorts of patients by investigating microbial composition in fecal samples (Table 1, samples from humans). In order to recapitulate and study the importance of certain microbes in human diseases, germfree mice can be further associated with selective patient-derived bacterial consortia (Faith *et al.* 2010, Goodman *et al.* 2011, Faith *et al.* 2014). So called gnotobiotic (Greek: gnotos 'known' and bios: 'life') mice are then used for more specific and targeted microbiota analyses (Clavel *et al.* 2016). So far, there is no standardized microbiota for gnotobiotic mice that can be shared between research facilities. An investigation conducted by Rausch and colleagues revealed that the microbiota composition of laboratory mice differs between animal facilities (Rausch *et al.* 2016). Hence, results obtained by different investigations might be biased by differences in base line microbiota composition observed between different animal facilities.

To date, most microbiota analyses are based on 16S rRNA gene sequencing using next generation sequencing (NGS) techniques and reference data bases which enable assigning certain reads to

Introduction

published 16S rRNA gene sequences and thereby determine bacteria. In addition, strain-specific quantitative real-time PCR (qPCR) can be used to quantify and detect bacteria (Ganesh *et al.* 2013).

1.1.4 Defined microbial consortia for gnotobiotic mouse models

Since the gut microbiota is highly complex harboring up to 1000 different species (Marchesi and Shanahan 2007), it is challenging to mechanistically investigate host-microbe as well as microbe-microbe interactions in the intestine. Thus, animal models with reduced microbiota complexity ranging from one or two community members to intermediate complexity emerged in the past few years (Freter and Abrams 1972, Klaasen *et al.* 1991, Bry *et al.* 1996, Dewhirst *et al.* 1999, Mahowald *et al.* 2009, Becker *et al.* 2011, McNulty *et al.* 2011). The advantage of such gnotobiotic animal models is that the microbiota harbors known bacterial strains that can be composed according to the basic of the scientific problem investigated (Yi and Li 2012, Clavel *et al.* 2016). These models have mostly been based on bacteria isolated from humans (humanized microbiota model). Although humanized animal models may manifest as valuable research tools for studying disease associated host-microbe interactions (Turnbaugh *et al.* 2009, Faith *et al.* 2011), the successful colonization of human bacterial isolates to animals is dependent on genetic background (Wos-Oxley *et al.* 2012) and might not reflect true mutualistic microbiota-host effects developed by long-term co-evolution between host-specific bacteria and their host. It has been shown that humanized animal models do not recapitulate several aspects of gut physiology and immune maturation compared to association with indigenous microbiota (Chung *et al.* 2012). This problem can be overcome by using germfree mice associated with murine bacterial isolates. The microbiota from mice and humans is highly comparable at the phylum level, however there are marked differences in lower taxonomical levels (Ley *et al.* 2005, Oh *et al.* 2010) and functional categories (Xiao *et al.* 2015). In the past, a consortium of mouse-gut-derived bacteria termed the Altered Schaedler Flora (ASF) that consisted of 8 murine bacterial isolates has been widely used (Dewhirst *et al.* 1999, Geuking *et al.* 2011, Natividad *et al.* 2013, Collins *et al.* 2014). Unfortunately, this consortium is not available in public strain collections.

1.1.5 The Oligo-Mouse-Microbiota

We have recently developed a novel consortium based on 12 murine isolates, termed the Oligo-mouse-microbiota (Oligo-MM¹²) that confers partial colonization resistance against an avirulent *S. Tm* strain (Brugiroux *et al.* 2016). It was aimed to create a defined consortium of gut commensals that resembles the microbiota of conventional mice at the phylum level (Figure 1). By using a genome-informed design based on comparative (meta)genome analysis, we added additional bacteria which increased CR against *S. Tm*. We thereby show that the Oligo-MM¹² is a basic model microbiota that can be reduced or expanded by additional bacteria in order to investigate host-microbe or microbe-microbe interactions during enteric infection and other diseases.

Introduction

Linnenbrink and co-workers analyzed microbiota compositions of wild mice and showed that Bacteroidetes, Firmicutes, Deferribacteres and Proteobacteria were the dominating phyla in the mouse gut (Linnenbrink *et al.* 2013). Remarkably, the 12 mouse-adapted Oligo-MM¹² strains cover a spectrum of 5 eubacterial phyla identified by Linnenbrink and colleagues (Firmicutes, Bacteroidetes, Actinobacteria, Verrucomicrobia and Proteobacteria but not Deferribacteres). All Oligo-MM¹² strains were deposited in the German type culture collection (DSMZ) and are publically available. To this end, protocols for cryopreservation as well as FISH probes for individual Oigo-MM¹² were established and the genome of each Oligo-MM¹² strain is available.

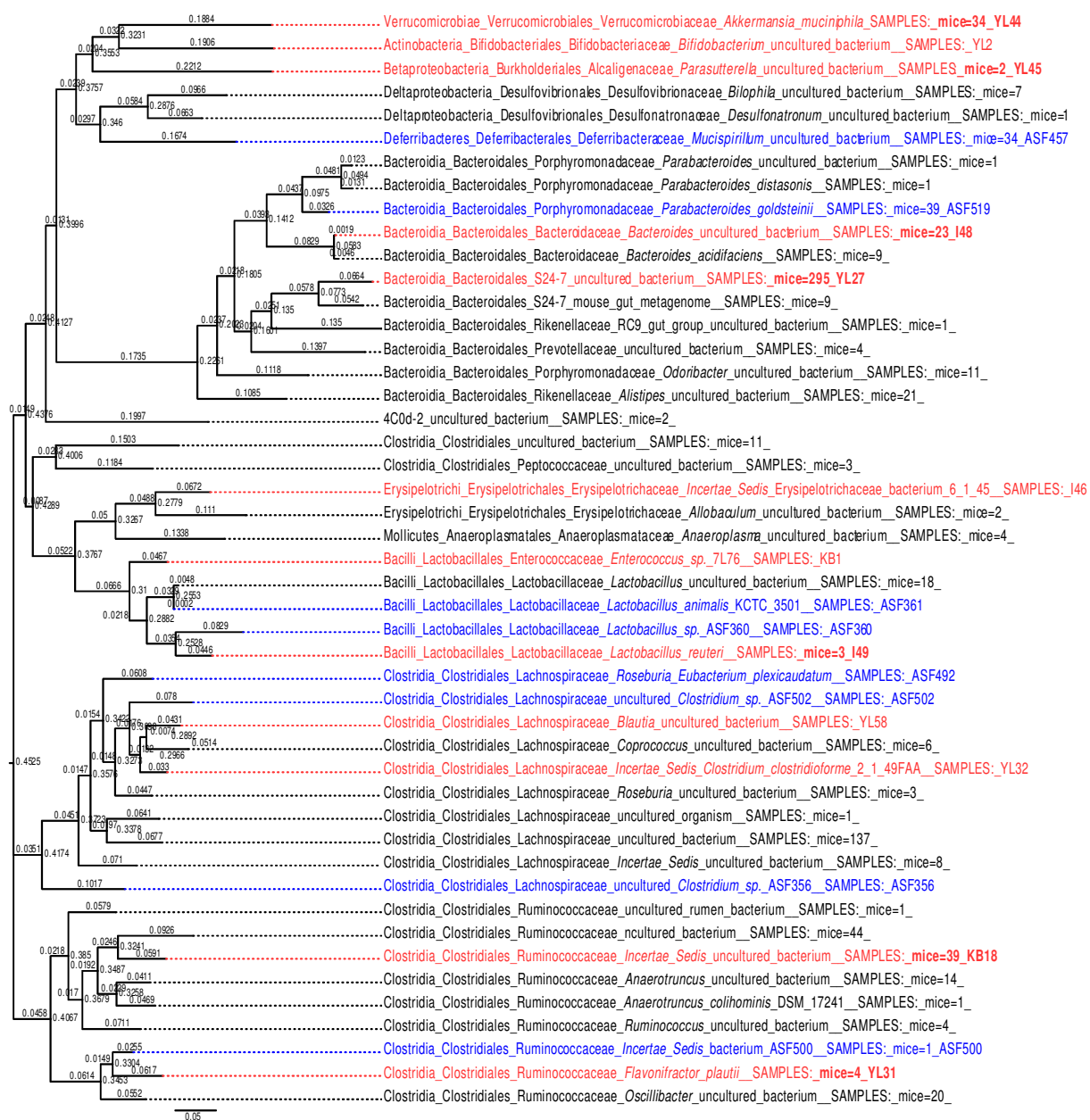


Figure 1: Phylogenetic placement and representation of the Oligo-MM¹² strains in conventional mice. The 16S rRNA sequences of the 12 Oligo-MM strains (red) as well as the 8 strains of the Altered Schaedler Flora (blue; ASF356, ASF360, ASF361, ASF457, ASF492, ASF500, ASF502 and ASF519) (Dewhirst *et al.* 1999) were compared against a set of 865 full-length high quality 16S rRNA gene sequences from 2 types of conventional

Introduction

unmanipulated SPF mice (Stecher *et al.* 2007). All sequences were aligned against the SILVA database version 111 NR (Quast *et al.* 2013) using MEGABLAST (version 2.2.28+) on a 97 % identity level, yielding 47 different taxonomic identities. The best hit of each of the 47 taxonomies from the database was used for the generation of a multiple sequence alignment using Infernal. A phylogenetic tree was generated using fasttree (Price *et al.* 2009). The number of sequences per taxonomic identity in the conventional mice is indicated (e.g. mice=20). The Oligo-MM¹² strains represent 10 of the 19 bacterial families (and candidate families), detected in this CON microbiota. Families represented only in CON mice include the Desulfobacteriaceae, Desulfonatronaceae (both δ -Proteobacteria), Deferribacteraceae (Deferribacteres phylum), Porphyromonadaceae, Rikenellaceae, Prevotellaceae (Bacteroidetes phylum), Peptococcaceae and Anaeroplasmataceae (Firmicutes phylum). It should be noted that ASF457 is a representative of the Deferribacteraceae and ASF519 is a representative of the Porphyromonadaceae. Oligo-MM¹² and the ASF⁸ consortia together cover 12 of the 19 abundant families in this CON microbiota. Figure and figure legend taken from (Brugiroux *et al.* 2016).

1.2 *Salmonella enterica* serovar Typhimurium pathogenesis and disease

1.2.1 Pathogenesis of *Salmonella enterica* serovar Typhimurium is dependent on type 3 secretion systems

S. Tm is a facultative anaerobic, non-spore-forming, Gram-negative food-borne pathogen belonging to the class of Gamma-Proteobacteria and is among the most clinically important serotypes that causes salmonellosis in humans with millions of infections every year worldwide (WHO 2013 (Mead *et al.* 1999, Flockhart *et al.* 2016)). The infection is usually self-limiting, however in very young, old or immunocompromised patients the *S. Tm* infection can become life-threatening with several thousands of deaths per year (WHO 2013 (Schulte and Hensel 2016)).

After oral uptake, *S. Tm* has to overcome host clearances such as stomach acid, the indigenous microbiota which provides colonization resistance (CR) as well as the mucus layer by using flagella and chemotaxis (Stecher *et al.* 2004). Upon reaching the epithelium, *S. Tm* adheres to polarized epithelial cells using a giant non fimbrial adhesin SiiE encoded on *Salmonella* pathogenicity island 4 (SPI-4). Expression of SPI-4 genes is co-regulated with expression of SPI-1 invasion genes (Gerlach *et al.* 2007). SPI-1 encodes a type 3 secretion system (T3SS-1) that injects effector proteins into the host cell (Kaiser *et al.* 2012). Secretion of T3SS-1 effector proteins is essential for bacterial uptake into epithelial cells that is associated with rearrangement of the actin cytoskeleton (Patel and Galán 2005) and induction of an inflammatory response (Hapfelmeier *et al.* 2004). In addition to T3SS-1 mediated invasion, *S. Tm* can also be taken up by dendritic cells which shuttle *S. Tm* across the epithelial barrier (Figure 2) (Rescigno *et al.* 2001). Once inside a host cell, *S. Tm* is surrounded by a vacuole made of plasma membrane, the so called *Salmonella*-containing vacuole (SCV) (Portillo *et al.* 1992) where *S. Tm* survives and replicates. In order to switch to this intracellular live style, *S. Tm* makes use of a second type 3 secretion system (T3SS-2). T3SS-2 effector protein secretion induces inhibited fusion of SCV with lysosomes in macrophages (Uchiya *et al.* 1999), intracellular replication, enhancement of inflammation and systemic dissemination (Hapfelmeier and Hardt 2005). SPI-1 and 2

Introduction

T3SSs additionally contribute to long-term infection and spread (Lawley *et al.* 2006). Moreover, *S. Tm* is able to form non-replicative, antibiotic resistant persister cells which reside within SCVs in macrophages. These persister cells might serve as a reservoir for relapsing infection (Helaine *et al.* 2014). After reaching an abundance of 10^8 bacteria per gram feces, *S. Tm* is effectively transmitted to the next host via the oral fecal route (Lawley *et al.* 2008). Transmission is additionally controlled by the indigenous microbiota.

It is worth mentioning, that most mechanistic studies of *S. Tm* infection have been done in the streptomycin pre-treated *S. Tm* infection model (Barthel *et al.* 2003), where the microbiota is manipulated by antibiotic treatment prior to infection (Stecher *et al.* 2007). In this model, antibiotic-induced dysbiosis renders mice susceptible to *S. Tm* induced colitis that is dependent on functional T3SSs (Hapfelmeier *et al.* 2005). Although the streptomycin pre-treated mouse model is excellent for mechanistic studies regarding host-pathogen interaction, it is not adequate for studying all aspects of microbiota-pathogen interactions since microbiota composition is influenced by antibiotic treatment. Therefore, in order to obtain unbiased insights into microbiota-pathogen interactions at the single species level, the gnotobiotic Oligo-MM¹² model was used in this study.

1.2.2 *S. Tm* invades the gut ecosystem and induces inflammation

As already outlined before in section 1.2.1, *S. Tm* has to break CR of the indigenous microbiota in order to successfully colonize and infect the host. Ferreyra and colleagues proposed that during infection there are five stages of microbiota-pathogen interaction: At stage 1, the healthy and complex microbiota mediates CR by occupying niches. Upon changes in bacterial diversity and density (moderate dysbiosis) that can be induced by disturbances such as antibiotics or changes in diet, the pathogen can colonize (stage 2). At stage 3, the pathogen expands and benefits from available nutrients (expansion phase). Stage 4 is characterized by pathogen outgrowth ('blooming' phase) that is accompanied by inflammation and massive dysbiosis. After clearing the pathogen in stage 5 the microbiota recovers from dysbiosis (resilience) (Ferreyra *et al.* 2014). The first 4 stages of ecosystem invasion are visualized in Figure 2.

CR which is mediated by niche occupation, competition for nutrients, by direct inhibition using antimicrobial peptides or T6SS mediated killing (Russell *et al.* 2014) and by stimulation of the immune defense can be overcome by the application of antibiotics (Barthel *et al.* 2003). It could be recently shown that antibiotic treatment facilitates *S. Tm* infection by depletion of *Clostridia* which is followed by a decrease in butyrate concentration and increased oxygenation of the epithelium. This oxygenation promotes *S. Tm* growth in a cytochrome oxidase dependent manner in early stages of infection (Rivera-Chávez *et al.* 2016). Furthermore, after antibiotic treatment, *S. Tm* as well as

Introduction

Clostridium difficile (another enteric pathogen) profit from microbiota-liberated mucosal carbohydrates like fucose and sialic acid (Ng *et al.* 2013). Antibiotic treatment also increases luminal galactarate and glucarate concentrations by leading to increased oxygenation of galactose and glucose, sugars selectively consumed by *Salmonella* (Faber *et al.* 2016). In addition, hydrogen that is produced by the unperturbed indigenous microbiota (Maier *et al.* 2013) boosts *S. Tm* growth and ecosystem invasion of *S. Tm* in early stages of infection. This effect was absent after antibiotic treatment, showing a link between specific metabolites provided by the microbiota and pathogen adaptation. Gnotobiotic mice used in this study were based on a low complex type of microbiota (LCM mice) (Stecher *et al.* 2010). Besides taking advantage of sugars, oxygenation and hydrogen during early stages of infection (stages 2 and 3), *S. Tm* induces gut inflammation via T3SS activity which creates an inflammatory milieu and is accompanied by *Salmonella* 'blooms' during later stages of infection (stage 4). *S. Tm* induced colitis causes dysbiosis (Stecher *et al.* 2007) and is characterized by infiltrating neutrophils (Loetscher *et al.* 2012). However, until now the impact of severe *S. Tm* induced gut inflammation on single species of the gut microbiota remains elusive.

1.2.3 *S. Tm* profits from an inflammatory gut milieu and outcompetes the indigenous microbiota

S. Tm induces acute gut inflammation by invading epithelial cells and survival in mucosal macrophages (Winter *et al.* 2010) which is followed by dramatic changes in microbiota composition as well as *Salmonella* 'blooms'. It has been shown that *S. Tm* thrives in the inflamed gut by profiting from the inflammatory milieu. In contrast to anaerobic commensals, *S. Tm* is able to use anaerobic electron acceptors that are generated during respiratory burst mediated by neutrophils attracted to the site of infection (Winter *et al.* 2010, Lopez *et al.* 2012). The most important anaerobic electron acceptors are tetrathionate ($S_4O_6^{2-}$) and nitrate (NO_3^-). Toxic hydrogen sulfide (H_2S) produced by the microbiota is converted into thiosulfate ($S_2O_3^{2-}$) by the mucosa (Levitt *et al.* 1999, Furne *et al.* 2001). During intestinal inflammation which is accompanied by neutrophil infiltration and the presence of reactive oxygen species, $S_2O_3^{2-}$ is further oxidized to tetrathionate ($S_4O_6^{2-}$) (Winter *et al.* 2010). Nitrate forms from NO that is generated by iNOS which further reacts with reactive oxygen species such as superoxide O_2^- produced by neutrophils (PHOX dependent) or by the epithelium (Winter *et al.* 2013) to peroxynitrite ($ONOO^-$) which can isomerize to nitrate (NO_3^-) (Szabó *et al.* 2007). *S. Tm* even actively seeks for energetically favorable regions where anaerobic electron acceptors or glycoconjugates are present using flagella-mediated motility and chemotaxis (Stecher *et al.* 2008, Rivera-Chávez *et al.* 2013). Ethanolamine that is liberated from dying epithelial and is selectively used by *Salmonella* serves as energy source for tetrathionate respiration (Thiennimitr *et al.* 2011).

Introduction

In addition to respiratory burst, antimicrobial peptides are released upon *S. Tm* infection. Infection of macrophages induces IL-23 expression which leads to T-cell dependent induction of IL-17 and IL-22 (Godinez *et al.* 2009). T-cell dependent cytokine production is essential for recruitment of neutrophils (Godinez *et al.* 2008) and for secretion of antimicrobials like lipocalin-2 (LCN-2). LCN-2 that is secreted by epithelial cells and neutrophils hampers iron uptake by sequestering bacterial siderophores like enterochelin (Flo *et al.* 2004, Berger *et al.* 2006, Raffatellu *et al.* 2009). Siderophores are needed for iron scavenging which is an essential micronutrient. Free iron concentrations in the host is restricted by iron-binding proteins like transferrin or ferritin (Andrews 2000). Besides enterochelin, *S. Tm* produces salmochelin a glycosylated variant of enterochelin which is not bound by LCN-2 (Raffatellu *et al.* 2009). Thus, salmochelin production provides a fitness advantage in the presence of LCN-2. In addition, low dietary iron intake was protective against enteric infection in a mouse model (Kortman *et al.* 2015). *S. Tm* is also resistant to host-mediated zinc sequestration by neutrophil dependent secretion of calprotectin (Liu *et al.* 2012). This resistance is conferred by expression of a high affinity zinc transporter (ZnuABC). Furthermore, *S. Tm* resists RegIII β , an antimicrobial peptide which is induced in enteric *S. Tm* infection and kills commensal gut bacteria while paving the way for *Salmonella* (Stelzer *et al.* 2011). Moreover, sialic acid catabolism favors *S. Tm* outgrowth and dysbiosis during inflammation (Huang *et al.* 2015).

However, the inflammatory host response is not only beneficial for *S. Tm*. On the one hand, immune defense that was thought to limit pathogen-invasion can actually promote infection by providing a growth advantage over the gut microbiota. On the other hand, during *S. Tm* infection granulocytes (mostly neutrophils) impose a tight bottleneck on the gut luminal pathogen population (Maier *et al.* 2014). Transmigrated granulocytes kill up to 99.999% of the luminal *Salmonella* population and only a subpopulation of *Salmonella* survives and thrives later in the inflamed gut, profiting from the inflammatory milieu. Until now it is unknown how infiltrating neutrophils impact on commensal bacteria and which nutritional factor of an inflammatory milieu (Figure 2) contributes most to *S. Tm* 'blooming' and dysbiosis.

Introduction

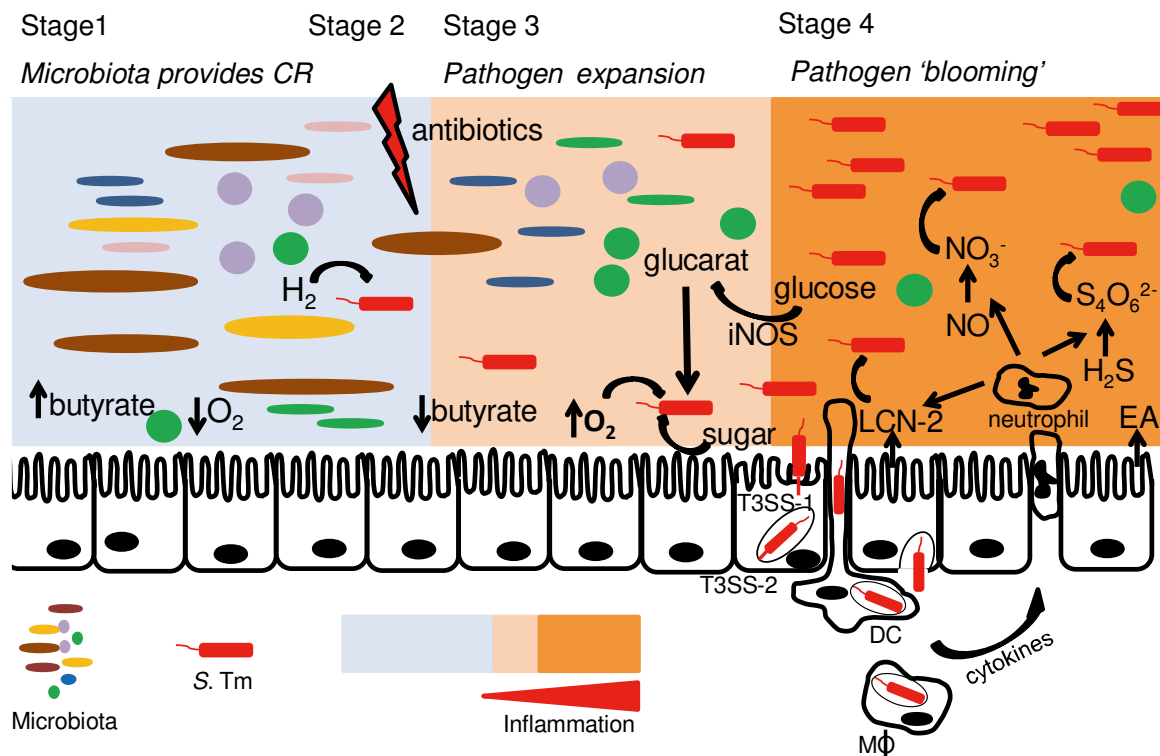


Figure 2: *S. Tm* ecosystem invasion and infection. A healthy and complex microbiota confers colonization resistance (CR) and protects from infection (stage 1). Upon disturbances of the microbiota (dysbiosis) induced by e.g. antibiotics, *S. Tm* colonizes the gut (stage 2). *S. Tm* profits from microbiota derived hydrogen (H_2), increased oxygenation, and sugars and expands in the already inflamed gut (stages 2 and 3). At stage 4, *S. Tm* induces systemic infection and severe inflammation including recruitment of dendritic cells (DC), macrophages (M ϕ) and neutrophils which is accompanied by *S. Tm* 'blooming' and massive dysbiosis. During this late stage of infection, *S. Tm* profits from nitrate (NO_3^-) and tetrathionate ($S_4O_6^{2-}$) respiration as well as from ethanolamine (EA) derived from dying epithelial cells.

1.3 Interactions of other enteric pathogens and the gut microbiota

1.3.1 *Citrobacter rodentium*, a model for human enteropathogenic *Escherichia coli* infection

Enteropathogenic *Escherichia coli* (EPEC) is an important pathogen inducing diarrheal disease in infants causing illness and morbidity (Nataro and Kaper 1998, Kotloff *et al.* 2013). EPEC has been shown to adhere to epithelial cells using bundle-forming pili (BFP) (Cleary *et al.* 2004). This adherence is further strengthened by T3SS mediated translocation of translocated intimin receptor (Tir) to the mammalian cell which induces formation of 'attaching and effacing' lesions (Kenny *et al.* 1997). In order to model EPEC induced pathology in humans which is a bad mouse-colonizer, mouse models of EPEC induced pathology are based on infections with *Citrobacter rodentium* (*C. rodentium*). Interestingly, *C. rodentium* causes transmissible colon hyperplasia in mice (Luperchio and Schauer 2001). The pathogenesis is comparable to EPEC infection in humans. It is characterized by intimate attachment of the pathogen to enterocytes, pedestral formation and effacement of microvilli

Introduction

(‘attaching and effacing’ lesion) (Mallick *et al.* 2012). In mice, *C. rodentium* infection causes colitis and induces microbiota shifts mainly characterized by increased abundance of facultative anaerobic bacteria belonging to the Enterobacteriaceae family (Lupp *et al.* 2007). Interestingly, commensal lactobacilli protect against *C. rodentium* infection (Vong *et al.* 2015). Furthermore, viable bacteria in fermented dairy products reduced colonic crypt hyperplasia upon *C. rodentium* infection by stabilizing the abundance of *Ruminococcus* and *Turicibacter* (Collins *et al.* 2014). This indicates that the microbiota plays a role in protection against *C. rodentium* infection. 16S rRNA amplicon sequencing of the microbiota revealed that *C. rodentium* infection is associated with changes in mucosally adherent as well as luminal microbiota. In particular, increased abundance of Proteobacteria, Deferribacteres and Clostridia as well as decreased abundance of *Lactobacillus* were observed (Hoffmann *et al.* 2009). However, data how *C. rodentium* alters microbial composition at the single species level are lacking (Table 1).

1.3.2 *Clostridium difficile*, a leading cause of antibiotic associated diarrhea (AAD)

Nosocomially acquired infections with *Clostridium difficile* (*C. difficile*) are associated with antibiotic therapy and have become a major health concern worldwide (Rupnik *et al.* 2009). While a healthy gut microbiota provides CR against *C. difficile* infection, antibiotic therapy increases the risk of acquiring *C. difficile* infection and disease (Britton and Young 2014). Especially *C. difficile* ribotype 027 spreads rapidly. This ribotype is linked to increased severity of disease and mortality (Valiente *et al.* 2014). Persistent infection correlates with a dysbiotic microbiota (Ananthakrishnan 2011). Interestingly, transfer of fecal samples from healthy donors ameliorated disease in patients (van Nood *et al.* 2013), indicating the beneficial potential of a healthy microbiota. Pathology of *C. difficile* depends on expression of different toxins such as toxin A (*tcdA*) and toxin B (*tcdB*) which are glycosyltransferases that inactivate Rho, Rac as well as Cdc42 involved in actin polymerization and regulation of the cell cycle (Voth and Ballard 2005). It was speculated that ribotype 027 produces more toxin A and B because it lacks *tcdC* which is a negative regulator of these toxins (Warny *et al.* 2005) and thereby increases virulence. However, this is controversial since Aitken and colleagues could not confirm hyper-virulence of ribotype 027 (Aitken *et al.* 2015). Besides toxin A and toxin B, *C. difficile* ribotypes can additionally express a binary toxin (CDT) which exerts actin-specific ADP-ribosyltransferase activity and is encoded by *cdtA* (enzymatic domain) and *cdtB* (binding domain) (Stubbs *et al.* 2000). CDT which is expressed by two-third of the *C. difficile* strains including ribotype 027 is thought to further aggravate *C. difficile*-induced disease (Barbut *et al.* 2005, McEllistrem *et al.* 2005, Valiente *et al.* 2014). Toxins are only produced by vegetative cells, not by spores (Lawley *et al.* 2009), underlining the importance of spore germination for pathogenesis. Germination is dependent on bile acids (Sorg and Sonenshein 2010) which is modulated by the microbiota (Narushima *et al.*

Introduction

2006, Ridlon *et al.* 2006). Manipulation of the microbiota with broad-spectrum antibiotics reduces abundance of Lachnospiraceae and Ruminococcaceae which correlates with decreased concentrations of secondary bile acids in the gut. Secondary bile acid producers like *Clostridium scindens* increased CR against *C. difficile* infection (Buffie *et al.* 2015, Theriot *et al.* 2016). Furthermore, cohort studies conducted with patients that had received fecal microbiota transplantation revealed that protective microbial taxa belong to the *Bacteroides* spp., *Parabacteroides* spp., *Alistipes*, Ruminococcaceae, Clostridium cluster IV and XIVa (*Faecalibacterium prausnitzii*, *Roseburia intestinalis*, *Eubacterium rectale*), Lachnospiraceae, Peptostreptococcaceae and Verrucomicrobiaceae and negatively correlate with *C. difficile* colonization. In contrast, the abundance of *Lactobacillus* spp., Streptococcaceae, Enterobacteriaceae, *Enterococcus* spp., *Salmonella* spp., *Sutterella* spp. and Verrucomicrobia correlates positively with *C. difficile* colonization (Seekatz and Young 2014).

1.4 Dysbiosis and inflammatory bowel diseases

Inflammatory bowel diseases (IBD) include Crohn's disease (CD) and Ulcerative Colitis (UC). Especially, IBD are emerging in countries of the western world. IBD are characterized by barrier disruption, chronic inflammation and dysbiosis (Vivinus-Nébot *et al.* 2014, Ridler 2016, Willing *et al.* 2016). The incidence of IBD has been further associated with genetic predisposition and western diet rich in fat and sugars (Agus *et al.* 2016). Furthermore, the epithelial barrier, innate and adaptive immunity, environmental factors and the microbiota apparently play a key role in the pathogenesis of IBD (Xavier and Podolsky 2007).

Compositional microbiota analysis of samples obtained from inflamed guts revealed that *Bacteroides* spp. and Fusobacteria are increased in CD patients, whereas Proteobacteria and Firmicutes are increased in UC patients (Forbes *et al.* 2016). In addition, butyrate-producing bacteria like *Blautia faecis*, *Roseburia inulinivorans*, *Ruminococcus torques*, *Clostridium lavalense*, *Bacteroides uniformis* and *Faecalibacterium prausnitzii* are reduced and bacteria belonging to the genera *Actinomyces* and *Bifidobacterium* are enriched in CD patients (Takahashi *et al.* 2016). Patients suffering from UC display reduced diversity of Clostridium cluster IV and decreased abundance of bacteria involved in butyrate and propionate metabolism like *Ruminococcus bromii*, *Eubacterium rectale*, *Roseburia* spp., and *Akkermansia* spp.. In contrast, increased abundance of *Fusobacterium* spp., *Peptostreptococcus* spp., *Helicobacter* spp., *Campylobacter* spp. and *C. difficile* is observed in patients suffering from UC (Rajilic-Stojanovic *et al.* 2013). However, until now it remains elusive whether dysbiosis observed during IBD is cause or consequence of the disease (Buttó and Haller 2016). Interestingly, some microbiota members protect the host from colitis. For example *Bacteroides thetaiotaomicron* as well

Introduction

as *B. fragilis* have evolved beneficial immune modulatory properties (Hoffmann *et al.* 2015, Chu *et al.* 2016) and *Faecalibacterium prausnitzii* mediates anti-inflammatory activity (Sokol *et al.* 2008).

1.5 Common changes in microbiota composition upon enteric infection and inflammatory bowel diseases

In the past years, it has become evident that IBD as well as pathogen induced inflammation are accompanied by microbiota shifts and decreased bacterial diversity. Shifts have in common that the abundance of obligate anaerobic bacteria is decreased. This gives way to overgrowth of facultative anaerobic bacteria (Winter and Bäumlér 2014). Thus, shifts were mainly characterized by Enterobacteriaceae (Proteobacteria) ‘blooms’ (Lupp *et al.* 2007, Stecher *et al.* 2007, Seekatz and Young 2014) and reduced abundance of butyrate producing bacteria such as *Blautia faecis*, *Roseburia inulinivorans*, *Ruminococcus torques*, *Clostridium lavalense*, *Bacteroides uniformis*, *Faecalibacterium prausnitzii*, *Ruminococcus bromii*, *Eubacterium rectale* and *Roseburia* spp (Rajilic-Stojanovic *et al.* 2013, Takahashi *et al.* 2016). However, studies conducted so far were mostly done in different animal models or are obtained from human patients (Table 1). In order to investigate parallels and mechanisms of dysbiosis induced by infections or chronic inflammation, it is key to make use of standardized and highly defined microbial minimal consortia with strain-specific analysis tools. In this thesis, we compare dysbiosis induced by infection or chronic inflammation using gnotobiotic mice associated with the Oligo-MM¹².

Table 1: Changes in microbiota composition upon enteric infection and inflammatory bowel diseases

Pathology	Enriched or positively correlated bac. taxa	Depleted or negatively correlated bac. taxa	Organism / analysis method	Reference
S. Tm infection	Proteobacteria, <i>Enterococcus</i> spp., <i>Salmonella</i>	Bacteroidales, Firmicutes, Verrucomicrobia, Deferribacteres, <i>Lactobacillus</i> spp., <i>Clostridium</i> spp., <i>Bacteroides</i> spp.	C57BL/6J mice (strep. pre-treated mouse) / 16S rRNA sequencing and culturing	(Stecher <i>et al.</i> 2007)
S. Tm infection	<i>Enterococcus</i> spp., <i>Salmonella</i>	Bacteroidetes, Firmicutes, <i>Barnesiella</i> spp.	129/SvJ mice (no antibiotic prior to infection) / 16S rRNA sequencing	(Kaiser <i>et al.</i> 2013)
S. Tm infection	<i>Salmonella</i>	<i>Anaerostipes caccae</i> , <i>Bifidobacterium longum</i> , <i>Blautia producta</i> , <i>Bacteroides thetaiotaomicron</i> , <i>Clostridium ramosum</i> , <i>E. coli</i> , <i>C. butyricum</i> , <i>Akkermansia muciniphila</i>	C3H mice (human bacteria SIHUMI) / strain-specific qPCR	(Ganesh <i>et al.</i> 2013)
S. Tm infection	<i>Catenibacterium</i> , <i>Xylanibacter</i>	<i>Prevotella</i>	Swine / 16S rRNA sequencing and qPCR	(Bearson <i>et al.</i> 2013)
S. Tm infection	<i>Clostridium perfringens</i> , <i>Salmonella</i>	<i>Eubacterium rectale</i> , <i>Clostridium coccoides</i> ,	FvB mice (no antibiotic prior to	(Barman <i>et al.</i> 2008)

Introduction

Pathology	Enriched or positively correlated bac. taxa	Depleted or negatively correlated bac. taxa	Organism / analysis method	Reference
		<i>Lactobacillus</i> spp., <i>Bacteroides</i> spp.	infection) / qPCR	
<i>C. rodentium</i> infection	Enterobacteriales	Bacteroidales, Clostridiales	C57BL/6J mice / 16S rRNA sequencing	(Lupp <i>et al.</i> 2007)
<i>C. rodentium</i> infection	Deferribacteres, Proteobacteria	Lactobacillaceae	C57BL/6J mice / 16S rRNA sequencing	(Hoffmann <i>et al.</i> 2009)
<i>C. difficile</i> infection	<i>Ruminococcus gnavus</i> , <i>Klebsiella pneumoniae</i>	<i>Bifidobacterium longum</i>	Human infants / TTGE* + 16S rRNA sequencing	(Rousseau <i>et al.</i> 2011)
<i>C. difficile</i> infection		Ruminococcaceae, Lachnospiraceae	Human / 16S rRNA sequencing	(Antharam <i>et al.</i> 2013)
<i>C. difficile</i> infection	Firmicutes, Proteobacteria, Actinobacteria	Bacteroidetes	Human / microarray + 16S rRNA sequencing	(Manges <i>et al.</i> 2010)
<i>C. difficile</i> infection	<i>Lactobacillus</i> spp., Streptococcaceae, Enterobacteriaceae, <i>Enterococcus</i> spp., <i>Salmonella</i> spp., <i>Sutterella</i> spp., Verrucomicrobia	<i>Bacteroides</i> spp., <i>Parabacteroides</i> spp., <i>Alistipes</i> , Ruminococcaceae, Clostridium cluster IV and XIVa (<i>Faecalibacterium prausnitzii</i> , <i>Roseburia intestinalis</i> , <i>Eubacterium rectale</i>), Lachnospiraceae, Peptostreptococcaceae, Verrucomicrobiaceae	Human (after fecal transplantation).	(Seekatz and Young 2014)
CD	Bacteroidetes, Fusobacteria		Human / 16S rRNA sequencing	(Forbes <i>et al.</i> 2016)
CD	Actinomyces, <i>Bifidobacterium</i>	<i>Bacteroides</i> , <i>Eubacterium</i> , <i>Faecalibacterium</i> , <i>Ruminococcus</i> (<i>Blautia faecis</i> , <i>Roseburia inulinivorans</i> , <i>Ruminococcus torques</i> , <i>Clostridium lavalense</i> , <i>Bacteroides uniformis</i> and <i>Faecalibacterium prausnitzii</i>) butyrate producer	Human / 16S rRNA sequencing	(Takahashi <i>et al.</i> 2016)
UC	Proteobacteria, Firmicutes		Human / 16S rRNA sequencing	(Forbes <i>et al.</i> 2016)
UC	<i>Fusobacterium</i> spp., <i>Peptostreptococcus</i> spp., <i>Helicobacter</i> spp., <i>Campylobacter</i> spp., <i>C. difficile</i>	<i>Ruminococcus bromii</i> , <i>Eubacterium rectale</i> , <i>Roseburia</i> spp., and <i>Akkermansia</i> spp., Clostridium cluster IV	Human / phylogenetic microarray	(Rajilic-Stojanovic <i>et al.</i> 2013)
IBD	Alphaproteobacteria; Actinobacteria (<i>Actinomyces oxydans</i>); Gammaproteobacteria; Betaproteobacteria (<i>Pseudomonas</i> spp.), Firmicutes, Bacilli (<i>B. licheniformis</i>)	Firmicutes, Lachnospiraceae (<i>Clostridium</i> spp.); Bacteroidetes, Bacteroidales (<i>B. thetaiotaomicron</i> , <i>Alistipes</i> spp.)	Human / qPCR	(Frank <i>et al.</i> 2007)

S. Tm: *Salmonella* Typhimurium, *C. rodentium*: *Citrobacter rodentium*, *C. difficile*: *Clostridium difficile*, CD: Crohn's disease, UC: ulcerative colitis, IBD: inflammatory bowel disease, Strep.: streptomycin, *TTGR: PCR-temporal temperature gradient gel electrophoresis, bac.: bacterial

Introduction

1.6 Aims of the study

The composition of the gut microbiota is highly complex and several aspects of host-pathogen-microbiota interactions still remain elusive. In order to investigate mechanisms underlining such interactions, we established a novel mouse derived bacterial consortium termed the Oligo-mouse-microbiota (Oligo-MM¹²) that is constituted of 12 bacterial isolates which cover the main eubacterial phyla (Brugiroux *et al.* 2016).

(1) The first aim of my thesis was to establish strain-specific qPCR assays that allow for absolute quantification of the 12 individual Oligo-MM strains. In addition for specific research question, qPCR assays should be also extended to quantification of 7 ASF strains, *Salmonella* Typhimurium, *Citrobacter rodentium*, *Helicobacter typhlonius*, *Clostridium difficile*, *Clostridium scindens*, *Escherichia coli*, *Streptococcus danieliae* and *Staphylococcus xylosus* in complex consortia. qPCR was chosen because it is a fast, affordable and sensitive method for absolute quantification of individual bacterial species. This method shall then be employed to monitor bacterial colonization in gnotobiotic mice over time, analyze vertical transmission, microbial stability over generations, changes in microbial composition upon exposure to different diet and compare Oligo-MM¹² composition between different animal facilities.

S. Tm induces acute gut inflammation engaging effector protein secretion via type 3 secretion systems which is followed by dramatic changes in microbiota composition (dysbiosis) as well as *Salmonella* overgrowth ('blooming'). Recently, first insights into the underlying mechanisms have been obtained: On the one hand, anaerobic electron acceptors like nitrate and tetrathionate, ethanolamine and iron are selectively used by the pathogen conferring a fitness advantage over the indigenous microbiota. On the other hand, the microbiota might experience collateral damage by neutrophils which infiltrate the gut lumen in response to *Salmonella*-induced inflammation. However, it is still unclear which of these mechanisms is more important for the induction of pathogen 'blooming' and concomitant dysbiosis: the altered nutritional environment or differential killing by the inflammatory immune response. Furthermore, it has remained elusive how the environment of an inflamed gut impacts on individual species of a normal microbiota, which properties are important for survival in the inflamed gut and whether or how the microbiota is able to recover from inflammation induced dysbiosis (resilience).

(2) The second aim was to study the course of *S. Tm* infection in the gnotobiotic Oligo-MM¹² model. Furthermore, the influence and importance of single nutrients provided by an inflammatory milieu as well as long-term infection should be investigated using strain-specific qPCR assays as well as *S. Tm* strains deficient in nitrate and tetrathionate respiration, ethanolamine utilization, siderophore

Introduction

production and functional type 3 secretion systems (T3SSs). Functional genomic analysis of Oligo-MM¹² genome sequences should be performed to identify genes of commensals characteristic for survival in the inflamed gut. In addition, besides the influence of an inflammatory milieu, I aimed to investigate the role of neutrophils in dysbiosis during *Salmonella*-induced inflammation by antibody-mediated depletion of neutrophils and mice deficient in extravasation of neutrophils.

Pathogen infection as well as chronic inflammation correlates with decreased abundance of obligate anaerobic bacteria and increased abundance of Proteobacteria. However, data showing the fate of individual bacteria during dysbiosis at the species level are lacking so far. Studies have been performed in different animal models or are patient-derived and employ different analysis tools (Table 1). Thus, I wanted to identify differences and common effects between infections with different pathogens and chronic inflammation on the gut microbiota using the same model microbiota and analysis tools.

(3) My third aim was to compare the influence of infections with *S. Tm*, *C. rodentium*, *C. difficile* as well as T-cell-induced colitis on individual microbiota species using the defined Oligo-MM¹² model and strain-specific qPCR assays.

2. Material and Methods

2.1 Strains and plasmids

2.1.1 Strains

Table 2: Mouse derived bacterial strains constituting the Oligo-Mouse-Microbiota (Oligo-MM¹²)

Strain ID	Taxonomy at species level	DSM No.	Isolated by	Publication
YL2	<i>Bifidobacterium longum</i> subsp. <i>animalis</i>	26074	Yvonne Loetscher	(Brugiroux <i>et al.</i> 2016)
YL27	'Muribaculum intestinale'	28989	Yvonne Loetscher	(Brugiroux <i>et al.</i> 2016)
YL31	<i>Flavonifractor plautii</i>	26117	Yvonne Loetscher	(Brugiroux <i>et al.</i> 2016)
YL32	<i>Clostridium clostridioforme</i>	26114	Yvonne Loetscher	(Brugiroux <i>et al.</i> 2016)
YL44	<i>Akkermansia muciniphila</i>	26127	Yvonne Loetscher	(Brugiroux <i>et al.</i> 2016)
YL45	'Turicimonas caecimuris'	26109	Yvonne Loetscher	(Brugiroux <i>et al.</i> 2016)
YL58	<i>Blautia coccoides</i>	26115	Yvonne Loetscher	(Brugiroux <i>et al.</i> 2016)
I46	<i>Clostridium innocuum</i>	26113	Ricco Robbiani	(Brugiroux <i>et al.</i> 2016)
I48	'Bacteroides caecimuris'	26085	Ricco Robbiani	(Brugiroux <i>et al.</i> 2016)
I49	<i>Lactobacillus reuteri</i>	32035	Ricco Robbiani	(Brugiroux <i>et al.</i> 2016)
KB1	<i>Enterococcus faecalis</i>	32036	Sandrine Brugiroux	(Brugiroux <i>et al.</i> 2016)
KB18	'Acutalibacter muris'	26090	Sandrine Brugiroux	(Brugiroux <i>et al.</i> 2016)

Table 3: *Salmonella*, *E. coli* and *Yersinia enterocolitica* strains

Strains	strain ID	Genotype	Reference
S.Tm ^{WT}	SB300	S. Tm strain S1344	(Hoiseh and Stocker 1981)
S.Tm ^{Avir}	M557	$\Delta invG$; <i>sseD::aphT</i>	(Hapfelmeier <i>et al.</i> 2004)
S.Tm ^{SPI-1}	SB161	$\Delta invG$	(Kaniga <i>et al.</i> 1994)
S.Tm ^{SPI-2}	M556	<i>sseD::aphT</i>	(Hapfelmeier <i>et al.</i> 2004)
MBE1	MBE1	<i>narZ::cat</i>	This study
MBE2	MBE2	<i>narG::cat</i>	This study
MBE3	MBE3	<i>napA::aphT</i>	This study
MBE4	MBE4	<i>narZ::cat</i> (P22-phage lysate of MBE1 on SB300)	This study
MBE5	MBE5	$\Delta narZ$	This study

Material and Methods

Strains	strain ID	Genotype	Reference
MBE6	MBE6	$\Delta narZ$; $narG::cat$	This study
<i>S.Tm</i> ^{Ni.}	MBE7	$\Delta narZ$; $narG::cat$; $napA::aphT$	This study
<i>S.Tm</i> ^{Ni. + Te.}	MBE8	$\Delta narZ$; $narG::cat$; $napA::aphT$; $ttrS::tet$	This study
MBE9	MBE9	$entA::cat$	This study
<i>S.Tm</i> ^{EntA}	MBE10	$entA::cat$ (P22-phage lysate of MBE9 on SB300)	This study
MBE11	MBE11	$eutC::aphT$	This study
<i>S.Tm</i> ^{EA}	MBE12	$eutC::aphT$ (P22-phage lysate of MBE11 on SB300)	This study
<i>E.coli</i> DH5 α			Invitrogen
HB 1852S WA-CS			(Stojiljkovic <i>et al.</i> 1999)
WA-TS		$ybtA::aphT$	(Pelludat 1999)
<i>Clostridium difficile</i>	DH196		(Studer <i>et al.</i> 2016)
<i>Citrobacter rodentium</i>	DBS100		(Schauer and Falkow 1993, Schauer <i>et al.</i> 1995)
<i>Helicobacter typhlonius</i>	CCUG48335T		(Brasseit <i>et al.</i> 2016)

2.1.2 Plasmids

Table 4: Plasmids used for λ red and Flp recombination

Plasmid	Function	Genotype	Reference
pKD3	Harbors a chloramphenicol resistance gene (<i>cat</i>)	<i>cat</i> with FRT sites, Amp ^R	(Datsenko and Wanner 2000)
pKD4	Harbors a kanamycin resistance gene (<i>aphT</i>)	<i>aphT</i> with FRT sites, Amp ^R	(Datsenko and Wanner 2000)
pKD46	Harbors 2,154 nt (31088–33241) of phage λ , enzymes for recombination	<i>araC</i> , ParaB γ , β and <i>exo</i> , <i>repA101</i> ^{ts} , Amp ^R	(Datsenko and Wanner 2000)
pCP20	Harbors FLP-recombinase	<i>FLP</i> ⁺ , λ <i>ci857</i> ⁺ , λ <i>p_R</i> , Rep ^{ts} , Amp ^R , Cm ^R	(Cherepanov and Wackernagel 1995)

Material and Methods

Table 5: Plasmids harboring 16S rRNA full length gene sequences

Plasmid	Backbone	Taxonomy and strain ID	Digest*	Reference
pM1411	pSB-Bluescript	<i>Clostridium</i> spp. ASF356	<i>NotI</i>	(Brugiroux <i>et al.</i> 2016)
pM1412	pSB-Bluescript	<i>Lactobacillus intestinalis</i> ASF360	<i>NotI</i>	(Brugiroux <i>et al.</i> 2016)
pM1413	pSB-Bluescript	<i>Lactobacillus murinus</i> ASF361	<i>NotI</i>	(Brugiroux <i>et al.</i> 2016)
pM1414	pSB-Bluescript	<i>Mucispirillum schaedleri</i> ASF457	<i>NotI</i>	(Brugiroux <i>et al.</i> 2016)
pM1417	pSB-Bluescript	<i>Parabacteroides goldsteinii</i> ASF519	<i>NotI</i>	(Brugiroux <i>et al.</i> 2016)
pM1452	pCR2.1-topo	<i>Bifidobacterium longum</i> subsp. <i>animalis</i> YL2	<i>HindIII</i>	(Brugiroux <i>et al.</i> 2016)
pM1456	pCR2.1-topo	<i>Flavonifractor plautii</i> YL31	<i>HindIII</i>	(Brugiroux <i>et al.</i> 2016)
pM1457	pCR2.1-topo	<i>Clostridium clostridioforme</i> YL32	<i>HindIII</i>	(Brugiroux <i>et al.</i> 2016)
pM1459	pCR2.1-topo	<i>Akkermansia muciniphila</i> YL44	<i>HindIII</i>	(Brugiroux <i>et al.</i> 2016)
pM1460	pCR2.1-topo	' <i>Turicimonas caecimuris</i> ' YL45	<i>NcoI</i>	(Brugiroux <i>et al.</i> 2016)
pSAB3	pJET1.2	' <i>Muribaculum intestinale</i> ' YL27	<i>NotI</i>	(Brugiroux <i>et al.</i> 2016)
pSAB4	pJET1.2	<i>Blautia coccooides</i> YL58	<i>HindIII</i>	(Brugiroux <i>et al.</i> 2016)
pSAB6	pJET1.2	<i>Clostridium innocuum</i> I46	<i>NotI</i>	(Brugiroux <i>et al.</i> 2016)
pSAB7	pJET1.2	' <i>Bacteroides caecimuris</i> ' I48	<i>HindIII</i>	(Brugiroux <i>et al.</i> 2016)
pSAB8	pJET1.2	<i>Lactobacillus reuteri</i> I49	<i>HindIII</i>	(Brugiroux <i>et al.</i> 2016)
pSAB9	pJET1.2	<i>Enterococcus faecalis</i> KB1	<i>NotI</i>	(Brugiroux <i>et al.</i> 2016)
pSAB10	pJET1.2	<i>Clostridium</i> spp. ASF502/SB2	<i>NotI</i>	(Brugiroux <i>et al.</i> 2016)
pSAB12	pJET1.2	' <i>Acutalibacter muris</i> ' KB18	<i>HindIII</i>	(Brugiroux <i>et al.</i> 2016)
pSAB13	pJET1.2	<i>Pseudoflavonifractor</i> spp. ASF500	<i>NotI</i>	(Brugiroux <i>et al.</i> 2016)
pMB1	pJET1.2	<i>Salmonella</i> Typhimurium	<i>HindIII</i>	This study
pMB2	pJET1.2	<i>Citrobacter rodentium</i> DBS100	<i>NotI</i>	This study
pMB4	pJET1.2	<i>Helicobacter typhlonius</i> CCUG48335T	<i>NotI</i>	This study
pMB5	pJET1.2	<i>Clostridium difficile</i> DH196	<i>NotI</i>	This study
pMB6	pJET1.2	<i>Clostridium scindens</i> ATCC35704	<i>NotI</i>	This study

*The indicated restriction enzymes were used to linearize vectors that contain strain-specific 16S rRNA gene sequences.

Material and Methods

2.2 Buffers, media and Oligonucleotides

2.2.1 Buffers and media

Buffers and media were made up in desalted water (dH₂O), autoclaved at 121°C and 1 bar for 20 min -if not indicated differently- and prepared according to the following recipes:

Table 6: Luria-Bertani (LB) medium

Components	Per liter medium
NaCl	5 g
Yeast extract	5 g
Tryptone	10 g

All components were dissolved in dH₂O.

Table 7: LB agar

Components	Per liter medium
NaCl	5 g
Yeast extract	5 g
Tryptone	10 g
Agar	15 g

All components were dissolved in dH₂O.

Table 8: LB 0.3 M NaCl

Components	Per liter medium
NaCl	17.53 g
Yeast extract	5 g
Tryptone	10 g

All components were dissolved in dH₂O.

Table 9: Peptone-glycerol broth

Components	Per liter broth
Peptone	20 g
Glycerol	50 ml

All components were dissolved in dH₂O.

Material and Methods

Table 10: M9 medium

Components	Final concentration
$\text{Na}_2\text{HPO}_4 \cdot 2\text{H}_2\text{O}$	40 mM
KH_2PO_4	20 mM
NaCl	9 mM
NH_4Cl	2 g/l
D-glucose	2 g/l
MgSO_4	1 mM
CaCl_2	100 μM
Thiamine	10 mg/ml
Histidine	500 mg/l
Optional NaNO_3	20 mM

All components were dissolved in dH_2O .

Table 11: Mucin broth

Components	Per liter medium
Type II porcine mucin	2.5 g
Morpholino propanesulfonic acid (MOPS)	9.25 g
Sodium	
MgSO_4	0.265 g
Optional: NaNO_3 or $\text{Na}_2\text{O}_6\text{S}_4 \cdot 2\text{H}_2\text{O}$	40 mM
Trace elements (1,000x)	1 ml
Trace elements	Final concentration
$\text{CaCl}_2 \cdot 2\text{H}_2\text{O}$	0.3 mM
$\text{ZnSO}_4 \cdot 7\text{H}_2\text{O}$	0.1 mM
$\text{FeSO}_4 \cdot 7\text{H}_2\text{O}$	0.045 mM
Na_2SeO_3	0.2 mM
$\text{Na}_2\text{MoO}_4 \cdot 2\text{H}_2\text{O}$	0.2 mM
$\text{MnSO}_4 \cdot \text{H}_2\text{O}$	2 mM
$\text{CuSO}_4 \cdot 5\text{H}_2\text{O}$	0.1 mM
$\text{CoCl}_2 \cdot 6\text{H}_2\text{O}$	3 mM
$\text{NiSO}_4 \cdot 6\text{H}_2\text{O}$	0.1 mM

All components were dissolved in dH_2O . The 1,000x trace element stock was autoclaved separately.

Material and Methods

Table 12: *Akkermansia* medium (AAM) without mucin

Components	Per liter medium
Brain Heart Infusion	18.5 g
Trypticase soy broth	15 g
Yeast extract	5 g
K ₂ HPO ₄	2.5 g
Hemin	1 mg
Glucose	0.5 g
Autoclave and add the following components under sterile conditions:	
Na ₂ CO ₃ (5% stock solution) [‡]	0.4 g
Cysteine hydrochloride [#]	0.5 g
Menadione [#]	0.5 g
Complement inactivated FCS [#]	3 %

All components but hemin, that was resuspended in ethanol p.a. and supplemented with NaOH until dissolved and menadione, which was resuspended in ethanol p.a. were dissolved in dH₂O. [‡] Autoclaved. [#] Sterile filtered.

The following Tables 13 - 17 list ingredients needed for the preparation of Chromazurol S (CAS) agar:

Table 13: CAS stock solution A

Components	Per 60ml
Chromazurol S	60.5 mg
1 mM FeCl ₃ · 6H ₂ O dissolved in 10 mM HCl	10 ml

Chromazurol S was dissolved in 50 ml of dH₂O and subsequently 10 ml of FeCl₃ solution were added.

Table 14: CAS stock solution B

Component	Per 40 ml
Hexadecyltrimethylammonium bromide (HDTMA)	72.9 mg

HDTMA was dissolved in 40 ml of dH₂O and subsequently solution A was added under constant stirring. Solution B was finally autoclaved.

Table 15: 10x LB medium

Components	Per 200 ml
Tryptone	20 g
Yeast extract	10 g
NaCl	10 g

Components were dissolved in 200 ml of dH₂O and autoclaved.

Material and Methods

Table 16: 10x MM9

Components	Per 200 ml
KH ₂ PO ₄	0.6 g
NH ₄ Cl	2 g

Components were dissolved in 200 ml of dH₂O.

Table 17: PIPES agar

Components	Per 850 ml
dH ₂ O	500 ml
10x MM9	100 ml
Agar	15 g
1,4-Piperazinediethanesulfonic acid (PIPES)	31.1 g

PIPES was added under constant stirring, the pH was adjusted to 6.8 using NaOH pellets and dH₂O was added ad 850 ml. The solution was subsequently autoclaved and allowed to cool down to 50°C. The following already sterile watery solutions were then added: 30 ml of 10x LB (autoclaved), 10 ml of 20% glucose (sterile filtered), 2 ml of 1 M MgSO₄ (sterile filtered), 2 ml of 1 M Na₂SO₄ (autoclaved), 1 ml of 0.1 M CaCl₂ and 100 ml of CAS stock solution A + B. The CAS agar was finally poured in petri dishes.

Table 18: 10x phosphate Buffered Saline (PBS)

Components	Per liter buffer
NaCl	80 g
KCl	2 g
Na ₂ HPO ₄ unhydrated	6.1 g
KH ₂ PO ₄	2.4 g

All components were dissolved in dH₂O.

Table 19: TE Buffer

Components	Final concentration
Tris	10 mM
EDTA	1 mM

All components were dissolved in ddH₂O (Ampuwa). pH was adjusted to 8.0 with HCl.

Material and Methods

Table 20: 4% Paraformaldehyde (PFA)

Components	Per liter buffer
ddH ₂ O	300 ml
PFA	40 g
1 M NaOH	100 µl
10x PBS in ddH ₂ O, pH 7.4	100 ml

Components were heated up to 60 °C and stirred vigorously until PFA is dissolved. DdH₂O (Ampuwa) was filled up to 1 l and pH was adjusted. Buffer was sterile filtered and stored at -20 °C.

Table 21: TFB1 buffer

Components	Volume
Potassium acetate	0.29 g
MnCl ₂ · 4H ₂ O	2 g
1 M RbCl	10 ml
1 M CaCl ₂	1 ml
Glycerol 87%	17.2 ml
ddH ₂ O (Ampuwa)	Ad 100 ml

pH was adjusted to 7.0 and filter sterilized.

Table 22: TFB2 buffer

Components	Volume
1 M NaMOPS pH 7.0	1 ml
1 M RbCl	1 ml
1 M CaCl ₂	7.5 ml
Glycerol 87%	17.5 ml
ddH ₂ O (Ampuwa)	Ad 100 ml

pH was adjusted to 7.0 and filter sterilized.

Table 23: 50x TAE buffer

Components	Per 5 l buffer
Tris	1,210 g
Glacial acetic acid	285.5 ml
0.5 M EDTA pH 8.0	500 ml
dH ₂ O	ad 5 l

Material and Methods

Table 24: 10x loading dye

Components	Final concentration
Sucrose	40%
Bromphenol blue	0.25%
Xylene Cyanol	0.25%

Table 25: SOC medium

Components	Per 250 ml medium
Tryptone	5 g
Yeast extract	1.25 g
NaCl	0.125 g
250 mM KCl	2.5 ml
Ad 250 ml with ddH ₂ O (Ampuwa), adjust pH to 7.0 with 5 M NaOH and autoclave.	
1 M glucose (sterile filtered)	5 ml

Table 26: 20% glycerol-palladium solution

Components	Per 50 ml solution
100% glycerol	10 ml
Palladium crystals	Tip of spatula
ddH ₂ O	40 ml

After autoclaving, the warm solution (60°C) was imported in the anaerobic tent.

Table 27: Lysis buffer for DNA extraction (Stool kit, Qiagen)

Components	Final concentration
Tris	20 mM
EDTA	2 mM
Triton X 100	1%
Adjust pH to 8.0 with HCl, autoclave and add:	
Lysozyme	20 mg/ml

Components were dissolved in ddH₂O (Ampuwa)

Material and Methods

Table 28: Extraction buffer for DNA extraction (Turnbaugh/Ubeda)

Components	Final concentration
Tris	200 mM
NaCl	200 mM
EDTA	20 mM

Components were dissolved in ddH₂O (Ampuwa). pH was adjusted to 8.0 using HCl and the solution was finally autoclaved.

Table 29: PBT

Components	Per 200 ml
BSA fraction V	200 mg
TM 10 tergitol	200 µl
1x PBS	ad 200 ml

Solution was sterile filtered.

Material and Methods

2.2.2 Oligonucleotides

Table 30: Oligonucleotides and hydrolysis probes for qPCR

Primers and corresponding probe (targeted strain)	Sequence 5' - 3'	Tm°C	GC%	Length (bp)	Ampl. (bp)
Isol46_Exonucl.2_fwd	CGGATCGTAAAGCTCTGTTGTAAG	58	45.8	24	
Isol46_Exonucl.3_rev	GCTACCGTCACTCCCATAGCA	59	57.1	21	
Probe3_Isol46 (<i>Clostridium innocuum</i> I46)	FAM-AAGAACGGCTCATAGAGG-BHQ1	70	50.0	18	68
Isol49_Exonucl._fwd	GCACTGGCTCAACTGATTGATG	59.0	50.0	22	
Isol49_Exonucl._rev	CCGCCACTCACTGGTGATC	59.0	63.2	19	
Probe_Isol49 (<i>Lactobacillus reuteri</i> I49)	HEX-CTTGACCTGATTGACGA-BHQ1	69.0	50.0	18	64
YL58_Exonucl._fwd	GAAGAGCAAGTCTGATGTGAAAGG	58.0	45.8	24	
YL58_Exonucl._rev	CGGCACTCTAGAAAAACAGTTTCC	59.0	45.8	24	
Probe_YL58 (<i>Blautia coccooides</i> YL58)	FAM-TAACCCAGGACTGCAT-BHQ1	69.0	52.9	17	74
YL27_Exonucl.2_fwd	TCAAGTCAGCGGTAAAAATTCG	58.0	40.9	22	
YL27_Exonucl.2_rev	CCCACTCAAGAACATCAGTTTCAA	59.0	41.7	24	
Probe2_YL27 (<i>Muribaculum intestinale</i> YL27)	HEX-CAACCCCGTCGTGCC-BHQ1	70.0	73.3	15	67
YL31_Exonucl.2_fwd	AGGCGGGATTGCAAGTCA	59.0	55.6	18	
YL31_Exonucl.3_rev	CCAGCACTCAAGAACTACAGTTTCA	59.0	44.0	25	
Probe2_YL31 (<i>Flavonifractor plautii</i> YL31)	FAM-CAACCTCCAGCCTGC-BHQ1	70.0	66.7	15	80
YL32_Exonucl.2_fwd	AATACCGCATAAGCGCACAGT	58.0	47.6	21	
YL32_Exonucl.2_rev	CCATCTCACACCACAAAGTTTT	59.0	43.5	23	
Probe2_YL32 (<i>Clostridium clostridioforme</i> YL32)	HEX-CGCATGGCAGTGTGT-BHQ1	69.0	60.0	15	63
KB1_Exonucl._fwd	CTTCTTCTCCCGAGTGCTT	59.0	52.4	21	
KB1_Exonucl._rev	CCCCTCTGATGGGTAGGTTACC	60.0	59.1	22	
Probe_KB1 (<i>Enterococcus faecalis</i> KB1)	FAM-CACTCAATTGGAAAGAGGAG-BHQ1	70.0	45.0	20	88
YL2_Exonucl._fwd	GGGTGAGTAATGCGTGACCAA	59.0	52.4	21	
YL2_Exonucl._rev	CGGAGCATCCGGTATTACCA	59.0	55.0	20	
Probe_YL2 (<i>Bifidobacterium longum</i> subsp. <i>animalis</i> YL2)	HEX-CGGAATAGCTCCTGGAAA-BHQ1	69.0	50.0	18	77
KB18_Exonucl.2_fwd	TGGCAAGTCAGTAGTGAAATCCA	58.0	43.5	23	
KB18_Exonucl.2_rev	TCACTCAAGCTCGACAGTTTCAA	59.0	43.5	23	

Material and Methods

Primers and corresponding probe (targeted strain)	Sequence 5' - 3'	Tm°C	GC%	Length (bp)	Ampl. (bp)
Probe2_KB18 (<i>'Acutalibacter muris'</i> KB18)	FAM-CTTAACCCATGAACTGC-BHQ1	69.0	47.1	17	69
YL44_Exonucl._fwd	CGGGATAGCCCTGGGAAA	59.0	61.1	18	
YL44_Exonucl._rev	GCGCATTGCTGCTTTAATCTTT	60.0	40.9	22	
Probe_YL44 (<i>Akkermansia muciniphila</i> YL44)	HEX-TGGGATTAATACCGCATAGTA-BHQ1	69.0	38.1	21	65
YL45_Exonucl._fwd	AGACGGCCTTCGGGTTGTA	59.0	57.9	19	
YL45_Exonucl._rev	CGTCATCGTCTATCGGTATTATCAA	58.0	40.0	25	
Probe_YL45 (<i>'Turicimonas caecimuris'</i> YL45)	FAM-ACCACTTTTGTAGAGAACGA-BHQ1	69.0	40.0	20	73
Isol48_Exonucl._fwd	GGCAGCATGGGAGTTTGCT	60.0	57.9	19	
Isol48_Exonucl._rev	TTATCGGCAGGTTGGATACGT	58.0	47.6	21	
Probe_Isol48 (<i>'Bacteroides caecimuris'</i> I48)	HEX-CAAACCTCCGATGGCGAC-BHQ1	69.0	55.6	18	79
ASF356_Exonucl.2_fwd	CGGCAAGGTAAGCGATATGTG	59.0	52.4	21	
ASF356_Exonucl.2_rev	CGCTTCTCTCTCTGTACTCTAGCT	60.0	52.0	25	
Probe2_ASF356 (<i>Clostridium</i> spp. ASF356)	FAM-TAACTTAAGGATAGCATAACGAACT-BHQ1	69.0	32.0	25	88
ASF360_Exonucl.4_fwd	TGAGTGCTAAGTGTTGGGAGGTT	59.0	47.8	23	
ASF360_Exonucl.4_rev	CGGAGTGCTTAATGCGTTAGCT	60.0	50.0	22	
Probe4_ASF360 (<i>Lactobacillus intestinalis</i> ASF360)	FAM-CCGCCTCTCAGTGCT-BHQ1	70.0	66.7	15	63
ASF361_Exonucl._fwd	TCGGATCGTAAAACCTGTTG	59.0	47.6	21	
ASF361_Exonucl._rev	ACCGTCGAAACGTGAACAGTT	58.0	47.6	21	
Probe_ASF361 (<i>Lactobacillus murinus</i> ASF361)	HEX-TAGAGAAGAAAGTGCCTGAGAG-BHQ1	70.0	45.5	22	66
ASF457_Exonucl._fwd	GACTGGAACAACCTACCGAAAGGT	59.0	45.8	24	
ASF457_Exonucl._rev	CAGGTCTCCCAACTTTTCCT	58.0	52.4	21	
Probe_ASF457 (<i>Mucispirillum schaedleri</i> ASF457)	FAM-TAATGCCGGATGAGTTATA-BHQ1	69.0	36.8	19	85
ASF500_Exonucl._fwd	AGGCGGGACTGCAAGTCA	59.0	61.1	18	
ASF500_Exonucl._rev	CAAATGCAGGCCACAGGTT	58.0	52.6	19	
Probe_ASF500 (<i>Pseudoflavonifactor</i> spp. ASF500)	HEX-ATGTGAAAACCGGGC-BHQ1	68.0	52.9	17	57
ASF502_Exonucl.3_fwd	GACCCAGTACCGCATGGTA	59.0	60.0	20	
ASF502_Exonucl.3_rev	TCAGACGCGGGCCTATCTTA	59.0	55.0	20	
Probe3_ASF502(SB2) (<i>Clostridium</i> spp. ASF502/SB2)	HEX-AGAGGTAAAACTGAGGTGGT-BHQ1	69.0	42.9	21	63
ASF519_Exonucl._fwd	TGTGGCTCAACCATAAAATTGC	59.0	40.9	22	

Material and Methods

Primers and corresponding probe (targeted strain)	Sequence 5' - 3'	Tm°C	GC%	Length (bp)	Ampl. (bp)
ASF519_Exonucl._rev	GCATTCCGCCTACCTCAAATAT	58.0	45.5	22	
Probe_ASF519 (<i>Parabacteroides goldsteinii</i> ASF519)	HEX-TTGAAACTGGTTGACTTGAG-BHQ1	69.0	40.0	20	67
Salmo_Exonucl._fwd	TGGGAAACTGCCTGATGGA	59.0	52.6	19	
Salmo_Exonucl._rev	CTTGCGACGTTATGCGGTATT	59.0	47.6	21	
Probe_Salmo (<i>Salmonella</i> SL1344)	FAM-ATAACTACTGGAAACGGTGGC-BHQ1	70.0	47.6	21	67
C.rod_Exonucl._fwd	GGGACCTTCGGGCCTCTT	60.0	66.7	18	
C.rod_Exonucl._rev	TCACCAACAAGCTAATCCCATCT	59.0	43.5	23	
Probe_C.rod (<i>Citrobacter rodentium</i> DBS100)	HEX-CCACCGGATGTGCC-BHQ1	70.0	71.4	14	57
H.typh_Exonucl.2_fwd	CAGCTCGGCTGAGCACTCTA	58.0	60.0	20	
H.typh_Exonucl.2_rev	GACTTGACGTCGTCCTCACCTT	59.0	54.5	22	
Probe2_H.typhlonius (<i>Helicobacter typhlonius</i> CCUG48335T)	HEX-AGACTGCCTTCGTAAGG-BHQ1	68.0	52.9	17	68
C.diff_Exonucl._fwd	TCGGTGCCGCAGCTAAC	58.0	64.7	17	
C.diff_Exonucl._rev	AGTTTCACTCTTGCGAGCGTACT	58.0	47.8	23	
Probe_C.difficile (<i>Clostridium difficile</i> DH196)	HEX-CATTAAGTACTCCGCCTGGG-BHQ1	70.0	55.0	20	62
C.scin_Exonucl._fwd	TGCAAGCCAGATGTGAAAGC	59.0	50.0	20	
C.scin_Exonucl._rev	AGCCACGCAGTTCCAAATG	58.0	52.6	19	
Probe_C.scindens (<i>Clostridium scindens</i> ATCC35704)	HEX-CTCAACCCCGGGACT-BHQ1	69.0	66.7	15	61
E.coli_Exonucl._fwd	GGACCTTCGGGCCTCTTG	59	66.7	18	
E.coli_Exonucl._rev	CCTTTACCCACCTACTAGCTAATCC	60	50.0	26	
Probe_E.coli(Mt1B1) (<i>Escherichia coli</i> Mt1B1)	FAM-ATCGGATGTGCCAGAT-BHQ1	69	52.9	17	64
Strep._Exonucl._fwd	CAACTGCATCACTACCAGATGGA	59	47.8	23	
Strep._Exonucl._rev	CGCCTAGGTGAGCCTTTACCT	59	57.1	21	
Probe_Strep.daniel. (<i>Streptococcus danieliae</i> ERD01G)	HEX-CTGCGTTGTATTAGCTAGTAG-BHQ1	69	42.9	21	69
Staph._Exonucl._fwd	GGAGCTAATACCGGATAACATTTAGAA	58	37.0	27	
Staph._Exonucl._rev	CCATCTATAAGTGATAGCAAAACCATCT	58	35.7	28	
Probe_Staph.xylosus (<i>Staphylococcus xylosus</i> 33R13C)	HEX-CGCATGGTTCTAAAGTG-BHQ1	69	47.1	17	75
Univ_Exonucl.3_fwd	TGCAYGGYYGTCGTCAGC	59.0	63.9	18	
Univ_Exonucl.3_rev	CRTCRTCCYCRCTTCCTC	59.0	63.2	19	

Material and Methods

Primers and corresponding probe (targeted strain)	Sequence 5' - 3'	Tm°C	GC%	Length (bp)	Ampl. (bp)
Probe2_Univ (All bacteria but <i>C. difficile</i>)	HEX-AACGAGCGCAACCC-BHQ1	70.0	64.3	14	143
Probe3_Univ* (All bacteria listed)	HEX-ARCGAGCGYAACCC-BHQ1	70.0	64.3	14	143

*For samples including template DNA of *C. difficile*, the combination of Univ_Exonucl.3_fwd/rev3 + Probe3_Univ was used, since Probe2_Univ cannot detect *C. difficile*; Tm°C: melting temperature in °C, determined using Primer Express 3 (MGB protocol, Applied Biosystems, Life Technologies, USA), note: minor groove binder (MGB) protocol was chosen; GC%: guanine and cytosine content as percentage of all nucleotides constituting the oligo-nucleotide; length: length of the oligo-nucleotide in base pairs; ampl.: amplicon size that is amplified by the given primer pair, indicated in base pairs; FAM (6-carboxyfluoresceine); HEX (6-carboxyhexafluoresceine); BHQ1 (black hole quencher 1).

Table 31: Primers used for construction of *Salmonella* mutants

Designation	Sequence 5' - 3'	Construction of	Amplicon size (bp)
narZ-fwd-ko	AATGGTTTAACGCCAAATCGACAGGATGGCGGAAA ATTTATCGAAGCAGGAGAAATGTCatataaatatcctcc ttagtt	MBE1 (<i>narZ::cat</i>)	3948
narZ-rev-ko	GGTGTGACAGCCAATACATTTATCGAGATTAGTAC CATCCCAACCTGTGAGCGTATTTgtgttaggctggagctg cttc		
narZ fwd-check up	GCGTCGTAAGCCTAAACA		
narZ rev-check up	CCGGTCCAGACGTTTTTA		
narG-fwd-ko	CTTAGTTAAGCAATGTCGATTTATCAGAGAGCCGTA AGGTTCCACACAGGAGAAACCCGatatgaatatcctcctt agtt	MBE2 (<i>narG::cat</i>)	3921
narG-rev-ko	GGTATGACAGCCGATGCACTTATCGAGATTAGCA CCATGCCGACTTGTGAACGAATTTgtgttaggctggagct gcttc		
narG fwd-check up	TTCTCACGCCCATTCAGC		
narG rev-check up	CCAGACGTTTTTACAGGT		
napA-fwd-ko	GGCGTACTGGCGGTGTCGCTGTTTATCACCAGCA GGATGAGCAAGGTGAGGAAACACCatataaatatcctc cttagtt	MBE3 (<i>napA::aphT</i>)	2756
napA-rev-ko	ACATCACGCAGGAAGCGGCGGCGGCCATTTGGG GTTTCGCTGTACGGGACATAACGCGTgtgttaggctgga gctgcttc		
napA fwd-check up	ACAATTGAGTCAGTACGC		
napA rev-check up	GCTGGCGAAGACATTTTC		
ttrS fwd-check up	CGGCTTGTTGTTGATCTAA		
ttrS rev-check up	CCCAGACTTTCCAGTAAAA		
entA-fwd-ko	CTGGCGAAAAACCCGACCATTGACGCCTGGTGGGC GCTGCTTTCTCGCGGGGTAGAGTAatataaatatcctc tagtt		

Material and Methods

Designation	Sequence 5' - 3'	Construction of	Amplicon size (bp)
entA-rev-ko	AGTGTCTGACTGGTAGCGTTCAATTCATCCAGCGT TAAATGCCGTTTCCAGATCATCGtgtaggctggagctg cttc	MBE9 (<i>entA::cat</i>)	
entA fwd-check up	GTAAAGTACACGGCGATAT		
entA rev-check up	TAAACAATGCCCAGATGCG		932
eutC-fwd-ko	GTCTGACCAAACGGGCGGGCGATCCGTCCTGTTT TTCTGATGACGCGGGGATAACACCatatgaatctctcc ttagtt		
eutC-rev-ko	ATCACGCGCATGGCAGTCACTGAAGGTCGAATTAA ATCTAATGCAGGCATGATGTCTCctgttaggctggagct gcttc	MBE11 (<i>eutC::aphT</i>)	
eutC fwd-check up	CTGGAAACGATGGGCATTAT		
eutC rev-check up	TAATTTAAGTTCCGCGCAA		1086

Genes of interest were replaced by either chloramphenicol (*cat*) or kanamycin (*aphT*) resistance genes using the λ red recombination system (Datsenko and Wanner 2000). PCR products were generated with primers harboring a homology region adjacent to the gene of interest (capital letters) and a sequence targeting the plasmids pKD3 (*cat*) and pKD4 (*aphT*, small letters) (Table 4). Check-up primers were used to verify correct insertion of the antibiotic cassette.

Table 32: Further oligonucleotides used in this study

Designation	Sequence 5' - 3'	Purpose	Reference
fd1	CGATATCTCTAGAAGAGTTTGATCCTGGCTCAG	Amplification of bacterial 16S rRNA genes	(Weisburg <i>et al.</i> 1991)
fd2	CGATATCTCTAGAAGAGTTTGATCATGGCTCAG	Amplification of bacterial 16S rRNA genes	(Weisburg <i>et al.</i> 1991)
rP1	GATATCGGATCCACGGTTACCTTGTTACGACTT	Amplification of bacterial 16S rRNA genes	(Weisburg <i>et al.</i> 1991)
pJet1-FP	ACTACTCGATGAGTTTTTCGG	Amplification of insert in pJET1.2 vector	Fermentas
pJet1-RP	TGAGGTGGTTAGCATAGTTC	Amplification of insert in pJET1.2 vector	Fermentas

2.3 Chemicals, antibodies and devices

2.3.1 Chemicals

Table 33: Chemicals used in this study

Compound	Supplier
ABTS substrate	Merck (Darmstadt)
Acetic acid	Roth (Karlsruhe)
Agar	BD (Heidelberg)
Agarose	Bio&Sell (Feucht)

Material and Methods

Compound	Supplier
L-(+)-arabinose	Sigma-Aldrich (Munich)
BD™ CompBeads	BD (Franklin Lakes, USA)
BD FACS™ Lysing Solution	BD (Franklin Lakes, USA)
Brain Heart Infusion	Oxoid, Thermo Fisher Scientific biosciences (St. Leon-Rot)
Bromphenol blue	Sigma-Aldrich (Munich)
Bovine serum albumin (BSA)	PAA Laboratories GmbH (Austria)
BSA fraction V	Roth (Karlsruhe)
CaCl ₂	Roth (Karlsruhe)
CaCl ₂ · 2H ₂ O	Merck (Darmstadt)
Chloroform	Roth (Karlsruhe)
Chromazurol S	Roth (Karlsruhe)
CloneJET™ PCR Cloning kit	Fermentas, Thermo Scientific (USA)
CoCl ₂ · 6H ₂ O	Merck (Darmstadt)
Columbia agar with sheep blood plus	Oxoid, Thermo Fisher Scientific Biosciences (St. Leon-Rot)
CuSO ₄ · 5H ₂ O	Merck (Darmstadt)
Cysteine (-L) Hydrochloride Monohydrate	Sigma-Aldrich (Munich)
ddH ₂ O (Ampuwa)	Fresenius Kabi (Bad Homburg)
ddH ₂ O used for qPCR reactions	Gibco, Life Technologies (UK)
dNTPs	Fermentas, Thermo Scientific (USA)
DAPI	Roth (Karlsruhe)
Dipyridyl	Sigma-Aldrich (Munich)
DreamTaq PCR Master Mix (2x)	Fermentas, Thermo Scientific (USA)
DTPA	Sigma-Aldrich (Munich)
EDTA	Biomol (Hamburg)
EGTA	Sigma-Aldrich (Munich)
Eosin Y solution	Sigma-Aldrich (Munich)
Ethanol p.a.	Roth (Karlsruhe)
Ethidium bromide	Sigma-Aldrich (Munich)
FastStart Essential DNA Probes Master	Roche (Mannheim)
FastStart Taq polymerase	Roche (Mannheim)
FCS	Biochrom AG (Berlin)
FeCl ₃ · 6H ₂ O	Merck (Darmstadt)
FeSO ₄ · 7H ₂ O	Roth (Karlsruhe)
GeneRuler 1kb DNA Ladder	Thermo Fisher Scientific biosciences (St. Leon-Rot)
GeneRuler DNA ladder mix (100bp)	Thermo Fisher Scientific biosciences (St. Leon-Rot)
D-glucose	Roth (Karlsruhe)
Glycerol	Roth (Karlsruhe)
HCl	Roth (Karlsruhe)
Hemin	Sigma-Aldrich (Munich)
Hexadecyltrimethylammonium bromide (HDTMA)	Sigma-Aldrich (Munich)

Material and Methods

Compound	Supplier
Histidine	Sigma-Aldrich (Munich)
H ₂ O ₂	Merck (Darmstadt)
HRP-streptavidin	IBA (Göttingen)
K ₂ HPO ₄	Roth (Karlsruhe)
KCl	Fluka, Sigma-Aldrich (Munich)
KH ₂ PO ₄	Roth (Karlsruhe)
Lipocalin-2 standard	R&D Systems (Wiesbaden-Nordenstadt)
Lysozyme from hen egg	Sigma-Aldrich (Munich)
MacConkey agar	Oxoid, Thermo Fisher Scientific Biosciences (St. Leon-Rot)
Menadione	Sigma-Aldrich (Munich)
MgSO ₄	Roth (Karlsruhe)
MnSO ₄ · H ₂ O	Roth (Karlsruhe)
MnCl ₂ · 4H ₂ O	Merck (Darmstadt)
Morpholino propanesulfonic acid (MOPS) Sodium	Sigma-Aldrich (Munich)
Type II porcine mucin	Sigma-Aldrich (Munich)
NaCl	Roth (Karlsruhe)
Na ₂ CO ₃	Merck (Darmstadt)
Na ₂ HPO ₄ unhydrated	Roth (Karlsruhe)
Na ₂ HPO ₄ · 2H ₂ O	Roth (Karlsruhe)
Na ₂ MoO ₄ · 2H ₂ O	Merck (Darmstadt)
NaNO ₂	Sigma-Aldrich (Munich)
NaNO ₃	Roth (Karlsruhe)
NaOH	Roth (Karlsruhe)
NaOH pellets	Merck (Darmstadt)
Na ₂ O ₆ S ₄ · 2H ₂ O	Sigma-Aldrich (Munich)
Na ₂ SeO ₃	Sigma-Aldrich (Munich)
Na ₂ SO ₄	Merck (Darmstadt)
NH ₄ Cl	Merck (Darmstadt)
NiSO ₄ · 6H ₂ O	Merck (Darmstadt)
N-naphThylethylenediamine dihydrochloride monomethanolate (NEDD)	Sigma-Aldrich (Munich)
Normal goat serum	Biozol (Eching)
O.C.T.	Sakura Finetek (Torrance)
Palladium chloride	Sigma-Aldrich (Munich)
Paraformaldehyde (PFA)	Roth (Karlsruhe)
Phalloidin	Interchim (Mannheim)
Phenol:chloroform:isoamylalcohol (25:24:1)	Roth (Karlsruhe)
Piperazin Ethansulfonsäure (PIPES)	Roth (Karlsruhe)
Potassium acetate	Roth (Karlsruhe)
Oligonucleotides	Metabion (Martinsried)

Material and Methods

Compound	Supplier
Peptone	Oxoid, Thermo Fisher Scientific Biosciences (St. Leon-Rot)
Q5 [™] Hot Start High-Fidelity polymerase	New England BioLabs (Frankfurt am Main)
RbCl	Roth (Karlsruhe)
Restriction enzymes + buffers	Fermentas, Thermo Scientific (USA)
Rotimount	Roth (Karlsruhe)
Sabouraud dextrose agar	Oxoid, Thermo Fisher Scientific Biosciences (St. Leon-Rot)
Sodium acetate	Roth (Karlsruhe)
Sodium dodecyl sulfate (SDS)	Serva (Heidelberg)
Sucrose	Sigma-Aldrich (Munich)
Sulfanilamide	Merck (Darmstadt)
SYTOX green	Invitrogen, Thermo Fisher Scientific Biosciences (St. Leon-Rot)
SYTOX red	Life Technologies, Thermo Scientific (USA)
Thiamine hydrochloride	Roth (Karlsruhe)
TM 10 tergitol	Chemika (Australia)
Tris	MP Biomedicals (Eschwege)
Triton	Roth (Karlsruhe)
Trypticase soy broth	Oxoid, Thermo Fisher Scientific biosciences (St. Leon-Rot)
Tryptone	Roth (Karlsruhe)
Tween	Sigma-Aldrich (Munich)
VCL ₃	Sigma-Aldrich (Munich)
Vectashield	Enzo life science (UK)
Vector's Hämalaun solution	Roth (Karlsruhe)
VirkonS	V.P. Produkte (Schlächtern)
Xylene	Roth (Karlsruhe)
Xylene Cyanol	Sigma-Aldrich (Munich)
Yeast extract	MP Biomedicals (Eschwege)
Yeast t-RNA	Roche (Mannheim)
ZnSO ₄ · 7H ₂ O	Merck (Darmstadt)

Table 34: Antibiotics used in this study

Antibiotic	Supplier	Final concentration
Ampicillin	Roth (Karlsruhe)	100 µg/ml
Chloramphenicol	Roth (Karlsruhe)	30 µg/ml
Kanamycin sulfate	Roth (Karlsruhe)	30 µg/ml
Streptomycin sulfate	Roth (Karlsruhe)	50 or 100 µg/ml as indicated
Tetracycline hydrochloride	Roth (Karlsruhe)	12.5 µg/ml

Material and Methods

2.3.2 Antibodies

Table 35: Antibodies used for lipocalin-2 ELISA (mouse lipocalin-2/NGAL detection kit (R&D, DY1857))

Antibody	Origin	Supplier	Final concentration
Lipocalin-2 capture antibody	Rat	R&D, Part 842440	1:200
Lipocalin-2 detection antibody (biotinylated)	Rat	R&D, Part 842441	1:200

Table 36: Antibodies used for depletion of neutrophils and FACS analysis

Antibody	Origin	Supplier	Final amount or dilution
α -mouse G-CSF (clone: # 67604; depletion)	Rat	R&D Systems	10 μ g per mouse
Rat IgG ₁ (clone: # 43414, isotype control)	Rat	R&D Systems	10 μ g per mouse
α - m Ly-6G (clone: 1A8; depletion)	Rat	BioXCell	150 μ g per mouse
Rat IgG2a (clone: 2A3; isotype control)	Rat	BioXCell	150 μ g per mouse
α -CD45-PerCP (clone: 30-F11)	Rat	Biolegend	1:100
α -CD11b-APC-Cy7 (clone: M1/70)	Rat	Biolegend	1:200
α -Ly-6G-Pacific Blue (clone: 1A8)	Rat	Biolegend	1:200
α -Ly-6C-FITC (clone: AL-21)	Rat	BD	1:400
α -CD3-PE (clone: 17A2)	Rat	Biolegend	1:200
α -CD16/CD32 (93)	Rat	eBioscience	1:100

Table 37: Antibodies used for immuno-fluorescence staining of neutrophils

Antibody	Origin	Supplier	Final amount or dilution
Rat-anti CD18 (M18/2)	Rat	BD	1:300
Anti-rat Cy3	Goat	Jackson (112-165-167)	1:300

2.3.3 Devises and specific materials

Table 38: Devises and specific materials

Items	Supplier
ABI 7500 fast	Applied Biosystems (Darmstadt)
Acid washed glass beads (<106 μ m)	Sigma-Aldrich (Munich)
Aluminum crimp seals (diam. 11 mm)	Supelco (USA)
Aluminum crimp seals (diam. 20 mm)	Supelco (USA)
Amp for agarose gels (Power Pac)	Bio Rad (Munich)

Material and Methods

Items	Supplier
BioPhotometer	Eppendorf (Wesseling-Berzdorf)
Butyl-rubber stoppers (diam. 11 mm)	Supelco (USA)
Butyl-rubber stoppers (diam. 20 mm)	Geo-Microbial Technologies (USA)
Cannulas	B. Braun (Melsungen)
Crimper (diam. 11 mm)	VWR (Darmstadt)
Crimper (diam. 20 mm)	VWR (Darmstadt)
Cryotome	Leica Biosystems (Wetzlar)
Cryo-tubes	Thermo Fisher Scientific biosciences (St. Leon-Rot)
Decrimper (diam. 20 mm)	VWR (Darmstadt)
Dialysis membrane (pore size: 0.025 µm)	Merck, Millipore (Darmstadt)
Diagnostic slides (10 wells, 76 x 25 x 1 mm)	Thermo Fisher Scientific biosciences (St. Leon-Rot)
1.5 ml DNA loBind tubes	Eppendorf (Wesseling-Berzdorf)
Electroporation cuvette (1mm)	Peqlab (Erlangen)
Electroporation device (Micro Pulser)	Bio Rad (Munich)
Epi Centrifuge (5430 R)	Eppendorf (Wesseling-Berzdorf)
FACSCANTO II	BD (Franklin Lakes, USA)
FACS tubes	Hartenstein (Würzburg)
Filter Millex (0.22 µm)	Merck (Darmstadt)
Filter Millex (0.45 µm)	Merck (Darmstadt)
Gel documentation chamber	Bio Rad (Munich)
Glass slides (cover)	Marienfeld Laboratory Glassware (Lauda-Königshofen)
Gnoto cages	Han, Bioscape (Emmendingen)
Incubator (Heraeus oven)	Thermo Fisher Scientific biosciences (St. Leon-Rot)
Laminar flow (Safe 2020)	Thermo Fisher Scientific biosciences (St. Leon-Rot)
LightCycler480 Multiwell Plate 96, white	Roche (Mannheim)
LightCycler96	Roche (Mannheim)
40 µm mesh (cell strainer)	BD Falcon™ (USA)
NanoDrop	Thermo Fisher Scientific biosciences (St. Leon-Rot)
NucleoSipn Gel and PCR Clean-up kit	Macherey-Nagel (Düren)
NucleoSipn Plasmid kit	Macherey-Nagel (Düren)
Parafilm	BEMIS (USA)
Peqstar 2x gradient cyclor	Peqlab (Erlangen)
Plasmid Plus Midi Kit	Qiagen (Hilden)
Screw cap plastic tubes	A. Hartenstein (Würzburg)
1.5 ml plastic tubes (PCR grade)	Eppendorf (Wesseling-Berzdorf)
2 ml plastic tubes (PCR grade)	Eppendorf (Wesseling-Berzdorf)
15 ml plastic tubes	Greiner Bio-One (Frickenhausen)
50 ml plastic tubes	Greiner Bio-One (Frickenhausen)
Petri dishes	Greiner Bio-One (Frickenhausen)
Qiagen DNA (fast) stool kit	Qiagen (Hilden)

Material and Methods

Items	Supplier
Shaker (Certomat R)	B. Braun Biotech international (Melsungen)
Spectrophotometer (Sunrise)	Tecan (Crailsheim)
Superfrost Plus slides (75 x 25 x 1 mm)	A.Hartenstein (Wuerzburg)
Syringes	B. Braun (Melsungen)
Tissue lyzer	Qiagen (Hilden)
Vortex	Scientific industries (USA)
96-well ELISA plates (Brandplates)	Brand (Wertheim)
96-well plate for standard assays	TPP (Trasadingen)
Wheaton glass serum bottles (1.5 ml)	Sigma-Aldrich (Munich)
Wheaton glass serum bottles (100 ml)	Sigma-Aldrich (Munich)
Zirconia/silica beads (0.1 mm)	Roth (Karlsruhe)
Zirconia-beads (0.7 mm)	Roth (Karlsruhe)

2.4 Microbiological methods

2.4.1 Preparation of bacterial cryo-stocks (*S. Tm* and *E. coli* strains)

One bacterial colony was picked from a LB agar plate containing the appropriate antibiotic and was subsequently cultured in 5 ml of LB medium supplemented with the selective antibiotic. The bacterial culture was performed in glass tubes and incubated overnight (o/n) at 37°C in a wheel rotor. The following day, the o/n culture was transferred to a 15 ml plastic tube and spun down (15 min; 4°C; 4,000 x g). After the removal of the supernatant, the bacterial cell pellet was resuspended in 1 ml of peptone-glycerol broth, transferred into cryo-tubes and stored at -80°C.

2.4.2 Bacterial culture for *in vivo* experiments

S. Tm strains were streaked on LB agar plates containing a selective antibiotic, whereas *C. rodentium* was streaked on MacConkey (Oxoid) plates without antibiotic. 2 - 3 colonies were used to inoculate 3 ml starter cultures containing either LB medium with 0.3 M NaCl for *S. Tm* cultures or LB medium without supplements for *C. rodentium* cultures. Starter cultures were incubated for 12 h at 37°C in a wheel rotor. 2 ml subcultures in either LB medium with 0.3 M NaCl or regular LB medium were subsequently inoculated with 100 µl of the starter cultures and further incubated for 4 h at 37°C in a wheel rotor. In order to harvest cells, subcultures were centrifuged (2 min; 4°C; 9,660 x g), the supernatant was discarded and the cell pellet was resuspended in the same volume 1x PBS as the subculture. 50 µl aliquots of cell suspension were aliquoted in 1.5 ml plastic tubes and stored on ice until oral gavage. In order to determine the exact inoculum size, dilutions of the inoculum in sterile 1x PBS (10^{-4} and 10^{-6}) were additionally plated on MacConkey agar plates.

Material and Methods

Clostridium difficile DH196 spores that were used for infection were prepared by Prof. Hapfelmeier's group (Studer *et al.* 2016). *Helicobacter typhlonius* CCUG48335T used for the reversible colitis was prepared by Prof. Mueller's group (Brasseit *et al.* 2016).

2.4.3 *In vitro* growth assay of *S. Tm* strains

Bacteria from -80°C cryo-stocks were streaked on LB agar plates without antibiotics and grown o/n at 37°C. 3 individual colonies were used to inoculate aerobic starter cultures containing 5 ml of M9 medium without antibiotics. Starter cultures were performed in glass tubes and incubated for 12 h at 37°C in a wheel rotor. Aerobic as well as anaerobic subcultures with a starting OD₆₀₀ of 0.02 were subsequently carried out in 10 ml M9 medium with and without nitrate (20 mM). For testing *S. Tm* strains deficient in ethanolamine utilization, M9 medium was additionally supplemented with ethanolamine (5 mM) and tetrathionate (40 mM) as indicated in the experiments. Aerobic subcultures were performed in glass Erlenmeyer flasks sealed with aluminum foil, whereas anaerobic subcultures were conducted in 100 ml Wheaton glass serum bottles with pre-reduced medium (pre-reduction for at least 2 days under anoxic conditions: 3% H₂, rest N₂). The amount of starter culture required to meet a final OD₆₀₀ of 0.02 was spun down (10 min; 4°; 1,677 x g), imported in the anaerobic tent, resuspended in pre-reduced medium and used to inoculate anaerobic subcultures. The 100 ml culture bottles were plugged with a butyl-rubber stopper, exported, sealed with an aluminum crimp seals (diam. 20 mm) using a crimper and gassed (7% H₂, 10% CO₂, rest N₂). Both aerobic and anaerobic cultures were incubated at 37°C under constant shaking at 180 rpm. 1 ml samples for OD₆₀₀ measurement and for the determination of nitrate concentrations were taken at the indicated time points using a syringe. After the photometric OD₆₀₀ measurement in plastic cuvettes, samples were transferred into 1.5 ml plastic tubes. In order to pellet cells, tubes were subsequently centrifuged (5 min; RT; 4,293 x g). The supernatant was transferred to a new 1.5 ml plastic tube and stored at -20°C until measurement of nitrate concentrations.

2.4.4 *In vitro* competition assay

S. Tm strains from -80°C cryo-stocks were streaked out on LB plates without antibiotics and incubated o/n at 37°C. 3 colonies were picked and resuspended in 100 µl of either LB or M9 medium without antibiotic using sterile 1.5 ml plastic tubes. The bacterial suspension was used to inoculate starter cultures which were incubated for 12 h at 37°C in a wheel rotor. The starter cultures were performed in glass tubes containing 5 ml of either LB or M9 medium without antibiotics. Subsequently, co-cultures were prepared in mucin broth as described by (Lopez *et al.* 2012). Briefly, starter cultures of the competing strains were mixed in a 1:1 ratio with a starting OD₆₀₀ of 0.05 of each strain and used to inoculate 14 ml cultures with either plain mucin broth or mucin broth containing 40 mM nitrate. For competition assays between *S. Tm* strains deficient in nitrate

Material and Methods

respiration and *S. Tm* strains deficient in nitrate and tetrathionate respiration, the mucin broth was additionally supplemented with histidine (500 mg/l) to enhance growth and with tetrathionate (40 mM). The cultures were incubated in 15 ml plastic tubes and incubated statically for 24 h at 37°C. In order to determine CFUs of the strains, 100 µl samples of the 24 h cultures were taken at t=0 h and t=24 h, diluted in sterile 1x PBS (down to 10^{-4} – 10^{-6}) and plated on LB agar plates containing the respective selective antibiotics for individual strains (for streptomycin a concentration of 50 µg/ml was used, other concentrations as indicated in Table 34).

2.4.5 Preparation of starter inocula for growth assays of Oligo-MM¹² strains

The cecum of a male C57BL/6J mouse stably associated with the Oligo-MM¹² bacteria was aseptically dissected under anoxic conditions (anaerobic tent: 3% H₂, rest N₂) and transferred into a sterile 50 ml plastic tube. 20 ml of sterile 1x PBS were added and the bacteria were flushed out of the cecum by gently shaking. The bacterial suspension was subsequently filtered through a 40 µm nylon mesh (cell strainer) into a sterile 50 ml plastic tube. An equal amount of a 20% glycerol-palladium solution was added (final glycerol concentration of 10%) and 1 ml aliquots in 1.5 ml Wheaton glass serum bottles were prepared. The bottles were sealed with a butyl-rubber stopper and an aluminum crimp seal as well as finally stored at -80°C. All plastic ware and solutions used were already pre-reduced for at least 2 days in the anaerobic tent.

2.4.6 *In vitro* growth assay of Oligo-MM¹² strains

A 1 ml aliquot of frozen starter inoculum for *in vitro* growth curves (2.4.5) was thawed in 150 ml of pre-warmed 5% VirkonS. The sterile glass bottle was imported in the anaerobic tent, the aluminum crimp seal was opened with a screw driver and the butyl-rubber stopper was removed with a sterile forceps. Subsequently, 50 µl of bacterial suspension were added to a 100 ml Wheaton glass serum bottle filled with 10 ml of anaerobic *Akkermansia* medium without mucin, and the glass bottle was sealed with a butyl-rubber stopper (diam. 20 mm) and exported. Depending on the experiment, the medium was also supplemented with nitrate, dipyriddy or DTPA at concentrations indicated in the experiments. After the export, the bottles were sealed with aluminum crimp seals and gassed (7% H₂, 10% CO₂, rest N₂). The cultures were incubated at 37°C under constant shaking and 1 ml samples were anaerobically removed at the indicated time points using a 1 ml syringe. 100 µl of the sample were used to determine the OD₆₀₀ and the residual 900 µl were transferred to 2 ml plastic tubes and spun down (10 min; RT; 11,000 x g). With increasing OD₆₀₀, there was less culture volume used for pelleting cells (OD₆₀₀ of 0.350-0.699: 450 µl, OD₆₀₀ of 0.700-1.049: 300 µl and OD₆₀₀ above 1.050: 90 µl). The supernatant was discarded and the bacterial cell pellet was stored at -20°C until extraction of genomic DNA (gDNA). All devices, supplements and media used were already reduced for at least 2 days in the anaerobic tent.

Material and Methods

2.4.7 Chromazurol S (CAS) agar assay for siderophore production

Strains from -80°C cryo-stocks were streaked on LB agar plates containing the appropriate antibiotic and grown o/n at 37°C (no antibiotics for *Yersinia* control strains). 2 - 3 individual colonies were picked in order to inoculate 5 ml starter cultures containing LB medium without antibiotics. The starter cultures were performed in glass tubes and incubated for 12 h at 37°C in a wheel rotor. 1 ml of starter culture were spun down (10 min; 4°C; 2,415 x g), the supernatant was discarded and the pellet was resuspended in 1 ml of sterile and ice-cold 1x PBS. The bacteria in 1x PBS were diluted to an OD₆₀₀ of 0.1 and 5 µl of diluted bacteria were spotted on CAS agar plates and incubated at 37°C for 48 h. The diameters of the colony as well as the diameter of the colony + the orange CAS halo were measured and the CAS-reactive ring was calculated in mm according to the formula: 0.5 x [(diameter of colony + CAS halo) – diameter of colony].

2.4.8 Generation of chemo-competent cells

200 ml of LB medium were inoculated with 10 ml of an o/n culture of *E.coli* DH5α (1:20) and incubated at 37°C under constant shaking at 180 rpm until an OD₆₀₀ of 0.4 – 0.6 was reached. Cells were briefly chilled on ice and centrifuged (10 min; 4°C; 5,000 x g) in 50 ml plastic tubes. The supernatant was discarded and the pellets were resuspended in 60 ml of ice-cold TFB1 buffer. After 10 min incubation on ice, the cells were centrifuged again (10 min; 4°C; 5,000 x g), the supernatant was discarded and the pellets were resuspended in 8 ml of ice-cold TFB2 buffer. 200 µl of cell suspension were finally aliquoted in pre-cooled 1.5 ml plastic tubes, snap frozen in liquid nitrogen and stored at -80°C until usage.

2.4.9 Generation of electro-competent cells

50 ml subcultures in LB medium containing appropriate supplements (refer to 2.5.9.2 and 2.5.9.4) were incubated at either 30°C or 37°C under constant shaking at 180 rpm until an OD₆₀₀ of around 0.5 was reached. Subcultures were subsequently transferred into 50 ml plastic tubes, chilled on ice for 10 min and centrifuged (15 min; 4°C; 1,677 x g). The supernatants were discarded and the pellets were resuspended in 1 ml of ice-cold 10% glycerol, transferred to 1.5 ml plastic tubes and mixed by vortexing. Subsequently, cells were washed 5 times with ice-cold 10% glycerol [centrifugation (1 min; 4°C; full speed), discarding the supernatant and resuspending the cell pellet again in 1 ml of ice-cold 10% glycerol]. Finally, the electro-competent cells were resuspended in 80 µl of 10% glycerol and directly transferred into pre-cooled electroporation cuvettes. Cells were chilled on ice until electroporation.

Material and Methods

2.5 Molecular biological and biochemical methods

2.5.1 Agarose gel electrophoresis

1 – 2% agarose gels supplemented with ethidium bromide (0.1 µl/ml) were prepared in 1x TAE buffer and run for 30 min at 100 V. Usually, 10 µl of the DNA sample was mixed with 10x loading dye and loaded. The following standards: GeneRuler 1kb DNA ladder or GeneRuler DNA ladder mix (100 bp) were used as DNA markers. Gels were visualized under UV light using a gel documentation chamber.

2.5.2 Lipocalin-2 (LCN-2) ELISA (mouse lipocalin-2/NGAL detection kit (R&D, DY1857))

96-well ELISA plates were coated with 50 µl/well of lipocalin-2 capture antibody (Table 35) and incubated o/n at 4°C in a humid chamber. After 3 washing steps with washing buffer (0.05% Tween-20 in 1x PBS), the plates were blocked for 1 h at RT with 50 µl/well of blocking buffer (2% BSA in 1x PBS). The plates were washed again 3 times and samples were subsequently added in duplicates (50 µl/well, undiluted in PBT, 1:20 and 1:200 in 1x PBS). In order to quantify LCN-2 amounts, standard curves with a starting concentration of 50 ng/ml of LCN-2 were prepared (duplicates, 1:3 dilutions in blocking buffer). The plates were then incubated for 1 h at RT and washed again 6 times. 50 µl/well of LCN-2 detection antibody (Table 35) were added and the plates were incubated again for 1 h at RT, followed by 6 washing steps. Subsequently, 100 µl/well of HRP-streptavidin (1:1,000 diluted in 1x PBS) were added following 1 h of incubation and 6 washing steps. The plates were finally developed in the dark for 30 - 45 min using 100 µl/well of ABTS substrate (1 mg ABTS in 10 ml of 0.1 M NaH₂PO₄, pH 4 + 5 µl of H₂O₂). Finally, the absorbance was measured at 405 nm with a spectrophotometer (Tecan, Sunrise).

2.5.3 Cloning of 16S rRNA full length sequences into pJET1.2 cloning vector

Plasmids listed in Table 5 have been described previously (Brugiroux *et al.* 2016) as indicated or were constructed as described below (pMB1 + 2, pMB4 - 6): For construction of pMB1 - 5, bacterial 16S rRNA full length gene sequences were amplified by polymerase chain reaction (PCR) using DreamTaq Master mix with one initial denaturation step at 95°C for 5 min, followed by 35 cycles with one cycle consisting of 95°C for 30 sec, 50°C for 30 sec and 72°C for 1 min and one final elongation step at 72°C for 10 min. For construction of pMB6, PCR reaction was performed using Q5[™] Hot Start High-Fidelity polymerase which has proofreading activity (initial denaturation step at 98°C for 30 sec followed by 35 cycles with one cycle being 98°C for 10 sec, 50°C for 30 sec and 72°C for 35 sec and one final elongation step at 72°C for 2 min). 100 ng of bacterial gDNA was used as template. The gDNAs of *S. Tm* and *C. rodentium* were provided by B. Stecher, the gDNAs of *C. difficile* and *C. scindens* were provided by Nicolas Studer (University of Bern) and the gDNA of *H. typhlonius* was provided by Martin Faderl (University of Bern). PCR reactions were performed using a Pqstar 2x gradient cycler

Material and Methods

using 125 nM of each primer: fD1 and fD2 (250 nM for PCR reaction with Q5 polymerase) as well as 250 nM of the primer rP1 (500 nM for PCR reaction with Q5 polymerase) (Table 32). The reaction volume was 50 μ l. 5 μ l were loaded on a 1% agarose gel to visualize successful 16S rDNA amplification. The residual 45 μ l were purified using the NucleoSpin Gel and PCR Clean-up kit (Macherey-Nagel) according to the manufacturer's instructions and subsequently cloned into the high-copy expression vector pJET1.2 using the CloneJET™ PCR kit. Briefly, 2 μ l of PCR-amplified 16S rRNA gene were blunted in a 18 μ l reaction using the provided 2x reaction buffer, nuclease free water and 1 μ l of DNA blunting enzyme. The blunting reaction was performed at 70°C for 5 min. The blunted PCR product was then inserted into the pJET1.2 cloning vector using 50 ng of vector and 1 μ l of the provided T4 DNA ligase. The ligation mix was briefly vortexed and incubated for 30 min at RT. The ligation mix was finally transformed into chemo-competent *E. coli* DH5 α as described below (2.5.4).

Correct insertion of a full length 16S rRNA gene was checked by PCR using 5 μ l of boiled 1:20 diluted cultures used for stocking and DreamTaq Master mix (20 μ l reaction volume, reaction condition as described above). Plasmid DNA of clones harboring 16S rRNA full length sequences was extracted using the NucleoSpin plasmid extraction kit (Macherey-Nagel) and finally sequenced using the pJet1.2 specific primers pJet1-FP and pJet1-RP (Table 32). Sanger sequencing was performed at GATC, Germany. Sequences were analyzed using the software CLC DNA workbench 6.0.2 (CLC bio, Denmark).

2.5.4 Transformation chemo-competent cells

Plasmids were transformed in chemo-competent DH5 α cells (2.4.8). 100 μ l of chemo-competent DH5 α cells were thawed on ice and 5 μ l of ligation reaction were added. The cells were gently mixed and incubated on ice for 30 min. Hereafter, cells were heat shocked at 37°C for 45 sec and immediately cooled on ice for 2 min. 800 μ l of LB medium were subsequently added and the cells were incubated at 37°C for 1 h under constant shaking at 650 rpm. Cells were then centrifuged (2 min; RT; 8,117 x g), the supernatant was partially discarded and the cell pellet was resuspended in the residual supernatant (50 - 100 μ l). In order to select for pJET1.2 positive cells, 50 μ l of cell suspension were plated on LB agar plates containing ampicillin (100 μ g/ml). Positive clones were cryo-stocked as described previously (2.4.1) and stored at -80°C.

2.5.5 Total DNA extraction of fecal and cecal microbiota

Fecal and cecal DNA was directly extracted from samples stored in 2 ml plastic tubes at -80°C using the Qiagen DNA (fast) stool kit. The provided protocol was followed including additional modifications. First, samples were thawed and mixed with 150 μ l of acid washed glass beads (<106

Material and Methods

µm), 150 µl of zirconia-beads (0.7 mm) as well as 700 µl of Inhibit Ex buffer. The samples were then lyzed for 3 min at 50 Hz in a tissuelyzer, incubated at 95°C for 5 min, lyzed again (50 Hz, 5 min) and centrifuged (1 min; RT; 11,300 x g). The supernatant was transferred into a fresh 2 ml plastic tube and kept on ice. In order to increase the lysis efficiency of Gram-positive bacteria, the pellets were resuspended in 200 µl of sterile and DNA free lysis buffer including lysozyme (Table 27) and incubated for 30 min at 37°C. Subsequently, 500 µl of Inhibit Ex buffer were added, following lysis (50 Hz, 5 min), incubated at 95°C, lyzed (50 Hz, 5 min) again and centrifuged (1 min; RT; 11,300 x g). The supernatant was added to the supernatant that was previously harvested and kept on ice. 26 µl of proteinase K (provided solution) were pipetted into a fresh 2 ml plastic tube and 700 µl of total supernatant as well as 700 µl of AL buffer were added. Samples were vortexed for 15 sec and incubated at 70°C for 10 min. Hereafter, samples were briefly centrifuged in order to remove any drops from the lid and 700 µl of ethanol (96% p.a.) were added. Samples were then vortexed again, briefly centrifuged and loaded onto QIAamp spin columns. The DNA bound to the filter matrix was subsequently washed using the buffers AW1 and AW2 and finally eluted in 100 µl of pre-warmed ATE buffer (70°C). The DNA concentration was determined by NanoDrop.

2.5.6 DNA extraction from bacterial cell pellets harvested from *in vitro* cultures

gDNA from bacterial cell pellets was extracted as described previously (Turnbaugh *et al.* 2009, Ubeda *et al.* 2012). The bacterial cell pellet stored in a 2 ml plastic tube at -20°C was resuspended in 500 µl of extraction buffer (Table 28), 210 µl of sterile filtered 20% SDS and 500 µl of a phenol:chloroform:isoamylalcohol (25:24:1) mixture. 1 ml of zirconia / silica beads (0.1 mm diameter) was added. The sample was lyzed at 50 Hz for 4 min in a tissuelyzer at RT and subsequently centrifuged (5 min; RT; 11,300 x g). The upper phase was transferred into a fresh 2 ml plastic tube and 500 µl of phenol:chloroform:isoamylalcohol (25:24:1) mixture were added. The sample was mixed by inversion (2 - 3 times) and centrifuged (5 min; RT; 11,300 x g). The supernatant (~ 500 µl) was transferred into a fresh 2 ml tube and 1 ml of ethanol (96% p.a.) + 50 µl of NaAcetat (3M) were added and the sample was mixed by inversion (2 - 3 times), subsequently centrifuged (30 min; 4°C; 13,148 x g) and the supernatant was discarded. The DNA pellet was resuspended in 500 µl of ice-cold 70% ethanol and mixed again by inversion. After centrifugation (15 min; 4°C; 13,148 x g), the supernatant was discarded and the DNA pellet was air-dried (until dry under laminar airflow). The DNA pellet was finally resuspended in 50 µl of 10 mM Tris-HCl pH8 and the nucleic acid concentration was determined by NanoDrop.

2.5.7 Colorimetric quantification of nitrite concentrations

S. Tm culture supernatant processed as detailed in section 2.4.3 and colorimetric quantification of nitrite concentrations was performed as described by (Miranda *et al.* 2001). Briefly, 50 µl of the

Material and Methods

sample (undiluted, 1:10 as well as 1:100) were transferred in wells of a 96-well plate. 50 µl of 1:1.5 serial dilutions of a NaNO₂ with known concentrations (50 µM down to 7 µM) were used as a standard curve. 25 µl of a 1:1 mixture of 2% sulfanilamide in 3 M HCl and 0.1% *N*-(1-NaphThyl)ethylenediamine dihydrochloride monomethanolate (NEDD) in ddH₂O were added to each well. The plate was incubated in the dark at 37°C for 30 min and the absorbance at 540 nm was measured using a spectrometer (Tecan, Sunrise).

2.5.8 Hydrolysis probe based quantitative real-time PCR (qPCR)

2.5.8.1 Design of specific primers and hydrolysis probes

16S rRNA full length gene sequences of bacteria used in this study were aligned using CLC DNA Workbench 6.0.2 (CLC bio, Denmark) in order to identify hypervariable regions that are unique for each strain. Subsequently, specific primers and a hydrolysis probe were designed for each strain using the software Primer Express 3 (MGB protocol, Applied Biosystems, Life Technologies, USA; Table 30) and checked against the aligned 16S rRNA genes to ensure specificity. In order to enable duplex quantitative real-time PCR experiments, the hydrolysis probes were either labeled with 6-carboxyfluoresceine (FAM) or 6-carboxyhexafluoresceine (HEX) at the 5' end. Additionally, every probe was conjugated with the black hole quencher 1 (BHQ1) at the 3' end. There was no other additional chemical modification which might improve performance of MGB probes. All primers and hydrolysis probes were synthesized by Metabion International AG (Germany), delivered freeze dried and were either desalted (primers) or HPLC purified (hydrolysis probes). The quality was controlled by mass check (primer length: 18 – 28 nt; probe length: 15 – 25 nt.)

2.5.8.2 Preparation of plasmid DNA for standards curves

Linearized plasmids harboring full length 16S rRNA gene sequences were used as DNA templates for the standard curves used for absolute quantification. *E. coli* DH5α harboring the respective plasmid was grown in LB medium supplemented with ampicillin (50 - 100 µg/ml o/n cultures) and plasmids were purified using the Plasmid Plus Midi Kit (QIAGEN) according to the manufacturer's instructions. 30 µg of plasmid DNA were subsequently linearized in 100 µl o/n reactions at 37°C using 10x reaction buffers and endonucleases (20 units) to linearize the plasmids that have no recognition site within the 16S rRNA full length gene sequence (Table 5). After digesting, plasmids were purified using the NucleoSpin Gel and PCR Clean-up kit (Macherey-Nagel) according to the provided protocol. The final concentrations of the linearized plasmids were determined by NanoDrop. Agarose gel electrophoresis (1% agarose) was performed in order to verify complete linearization of the plasmids.

Material and Methods

2.5.8.3 Determination of 16S rRNA gene copy numbers

10 ng/μl stocks of each plasmid were prepared and the 16S rRNA gene copy numbers per μl were calculated: (i) the number of nucleotides of the plasmid was defined; (ii) the approximate molecular mass of the dsDNA was determined according to the formula: (number of nucleotides x 607.4) + 157.9; (iii) the gene copy numbers/μl of a 10 ng/μl stock were calculated: $((10 \times 10^{-9})/\text{molecular mass of dsDNA}) \times (6.022 \times 10^{23})$; (iv) 10 fold dilutions were prepared: range: $10^8 - 10^{-2}$ gene copies/μl; the DNA was diluted in yeast t-RNA solution (100 ng/μl) and 1.5 ml DNA loBind tubes (Eppendorf) were used. The dilutions were stored at -20°C.

2.5.8.4 qPCR reaction conditions

qPCR reactions were performed in white LightCycler480 Multiwell Plate 96 plates using the thermo cycler LightCycler96 and the FastStart Essential DNA Probes Master reaction kit. The reaction volume was 20 μl and the following conditions were applied: (i) an initial denaturation step at 95°C for 10 min followed by (ii) 45 cycles (95°C for 15 sec and 60°C for 1 min). qPCR reactions were performed with 5 ng template DNA as well as with 300 nM of each primer and 250 nM of the corresponding probe. The fluorescence for each cycle was recorded after each step.

Standard curves were run once in triplicates in order to evaluate the performance of the primer / probe combinations in mono- and duplexed qPCR reactions (Table 39). In further experiments, standard curves were reproduced by the LightCycler96 software 1.1 (Roche, Switzerland) based on one single DNA standard with known DNA quantity and the efficiency derived from the standard curve that was run initially. DNA samples from feces or cecal content were run in duplicates. The quantification cycle (Cq) as well as the baseline were automatically determined by the LightCycler96 software 1.1 (Roche, Switzerland).

2.5.8.5 Titration of primers and probes as well as template DNA concentrations

Different concentrations of forward and reverse primers as well as hydrolysis probes (100 – 500 nM) were tested with 2 different amounts of linearized plasmid DNA (2.5×10^6 and 2.5×10^2 16S rRNA gene copies). Optimal concentrations of forward and reverse primers (300 nM each) as well as of hydrolysis probe (250 nM) were derived from qPCR reaction with YL2_Exonucl._fwd/rev with Probe_YL2, YL44_Exonucl._fwd/rev with Probe_YL44, YL45_Exonucl._fwd/rev with Probe_YL45, YL58_Exonucl._fwd/rev with Probe_YL58, Isol46_Exonucl._fwd/rev with Probe_Isol46, Isol49_Exonucl._fwd/rev with Probe_Isol49, Isol48_Exonucl._fwd/rev with Probe_Isol48. The titration of primers and probes was performed using the thermocycler ABI 7500 fast.

In order to determine the optimal quantity of template DNA, qPCR reactions with 1:2 dilutions of 25 ng of fecal DNA were performed in triplicates. The 1:2 dilutions of template DNA resulted in parallel

Material and Methods

amplification curves. 5 ng of template DNA were found to be an optimal quantity that yields results within the dynamic range of the qPCR assay (C_q over 15 cycles) and were subsequently used as template amount for all further qPCR reactions. This titration experiment was performed with one primer / probe combination that targets a strain that is highly abundant in fecal DNA samples ('*Bacteroides caecimuris* I48').

2.5.8.6 Evaluation of qPCR efficiency and establishment of a duplex qPCR assay

The efficiency of each primer / probe combination was calculated based on the slope of standard curves with 1:10 dilutions of linearized plasmids harboring specific 16S rRNA gene sequences (qPCR efficiency: $(10^{(-1/\text{slope of standard curve})} - 1) \times 100$). DNA amounts for standard curves were titrated down until the assay was dynamic: around 3.3 C_qs decrement between 1:10 dilutions and high endpoint fluorescence levels. Efficient qPCR reactions were within the range of 90 - 110% efficiency (duplication of the DNA amount per qPCR cycle) which guaranteed accurate determination of gene copy numbers. Standard curves were performed in mono- and duplex qPCR reactions in order to rule out any mutually inhibitory effects between the duplexed primers and probe combinations. For duplex reactions, assays with similar qPCR efficiencies and endpoint fluorescence levels were combined.

2.5.8.7 Validation of specificity and determination of the limit of detection

Besides testing the specificity *in silico* using the aligned 16S rRNA gene sequences, the strain-specificity of all primer / probe combinations was additionally investigated with plasmid pools harboring all 16S rRNA gene sequences excluding the one that was tested (2.5×10^6 gene copies per linearized plasmid per μl).

The limit of detection of each primer / probe combination was either the LOD₉₅ (amount of template DNA that results in a positive signal in 95% of the qPCR runs), the assay specific limit of detection or the gene copy number determined from late unspecific amplification using plasmid pools. The highest value was set to be the limit of detection. The LOD₉₅ was determined by titrating standard curves down to 2.5×10^{-2} gene copies. The percentage of signals that were above threshold was subsequently determined for each DNA template quantity. These data were used for a sigmoidal curve fit (plot: % positives against DNA template amount; GraphPad Prism 5, GraphPad Software, Inc., USA) and the LOD₉₅ was determined by interpolation. If the standard curve went out of the dynamic range (clearly less than 3.3 C_qs decrement between 1:10 dilutions and inhibited endpoint fluorescence levels) before reaching DNA amounts for the determination of the LOD₉₅, an assay specific limit of detection was set.

Material and Methods

2.5.9 Generation of gene deletion mutants in *S. Tm* by λ red recombination

2.5.9.1 Generation of PCR fragments

For in frame gene deletions, antibiotic-resistance markers were inserted into the chromosome of *S. Tm* applying λ red recombination. The procedure was described by (Datsenko and Wanner 2000). Briefly, PCR reactions were performed using the Pqstar 2x gradient cycler, FastStart Taq polymerase with 10x MgCL₂ reaction buffer, dNTPs (200 μ M of each nucleotide), 5 - 50 ng of template DNA and oligonucleotides (200 nM each) that amplify an antibiotic-resistance cassette as well as FRT sites for gene deletion from one of the following plasmids: pKD3 (*cat*: chloramphenicol resistance) or pKD4 (*aphT*: kanamycin resistance) (Table 4). The primers harbored 5' extensions (59 bp) that were homologous to sequences upstream of the start codon and downstream of the stop codon of the gene of interest (Table 31). The total volume of the PCR reaction was 4 x 50 μ l and the following cycling conditions were used: one initial denaturation step at 95°C for 6 min followed by: (i) five cycles with one cycle being 95°C for 30 sec, 55°C for 30 sec and 72°C for 2 min, (ii) 25 cycles with one cycle consisting of 95°C for 30 sec, 65°C for 30 sec and 72°C for 2 min and (iii) a final elongation step at 72°C for 10 min. PCR products were pooled, visualized on a 1% agarose gel to ensure successful amplification of the antibiotic cassette (5 μ l loaded) and purified by ethanol precipitation: 1/10 volume of 3 M NaAcetat (ddH₂O solution) as well as 2 volumes of ice-cold ethanol (96% p.a.) were added to the pooled PCR product, following centrifugation (15 min; 4°C; 13,148 x g). The supernatant was discarded and the pellet was resuspended in 500 μ l of ice-cold 70% ethanol and centrifuged again (15 min; 4°C; 13,148 x g). After discarding the supernatant, the pellet was subsequently air-dried at 37°C and resuspended in 22 μ l of nuclease free ddH₂O (Gibco).

In order to desalt the DNA, the ethanol precipitated PCR product was dialyzed for 60 min against ddH₂O (Ampuwa) using petri dishes and a dialysis membrane (pore size: 0.025 μ m). The DNA concentration was determined by NanoDrop.

2.5.9.2 Electroporation of electro-competent *S. Tm* harboring pKD46

S. Tm^{WT} harboring the plasmid pKD46 (Datsenko and Wanner 2000) were streaked on LB agar plates containing ampicillin and were incubated o/n at 30°C. 2 - 3 colonies were subsequently used to inoculate starter cultures containing 10 ml of LB medium supplemented with ampicillin that were incubated o/n at 30°C and 180 rpm. In order to generate electro-competent cells, starter cultures were used to inoculate subcultures in LB medium supplemented with 10 mM L-(+)-arabinose and ampicillin that were grown at 30°C under constant shaking at 180 rpm. Further steps are detailed in section 2.4.9.

Material and Methods

Subsequently, 80 µl of electro-competent cells were mixed with 5 - 10 µl of the PCR product containing the antibiotic cassette as well as the homologous flanking regions and transferred into pre-cooled electroporation cuvettes. Electroporation was performed at 1800 V for 5 msec. Cells were immediately recovered in 1 ml of pre-warmed (37°C) SOC medium and further incubated at 37°C and 500 rpm for 1.5 h. Afterwards, 500 µl of the transformed cells were transferred into a new 1.5 ml plastic tube and further incubated o/n at RT. The residual 500 µl were reduced to around 50 µl (centrifugation and re-suspending in residual supernatant), plated on LB agar plates supplemented with the appropriate antibiotic (either chloramphenicol or kanamycin both 30 µg/ml) and incubated o/n at 37°C. Clones were re-streaked, cryo-stocked and PCR checked using the Dream Taq mastermix and 500 nM of each check-up primer (Table 31). The reaction volume of the PCR was 20 µl and 5 µl of boiled cells from o/n cultures that were 1:20 diluted with sterile nuclease free ddH₂O (Gibco) were directly used as template. The following cycling conditions were applied: (i) 95°C for 5 min, (ii) 35 cycles with one cycle being 95°C for 30 sec, either 55°C for 30 sec (*narZ*, *narG*, *entA* and *eutC*) or 56°C for 30 sec (*napA*) and 72°C for either 1 min (*eutC*), 2 min (*entA*), 3 min (*napA*) or 4 min (*narZ* and *narG*) and (iii) 72°C for 10 min. PCR products were run on a 1% agarose gel in order to confirm successful gene replacement.

2.5.9.3 P22 transduction

Preparation of P22-phage lysates. 3 ml cultures in either pure LB medium or LB medium containing 5 mM CaCl₂ were inoculated with 3 colonies of the donor strain that was picked from a LB agar plate supplemented with appropriate antibiotic. The cultures were grown o/n in glass tubes at 37°C in a wheel rotor. 10 µl of P22-phage (Schmieger 1972) lysate were transferred into a sterile 1.5 ml plastic tube and 500 µl of the o/n culture of the donor strain were added. The culture containing the P22-phage lysate was subsequently transferred into a glass tube with aluminum lid and statically incubated at 37°C for 15 min. Afterwards, 5 ml of LB medium were added to the glass tube and further incubated o/n at 37°C under constant shaking at 180 rpm. The next day, 50 µl of chloroform were added to the glass tube following a 30 min incubation at RT. 2 ml of the culture were then transferred to a sterile 1.5 ml plastic tube and spun down (10 min; 4°C; 2,415 x g). The supernatant was filtered through a sterile 0.45 µm filter into a sterile screw cap plastic tubes and 10 µl of chloroform were added. The plastic tube was sealed with parafilm and stored at 8°C. In order to ensure sterility, 50 µl of the lysate were plated on a LB agar plate without antibiotics and incubated o/n at 37°C.

P22-transduction. 3 colonies of the acceptor strain from a LB agar plate with appropriate antibiotic were used to inoculate cultures containing 3 ml of LB medium supplemented with 5 mM CaCl₂. The cultures were grown o/n in glass tubes at 37°C on a wheel rotor. 10 µl of the P22-phage lysate of the

Material and Methods

donor strain were transferred into a sterile 1.5 ml plastic tube, 100 µl of o/n culture of the acceptor strain were added and incubated statically for 15 min at 37°C. 900 µl of LB medium supplemented with 10 mM EGTA were subsequently added and the tube was incubated under constant shaking (550 rpm) for 1 h at 37°C. Finally, the cultures were centrifuged (3 min; RT; 8,117 x g), the supernatant was reduced to around 100 µl, the pellet was resuspended in the residual supernatant and 50 µl were plated on LB agar plates containing the appropriate antibiotic +/- 10 mM EGTA and incubated o/n at 37°C. In order to obtain phage free bacteria, clones were finally picked and re-streaked for two times before cryo-stocking at -80°C. Successful transduction was confirmed by PCR using the same condition as described in section 2.5.9.2 (check-up PCR).

2.5.9.4 Deletion of antibiotic-resistance markers using the Flp-recombinase

Strains containing an antibiotic-resistance marker flanked by FRT sites that were generated by λ red recombination as described previously (2.5.9) were picked from LB plates containing the appropriate antibiotic. 3 colonies were used to inoculate 5 ml starter cultures that were grown o/n in a wheel rotor in LB medium containing the appropriate antibiotic. Subsequently, 50 ml subcultures in LB medium supplemented with the appropriate antibiotic were inoculated with 500 µl of starter culture (1:100 dilution) and grown at 37°C under constant shaking at 180 rpm until an OD₆₀₀ of around 0.5 was reached. Further steps of the preparation of electro-competent cells are described in section 2.4.9.

Subsequently, electro-competent cells were electroporated with 1 µg of pCP20 harboring the Flp-recombinase (Table 4). The procedure of electroporation is described in section 2.5.9.2. After electroporation, the cells were immediately recovered in 1 ml of pre-warmed LB medium (30°C) and incubated at 30°C for 1.5h under constant shaking (500 rpm). The bacteria were then spun down (3 min; RT; 6,708 x g), resuspended in 100 µl of supernatant and finally plated on LB agar plates containing ampicillin. Plates were incubated o/n at 30°C, the permissive temperature for pCP20. The next day, clones were re-streaked on LB agar plates and incubated o/n at 43°C, in order to induce expression of Flp-recombinase. The antibiotic sensitive strains in which recombination has occurred were identified by double picking on LB agar plates with and without the respective antibiotic and incubation at 37°C, in order to select for loss of pCP20. In order to confirm the loss of pCP20, the antibiotic sensitive strains were double plated again on LB agar plates with and without ampicillin (100 µg/ml) and incubated at 37°C. Clones that were ampicillin sensitive were cryo-stocked and stored at -80°C. Successful deletion of the antibiotic marker was confirmed by PCR according to the protocol described in section 2.5.9.2 (check-up PCR).

Material and Methods

2.5.9.5 Construction of *S. Tm* mutants

Construction of *S.Tm*^{Ni} (MBE7). In order to construct the nitrate respiration deficient *S. Tm* strain that lacks the three main nitrate reductases ($\Delta narZ$, *narG::cat*, *napA::aphT*) (Lopez *et al.* 2012), the genes *narZ*, *narG* and *napA* were either deleted or in frame replaced by antibiotic resistance markers. First, single *S. Tm* mutant strains were generated (Table 3, MBE1: *narZ::cat*, MBE2: *narG::cat* and MBE3: *napA::aphT*) using λ red recombination as described in the previous section 2.5.9. Briefly, antibiotic resistance genes were PCR amplified from plasmids (Table 4) using the ko-primers listed in Table 31 and electroporated into *S. Tm*^{WT} harboring pKD46. Effective recombination was verified by PCR using the check-up primers and agarose gel electrophoresis (1% agarose). Subsequently, the *narZ::cat* allele from MBE-1 was transduced to *S. Tm*^{WT} by P22 transduction in order to create MBE4. Correct insertion was tested by PCR using the primers narZ fwd-check up / narZ rev-check up (Table 31). The *narZ::cat* allele of MBE4 was subsequently deleted using the FLP recombinase as described in section 2.5.9.4. The resulting strain MBE5 ($\Delta narZ$) was checked by PCR using the primers narZ fwd-check up / narZ rev-check (Table 31). MBE5 was further transduced with P22-phage lysate of MBE2 in order to create MBE6 ($\Delta narZ$, *narG::cat*). Correct insertion was verified by PCR using the oligonucleotides narG fwd-check up / narG rev-check up. Finally, MBE6 was transduced with P22-phage lysate from MBE3 in order to construct MBE7 ($\Delta narZ$, *narG::cat*, *napA::aphT*). The correct genotype of MBE7 was assessed by PCR using the primers: narZ fwd-check up / narZ rev-check up, narG fwd-check up / narG rev-check up and napA fwd-check up / napA rev-check up. Conditions of check-up PCR reactions are detailed in section 2.5.9.2 (check-up PCR). All strains are listed in Table 3.

Construction of *S.Tm*^{Ni. + Te.} (MBE8). In order to generate MBE8 that is deficient in nitrate and tetrathionate respiration, the *ttrS::tet* allele from *S. Tm* strain M961 ($\Delta sodCI$, $\Delta sodCII$, *BCB4::tet* from (Hensel *et al.* 1999)) was transduced to MBE7 by P22-transduction. The correct genotype of MBE8 ($\Delta narZ$, *narG::cat*, *napA::aphT*, *ttrS::tet*) was verified by PCR using the primers: narZ fwd-check up / narZ rev-check up, narG fwd-check up / narG rev-check up, napA fwd-check up / napA rev-check up and ttrS fwd-check up / ttrS rev-check up. PCR conditions of check-up reactions are detailed in section 2.5.9.2 (check-up PCR).

Construction of *S.Tm*^{EntA} (MBE10). MBE10 (*S. Tm*, *entA::cat*) that is deficient in siderophore production was constructed by P22-transduction of the *entA::cat* allele from MBE9 to *S. Tm*^{WT}. MBE9 was generated previously by λ red recombination using pKD3 and the entA-fwd-ko / entA-rev-ko knock out primers (Table 31). Correct insertion of the *entA::cat* allele in MBE9 and MBE10 was assessed by PCR using entA fwd-check up / entA rev-check up primers (Table 31). Conditions of check-up PCR reactions are detailed in section 2.5.9.2 (check-up PCR).

Material and Methods

Construction of *S. Tm*^{EA} (MBE12). In order to construct MBE12 (*S. Tm*, *eutC::aphT*) that is deficient in ethanolamine utilization (Thiennimitr *et al.* 2011), *eutC* of *S. Tm*^{WT} harboring pKD46 was first replaced by a kanamycin resistance cassette performing λ red recombination using pKD4 as template and the knock out primers: *eutC*-fwd-ko / *eutC*-rev-ko. The genotype of the resulting strain MBE11 (*S. Tm*, *eutC::aphT*) was checked by PCR using the oligonucleotides: *eutC* fwd-check up / *eutC* rev-check up (Table 31). The allele *eutC::aphT* from MBE11 was finally P22-transduced to a fresh *S. Tm*^{WT} strain and verified by PCR using the primers: *eutC* fwd-check up / *eutC* rev-check up (Table 31). Conditions of check-up PCR reactions are detailed in section 2.5.9.2 (check-up PCR).

2.5.10 Immuno-fluorescence staining

PFA fixed cecum tips were taken from -80°C, cut in 7 μ m sections using a cryotome (Leica) and fixed on cover glass slides by air-drying for 2 h at RT. Sections were subsequently fixed with 100 μ l of 4% PFA for 5 min. After 3 washing steps with 1x PBS, sections were blocked with 100 μ l of 10% normal goat serum in 1x PBS for 60 min at RT. Next, 100 μ l of 10% normal goat serum containing 1.67 μ g/ml of α -CD18 antibody (Table 37) were added and incubated for 60 min at RT. After 3 washing steps with 1x PBS, sections were additionally stained for 30 min with 100 μ l of 10% normal goat serum containing the secondary anti rat antibody conjugated with Cy3 (4.17 μ g/ml, Table 37), DAPI (1 μ g/ml), SYTOX green (0,5 μ M) and Phalloidin (22 pmol/ml). Sections were washed again 3 times with 1x PBS, dried in the dark and mounted with a glass cover slip, Vectashield and nail varnish. Pictures were acquired using the confocal microscope TCS SP5 (Leica).

2.6 Animal experiments

2.6.1 Ethics

All animal experiments performed at the Max von Pettenkofer Institut (MvP) of the Ludwig-Maximilians-University Munich were reviewed and approved by the government of Oberbayern (55.2-1-54-2532-13-15).

2.6.2 Generation of gnotobiotic Oligo-MM¹² mice

Germfree C57BL/6J mice were associated with the 12 Oligo-MM strains (Table 2) by oral and rectal inoculation, Clean Mouse Facility (CMF) of the University of Bern (Brugiroux *et al.* 2016). Oligo-MM¹² mice, also termed stable Defined Moderately Diverse Microbiota mouse (sDMDMm2) were bred under germfree conditions in flexible film isolators (Harlan Laboratories) in order to maintain the defined microbiota. Oligo-MM¹² mice were also transferred to the gnotobiotic mouse facility of the MvP and to the ETHZ where mice were further bred under sterile conditions. Sterility was verified monthly by plating cecal content of sentinel mice on MacConkey (Oxoid), sheep blood (Oxoid) and Sabouraud dextrose (Oxoid) agar plates.

Material and Methods

2.6.3 High fat diet and oleic acid supplementation

Animal experiments and DNA extraction were performed by Sandra Wotzka, ETH Zurich. For high-fat diet, standard diet (KLIBA NAFAG, 3437) was switched to high-fat diet (Bio Serv, mouse high-fat diet) containing 20.5% protein, 36% fat and 35.7% carbohydrates. Oligo-MM¹² mice receiving high-fat diet were euthanized 6, 12 and 24 h post diet switch and cecal content was harvested for DNA extraction. For oleic acid supplementation, Oligo-MM¹² mice receiving standard diet were gavaged two times with 200 µl of oleic acid (Sigma) at time points 0 h and 4 h post initial gavage. Mice were sacrificed at 6, 12 and 24 h post initial oleic acid gavage and cecal content was taken for subsequent DNA extraction. Oligo-MM¹² mice fed with standard diet served as control.

2.6.4 Infection of gnotobiotic Oligo-MM¹² mice with *S. Tm* and *C. rodentium*

One day prior to infection Oligo-MM¹² mice were exported from the isolator in autoclaved gnotocages (Han, Bioscience) equipped with sterile ddH₂O (Ampuwa), food, bedding and enrichment. On the day of infection the laminar flow was disinfected with a sporicidal disinfectant (5% VirkonS, 30 min incubation). All instruments used (additional cage for handling, gavage needles and forceps in metal boxes) were previously enwrapped in tissues, autoclaved and imported under the laminar flow. In order to handle and manipulate Oligo-MM¹² mice under germfree conditions, infections were performed by two persons. Mice were directly handled by person 1 who was equipped with sterile cloths and gloves whereas person 2 handled unsterile material and opened the gnotocage. For infection, mice were taken out of the gnotocage, placed on the sterile grid of a handling cage and subsequently infected by oral gavage with either 5 x 10⁷ CFUs of *S. Tm* strains or 1 x 10⁸ CFUs of *C. rodentium* DBS100 in 50 µl of sterile 1x PBS using sterile gavage needles and syringes. The mice were placed back into the gnotocage that was sealed with Hepa-filter top. The preparation of bacterial cultures for *in vivo* experiments is detailed in section 2.4.2.

During the experiment, mice were monitored daily for signs of illness or suffering without taken them out of the cage because of high risk of contamination. The experiment was terminated prematurely, when individual mice showed signs of terminal illness according to a cumulative scoring system. At the end of the experiment, mice were euthanized by cervical dislocation.

2.6.5 Infection of CD18^{-/-} mice with *S. Tm*

In order to break microbiota-mediated colonization resistance, CD18^{-/-} mice B6.129S7-Itgb2^{tm2Bay} (Scharffetter-Kochanek *et al.* 1998) which are associated with a specific pathogen free (SPF) microbiota were orally gavaged with 25 mg of streptomycin-sulfate in 0.05 ml of dH₂O 24 h prior to infection with 5 x 10⁷ CFUs of *S. Tm*^{WT}. The preparation of *S. Tm*^{WT} cultures for *in vivo* experiments is

Material and Methods

detailed in section 2.4.2. Mice were euthanized at days 1 and 2 post infection by cervical dislocation and samples were taken.

2.6.6 Infection of Oligo-MM¹² mice with *C. difficile*

Infections with *C. difficile* were performed by Nicolas Studer in Prof. Hapfelmeier's group (University of Bern). Oligo-MM¹² mice were orally inoculated with 1×10^3 spores of *C. difficile* DH196 (Studer *et al.* 2016) and fecal pellets were collected daily, to determine LCN-2 levels and to perform microbiota analysis. The mice were sacrificed at day 3 post infection. LCN-2 levels were measured in Bern. DNA of feces and cecal content was extracted by Nicolas Studer as described in section 2.5.5. Fecal DNA was sent to the MvP and microbiota analysis was performed by qPCR.

2.6.7 Reversible colitis model: *H. typhlonius* infection and CD45RB^{hi} T-cell transfer

The reversible colitis model was established in Prof. Mueller's lab (University of Bern) (Brasseit *et al.* 2016). Mouse experiments shown in this study were performed by Martin Faderl. Briefly, germfree RAG1^{-/-} mice were either cohoused with C57BL/6J Oligo-MM¹² mice for 20 days in order to allow vertical bacterial transmission or were directly associated with the Oligo-MM¹². 14 days prior to the adoptive transfer of 250,000 colitogenic CD4⁺ CD45RB^{high} CD25⁻ T-cells isolated from C57BL/6J wildtype mice, mice were orally inoculated with 2×10^8 CFUs of *H. typhlonius* CCUG48335T. In order to induce remission from colitis, mice were treated with 250 µg of α-CD4 antibody (or isotype as control) in 3 day intervals starting from day 24 post T-cell transfer. Mice were euthanized at day 34 post T-cell transfer and intestinal content was collected. The DNA of the colon content was extracted by Martin Faderl and sent to the MvP for microbiota analysis by qPCR. LCN-2 levels were measured in Bern.

2.6.8 Antibody mediated depletion of neutrophils

Neutrophils were depleted as described in (Trautwein-Weidner *et al.* 2014). Briefly, Oligo-MM¹² mice were treated with one dose of α-m Ly-6G (Table 36, 150 µg) or isotype control (intraperitoneal (i.p.)) one day before infection with 5×10^7 CFUs of *S. Tm*^{WT}. In addition, α-mouse G-CSF (Table 36, 10 µg) or isotype control were daily administered via i.p. injections.

2.6.9 Monitoring depletion of neutrophils by FACS

3 - 4 drops of blood were directly collected from the tail vein in 1.5 ml of pre-cooled FACS buffer (1x PBS and 1% heat inactivated FCS) and kept on ice until erythrolysis. For lysing the erythrocytes, blood samples were centrifuged (2 min; 4°C; 1,677 x g), the supernatant was discarded and the cell pellet was resuspended in 1 ml of BD FACSTM Lysing Solution (1:10 diluted in ddH₂O, Ampuwa) following 10 min of incubation in the dark at RT. The blood cells were then centrifuged again (2 min; 4°C; 1,677 x g), the supernatant was discarded and the white blood cells were resuspended in FACS buffer (100 µl

Material and Methods

per staining). Cells were subsequently stained with antibodies listed in Table 36 using the indicated dilutions (FC-block (α -CD16/CD32) also included). Antibodies were added and samples were incubated for 30 min at 4 °C, following a washing step with 200 μ l of FACS buffer and centrifugation (5 min; 4°C; 1,677 x g). The supernatant was discarded and cells were resuspended in 200 μ l of FACS buffer and transferred to FACS tubes. For staining dead cells, SYTOX red (5 nM) was added to the samples directly before measurement. In addition, compensation controls were performed with single stained BD™ CompBeads (BD) beads. The FACS analysis was performed with the FACSCANTO II (BD) and data were recorded using the BD FACSDiva™ software (BD). Data were analyzed by Dr. Tamas Dolowschiak using the FlowJo software.

2.6.10 Collection of mouse tissues

Sampling of feces during the course of the experiments was performed by two persons under sterile conditions as described previously in 2.6.4. Feces and cecal content was collected in sterile 1.5 ml plastic tubes. *Salmonella* loads in feces, cecal content, mesenteric lymphnodes, liver and spleen (taken post mortem) were determined by plating appropriate dilutions (undiluted, 1:200 and 1:40,000) on MacConkey agar plates (Oxoid) containing streptomycin (100 μ g/ml). Samples containing *C. rodentium* were plated on MacConkey agar plates without antibiotics. Feces and cecal content for DNA extraction were also taken and stored in 2 ml PCR grade plastic tubes at -80°C until DNA extraction and subsequent microbiota analysis. Tissues of cecum, colon, small intestine, liver as well as spleen were embedded in O.C.T (Sakura, Torrance), subsequently frozen in liquid nitrogen and stored at -80°C until histology. Cecal content was also resuspended in PBT for LCN-2 ELISA.

2.6.11 Hematoxylin eosin (HE) staining and histopathology

Tissues embedded in O.C.T were directly taken from the -80°C freezer, and 5 μ m cross-sections were prepared using a cryotome (Leica) and transferred onto Superfrost Plus glass slides. The sections were air dried for at least 24 h at RT, fixed in Wollman solution (95% ethanol, 5% acetic acid) for 30 sec, washed with flowing tap water for 1 min and rinsed with dH₂O. Subsequently, the sections were incubated in Vector's Hämalalaun solution for 20 min and rinsed again with tap water for 5 min (blueing). The slides were hereafter dipped 1 - 2 times in de-staining solution (70% ethanol, 1% HCl), washed with flowing tap water for 5 min and rinsed with dH₂O, 70% and 90% ethanol. The cross-sections were then stained with alcoholic eosin y solution for 20 sec and rinsed again with dH₂O. The cross-sections were then dehydrated in 90% and 100% ethanol as well as xylene and finally mounted using coverslips and Rotimount (Roth).

Histopathology of cecal tissues was performed microscopically with H&E stained cross-sections as described previously (Stecher *et al.* 2007). Briefly, the cecal pathology score is based on formation of

Material and Methods

submucosal edema (0 - 3), infiltration of polymorphonuclear neutrophils (PMNs) (0 - 4), loss of goblet cells (0 - 3) and epithelial damage (0 - 3). The combined pathological score was subsequently determined by summing up scores: 0 – 3: no pathological change, 4 – 8: mild inflammation, 9 – 13: severe inflammation.

2.7 Bioinformatics and statistics

2.7.1 RAST automated gene annotation

The assembled bacterial genomes were annotated using the RAST (Rapid Annotations using Subsystems Technology) online server, an automatic annotation service based on manually curated subsystems and on protein families (Aziz *et al.* 2008).

2.7.2 Statistics

CFU data, LCN-2 levels, CAS halo and pathoscores were expressed as median. More than two different groups were compared to each other using Kruskal-Wallis test, with Dunn's multiple comparison test. Two groups were compared using the Mann Whitney test (Prism 5; GraphPad Software, San Diego, CA, USA).

The percentage of individual bacteria was expressed as mean \pm standard deviation (SD). Differences between groups were compared using a two-way ANOVA, with Bonferroni posttest (Prism 5; GraphPad Software, San Diego, CA, USA). Growth curves and data from immune-fluorescence microscopy were also shown as mean \pm SD. Differences between multiple samples at one time point were compared using 1 way ANOVA with Bonferroni's multiple comparison test. The difference between two groups was compared using unpaired t test (Prism 5; GraphPad Software, San Diego, CA, USA).

To analyze clustering of qPCR data, both a qualitative measure (Pearson) and a quantitative one (Bray-Curtis) were used to calculate distance matrices containing dissimilarity values for each pairwise comparison. Strength and statistical significance of sample grouping were determined applying the nonparametric Adonis method based on the permutational multivariate ANOVA (PERMANOVA), together with the parametric significance test PERMDISP, which analyzes multivariate homogeneity of group dispersions. The used scripts are available in QIIME (Caporaso *et al.* 2010).

In all cases, p values < 0.05 were considered as statistically significant.

Fold changes in absolute abundance were calculated with absolute values that were normalized to a million gene copies determined by universal probe.

3. Results

3.1 Establishment of a qPCR assay for specific detection and quantification of bacterial strains

3.1.1 General considerations: SYBR green versus hydrolysis probe based qPCR

It was initially planned to establish a SYBR green based qPCR assay. This assay relies on two specific primers that target variable regions in the bacterial 16S rRNA gene and a fluorescent dye (SYBR green) that intercalates into double stranded DNA (dsDNA) and allows quantification of the PCR amplicon. First, endpoint PCR reactions were performed in order to investigate and improve primer specificity by applying different annealing temperatures and DMSO concentrations. Unfortunately, these protocols were not transferrable to the qPCR system because of different reaction conditions e.g. the DMSO concentration in the mastermix was unknown in the SYBR green master mix. On top of that, pioneering SYBR green qPCR runs proved that most primer pairs performed inefficiently (out of the range between 90 - 110% efficiency). Another downside was that primer dimers resulted in false positive results because SYBR green intercalates unspecifically in dsDNA. Since bacteria were differentiated based on polymorphisms in the 16S rRNA gene which limits positioning of primers, it was very likely that the primers formed dimers.

In order to increase the efficiency and to avoid the issue of primer dimers, a hydrolysis probe based qPCR assay for absolute quantification of bacterial strains was established. Therefore new primers and fluorescently labeled hydrolysis probes were designed using the software Primer Express 3 (Applied Biosystems). The hydrolysis probe, a third oligonucleotide that binds within the amplicon, further increased specificity. Indeed, this strategy finally resulted in efficient and specific detection of bacterial strains in gnotobiotic mice.

3.1.2 Design of strain-specific primers and hydrolysis probes

16S rRNA gene sequences of 12 Oligo-MM strains, 7 ASF strains as well *Salmonella enterica* serovar Typhimurium, *Citrobacter rodentium* (DBS100), *Helicobacter typhlonius* (CCUG48335T), *Clostridium difficile* (DH196), *Clostridium scindens* (ATCC35704), *Escherichia coli* (Mt1B1), *Streptococcus danieliae* (ERD01G) and *Staphylococcus xylosus* (33R13C) were aligned using CLC DNA Workbench 6.0.2 (CLC bio, Denmark) and 9 hypervariable (V) regions were subsequently identified. V regions were localized and positioned according to (Chakravorty *et al.* 2007) with V regions spanning the following nucleotide position: V1: 69 - 99, V2: 137 - 242, V3: 433 - 497, V4: 576 - 682, V5: 822 - 879, V6: 986 - 1043, V7: 1117 - 1173, V8: 1243 - 1294 and V9: 1435 - 1465. The positioning is based on the 16S rRNA gene of *E. coli* published by (Brosius *et al.* 1978). Strain-specific primers and hydrolysis probes

Results

targeted hypervariable regions V1 - V5 and V7 (Table 30, Figure 42). Primers and hydrolysis probes were either constructed for experiments shown in this study or for experiments performed in collaboration: the qPCR assay for *Clostridium scindens* (ATCC35704) was designed for infection experiments with *Clostridium difficile* (DH196) performed in collaboration with Prof. Siegfried Hapfelmeier and Nicolas Studer. The qPCR assays for the 7 ASF strains as well as *Escherichia coli* (Mt1B1), *Streptococcus danieliae* (ERD01G) and *Staphylococcus xylosus* (33R13C) were designed for experiments performed in collaboration with Sandrine Brugiroux and Simone Herp.

3.1.3 Optimization of primer and hydrolysis probe concentrations

In order to determine suitable concentrations of qPCR primers and hydrolysis probes, oligonucleotides were titrated (100 - 500 nM) using two different DNA template amounts (2,500,000 and 250 gene copies). The lowest primer and probe concentrations enabling early detection (low quantification cycle) using high and low DNA template amounts were regarded as optimal and finally chosen. Optimal qPCR performance was obtained using 300 nM of each primer and 250 nM of the corresponding hydrolysis probe (Figure 3). The titration test was performed with the following primer / probe combinations: YL2_Exonucl._fwd/rev with Probe_YL2, YL44_Exonucl._fwd/rev with Probe_YL44, YL45_Exonucl._fwd/rev with Probe_YL45, YL58_Exonucl._fwd/rev with Probe_YL58, Isol46_Exonucl._fwd/rev with Probe_Isol46, Isol49_Exonucl._fwd/rev with Probe_Isol49, Isol48_Exonucl._fwd/rev with Probe_Isol48. The example shown in (Figure 3) is representative for all primer and probe titration experiments.

Results

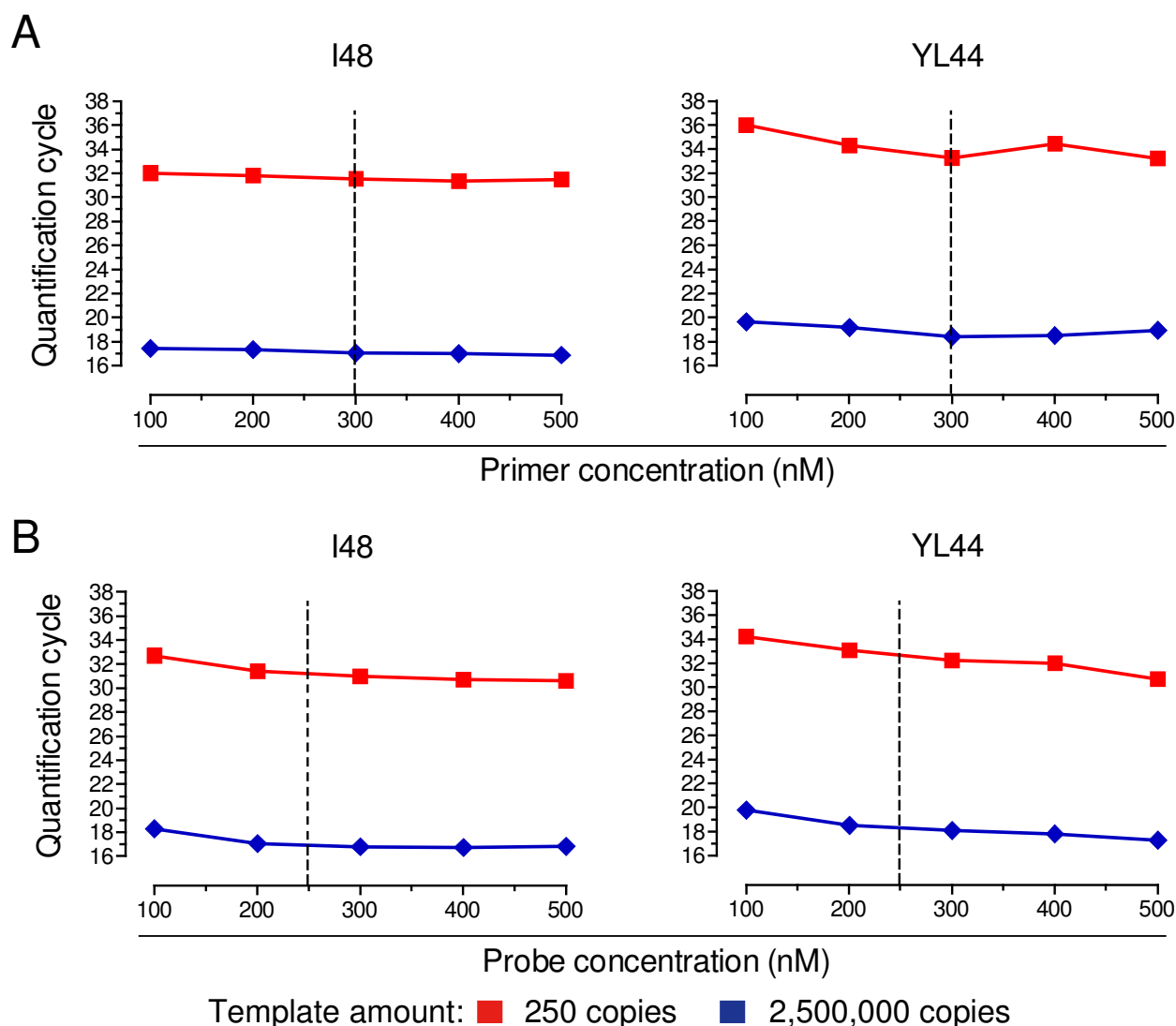


Figure 3: Optimization of primer and hydrolysis probe concentrations. Different concentrations (100 - 500 nM) of **(A)** forward and reverse primers as well as **(B)** hydrolysis probes were tested with different amounts of linearized plasmid template DNA (250 (red) and 2,500,000 (blue) gene copies). An equimolar concentration of forward and reverse primers was applied for qPCR reactions. In order to optimize the primer concentrations, the concentration of the probe was kept constant (200 nM) and the primers were titrated. The optimal primer concentration was found to be 300 nM. The optimal concentration of the hydrolysis probe (250 nM) was identified with qPCR reactions using 300 nM of each primer. qPCR reactions shown in this example were performed with the following primer / probe combinations: Isol48_Exonucl._fwd/rev with Probe_Isol48 and YL44_Exonucl._fwd/rev with Probe_YL44 and respective template DNA. Dashed lines indicate optimal primer and probe concentrations.

Results

3.1.4 Multiplexing and qPCR performance

Duplex qPCR reactions were performed order to increase speed and lower costs of the qPCR assays. A duplex qPCR reaction is based on two differently labeled hydrolysis probes (FAM or HEX), targeting different strains to be detected within one qPCR reaction. For duplex reactions, primers and probes with similar qPCR efficiencies and endpoint fluorescence levels were combined. In addition, in order to guarantee detection of low amounts of DNA template, duplex qPCR reactions were performed targeting trace amounts of template A in the presents of excessive DNA amounts of template B and vice versa (Figure 4C,D). qPCR efficiencies, R^2 values, slopes and Y-intercepts listed in Table 39 are all derived from standard curves with 10-fold dilutions of template DNA performed in either mono- or duplex qPCR reactions (Figure 4A). Plasmid pools were used to determine unspecific amplification. Since evaluation of primers and hydrolysis probes was based on plasmid DNA, gDNA was additionally applied to verify detection of real strains (Figure 4B).

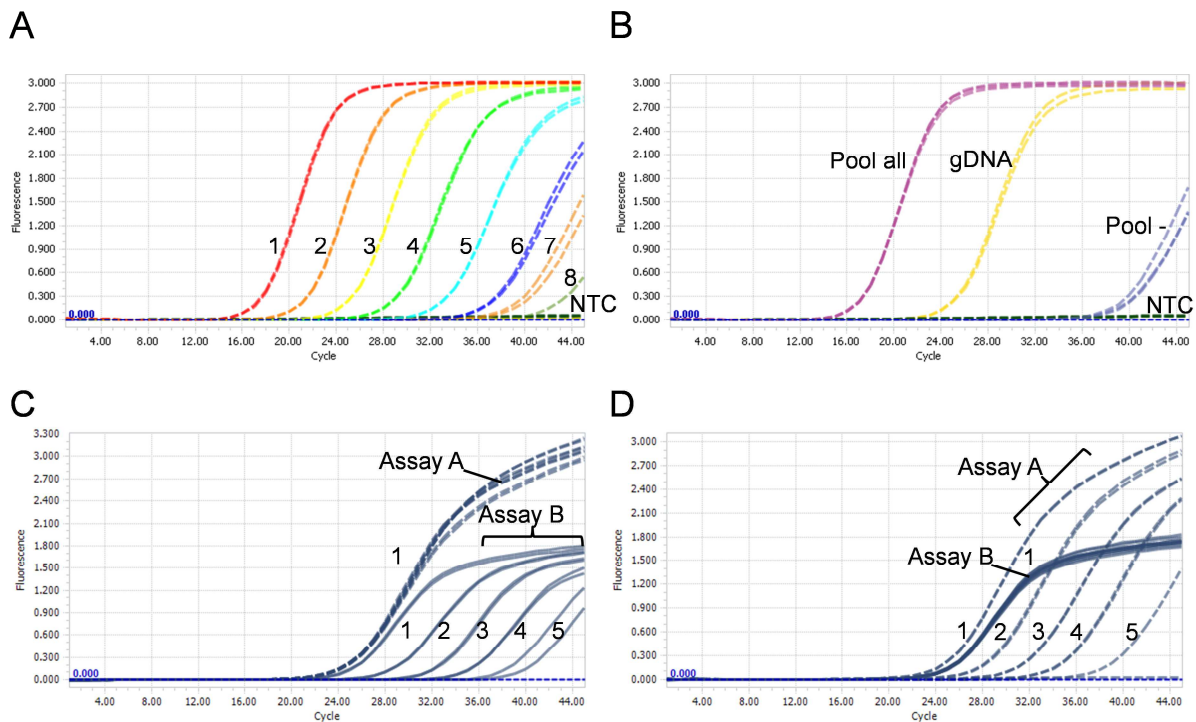


Figure 4: Example of qPCR performances. (A) A standard curve was performed in triplicates with 10-fold dilutions of linearized plasmid ranging from 2,500,000 - 0.025 copies. Amplification curves with a distance of around 3.33 cycles were observed between 10-fold dilutions down to 2.5 copies (1 - 7), whereas 0.25 (8) and 0.025 copies could not be detected by the qPCR assay (ASF502_Exonucl.3_fwd/rev and Probe3_ASF502(SB2)). (B) Specificity test with plasmid pools with an equimolar mixture of either all plasmids (pool all; 2,500,000 copies / strain), or a mixture including all but the DNA of the strain to be tested (pool -) and genomic DNA (gDNA). NTC: non template control. (C) and (D) control experiment for duplex assays: The amount of template DNA of either assay A or B was kept at 25,000 gene copies whereas the template amount of the duplex partner was diluted in 10-fold steps to 2.5 gene copies. 1 - 5: 25,000 - 2.5 gene copies; the standard curves were performed in duplicates.

Results

Table 39: Performance of primer / probe combinations in mono and duplex qPCR reactions

qPCR assay partners (targeted strain)	Standard curve (duplex)				Standard curve (monoplex)				LOD ^A
	Sl.*	Y-int. [#]	E ^S	R ^{2S}	Sl.	Y-int.	E	R ²	
Isol46_Exonucl.2_fwd/.3_rev Probe3_Isol46 (<i>Clostridium innocuum</i> I46)	-3.25	38.73	103%	0.99	-3.48	39.89	94%	1	100
Isol49_Exonucl.2_fwd/rev Probe_Isol49 (<i>Lactobacillus reuteri</i> I49)	-3.41	37.04	96%	1	-3.37	36.59	98%	0.99	306
YL58_Exonucl.2_fwd/rev Probe_YL58 (<i>Blautia coccooides</i> YL58)	-3.60	39.65	90%	0.98	-3.31	38.74	101%	1	113
YL27_Exonucl.2_fwd/.2_rev Probe2_YL27 (‘ <i>Muribaculum intestinale</i> ’ YL27)	-3.26	35.16	103%	0.99	-3.25	34.93	103%	0.99	4
YL31_Exonucl.2_fwd/.3_rev Probe2_YL31 (<i>Flavonifractor plautii</i> YL31)	-3.47	40.54	94%	1	-3.49	40.82	93%	0.99	4 (LOD ₉₅)
YL32_Exonucl.2_fwd/.2_rev Probe2_YL32 (<i>Clostridium clostridioforme</i> YL32)	-3.55	35.95	91%	1	-3.47	35.45	94%	0.99	4
KB18_Exonucl.2_fwd/.2_rev Probe2_KB18 (‘ <i>Acutalibacter muris</i> ’ KB18)	-3.24	40.83	104%	0.99	-3.39	41.24	97%	0.99	1 (LOD ₉₅)
YL44_Exonucl.2_fwd/rev Probe_YL44 (<i>Akkermansia muciniphila</i> YL44)	-3.27	38.82	102%	0.99	-3.32	39.36	100%	1	10
KB1_Exonucl.2_fwd/rev Probe_KB1 (<i>Enterococcus faecalis</i> KB1)	-3.51	41.41	93%	0.99	-3.49	41.29	93%	1	25 (as. sp.)
YL2_Exonucl.2_fwd/rev Probe_YL2 (<i>Bifidobacterium longum</i> <i>subsp. animalis</i> YL2)	-3.17	40.79	107%	0.98	-3.39	41.81	97%	1	13 (LOD ₉₅)
YL45_Exonucl.2_fwd/rev Probe_YL45 (‘ <i>Turicimonas caecimuris</i> ’ YL45)	-3.39	41.64	97%	0.99	-3.13	40.76	109%	0.99	2 (LOD ₉₅)
Isol48_Exonucl.2_fwd/rev Probe_Isol48 (‘ <i>Bacteroides caecimuris</i> ’ I48)	-3.48	39.57	94%	0.99	-3.27	38.23	102%	0.99	21
ASF356_Exonucl.2_fwd/.2_rev Probe2_ASF356 (<i>Clostridium</i> spp. ASF356)	-3.32	41.16	100%	0.99	-3.21	40.93	105%	0.99	5
ASF361_Exonucl.2_fwd/rev Probe_ASF361 (<i>Lactobacillus murinus</i> ASF361)	-3.58	38.70	90%	1	-3.32	37.78	100%	0.98	11
ASF457_Exonucl.2_fwd/rev Probe_ASF457 (<i>Mucispirillum schaedleri</i> ASF457)	-3.12	39.12	109%	1	-3.39	41.05	97%	1	9
ASF519_Exonucl.2_fwd/rev Probe_ASF519 (<i>Parabacteroides goldsteinii</i> ASF519)	-3.42	38.38	96%	1	-3.37	38.09	98%	0.99	25 (as. sp.)
ASF360_Exonucl.4_fwd/.4_rev Probe4_ASF360 (<i>Lactobacillus intestinalis</i> ASF360)	-3.29	36.78	101%	1	-3.28	37.10	102%	1	25 (as. sp.)

Results

qPCR assay partners (targeted strain)	Standard curve (duplex)				Standard curve (monoplex)				LOD [^]
	Sl.*	Y-int. [#]	E [§]	R ^{2§}	Sl.	Y-int.	E	R ²	
ASF500_Exonucl._fwd/rev Probe_ASF500 (<i>Pseudoflavonifactor</i> spp. ASF500)	-3.36	37.17	99%	0.99	-3.38	37.14	98%	0.99	31
ASF502_Exonucl.3_fwd/.3_rev Probe3_ASF502(SB2) (<i>Clostridium</i> spp. ASF502)	NA	NA	NA	NA	-3.58	38.71	90%	0.97	5
Salmo_Exonucl._fwd/rev Probe_Salmo (<i>Salmonella</i> Typhimurium)	NA	NA	NA	NA	-3.22	37.04	104%	0.99	25 (as. sp.)
C.rod_Exonucl._fwd/rev Probe_C.rod (<i>Citrobacter rodentium</i>)	NA	NA	NA	NA	-3.65	37.06	90%	1	2500 (as. sp.)
H.typh_Exonucl.2_fwd/.2_rev Probe2_H.typhlonius (<i>Helicobacter typhlonius</i>)	NA	NA	NA	NA	-3.34	39.02	99%	0.99	4 (LOD ₉₅)
C.diff_Exonucl._fwd/rev Probe_C.difficile (<i>Clostridium difficile</i>)	NA	NA	NA	NA	-3.26	36.52	103%	0.98	25 (as. sp.)
E.coli_Exonucl._fwd/rev Probe_E.coli(Mt1B1) (<i>Escherichia coli</i>)	NA	NA	NA	NA	-3.16	35.83	107%	1	25 (as. sp.)
Strep._Exonucl._fwd/rev Probe_Strep.daniel. (<i>Streptococcus danieliae</i>)	NA	NA	NA	NA	-3.34	38.68	99%	1	3
Staph._Exonucl._fwd/rev Probe_Staph.xylosus (<i>Staphylococcus xylosus</i>)	NA	NA	NA	NA	-3.46	40.98	95%	1	25 (as. sp.)
C.scin_Exonucl._fwd/rev Probe_C.scindens (<i>Clostridium scindens</i>)	NA	NA	NA	NA	-3.45	39.68	95%	1	25 (as. sp.)
Univ_Exonucl.3_fwd/rev Probe2_Univ. (all strains but <i>C.diff.</i>)	NA	NA	NA	NA	-3.36	35.69	99%	1	2500
Univ_Exonucl.3_fwd/rev Probe3_Univ. (<i>C.diff.</i> + <i>C.scind.</i> + Oligo-MM)	NA	NA	NA	NA	-3.40	38.97	97%	1	2500

*Sl.: slope of the standard curve; [#]Y-int.: Y-intercept of the standard curve; [§]E: qPCR efficiency; in case qPCR efficiency is 100%, the DNA amount will double per qPCR cycle; [§]R²: Regression coefficient (a value of 1 indicates a perfect fit between the regression line of the standard curve and the data points); the qPCR assays were validated with standard curves performing either mono- or duplex qPCR reactions; [^]LOD: limit of detection that was either (i) the LOD₉₅ (DNA template amount that results in above threshold signals in 95% of the qPCR runs, determined with duplex qPCR reactions), (ii) the assay specific limit (as. sp.): until the qPCR assay is dynamic (around 3.3 Cqs decrement between 1:10 dilutions and high endpoint fluorescence levels), or (iii) if higher, the gene copy number derived from unspecific amplification with pooled plasmid DNA of the remaining strains; for the Univ qPCR assay, the LOD is the gene copy number derived from signals of the non template control (NTC); NA: not available.

Results

3.2 Composition and characteristics of the Oligo-MM¹²

3.2.1 Selection of strains constituting the Oligo-Mouse-Microbiota (Oligo-MM¹²)

12 Bacterial strains that constitute the Oligo-MM (Figure 5; Table 2) were isolated from the intestinal content of specific pathogen free (SPF) mice as described in (Brugiroux *et al.* 2016). Isolation was performed by Yvonne Loetscher, Ricco Robbiani and Sandrine Brugiroux. The aim was to establish a model microbiota that covers the main bacterial phyla of the intestinal microbiota of laboratory mice. Finally, 12 strains that grew reliably after freezing were selected. Remarkably, these 12 strains covered 5 main phyla. 6 strains could be assigned to the phylum Firmicutes ('*Acutalibacter muris*' KB18, *Flavonifractor plautii* YL31, *Clostridium clostridioforme* YL32, *Blautia coccoides* YL58, *Clostridium innocuum* I46, *Lactobacillus reuteri* I49 and *Enterococcus faecalis* KB1), two strains to the Bacteroidetes ('*Bacteroides caecimuris*' I48, '*Muribaculum intestinale*' YL27), one strain to the Actinobacteria (*Bifidobacterium longum* subsp. *animalis* YL2), one strain to the β -Proteobacteria ('*Turicimonas muris*' YL45) and one strain to the Verrucomicrobia (*Akkermansia muciniphila* YL44) (Figure 5). It is worth mentioning that '*Muribaculum intestinale*' YL27 is a member of a novel family ('Muribaculaceae') and that the strains KB18 and YL45 are representatives of novel genera within the Lachnospiraceae ('*Acutalibacter muris*') and Sutterellaceae ('*Turicimonas muris*'), respectively. Strain I48 is proposed to be a novel species ('*Bacteroides caecimuris*'). Additional information of taxonomic classification is detailed in (Brugiroux *et al.* 2016). Protocols of bacterial culture and cryopreservation were established by Sandrine Brugiroux (PhD thesis of Sandrine Brugiroux).

Results

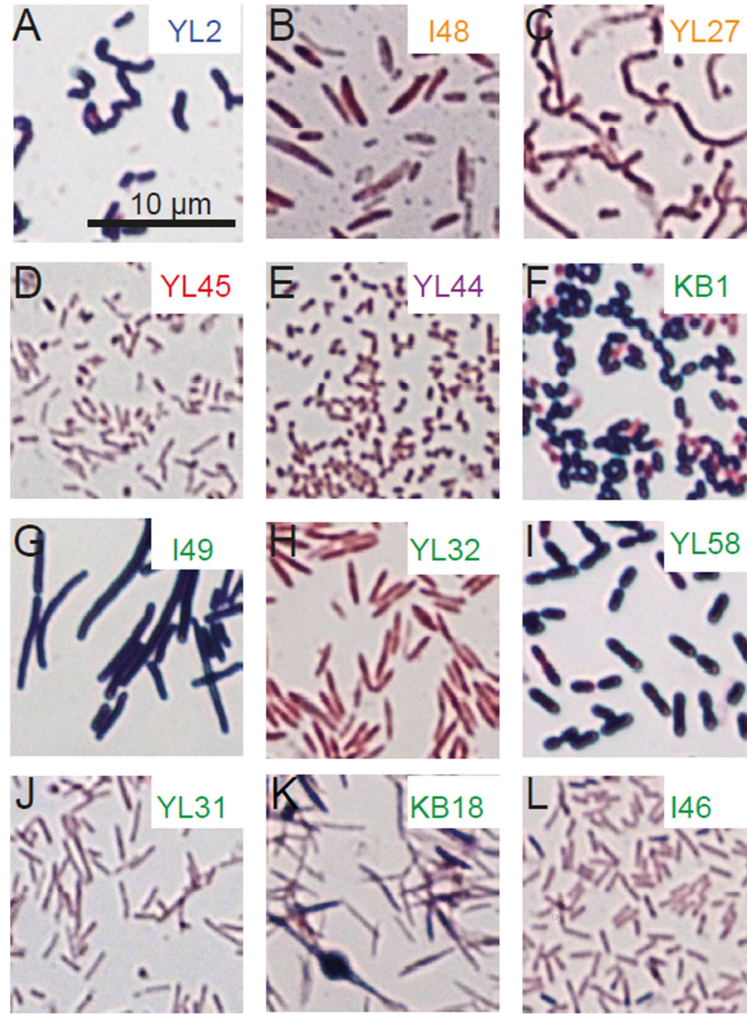


Figure 5: 12 strains constituting the Oligo-Mouse-Microbiota (Oligo-MM¹²). Gram-staining and light microscopy (100-fold magnification, oil immersion) of individually grown strains in liquid culture is shown (Brugiroux *et al.* 2016). Color code based on phylogeny of Oligo-MM¹² strains: blue: Actinobacteria, orange: Bacteroidetes, red: Proteobacteria, purple: Verrucomicrobia and green: Firmicutes. Representatives of the Bacteroidetes, Proteobacteria and Verrucomicrobia phyla ('*Bacteroides caecimuris*' I48, '*Muribaculum intestinale*' YL27, '*Turicimonas caecimuris*' YL45 and '*Akkermansia muciniphila*' YL44) stained Gram-negative. '*Bifidobacterium longum* subsp. *animalis*' YL2 (Actinobacteria) as well as '*Enterococcus faecalis*' KB1, '*Lactobacillus reuteri*' I49 and '*Blautia coccoides*' YL58 (Firmicutes) appear Gram-positive. In contrast, the other Firmicutes strains ('*Flavonifractor plautii*' YL31, '*Clostridium clostridioforme*' YL32, '*Acutalibacter muris*' KB18 and '*Clostridium innocuum*' I46) are stained Gram-negative or Gram-variable. Scale bar: 10 µm.

3.2.2 The Oligo-MM¹² matures and stably colonizes germfree mice

In order to monitor early colonization of the Oligo-MM¹² and its changes in composition over time, germfree C57BL/6J AGR2^{+/-} mice which develop a wild type like mucus layer (Bergström *et al.* 2014) were inoculated with a frozen mixture of Oligo-MM¹² strains. Feces was taken at the indicated time points (Figure 6A) and the microbiota composition was analyzed using strain-specific qPCR. Microbiota was clustered in 3 different stages (maturation stage): early: day 1, intermediate: from days 2 - 4 post inoculation (p.in.) and stable: after day 6 p.in. (Figure 6; Table 40). Clustering by

Results

maturation stage was significant, according to Bray Curtis ($p < 0.001$, Adonis) and Pearson ($p < 0.001$, Adonis) correlation with 66% (Bray Curtis) and 78% (Pearson) of variation explained. Additional PERMDISP analyses based on Bray Curtis and Pearson distance matrices revealed statistically significant differences in microbiota composition between early, intermediate and stable maturation stage (Figure 6B,C). The initial early stage at day 1 p.in. was dominated by *Akkermansia muciniphila* YL44 (mean: 64.01% +/- standard deviation: 27.68%), 'Bacteroides caecimuris' I48 (27.38% +/- 28.42%) and *Bifidobacterium longum* subsp. *animalis* YL2 (6.36% +/- 2.69%). The Firmicutes, 'Muribaculum intestinale' YL27 as well as 'Turicimonas caecimuris' YL45 were less abundant in this early stage. The most prevalent strain of the second stage of maturation, the intermediate stage, was 'Bacteroides caecimuris' I48 (75.70% +/- 8.29%). Its presence was significantly increased compared to early stage ($p < 0.001$, two-way ANOVA with Bonferroni posttest). 'Turicimonas caecimuris' YL45 and 'Muribaculum intestinale' YL27 increased by trend in this stage. The relative abundance of the Firmicutes was not altered, only *Flavonifractor plautii* YL31 slightly increased. Compared to early phase, the relative abundance of *Akkermansia muciniphila* YL44 (13.07% +/- 6.16%) significantly decreased ($p < 0.001$, two-way ANOVA with Bonferroni posttest). Remarkably, the abundance of *Bifidobacterium longum* subsp. *animalis* YL2 dropped down to (1.40% +/- 1.56%) in this intermediate stage. From day 7 post inoculation on, the composition of the Oligo-MM¹² was considered to be stable (Figure 6). The most abundant strains in this stage were 'Bacteroides caecimuris' I48 (57.52% +/- 9.31%), *Akkermansia muciniphila* YL44 (21.97% +/- 8.84%) and 'Muribaculum intestinale' YL27 (12.85% +/- 3.16%). In comparison to intermediate stage the relative abundance of 'Bacteroides caecimuris' I48 decreased, whereas the relative abundance of 'Muribaculum intestinale' YL27 and *Akkermansia muciniphila* YL44 increased ($p < 0.001$, two-way ANOVA with Bonferroni posttest). The relative abundance of 'Turicimonas caecimuris' YL45 and the Firmicutes was not changed compared to intermediate stage, whereas *Bifidobacterium longum* subsp. *animalis* YL2 was hardly detectable in stable stage. 'Acutalibacter muris' KB18 was only detectable in the inoculum, and undetectable or very close to the limit of detection in fecal DNA samples during all stages of maturation. The relative abundance of the Oligo-MM¹² strains in all 3 stages of maturation is summarized in (Table 40).

Results

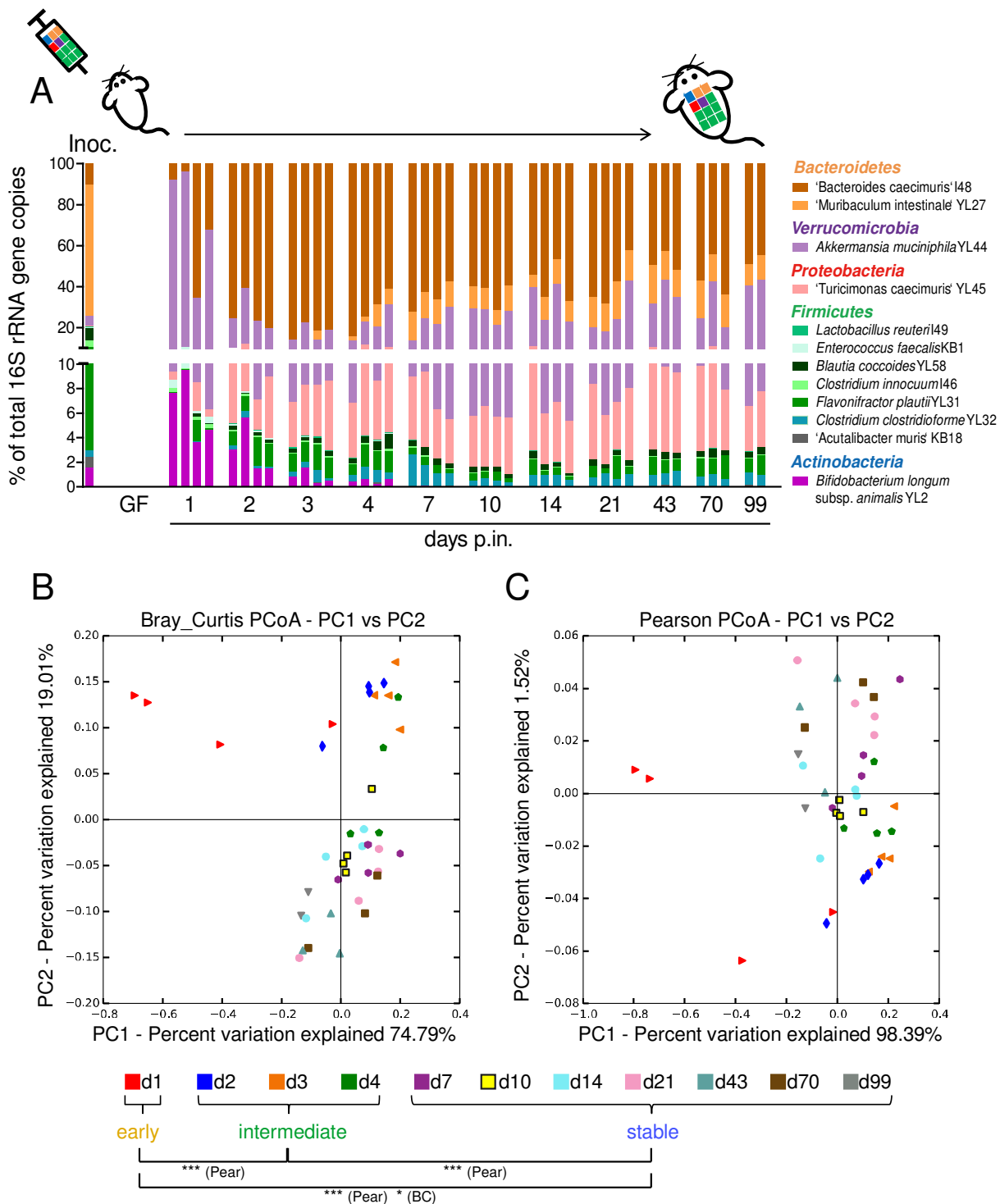


Figure 6: Changes in Oligo-MM¹² community composition over time after inoculation of germfree mice. Germfree (GF) C57BL/6J AGR2^{+/+} which exhibit wildtype like mucus layer (Bergström *et al.* 2014) were orally and rectally inoculated with freshly thawed cryostocks containing the Oligo-MM¹² strains and housed in a germfree isolator. **(A)** Fecal samples were sampled at the indicated time points (GF - day 99 post inoculation), the fecal DNA was extracted using a modified protocol for DNA stool kit (Qiagen) and microbiota composition was analyzed by qPCR. Microbiota composition is shown as relative abundance and is expressed as % of cumulated 16S rRNA gene copy numbers (% of total 16S rRNA gene copies). Cluster analysis based on Bray Curtis **(B)** or Pearson **(C)** distance matrices visualized as PCoA plots. Fecal microbiota samples were grouped by maturation stage of the Oligo-MM¹² in 'early' (day 1 post inoculation), 'intermediate' (days 2, 3 and 4 post inoculation) and 'stable' (from days 7 post inoculation on) which was significant, according to Bray Curtis ($p < 0.001$, Adonis) and Pearson ($p < 0.001$, Adonis) with 66% (Bray Curtis) and 78% (Pearson) of variation explained. PERMDISP analyses

Results

based on Bray Curtis and Pearson distance matrices revealed statistically significant differences in microbiota composition between early, intermediate and stable (*p<0.05, *** p<0.001).

Table 40: Relative abundance of individual Oligo-MM¹² strains at different maturation stages

Strain	Mean % of cumulated 16S rRNA gene copy numbers (+/- SD)		
	Maturation grade		
	early	intermediate	stable
'Bacteroides caecimuris' l48	27.38 (28.42)	75.70 ^a (8.29)	57.52 ^{b,c} (9.31)
'Muribaculum intestinale' YL27	0*	2.25 (3.57)	12.85 ^{b,c} (3.16)
<i>Akkermansia muciniphila</i> YL44	64.01 (27.68)	13.07 ^a (6.16)	21.97 ^{b,c} (8.84)
'Turicimonas caecimuris' YL45	0.89 (1.02)	4.74 (1.23)	5.26 (1.36)
<i>Lactobacillus reuteri</i> l49	0.02 (0.02)	0.05 (0.03)	0.01 (0.02)
<i>Enterococcus faecalis</i> KB1	0.50 (0.20)	0.07 (0.05)	0.001 (0.003)
<i>Blautia coccooides</i> YL58	0.07 (0.13)	0.43 (0.28)	0.46 (0.12)
<i>Clostridium innocuum</i> l46	0.27 (0.12)	0.12 (0.03)	0.05 (0.02)
<i>Flavonifractor plautii</i> YL31	0.48 (0.86)	1.61 (0.42)	0.89 (0.50)
<i>Clostridium clostridioforme</i> YL32	0.02 (0.02)	0.53 (0.33)	0.96 (0.44)
'Acutalibacter muris' KB18	0*	0.01 (0.03)	0.02 (0.05)
<i>Bifidobacterium longum</i> subsp. <i>animalis</i> YL2	6.36 (2.69)	1.40 (1.56)	0.01 (0.02)

Significant differences between groups are indicated with **a** for early vs intermediate, **b** for early vs stable and **c** for intermediate vs stable; p values were less than 0.001, two-way ANOVA with Bonferroni posttest. Values are indicated as mean % of cumulated 16S rRNA gene copy numbers +/- standard deviation (SD). Early: n=4, intermediate: n=12, stable n=24. *Very low abundant.

Results

3.2.3 The Oligo-MM¹² is vertically transmitted and remains stable over 6 filial generations

It was further investigated whether the Oligo-MM¹² that stably colonizes mice is vertically transmitted from parental mice to offspring and whether the consortium is stable over filial generations. By breeding C57BL6/J mice associated with Oligo-MM¹² in germfree isolators and analyzing fecal DNA by qPCR, it could be shown that the Oligo-MM¹² is vertically transmitted after a single gavage of Oligo-MM¹² strains. Moreover, the composition of the Oligo-MM¹² was stable over at least 6 filial generations. *Bifidobacterium longum* subsp. *animalis* YL2 was not detected in fecal samples and 'Acutalibacter muris' KB18 was detectable in samples of the parental (P) and filial generation 1 (F2 - F6 below limit of detection; Figure 7; Table 41). Although the composition of the microbiota was stable overall, there were statistically significant alterations in relative abundance of 'Bacteroides caecimuris' I48 and *Akkermansia muciniphila* YL44 between generations F1 - F4 (Table 41). Of note, P and F1 generation were housed at the CMF in Bern and F2 – F6 at the gnotobiotic facility of the MvP in Munich.

Cluster analysis was performed on relative abundance of the strains. According to Bray Curtis ($p < 0.001$, Adonis) and Pearson ($p < 0.005$, Adonis) distance matrices, grouping of microbiota composition by generations was significant, with 65% (Bray Curtis) and 77% (Pearson) of variation explained (Figure 7B,C). Non parametric PERMDISP procedure revealed that the Oligo-MM¹² composition of the P generation differed compared to the filial generations (Figure 7B,C). There was also a significant difference in microbiota composition between generations F3 and F4 ($p < 0.05$, non parametric PERMDISP procedure according to Pearson correlation). However, according to Bray Curtis distance there was no statistically significant difference between Oligo-MM¹² communities of the filial generations, indicating that the Oligo-MM¹² remains relatively stable over generations.

Results

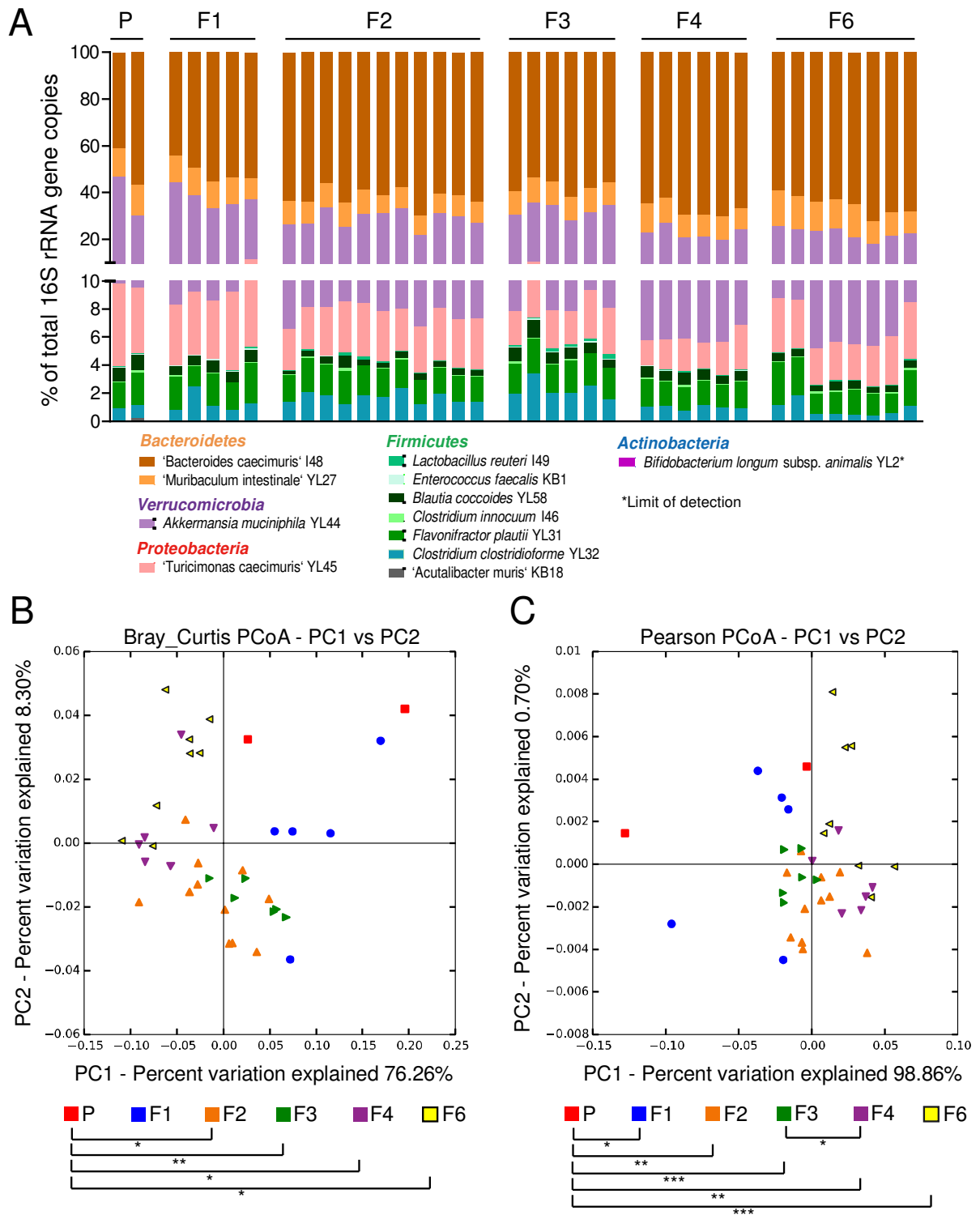


Figure 7: The Oligo-MM¹² is vertically transmitted and stable over 6 filial generations. (A) C57BL/6J mice associated with the Oligo-MM¹² consortium were bred in germfree isolators until filial generation 6 (F6). The inoculation of the parental generation (P) as well as the breeding of F1 generation took place at the CMF in Bern. The generations F2 – F6 were subsequently bred at the gnotobiotic mouse facility of the MvP in Munich. Fecal samples were collected, the fecal DNA was extracted and qPCR was performed in order to determine the microbiota composition in each generation. Microbiota composition is shown as relative abundance and is expressed as % of cumulated 16S rRNA gene copy numbers (% of total 16S rRNA gene copies). Cluster analysis based on Bray Curtis (B) or Pearson (C) distance matrices visualized as PCoA plots. Grouping by generations was significant, according to Bray Curtis ($p < 0.001$, Adonis) and Pearson ($p < 0.005$, Adonis) with 65% (Bray Curtis) and 77% (Pearson) of variation explained. PERMDISP analyses based on Bray Curtis and Pearson distance matrices

Results

revealed statistically significant differences in microbiota composition between groups, especially between the parental and the filial generations (* $p < 0.05$, ** $p < 0.01$, *** $p < 0.001$).

Table 41: Stability of Oligo-MM¹² community over consecutive mouse filial generations

Strain	Mean % of cumulated 16S rRNA gene copies (+/- SD)					
	Generations					
	P	F1	F2	F3	F4	F6
'Bacteroides caecimuris' I48	49.09 (11.00)	51.38 (4.67)	61.96 ^a (3.87)	57.38 ^b (3.04)	67.17 ^c (3.16)	65.23 (4.19)
'Muribaculum intestinale' YL27	12.63 (0.98)	10.89 (1.14)	9.15 (0.94)	10.21 (0.34)	10.16 (1.30)	12.23 (2.28)
<i>Akkermansia muciniphila</i> YL44	28.60 (11.77)	28.36 (4.70)	21.17 ^a (3.36)	23.90 ^b (2.60)	16.73 ^c (2.43)	15.84 (2.08)
'Turicimonas caecimuris' YL45	5.32 (0.83)	4.97 (0.89)	3.40 (0.30)	2.83 (0.45)	2.30 (0.50)	3.22 (0.59)
<i>Lactobacillus reuteri</i> I49	0.05 (0.01)	0.03 (0.04)	0.11 (0.06)	0.21 (0.07)	0.06 (0.03)	0.05 (0.02)
<i>Enterococcus faecalis</i> KB1	0.08 (0.03)	0.08 (0.04)	0.01 (0.01)	0.05 (0.02)	0.02 (0.01)	0*
<i>Blautia coccoides</i> YL58	1.03 (0.11)	0.77 (0.11)	0.45 (0.16)	0.86 (0.24)	0.73 (0.11)	0.53 (0.07)
<i>Clostridium innocuum</i> I46	0.13 (0.04)	0.06 (0.02)	0.07 (0.04)	0.09 (0.03)	0.09 (0.04)	0.11 (0.04)
<i>Flavonifractor plautii</i> YL31	2.06 (0.33)	2.19 (0.53)	2.02 (0.24)	2.25 (0.14)	1.77 (0.12)	2.00 (0.65)
<i>Clostridium clostridioforme</i> YL32	0.94 (0.06)	1.27 (0.72)	1.67 (0.38)	2.24 (0.65)	0.99 (0.14)	0.82 (0.50)
'Acutalibacter muris' KB18	0.10 (0.13)	0.01 (0.03)	DTL	DTL	DTL	DTL
<i>Bifidobacterium longum</i> subsp. <i>animalis</i> YL2	DTL	DTL	DTL	DTL	DTL	DTL

Significant differences between groups are indicated with **a** for F1 vs F2, **b** for F2 vs F3 and **c** for F3 vs F4; p values were less than 0.001, except: YL44 F2 vs F3 $p < 0.05$, two-way ANOVA with Bonferroni posttest. There were no statistically significant difference in microbiota composition between P and F1 and between F4 and F6. Values are expressed as mean % of cumulated 16S rRNA gene copy numbers +/- standard deviation (SD). P: $n=2$, F1: $n=5$, F2: $n=11$, F3: $n=6$, F4: $n=6$, F6: $n=8$. DTL: below limit of detection. *Very low abundant.

Results

3.2.4 The composition of the Oligo-MM¹² is comparable between different animal facilities

The Oligo-MM¹² was designed to be used as a standardized mouse microbiota that can be easily distributed and shared between different laboratories, in order to generate isobiotic mice. C57BL6/J mice associated with the Oligo-MM¹² were generated at the CMF in Bern in 2012 and distributed to the Mvp in Munich as well as to the ETHZ and further bred in germfree isolators. To investigate differences in microbiota composition between the different facilities, fecal samples were obtained and analyzed using the same DNA extraction protocol and strain-specific qPCR (Figure 8). Overall, the Oligo-MM¹² composition was comparable between the CMF (mice from isolators or individually ventilated cages (IVC)), the MvP or the ETHZ. However, statistically significant differences in relative abundance of 'Bacteroides caecimuris' I48, 'Muribaculum intestinale' YL27, *Akkermansia muciniphila* YL44 and 'Turicimonas caecimuris' YL45 were observed between animal facilities (Table 42). Compared to the Oligo-MM¹² composition of mice bred at the MvP, the microbiota composition of the CMF-IVC differed the most (Figure 8; Table 42). 'Bacteroides caecimuris' I48 was around 17% less abundant in CMF-IVC ($p < 0.001$, two-way ANOVA with Bonferroni posttest), whereas the relative abundance of 'Muribaculum intestinale' YL27, *Akkermansia muciniphila* YL44 and 'Turicimonas caecimuris' YL45 was increased ($p < 0.001$, two-way ANOVA with Bonferroni posttest; Table 42; Figure 8). *Bifidobacterium longum* subsp. *animalis* YL2 was not detectable in fecal samples taken in the CMF and MvP. *Bifidobacterium longum* subsp. *animalis* YL2 could be detected in one sample of the ETHZ, but was otherwise under the limit of detection. 'Acutalibacter muris' KB18 was below the limit of detection in Oligo-MM¹² mice of the MvP.

In addition, cluster analysis was performed on relative abundance of the strains. According to Bray Curtis ($p < 0.001$, Adonis) and Pearson ($p < 0.001$, Adonis) distance matrices, grouping of microbiota composition by the different animal facilities was significant, with 53% (Bray Curtis) and 72% (Pearson) of variation explained (Figure 8B,C). The Oligo-MM¹² compositions of the different facilities clustered similarly (Figure 8B,C). However, non parametric PERMDISP procedure according to Bray Curtis revealed significant differences ($p < 0.01$) between microbiota compositions of mice bred at the MvP and CMF-IVC. Additionally based on Pearson, the Oligo-MM¹² composition of the MvP was significantly different compared to the Oligo-MM¹² compositions of mice bred at the ETHZ and CMF ($p < 0.01$, non parametric PERMDISP procedure; Figure 8B,C). There was no statically significant difference in microbiota composition between the CMF and ETHZ (Figure 8B,C).

Results

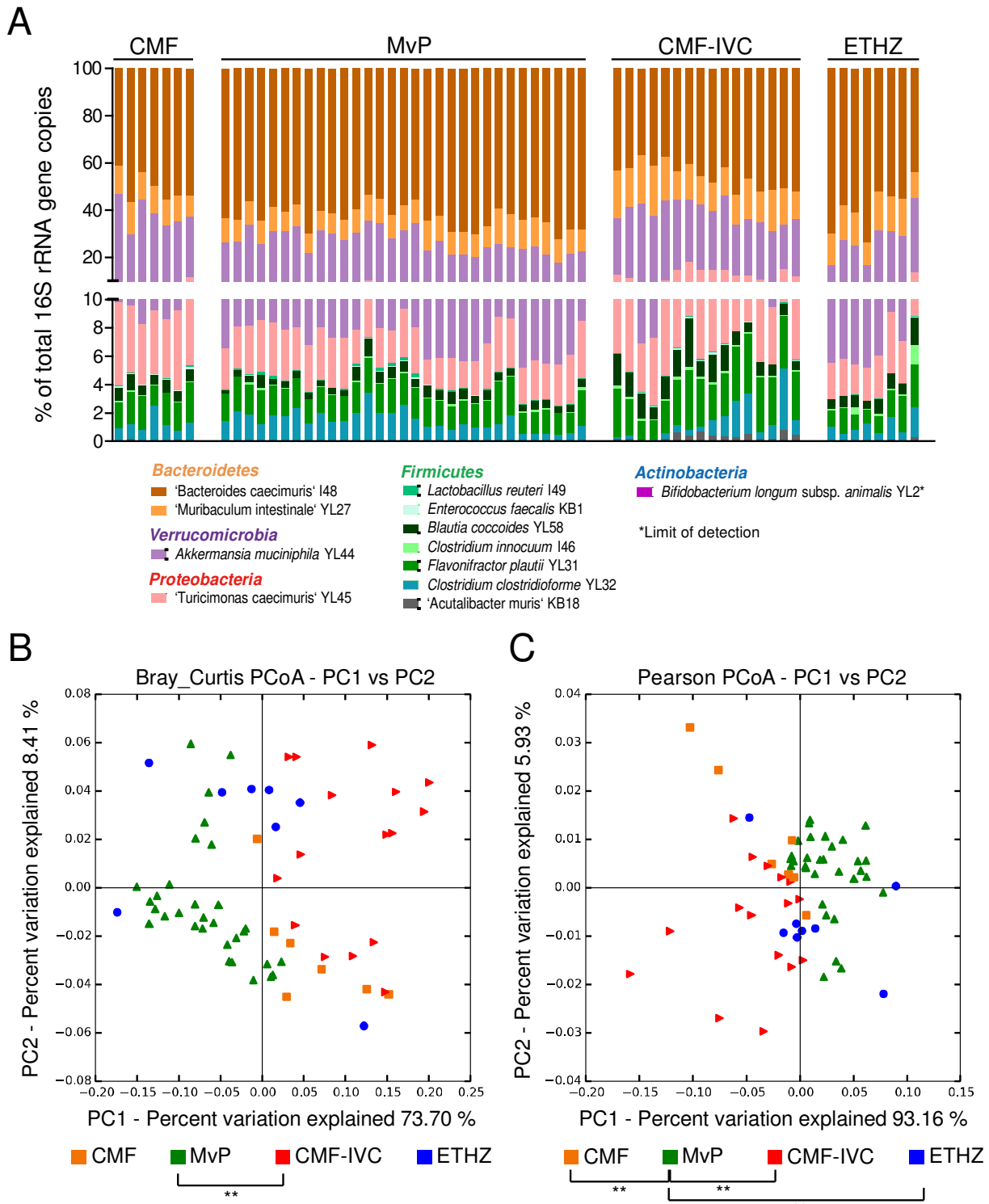


Figure 8: Composition of Oligo-MM¹² between different animal facilities. Fecal sample from mice associated with the Oligo-MM¹² were sampled, the DNA was extracted using the same DNA extraction protocol (modified stool kit, Qiagen) and qPCR was performed in order to determine the microbiota composition. **(A)** Oligo-MM¹² composition of mice from different animal facilities. Microbiota composition is shown as relative abundance and is expressed as % of cumulated 16S rRNA gene copy numbers (% of total 16S rRNA gene copies). * Limit of detection. Cluster analysis based on Bray Curtis **(B)** or Pearson **(C)** distance matrices visualized as PCoA plots. Fecal microbiota samples were grouped by different animal facilities which was significant, according to Bray Curtis ($p < 0.001$, Adonis) and Pearson ($p < 0.001$, Adonis) with 53% (Bray Curtis) and 72% (Pearson) of variation explained. PERMDISP analyses based on Bray Curtis and Pearson distance matrices revealed statistically

Results

significant differences in microbiota composition especially between the MvP and CMF as well as ETHZ (** p<0.01).

Table 42: Oligo-MM¹² composition in different animal facilities

Strain	Mean % of cumulated 16S rRNA gene copy numbers (+/- SD)			
	Animal facilities			
	CMF	MvP	CMF-IVC	ETHZ
'Bacteroides caecimuris' I48	50.72 (5.99)	62.92 ^a (4.88)	45.55 ^{b,d} (5.38)	58.70 ^{c,e,f} (9.66)
'Muribaculum intestinale' YL27	11.39 (1.32)	10.34 (1.81)	15.39 ^{b,d} (3.44)	13.55 ^e (2.34)
<i>Akkermansia muciniphila</i> YL44	28.42 (6.15)	19.46 ^a (4.11)	26.82 ^d (4.76)	20.57 ^{c,f} (6.75)
'Turicimonas caecimuris' YL45	5.07 (0.82)	3.03 (0.60)	6.07 ^d (1.83)	3.05 ^f (0.93)
<i>Lactobacillus reuteri</i> I49	0.03 (0.03)	0.10 (0.07)	0.06 (0.04)	0.06 (0.03)
<i>Enterococcus faecalis</i> KB1	0.08 (0.03)	0.01 (0.02)	0.04 (0.04)	0.001 (0.004)
<i>Blautia coccoides</i> YL58	0.84 (0.16)	0.60 (0.22)	1.46 (0.73)	0.95 (0.46)
<i>Clostridium innocuum</i> I46	0.08 (0.04)	0.09 (0.04)	0.13 (0.06)	0.33 (0.44)
<i>Flavonifractor plautii</i> YL31	2.15 (0.46)	2.01 (0.38)	3.12 (0.87)	1.69 (0.75)
<i>Clostridium clostridioforme</i> YL32	1.17 (0.61)	1.43 (0.69)	1.05 (1.22)	1.04 (0.58)
'Acutalibacter muris' KB18	0.04 (0.07)	DTL	0.33 (0.22)	0.06 (0.09)
<i>Bifidobacterium longum</i> subsp. <i>animalis</i> YL2	DTL	DTL	DTL	0.004 (0.011)

Significant differences between groups are indicated with **a** for CMF vs MvP, **b** for CMF vs CMF-IVC, **c** for CMF vs ETHZ, **d** for MvP vs CMF-IVC, **e** MvP vs ETHZ and **f** CMF-IVC vs ETHZ; p values were less than 0.001, except: YL27 CMF vs CMF-IVC p<0.01, YL27 MvP vs ETHZ p<0.01 and YL45 CMF-IVC vs ETHZ p<0.05, two-way ANOVA with Bonferroni posttest. Values are expressed as mean % of cumulated 16S rRNA gene copy numbers +/- standard deviation (SD). CMF: n=7, MvP: n=31, CMF-IVC: n=16, ETHZ: n=8. DTL: limit of detection.

Results

3.2.5 High-fat diet as well as oleic acid supplementation shift Oligo-MM¹² composition

In this section the influence of high-fat (HF) diet and oleic acid (OA) supplementation on the Oligo-MM¹² composition was investigated. Thus, C57BL/6J mice associated with the Oligo-MM¹² were either fed with standard diet, HF diet or with a standard diet supplemented with OA. Mice were then sacrificed at 6, 12 and 24 h post diet change, cecal content was harvested and DNA was extracted using the modified Stool kit (Qiagen). DNA was subsequently sent to the MvP for microbiota analysis by qPCR. Animal experiments and DNA extraction were performed by Sandra Wotzka, ETHZ.

The microbiota composition was comparable between groups 6 h post diet change (Figure 9A). At this time point, samples clustered together irrespective of diet fed (Figure 9B). Grouping of microbiota composition by different diet and time point was significant, according to Bray Curtis ($p < 0.001$, Adonis) and Pearson ($p < 0.001$, Adonis) distance matrices, with 86% (Bray Curtis) and 98% (Pearson) of variation explained (Figure 9B,C). Remarkably, starting from 12 h after diet change, the Oligo-MM¹² composition of the HF and OA group clustered apart from each other (Figure 9B), whereas Oligo-MM¹² composition of the standard diet group still clustered together with time points 6 and 24 h. In more detail, the relative abundance of '*Bacteroides caecimuris*' I48 decreased 24 h after feeding HF or standard diet supplemented with OA compared to standard diet from 62.77% \pm 2.70% to 26.48% \pm 9.07% and 14.03% \pm 6.80%, respectively ($p < 0.001$, two-way ANOVA with Bonferroni posttest; Table 43; Figure 9A). The lower abundance of '*Bacteroides caecimuris*' I48 after OA supplementation compared to HF was also statistically significant ($p < 0.001$, two-way ANOVA with Bonferroni posttest; Table 43). In contrast, compared to standard diet, the relative abundance of *Akkermansia muciniphila* YL44 increased around 35% after feeding HF and 43% after supplementing OA ($p < 0.001$, two-way ANOVA with Bonferroni posttest; Table 43; Figure 9A). There was significantly more *Akkermansia muciniphila* YL44 present 24 h after supplementing OA compared to HF diet ($p < 0.05$, two-way ANOVA with Bonferroni posttest; Table 43). The number of total bacteria was constant during the course of the experiment and independent of diet.

Results

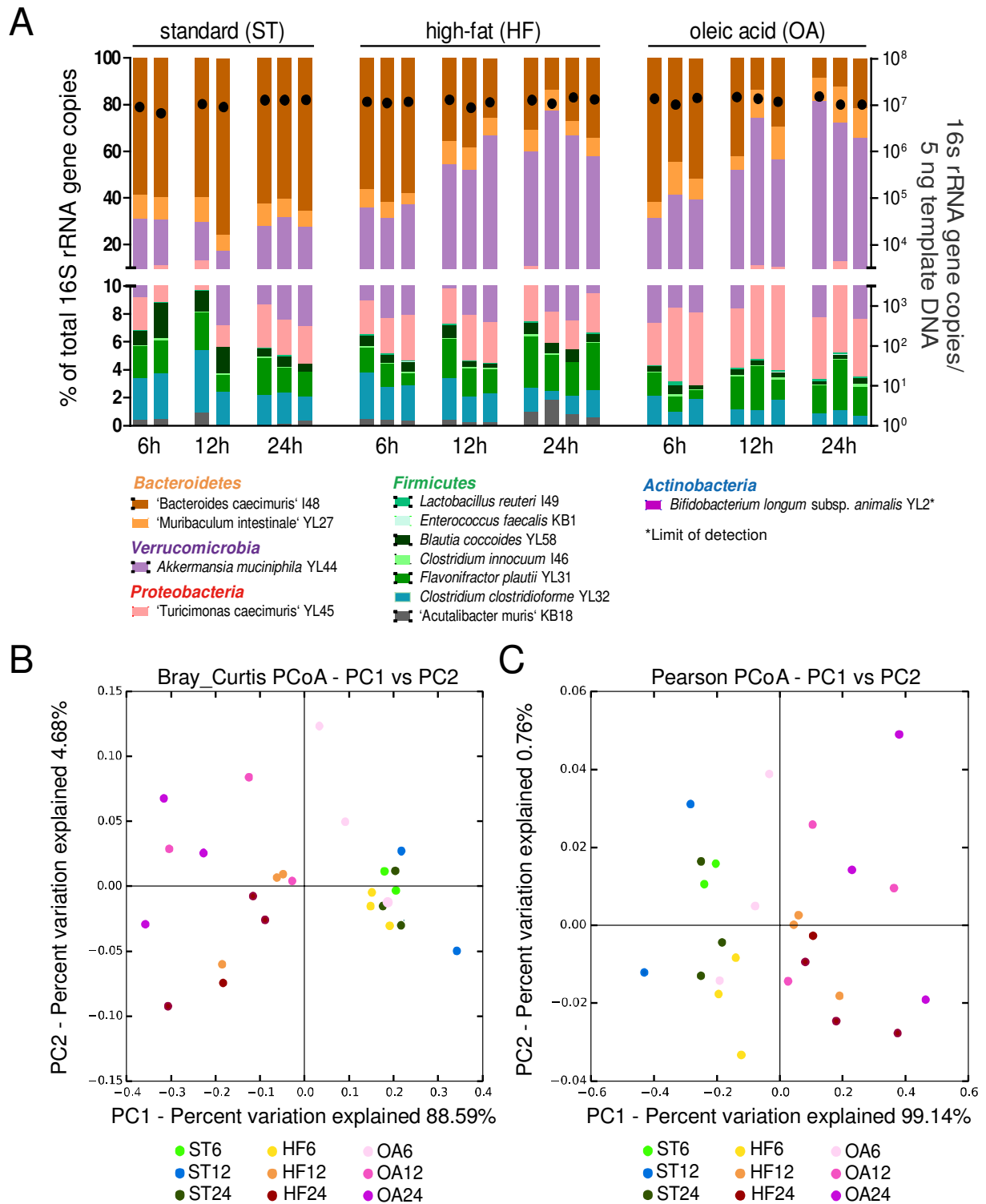


Figure 9: Oligo-MM¹² responds to changes in diet. Oligo-MM¹² mice were either fed with standard (ST) diet, high-fat (HF) or standard diet supplemented with oleic acid (OA). Mice were sacrificed 6, 12 and 24 h after diet change and cecal content was harvest for subsequent DNA extraction and microbiota analysis by qPCR. **(A)** Analysis of microbiota composition in cecal content. Microbiota composition is shown as relative abundance and expressed as % of cumulated 16S rRNA gene copy numbers (% of total 16S rRNA gene copies). The amount of absolute 16S rRNA gene copies (determined by an universal primer / probe combination) is illustrated as black dots (right y axis). Cluster analysis based on Bray Curtis **(B)** or Pearson **(C)** distance matrices visualized as PCoA plots. Microbiota samples were grouped by different diet and time point which was significant, according to Bray Curtis ($p < 0.001$, Adonis) and Pearson ($p < 0.001$, Adonis) with 86% (Bray Curtis) and 98% (Pearson) of variation explained.

Results

Table 43: Influence of high-fat diet and oleic acid supplementation on Oligo-MM¹² composition

Strain	Mean % of cumulated 16S rRNA gene copy numbers (+/- SD)		
	different diets (24h post diet change)		
	standard	high-fat	oleic acid
'Bacteroides caecimuris' I48	62.77 (2.70)	26.48 ^a (9.07)	14.03 ^{b,c} (6.80)
'Muribaculum intestinale' YL27	8.16 (1.25)	7.95 (1.22)	12.86 (2.84)
<i>Akkermansia muciniphila</i> YL44	21.27 (2.43)	56.61 ^a (9.93)	63.80 ^{b,c} (8.72)
'Turicimonas caecimuris' YL45	2.78 (0.24)	2.60 (0.57)	5.30 (1.74)
<i>Lactobacillus reuteri</i> I49	0.05 (0.02)	0.05 (0.04)	0.12 (0.04)
<i>Enterococcus faecalis</i> KB1	0* (0.01)	0.01 (0.01)	0.01 (0.01)
<i>Blautia coccoides</i> YL58	0.64 (0.13)	0.76 (0.12)	0.32 (0.10)
<i>Clostridium innocuum</i> I46	0.06 (0.01)	0.09 (0.02)	0.12 (0.07)
<i>Flavonifractor plautii</i> YL31	2.06 (0.50)	3.01 (0.64)	2.54 (0.95)
<i>Clostridium clostridioforme</i> YL32	2.04 (0.25)	1.41 (0.56)	0.91 (0.18)
'Acutalibacter muris' KB18	0.17 (0.16)	1.06 (0.54)	0*
<i>Bifidobacterium longum</i> subsp. <i>animalis</i> YL2	0* (0.005)	0.003 (0.005)	0*

Significant differences between groups are indicated with **a** for standard vs high fat, **b** for standard vs oleic acid and **c** for high-fat vs oleic acid; p values were less than 0.001, except: YL44 high-fat vs oleic acid p<0.05, two-way ANOVA with Bonferroni posttest. For the calculation of mean % values 24 h post diet change were used. Values are expressed as mean % of cumulated 16S rRNA gene copy numbers +/- standard deviation (SD). Standard: n=3, high-fat: n=4, oleic acid: n=3. * Very low abundant.

Results

3.3 The Oligo-MM¹² is a tool to study inflammation induced dysbiosis

3.3.1 Infection with wild type *S. Typhimurium* causes severe colitis and dysbiosis

Wildtype *S. Typhimurium* (*S. Tm*^{WT}) induces acute gut inflammation which triggers dysbiosis (Stecher *et al.* 2007). To date, studies investigating *Salmonella*-induced dysbiosis are based on human derived or not well defined murine microbiota, or use antibiotic pre-treated mice where the microbiota is already manipulated by antibiotic application before infection (Barthel *et al.* 2003, Barman *et al.* 2008, Ganesh *et al.* 2013) and might therefore generate biased datasets. In order to establish a new model for *Salmonella*-induced colitis, we address the influence of *Salmonella* infection on mice associated with Oligo-MM¹², a well-defined model microbiota consisting of murine bacterial isolates without antibiotic treatment prior to infection.

C57BL/6J mice associated with the Oligo-MM¹² consortium were infected with 5×10^7 CFUs of either *S. Tm*^{Avir} or *S. Tm*^{WT} without antibiotic treatment prior to infection. On each day post infection (p.i.) groups of mice (infection with *S. Tm*^{Avir}: day 1 p.i. n=5, day 2 p.i. n=5, day 3 p.i. n=6, day 4 p.i. n=6; infection with *S. Tm*^{WT}: day 1 p.i. n=5, day 2 p.i. n=5, day 3 p.i. n=7, day 4 p.i. n=7) were sacrificed and samples were taken for further analyses (Figure 10A). The avirulent *Salmonella* strain *S. Tm*^{Avir} that lacks functional type 3 secretion systems 1 and 2 ($\Delta invG$; $sseD::aphT$) was not able to induce colitis (Figures 10B; 11B). In stark contrast, mice infected with *S. Tm*^{WT} exhibited colitis starting at day 3 p.i. leading to profound colitis observed at day 4 p.i. that was accompanied by severe cecal pathology and a lipocalin-2 (LCN-2) peak of approximately 1,900 ng per mg cecal content (Figures 10B; 11B). Interestingly, the Oligo-MM¹² provided colonization resistance against *S. Tm*^{Avir} and *S. Tm*^{WT}, since *Salmonella* loads were significantly less in cecal content at day 1 p.i. compared to day 3 and day 4 p.i. ($p < 0.05$ and $p < 0.01$, Kruskal-Wallis test with Dunn's multiple comparison test; Figure 11A). At day 1 p.i., *S. Tm*^{Avir} exhibited higher loads in cecum than *S. Tm*^{WT} ($p < 0.05$, Mann Whitney test), whereas *S. Tm*^{WT} was significantly more abundant at day 3 p.i. ($p < 0.01$, Mann Whitney test) and increased further at day 4 p.i.. *S. Tm*^{WT} caused systemic infection and was already detected in mesenteric lymphnodes at day 1 p.i. as well as in liver and spleen as shown previously (Stecher *et al.* 2007). In contrast, *S. Tm*^{Avir} failed to systemically infect C57BL/6J mice associated with the Oligo-MM¹² (Figure 11C-E). Remarkably, shifts in microbiota composition coincided with strong inflammation after infection with *S. Tm*^{WT}, whereas *S. Tm*^{Avir} did not induce dysbiosis (Figure 10C).

Cluster analyses further supported this first observation. Since *S. Tm*^{WT} induced inflammation in Oligo-MM¹² mice, inflammation was categorized according to inflammation grade and cecal pathology: (i) non-inflamed (no colitis, pathoscore: 0 - 3, uninfected – day 2 p.i.), (ii) intermediate (moderate colitis, pathoscore: 3 - 9, day 3 p.i.) and (iii) inflamed (profound colitis, pathoscore: > 9,

Results

day 4 p.i.) (Figures 10B; 12C,D; 13C,D). Because no pathological changes were apparent after infection with *S. Tm*^{Avir} (Figures 10B; 11B), samples were simply grouped by days p.i.. According to Bray Curtis ($p < 0.002$, Adonis) and Pearson ($p < 0.004$, Adonis) distance matrices, grouping of microbiota composition in cecal content after infection with *S. Tm*^{Avir} by days post infection was statistically significant, with 41% (Bray Curtis) and 65% (Pearson) of the variation explained. According to both distance matrices, there was no statistically significant difference in overall microbiota composition between all 4 days p.i. with *S. Tm*^{Avir} ($p > 0.05$, non parametric PERMDISP procedure; Figure 12A,B). After infection with *S. Tm*^{WT}, grouping of microbiota composition by inflammation grade was also statistically significant according to Bray Curtis ($p < 0.001$, Adonis) and Pearson ($p < 0.001$, Adonis) distance matrices, with 97% (Bray Curtis) and 98% (Pearson) of variation explained (Figure 12C,D). There were significant difference between all groups of grades of inflammation, according Pearson ($p < 0.001$ and $p < 0.01$, non parametric PERMDISP procedure; Figure 12D). According to Bray Curtis, the uninflamed group was different compared to intermediate group ($p < 0.001$, non parametric PERMDISP procedure; Figure 12C) and there was a statistically significant difference between the intermediate and the inflamed group ($p < 0.01$, non parametric PERMDISP procedure; Figure 12C).

The same trend was observed in fecal microbiota composition: Grouping of fecal microbiota composition after *S. Tm*^{Avir} infection by days post infection was significant, according to Bray Curtis ($p < 0.001$, Adonis) and Pearson ($p < 0.001$, Adonis) distance matrices, with 68% (Bray Curtis) and 93% (Pearson) explained. There was no statistically significant difference in overall microbiota composition between all 4 days p.i. with *S. Tm*^{Avir} ($p > 0.05$, non parametric PERMDISP procedure based on Bray Curtis and Pearson; Figure 13A,B). As it was observed in cecal content, grouping of the microbiota composition after infection with *S. Tm*^{WT} by inflammation grade was statistically significant according to Bray Curtis ($p < 0.001$, Adonis) and Pearson ($p < 0.001$, Adonis) distance matrices, with 98% (Bray Curtis) and 100% (Pearson) of variation explained (Figure 13C,D). There were significant differences between all groups of grades of inflammation, according to Pearson ($p < 0.01$ and $p < 0.05$, non parametric PERMDISP procedure; Figure 13D). According to Bray Curtis, the uninflamed group was different compared to the inflamed group ($p < 0.01$, non parametric PERMDISP procedure; Figure 13C) and there was a statistically significant difference between the intermediate and the inflamed group ($p < 0.05$, non parametric PERMDISP procedure; Figure 13C).

Taken together, *S. Tm*^{Avir} was unable to induce inflammation and concomitant dysbiosis, whereas *S. Tm*^{WT} induced colitis starting at day 3 p.i.. Inflammation was additionally paralleled with drastic changes in microbiota composition at day 4 p.i. with *S. Tm*^{WT}.

Results

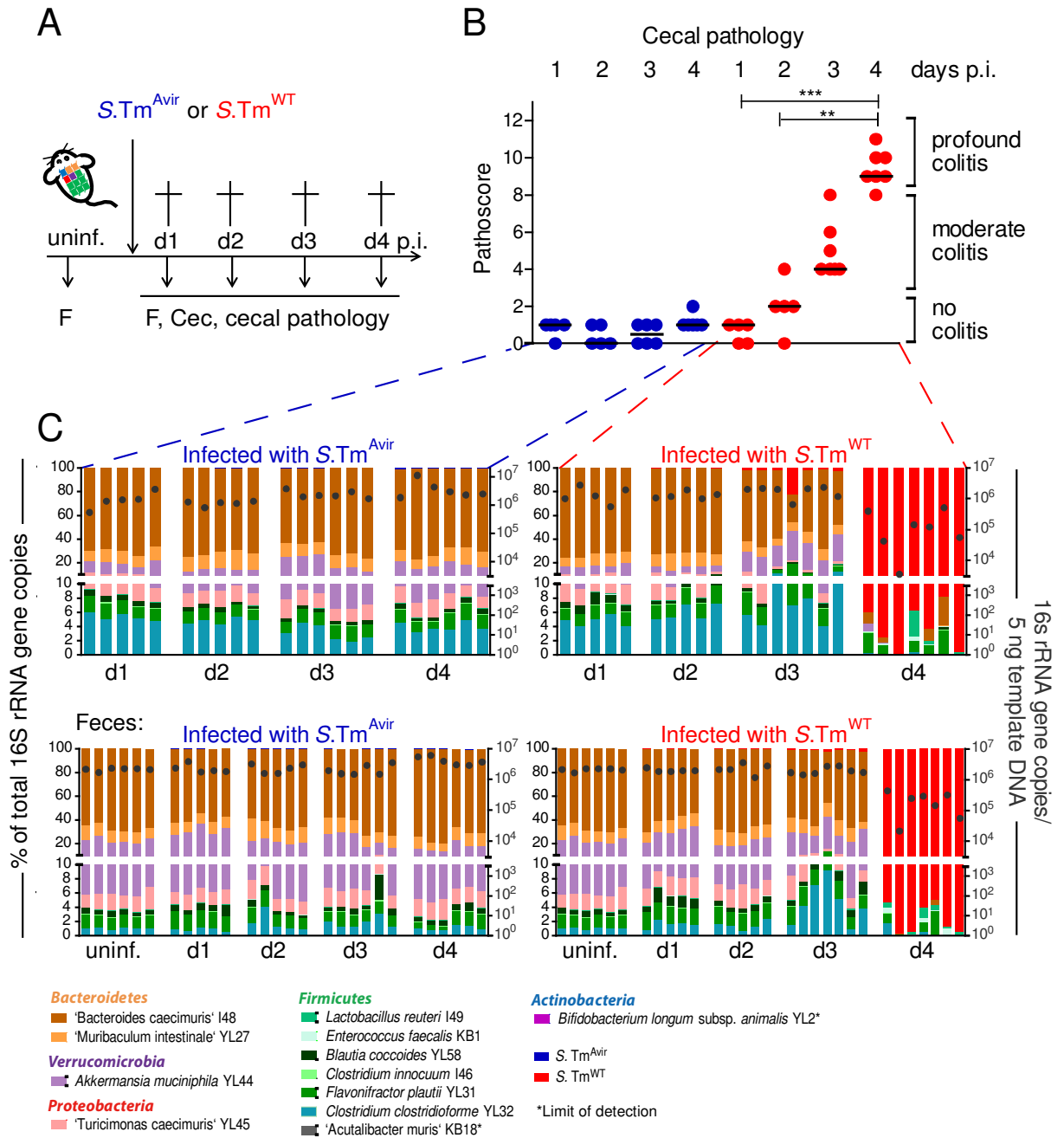


Figure 10: *S. Tm*^{WT} causes severe colitis and dysbiosis at day 4 post infection. (A) Experimental set-up: Oligo-MM¹² mice were orally infected with 5×10^7 CFUs of either *S. Tm*^{Avir} or *S. Tm*^{WT}. Animals were euthanized at days 1, 2, 3 and 4 p.i. and samples were taken: feces (F), cecal content (Cec). As control, there was also a fecal sample taken at d0 before infection. **(B)** Cecal pathology determined by microscopy of HE stained cecal sections. Colitis was observed at d4 p.i. with *S. Tm*^{WT}, whereas infection with *S. Tm*^{Avir} did not induce colitis. **(C)** Analysis of microbiota composition in cecal content (upper panel) and feces (lower panel). Microbiota composition is shown as relative abundance and expressed as % of cumulated 16S rRNA gene copy numbers (% of total 16S rRNA gene copies). The amount of absolute 16S rRNA gene copies (determined by an universal primer / probe combination) is illustrated as black dots (right y axis). Shifts in microbiota composition and drops in total bacteria paralleled with increased colitis following infection with *S. Tm*^{WT}. * limit of detection. Statistical analysis of cecal pathology was performed using Kruskal-Wallis test with Dunn's multiple comparison test (*** p < 0.001, ** p < 0.01).

Results

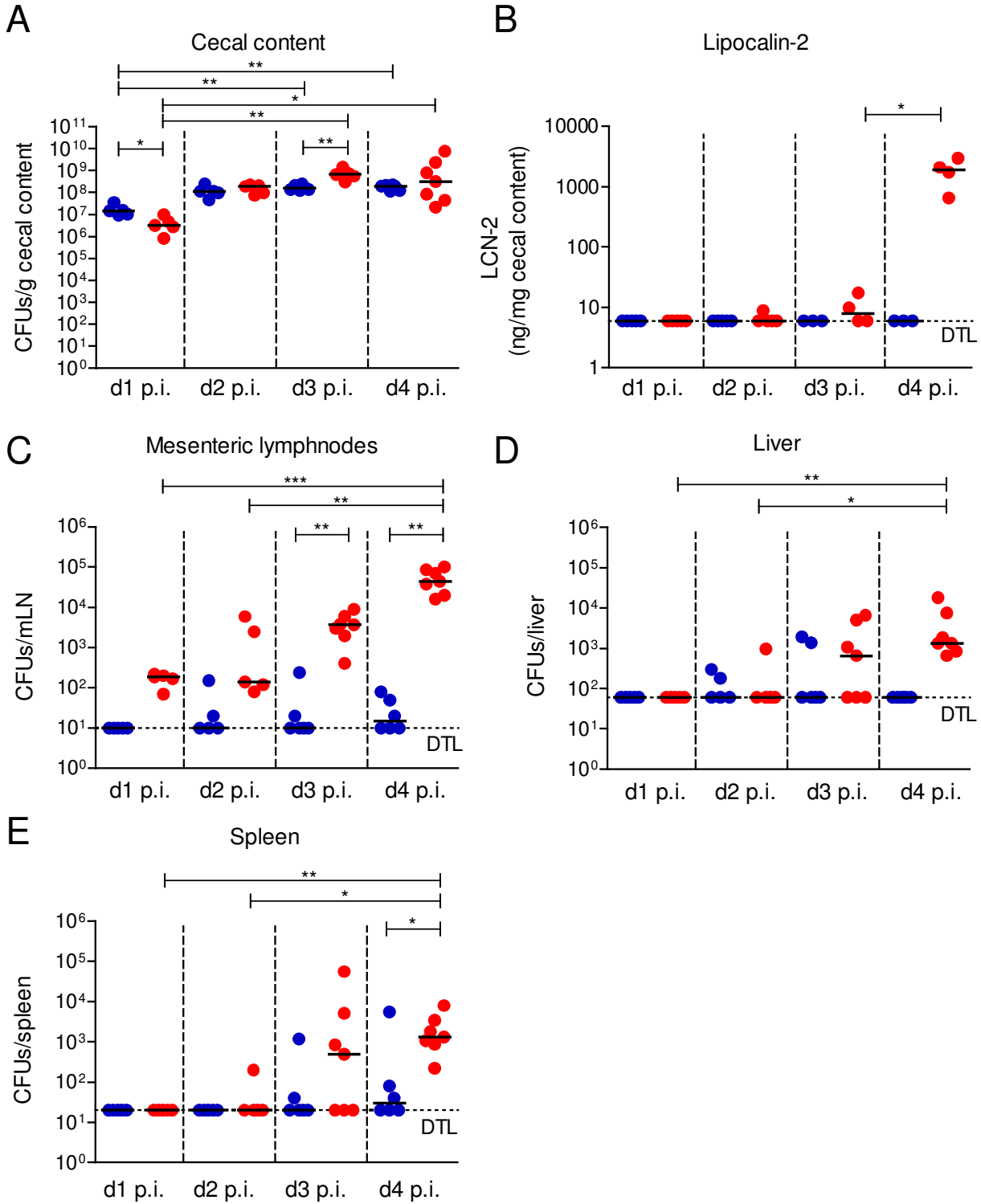


Figure 11: Course of enteric *S. Tm* infection and systemic dissemination. For experimental set-up refer to Figure 10A. Organs were additionally taken at the indicated time points. **(A)** *Salmonella* loads in cecal content (CFUs *S. Tm* / g content). **(B)** Lipocalin-2 (LCN-2) amount in cecal content measured by ELISA (ng / mg cecal content) **(C) – (E)** Systemic dissemination of *Salmonella* to mesenteric lymphnodes, liver and spleen (CFUs / organ). Statistical analysis between groups was performed using Kruskal-Wallis test with Dunn's multiple comparison test. Differences between groups (*S. Tm*^{WT} vs *S. Tm*^{Δvir}) at one given time point were compared using Mann Whitney test (* p<0.05, ** p<0.01, *** p<0.001). Dashed lines: DTL: limit of detection (mLN: 10 CFUs, liver: 60 CFUs, spleen: 20 CFUs).

Results

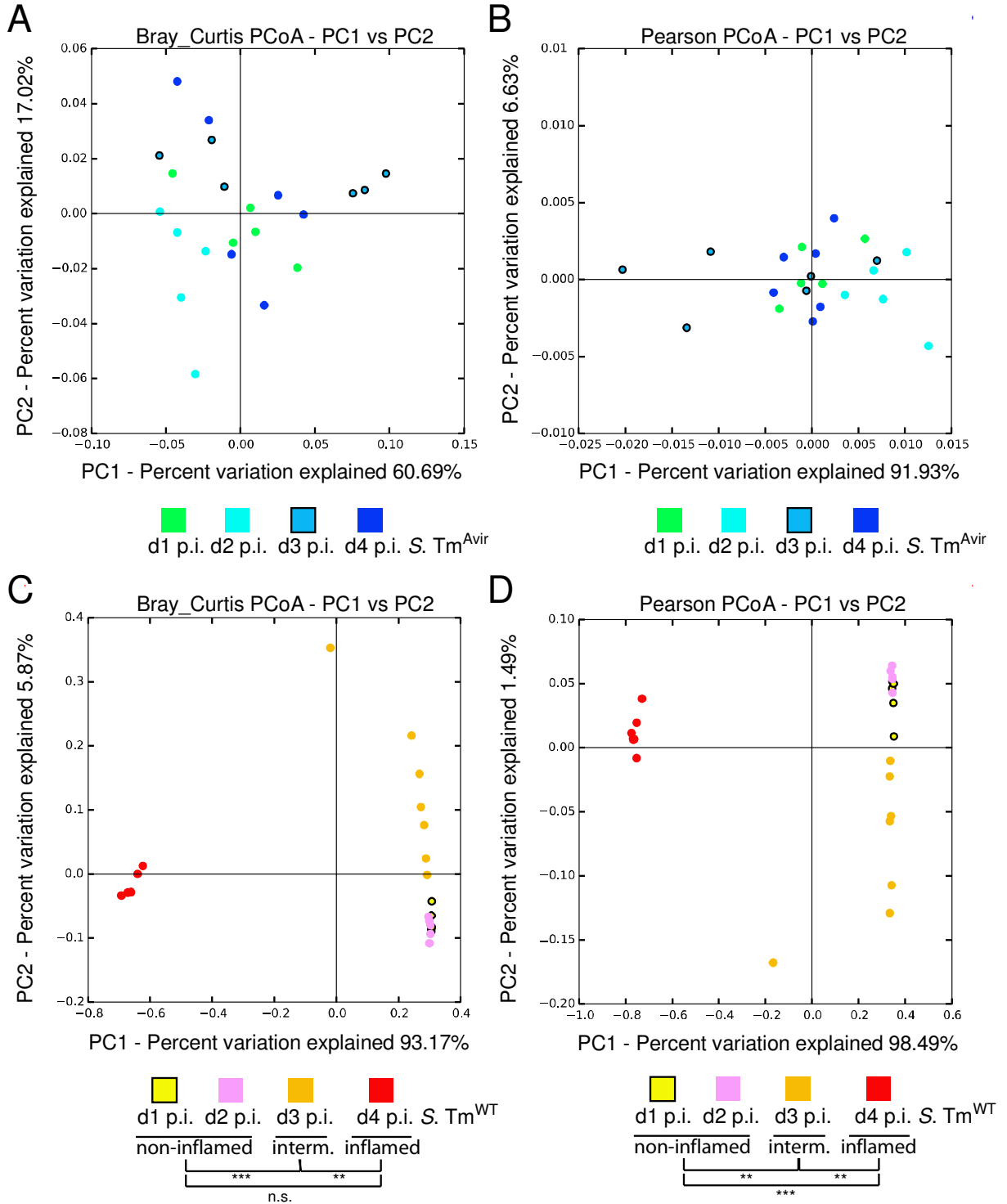


Figure 12: Clustering of Oligo-MM¹² composition in cecal content after infection with either *S. Tm^{Avir}* or *S. Tm^{WT}*. Cluster analysis based on Bray Curtis or Pearson distance matrices visualized as PCoA plots. **(A)** and **(B)** clustering of Oligo-MM¹² composition after infection with *S. Tm^{Avir}*. Microbiota samples from cecal content were grouped by days post infection since inflammation was absent. Grouping by days p.i. with *S. Tm^{Avir}* was significant, according to Bray Curtis ($p < 0.002$, Adonis) and Pearson ($p < 0.004$, Adonis) with 41% (Bray Curtis) and 65% (Pearson) of variation explained. PERMDISP analyses based on Bray Curtis and Pearson distance matrices revealed no statistically significant differences in microbiota composition in cecal content between days post infection with *S. Tm^{Avir}* ($p > 0.05$). **(C)** and **(D)** Oligo-MM¹² composition after infection with *S. Tm^{WT}*. Since *S. Tm^{WT}* caused inflammation, microbiota samples from cecal content were grouped according to inflammation grade (non-inflamed: days 1 + 2 p.i., intermediate: day 3 p.i. and inflamed: day 4 p.i.). Grouping by inflammation grade after infection with *S. Tm^{WT}* was significant, according to Bray Curtis ($p < 0.001$, Adonis) and Pearson

Results

($p < 0.001$, Adonis) with 97% (Bray Curtis) and 98% (Pearson) of variation explained. PERMDISP analyses based on Bray Curtis and Pearson distance matrices revealed statistically significant differences in microbiota composition of cecal content between all 3 inflammation grades (** $p < 0.01$, *** $p < 0.001$, n.s.: not significant).

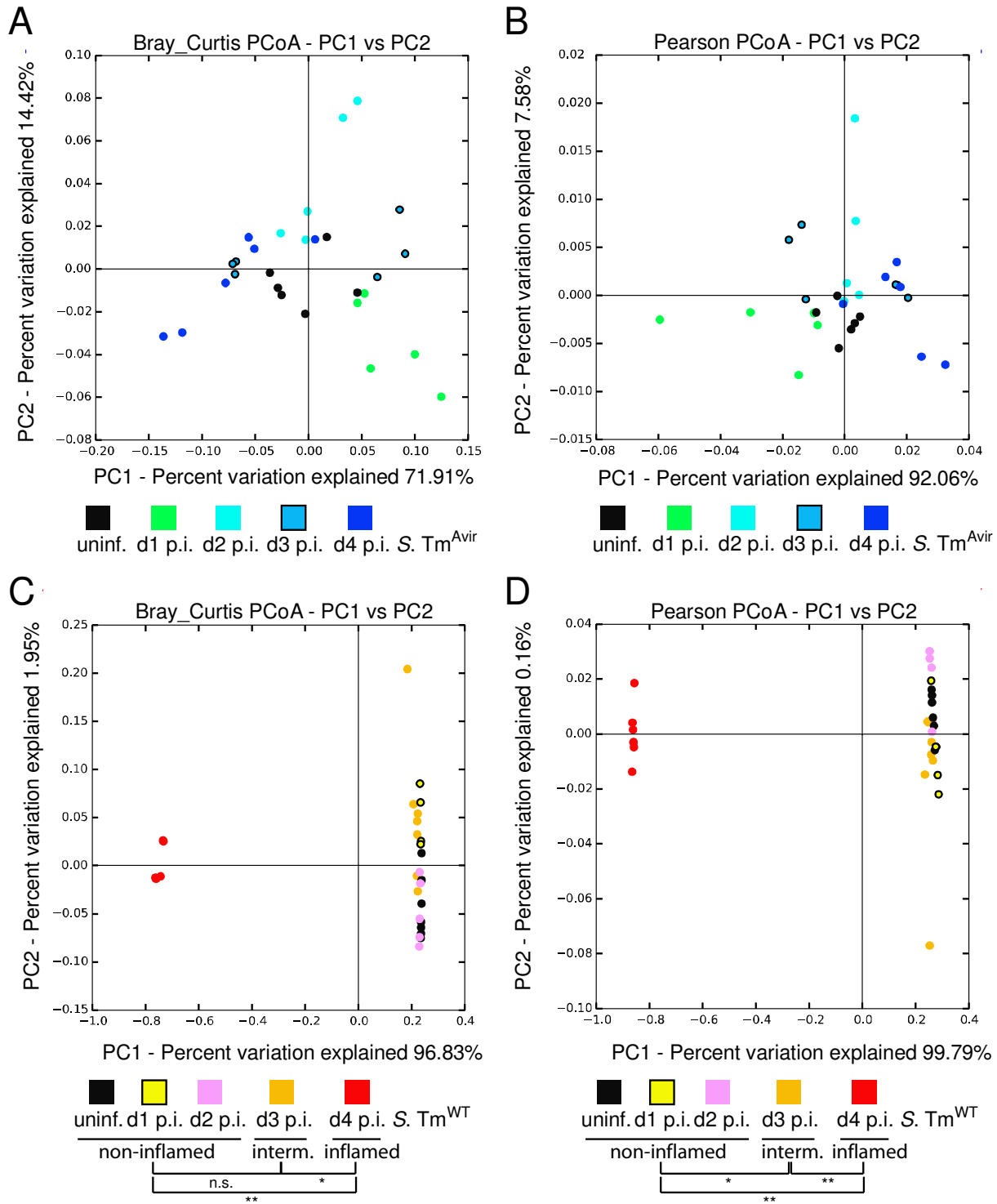


Figure 13: Clustering of Oligo-MM¹² composition in feces after infection with either *S. Tm^{Avir}* or *S. Tm^{WT}*. Cluster analysis based on Bray Curtis or Pearson distance matrices visualized as PCoA plots. (A) and (B) clustering of Oligo-MM¹² composition after infection with *S. Tm^{Avir}*. Fecal microbiota samples were grouped by

Results

days post infection since inflammation was absent. Grouping by days p.i. with *S. Tm*^{Avir} was significant, according to Bray Curtis ($p < 0.001$, Adonis) and Pearson ($p < 0.001$, Adonis) distance matrices, with 68% (Bray Curtis) and 93% (Pearson) of variation explained. PERMDISP analyses based on Bray Curtis and Pearson distance matrices revealed no statistically significant differences in fecal microbiota composition between days post infection with *S. Tm*^{Avir} ($p > 0.05$). **(C)** and **(D)** Oligo-MM¹² composition after infection with *S. Tm*^{WT}. Since *S. Tm*^{WT} caused inflammation, fecal microbiota samples were grouped according to inflammation grade (non-inflamed: uninfected + days 1 + 2 p.i., intermediate: day 3 p.i. and inflamed: day 4 p.i.). Grouping by inflammation grade after infection with *S. Tm*^{WT} was significant, according to Bray Curtis ($p < 0.001$, Adonis) and Pearson ($p < 0.001$, Adonis) with 98% (Bray Curtis) and 100% (Pearson) of variation explained. PERMDISP analyses based on Bray Curtis and Pearson distance matrices revealed statistically significant differences in fecal microbiota composition between all 3 inflammation grades (* $p < 0.05$, ** $p < 0.01$, n.s.: not significant).

3.3.2. Performance of individual Oligo-MM¹² strains during *S. Tm*^{WT} induced colitis

Oligo-MM¹² strains might be outcompeted by invading *S. Tm*^{WT}, that selectively uses nutrients such as anaerobic electron acceptors or ethanolamine which are present in an inflammatory milieu (Winter *et al.* 2010, Thiennimitr *et al.* 2011, Lopez *et al.* 2012). Moreover, individual Oligo-MM¹² strains could be directly killed by neutrophils infiltrating at the site of inflammation (Loetscher *et al.* 2012).

In order to better understand and characterize microbiota shifts observed at day 4 p.i. with *S. Tm*^{WT}, fold changes in absolute abundance of Oligo-MM¹² strains were calculated (day 1 versus day 4 p.i.). Calculations were based on absolute reads per 1 million gene copies determined by universal probe. 8,000 – 9,000 fold increase of *S. Tm*^{WT} in both cecal content and feces was observed (Figure 14). *S. Tm*^{WT} dominated the microbiota at day 4 p.i. (*Salmonella* ‘blooms’ (Stecher *et al.* 2012)). Remarkably, the individual members of the Oligo-MM¹² performed differently in the presence of *S. Tm*^{WT} induced inflammation. The Oligo-MM¹² strains were grouped in 3 categories according to their decreasing or increasing abundance during *Salmonella* ‘blooms’: (i) depleted, strains that decrease massively; (ii) intermediate, bacteria that remained stable during *S. Tm*^{WT} induced colitis and (iii) enriched, strains which abundance increased during inflammation. The grouping in the 3 categories was consistent between cecal content and feces. Depleted bacteria were mainly Gram-negatives and belonged to the phyla Bacteroidetes, Verrucomicrobia and Proteobacteria: ‘*Muribaculum intestinale*’ YL27, ‘*Turicimonas caecimuris*’ YL45, *Akkermansia muciniphila* YL44 and ‘*Bacteroides caecimuris*’ I48. The Gram-variable Firmicute *Clostridium clostridioforme* YL32 was also depleted during strong colitis. However, the Gram-positive or Gram-variable strains *Blautia coccoides* YL58, *Flavonifractor plautii* YL31 and *Clostridium innocuum* I46, that belong to the Firmicutes phylum decreased less and were assigned to the intermediate group. One has to mention here, that *Blautia coccoides* YL58 was mostly under the detection limit of the qPCR assay at day 4 p.i. with *S. Tm*^{WT} and that low baseline abundance before infection of this strain accounts for lower fold changes between day 1 and day 4

Results

p.i. with *S. Tm*^{WT}. Interestingly, *Lactobacillus reuteri* I49 and *Enterococcus faecalis* KB1, both Gram-positive bacteria were increased under inflammatory conditions and were grouped the third category (Figure 14). *Bifidobacterium longum* subsp. *animalis* YL2 and 'Acutalibacter muris' KB18 were below the limit of detection of the respective qPCR assay.

The absolute abundance of the strains after infection with *S. Tm*^{WT} was also in line with relative abundance expressed as mean % of cumulated 16S rRNA gene copy numbers. *S. Tm*^{WT} dominated the microbiota at day 4 p.i. with a relative abundance of 96.18% +/- 3.09% in cecal content and 97.64% +/- 2.14% in feces (Figure 10C; Tables 44; 46). In stark contrast, the *S. Tm*^{Avir} failed to dominate and its relative abundance remained below 1% (Tables 45; 47). Looking at the microbiota composition during *S. Tm*^{WT} 'blooms', there were drastic and statistically significant drops in relative abundance of 'Muribaculum intestinale' YL27, 'Bacteroides caecimuris' I48 and *Akkermansia muciniphila* YL44 between day 1 and day 4 ($p < 0.001$, two-way ANOVA with Bonferroni posttest; Table 44). The relative abundance of *Clostridium clostridioforme* YL32 at day 4 p.i. was also reduced by trend and 'Turicimonas caecimuris' YL45 was close to the limit of detection (Tables 44; 46). The relative abundance of *Blautia coccooides* YL58, *Flavonifractor plautii* YL31 and *Clostridium innocuum* I46 (intermediate group) was also reduced at day 4 p.i. (Tables 44; 46). Whereas, *Lactobacillus reuteri* I49 and *Enterococcus faecalis* KB1 increased by trend in relative abundance at day 4 p.i. (Tables 44; 46).

There was already moderate expansion of *S. Tm*^{WT} observed starting at day 3 p.i. (Tables 44; 46). The relative abundance of 'Bacteroides caecimuris' I48 in cecal content and feces started to decrease from day 3 p.i. on ($p < 0.001$, two-way ANOVA with Bonferroni posttest; Tables 44; 46) but was still the dominating strain in cecal content (52.75% +/- 15.21%) and feces (57.94% +/- 7.48%). The relative abundance of 'Muribaculum intestinale' YL27 and 'Turicimonas caecimuris' YL45 was quite stable between the days 1 - 3 p.i. (Tables 44; 46). Interestingly, the relative abundance of *Akkermansia muciniphila* YL44 increased between day 2 and day 3 p.i. of around 14% in cecal content ($p < 0.001$, two-way ANOVA with Bonferroni posttest; Table 44) and 6% in feces ($p < 0.001$, two-way ANOVA with Bonferroni posttest; Table 46). An increased relative abundance of *Clostridium clostridioforme* YL32 between day 2 and day 3 p.i. was also observed ($p < 0.05$, two-way ANOVA with Bonferroni posttest; Table 46). This might indicate that both strains *Akkermansia muciniphila* YL44 and *Clostridium clostridioforme* YL32 could profit from mild inflammation. The relative abundance of *Blautia coccooides* YL58, *Flavonifractor plautii* YL31, *Clostridium innocuum* I46 (intermediate group) as well as *Lactobacillus reuteri* I49 and *Enterococcus faecalis* KB1 (enriched group) was not significantly altered during this early stage of infection (days 1 - 3 p.i.; Tables 44; 46).

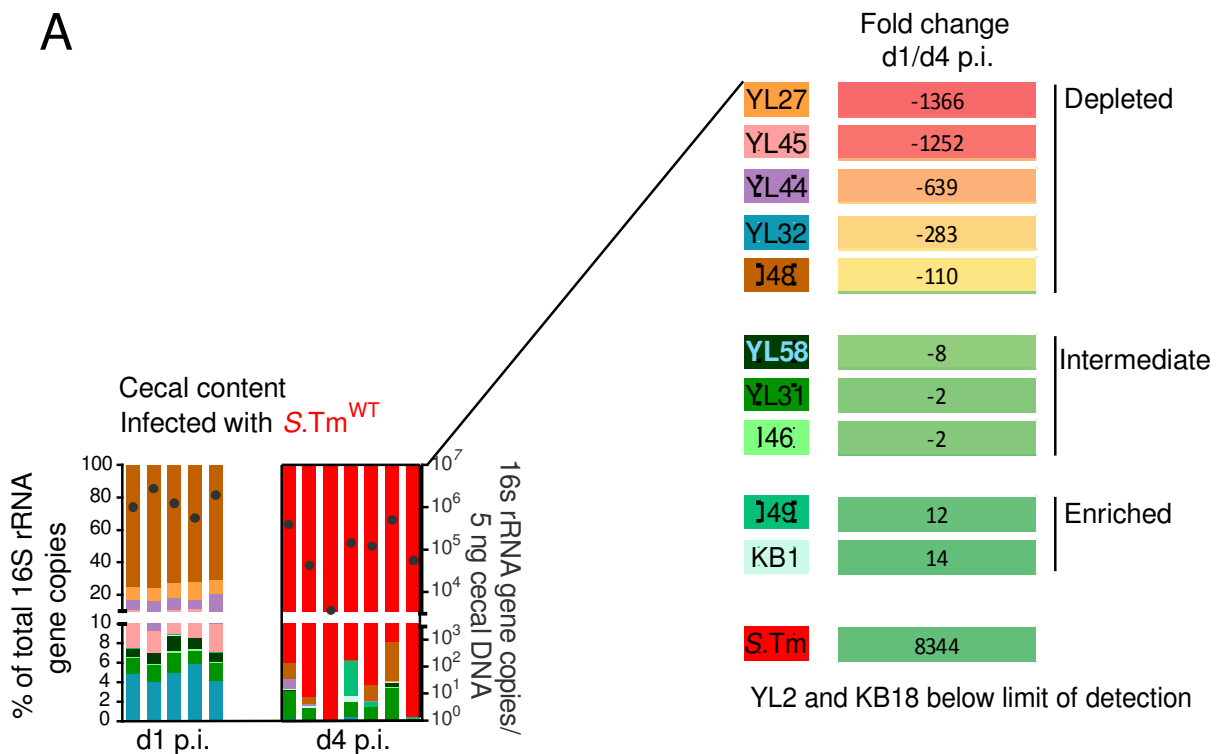
Infection with *S. Tm*^{Avir} did not induce dysbiosis at day 4 p.i. and no *Salmonella* 'blooms' were observed (Figure 10C). However, there were slight but statistically significant fluctuations in relative

Results

abundance of 'Bacteroides caecimuris' I48 and 'Muribaculum intestinale' YL27 during the course of infection with *S. Tm*^{Avir} (Tables 45; 47). Fluctuations were also observed in relative abundance of *Akkermansia muciniphila* YL44. It peaked at day 3 p.i. in cecal content and at day 1 p.i. in feces (Tables 45; 47).

Results

A



B

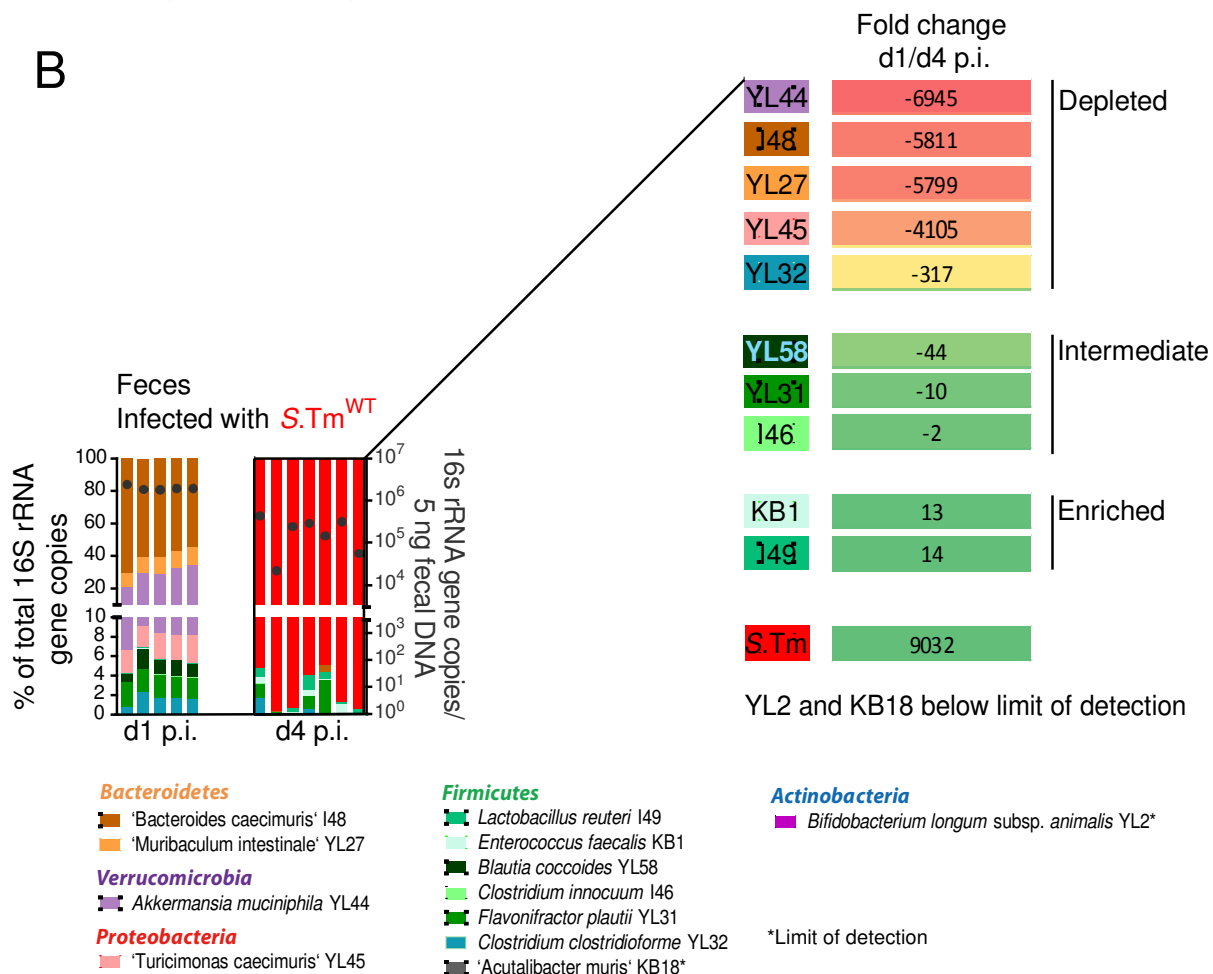


Figure 14: The performance of individual Oligo-MM¹² members during inflammation. Oligo-MM¹² mice were infected with 5×10^7 CFUs of *S. Tm*^{WT}. The experimental set-up is detailed in Figure 10A (same data used for fold-change calculations). Fold-changes in absolute abundance between day 1 and day 4 post infection were calculated with absolute values that were normalized to a million gene copies determined by universal probe.

Results

Fold changes in microbiota composition were determined in **(A)** cecal content and **(B)** feces and ranked according to decreasing abundance (red: highly decreased, green: less affected or enriched). Bacteria were subsequently grouped in 3 categories: depleted: bacteria that were highly depleted during *Salmonella* 'blooms'; intermediate: Oligo-MM¹² strains that were stable or decreased less during *Salmonella* induced colitis; enriched: strains that were enriched during inflammation. * Limit of detection.

Table 44: Relative abundance of Oligo-MM¹² strains in cecal content after infection with *S. Tm*^{WT}

Strain	Mean % of cumulated 16S rRNA gene copy numbers (+/- SD)			
	Days post infection with <i>S. Tm</i> ^{WT}			
	Day 1	Day 2	Day 3	Day 4
'Bacteroides caecimuris' I48	73.40 (2.20)	71.71 (0.82)	52.75 ^{a,c} (15.21)	1.15 ^{b,c} (1.47)
'Muribaculum intestinale' YL27	9.24 (1.48)	11.94 (1.88)	8.36 (1.46)	0.01 ^{b,c} (0.01)
<i>Akkermansia muciniphila</i> YL44	7.05 (1.91)	4.79 (0.80)	18.88 ^{a,c} (4.49)	0.17 ^{b,c} (0.38)
'Turicimonas caecimuris' YL45	2.50 (0.52)	2.33 (0.81)	2.14 (0.61)	0*
<i>Lactobacillus reuteri</i> I49	0.04 (0.01)	0.06 (0.03)	0.05 (0.03)	0.65 (1.34)
<i>Enterococcus faecalis</i> KB1	0.01 (0.01)	0.01 (0.004)	0.02 (0.03)	0.18 (0.19)
<i>Blautia coccoides</i> YL58	1.15 (0.32)	0.53 (0.10)	0.90 (0.47)	0.07 (0.16)
<i>Clostridium innocuum</i> I46	0.11 (0.03)	0.08 (0.02)	0.08 (0.05)	0.01 (0.02)
<i>Flavonifractor plautii</i> YL31	1.75 (0.24)	2.20 (0.26)	4.39 (3.38)	1.50 (1.28)
<i>Clostridium clostridioforme</i> YL32	4.72 (0.75)	5.90 (1.11)	7.40 (3.23)	0.09 ^b (0.15)
'Acutalibacter muris' KB18	DTL	DTL	DTL	DTL
<i>Bifidobacterium longum</i> subsp. <i>animalis</i> YL2	DTL	DTL	DTL	DTL
<i>S. Tm</i>	0.02 (0.02)	0.47 (0.23)	5.03 ^c (7.81)	96.18 ^{b,c} (3.09)

Significant differences between **a** day 2 vs day 3, **b** day 3 vs day 4 and **c** time point vs day 1 are indicated; p values were less than 0.001, except: *S. Tm* day 1 vs day 3 p<0.05, two-way ANOVA with Bonferroni posttest. There were no significant differences between day 1 vs day 2. Values are expressed as mean % of cumulated 16S rRNA gene copy numbers +/- standard deviation (SD). Day 1 p.i.: n=5, day 2 p.i.: n=5, day 3 p.i.: n=7, day 4 p.i.: n=7. DTL: limit of detection. * Very low abundant.

Results

Table 45: Relative abundance of Oligo-MM¹² strains in cecal content after infection with *S. Tm*^{Avir}

Strain	Mean % of cumulated 16S rRNA gene copy numbers (+/- SD)			
	Days post infection with <i>S. Tm</i> ^{Avir}			
	Day 1	Day 2	Day 3	Day 4
'Bacteroides caecimuris' I48	69.54 (2.91)	72.02 (2.33)	68.25 ^b (6.10)	70.18 (3.97)
'Muribaculum intestinale' YL27	10.60 (1.34)	13.65 ^a (1.86)	11.09 (0.71)	10.97 (2.35)
<i>Akkermansia muciniphila</i> YL44	9.06 (2.38)	4.96 ^a (1.06)	12.51 ^{b,d} (5.39)	9.56 ^c (2.02)
'Turicimonas caecimuris' YL45	2.36 (0.35)	2.05 (0.27)	2.10 (0.33)	2.05 (0.37)
<i>Lactobacillus reuteri</i> I49	0.07 (0.04)	0.01 (0.02)	0.03 (0.03)	0.08 (0.03)
<i>Enterococcus faecalis</i> KB1	0.02 (0.01)	0* (0.01)	0* (0.01)	0* (0.01)
<i>Blautia coccoides</i> YL58	0.74 (0.09)	0.52 (0.07)	0.52 (0.08)	0.60 (0.18)
<i>Clostridium innocuum</i> I46	0.11 (0.03)	0.06 (0.02)	0.07 (0.01)	0.08 (0.02)
<i>Flavonifractor plautii</i> YL31	1.93 (0.31)	1.65 (0.12)	1.87 (0.25)	1.86 (0.51)
<i>Clostridium clostridioforme</i> YL32	5.34 (0.52)	4.73 (0.49)	3.01 (1.10)	3.88 (0.64)
'Acutalibacter muris' KB18	DTL	DTL	DTL	DTL
<i>Bifidobacterium longum</i> subsp. <i>animalis</i> YL2	DTL	DTL	DTL	DTL
<i>S. Tm</i>	0.22 (0.17)	0.34 (0.12)	0.55 (0.14)	0.74 (0.12)

Significant differences between **a** day 1 vs day 2, **b** day 2 vs day 3, **c** day 3 vs day 4 and **d** time point vs day 1 are indicated; p values were less than 0.001, except: YL27 day 1 vs day 2 p<0.05, I48 day 2 vs day 3 p<0.01, YL44 day 3 vs day 4 p<0.05 and YL44 day 1 vs day 3 p<0.01, two-way ANOVA with Bonferroni posttest. There were no significant differences between day 1 vs day 4. Values are expressed as mean % of cumulated 16S rRNA gene copy numbers +/- standard deviation (SD). Day 1 p.i.: n=5, day 2 p.i.: n=5, day 3 p.i.: n=6, day 4 p.i.: n=6. DTL: limit of detection. * Very low abundant.

Results

Table 46: Relative abundance of Oligo-MM¹² strains in feces after infection with *S. Tm*^{WT}

Strain	Mean % of cumulated 16S rRNA gene copy numbers (+/- SD)				
	Days post infection with <i>S. Tm</i> ^{WT}				
	Uninf.	Day 1	Day 2	Day 3	Day 4
' <i>Bacteroides caecimuris</i> ' I48	67.17 (3.16)	60.69 ^a (6.31)	67.44 ^b (3.03)	57.94 ^{c,e} (7.48)	0.12 ^{d,e} (0.26)
' <i>Muribaculum intestinale</i> ' YL27	10.16 (1.30)	10.30 (1.26)	11.51 (1.35)	10.65 (2.62)	0 ^{d,e*}
<i>Akkermansia muciniphila</i> YL44	16.73 (2.43)	20.92 ^a (4.58)	13.55 ^{b,e} (3.17)	19.45 ^c (4.36)	0.001 ^{d,e} (0.004)
' <i>Turicimonas caecimuris</i> ' YL45	2.30 (0.50)	2.56 (0.28)	2.50 (0.49)	2.17 (0.70)	DTL
<i>Lactobacillus reuteri</i> I49	0.06 (0.03)	0.07 (0.02)	0.07 (0.04)	0.08 (0.05)	0.59 (0.52)
<i>Enterococcus faecalis</i> KB1	0.02 (0.01)	0.03 (0.02)	0.01 (0.004)	0.01 (0.01)	0.37 (0.38)
<i>Blautia coccoides</i> YL58	0.73 (0.11)	1.43 (0.47)	0.74 (0.17)	0.96 (0.43)	DTL
<i>Clostridium innocuum</i> I46	0.09 (0.04)	0.08 (0.02)	0.06 (0.02)	0.09 (0.03)	0.02 (0.05)
<i>Flavonifractor plautii</i> YL31	1.77 (0.12)	2.31 (0.16)	2.20 (0.23)	2.43 (0.63)	0.93 (1.29)
<i>Clostridium clostridioforme</i> YL32	0.99 (0.14)	1.59 (0.55)	1.48 (0.61)	4.54 ^{c,e} (2.95)	0.33 ^d (0.66)
' <i>Acutalibacter muris</i> ' KB18	DTL	DTL	DTL	DTL	DTL
<i>Bifidobacterium longum</i> subsp. <i>animalis</i> YL2	DTL	DTL	DTL	DTL	DTL
<i>S. Tm</i>	DTL	0.02 (0.02)	0.44 (0.10)	1.67 (0.67)	97.64 ^{d,e} (2.14)

Significant differences between **a** uninf. vs d1, **b** day 1 vs day 2, **c** day 2 vs day 3, **d** day 3 vs day 4 and **e** time point vs uninf. are indicated; p values were less than 0.001, except: YL44 uninf. vs d1 p<0.01, YL32 day 2 vs day 3 in p<0.05, YL44 uninf. vs day 2 p<0.05 and YL32 uninf. vs day 3 p<0.01, two-way ANOVA with Bonferroni posttest. Values are expressed as mean % of cumulated 16S rRNA gene copy numbers +/- standard deviation (SD). Uninf.: n=6, day 1 p.i.: n=5, day 2 p.i.: n=5, day 3 p.i.: n=7, day 4 p.i.: n=7; Uninf.: uninfected. DTL: limit of detection; * very low abundant.

Results

Table 47: Relative abundance of Oligo-MM¹² strains in feces after infection with *S. Tm*^{Avir}

Strain	Mean % of cumulated 16S rRNA gene copy numbers (+/- SD)				
	Days post infection with <i>S. Tm</i> ^{Avir}				
	Uninf.	Day 1	Day 2	Day 3	Day 4
'Bacteroides caecimuris' I48	67.17 (3.16)	59.46 ^a (3.63)	64.11 ^b (4.37)	65.12 (7.64)	73.19 ^{c,d} (5.43)
'Muribaculum intestinale' YL27	10.16 (1.30)	9.47 (1.01)	14.12 ^{b,d} (3.09)	11.08 (1.91)	9.36 (2.31)
<i>Akkermansia muciniphila</i> YL44	16.73 (2.43)	24.55 ^a (3.83)	14.87 ^b (0.98)	16.33 (6.31)	11.17 ^{c,d} (2.66)
'Turicimonas caecimuris' YL45	2.30 (0.50)	1.98 (0.17)	2.20 (0.46)	2.20 (0.44)	2.37 (0.26)
<i>Lactobacillus reuteri</i> I49	0.06 (0.03)	0.08 (0.04)	0.01 (0.01)	0.06 (0.04)	0.12 (0.03)
<i>Enterococcus faecalis</i> KB1	0.02 (0.01)	0.02 (0.02)	0.01 (0.004)	0.01 (0.02)	0.003 (0.005)
<i>Blautia coccoides</i> YL58	0.73 (0.11)	0.93 (0.34)	0.61 (0.29)	1.16 (1.21)	0.79 (0.19)
<i>Clostridium innocuum</i> I46	0.09 (0.04)	0.08 (0.02)	0.05 (0.02)	0.13 (0.09)	0.06 (0.02)
<i>Flavonifractor plautii</i> YL31	1.77 (0.12)	2.33 (0.15)	1.90 (0.32)	1.66 (0.23)	1.38 (0.73)
<i>Clostridium clostridioforme</i> YL32	0.99 (0.14)	0.83 (0.24)	1.79 (1.33)	1.79 (0.71)	1.05 (0.32)
'Acutalibacter muris' KB18	DTL	DTL	DTL	DTL	DTL
<i>Bifidobacterium longum</i> subsp. <i>animalis</i> YL2	DTL	DTL	DTL	DTL	DTL
<i>S. Tm</i>	DTL	0.26 (0.26)	0.33 (0.07)	0.47 (0.15)	0.52 (0.11)

Significant differences between **a** uninf. vs day 1, **b** day 1 vs day 2, **c** day 3 vs day 4 and **d** time point vs uninf. are indicated; p values were less than 0.001, except: YL27 and I48 day 1 vs day 2 p<0.01 as well as YL27 uninf. vs day 2 p<0.01, two-way ANOVA with Bonferroni posttest. There were no significant differences between day 2 vs day 3 and uninf. vs day 3. Values are expressed as mean % of cumulated 16S rRNA gene copy numbers +/- standard deviation (SD). Uninf.: n=6, day 1 p.i.: n=5, day 2 p.i.: n=5, day 3 p.i.: n=6, day4 p.i.: n=6; Uninf.: uninfected. DTL: limit of detection.

Results

3.4 Towards understanding the mechanisms causing shifts in microbiota composition

3.4.1 Influence of Type 3 secretion systems (T3SS) 1 and 2

3.4.1.1 Both T3SSs are necessary to cause colitis and dysbiosis

Next, the contribution of T3SS-1 and T3SS-2 that are encoded on the *Salmonella* pathogenicity islands 1 and 2 (SPI-1 and -2), respectively were investigated using *Salmonella* mutant strains lacking either a functional T3SS-1: *S. Tm*^{SPI-1} (Kaniga *et al.* 1994) or a functional T3SS-2: *S. Tm*^{SPI-2} (Hapfelmeier *et al.* 2004). Oligo-MM¹² mice were infected with 5×10^7 CFUs of either *S. Tm*^{SPI-1} or *S. Tm*^{SPI-2} and scarified at day 4 p.i.. Data were subsequently compared to infection experiments with *S. Tm*^{Avir} ($\Delta invG$, $sseD::aphT$) and *S. Tm*^{WT} shown in Figure 10 (Figures 15; 16; 17). As already shown before, infection with *S. Tm*^{Avir} that lacks functional T3SS-1 and 2 did not to induce dysbiosis at day 4 p.i. (Figure 10). The same was true for *S. Tm*^{SPI-1} that is deficient in secreting effector proteins via T3SS-1 (Figure 15). Interestingly, *S. Tm*^{SPI-2} that has a functional T3SS-1 but is deficient in T3SS-2 was able to induce dysbiosis in 1 out of 5 mice (Figure 15). Again, dysbiosis correlated with cecal pathology (Figure 15B) and elevated LCN-2 levels (Figure 16B). Mice infected with *S. Tm*^{Avir} and *S. Tm*^{SPI-1} showed almost no cecal pathology and LCN-2 levels close to the limit of detection, whereas mice infected with *S. Tm*^{SPI-2} already displayed moderate colitis and elevated LCN-2 levels at day 4 p.i.. The animal infected with *S. Tm*^{SPI-2} that exhibited a dysbiotic microbiota even showed profound colitis and high LCN-2 levels comparable to mice infected with *S. Tm*^{WT} (Figures 15; 16B). Regarding *Salmonella* loads in cecal content, *S. Tm*^{SPI-2} loads were significantly higher than compared to *S. Tm*^{Avir} ($p < 0.05$, Kruskal-Wallis test with Dunn's multiple comparison test; Figure 16A). There was no statistically significant difference in colonization of mesenteric lymphnodes, liver or spleen at day 4 p.i. between *S. Tm*^{SPI-1} and *S. Tm*^{SPI-2} (Figure 16C-E). Compared to *S. Tm*^{Avir}, CFUs of *S. Tm*^{SPI-1} and *S. Tm*^{SPI-2} in mesenteric lymphnodes were increased by trend which was comparable in liver as well as in spleen. Compared to *S. Tm*^{Avir}, *S. Tm*^{WT} showed significantly increase in tissue loads at systemic sites (Kruskal-Wallis test with Dunn's multiple comparison test; Figure 16C-E). Interestingly, the relative cecum size which is also a measure for inflammation (rel. cecal weight negatively correlates with inflammation) of mice infected with *S. Tm*^{SPI-2} was comparable to the relative cecum size of mice infected with *S. Tm*^{WT} (Figure 16F), indicating that a functional T3SS-1 is crucial for the induction of inflammation in Oligo-MM¹² mice. In contrast, the relative cecum size of Oligo-MM¹² mice infected with either *S. Tm*^{Avir} (no T3SS-1 + 2) or *S. Tm*^{SPI-1} (no T3SS-1) was significantly increased at day 4 p.i. compared to relative cecum size of mice infected with *S. Tm*^{WT} ($p < 0.01$, $p < 0.05$, Kruskal-Wallis test with Dunn's multiple comparison test; Figure 16F).

Results

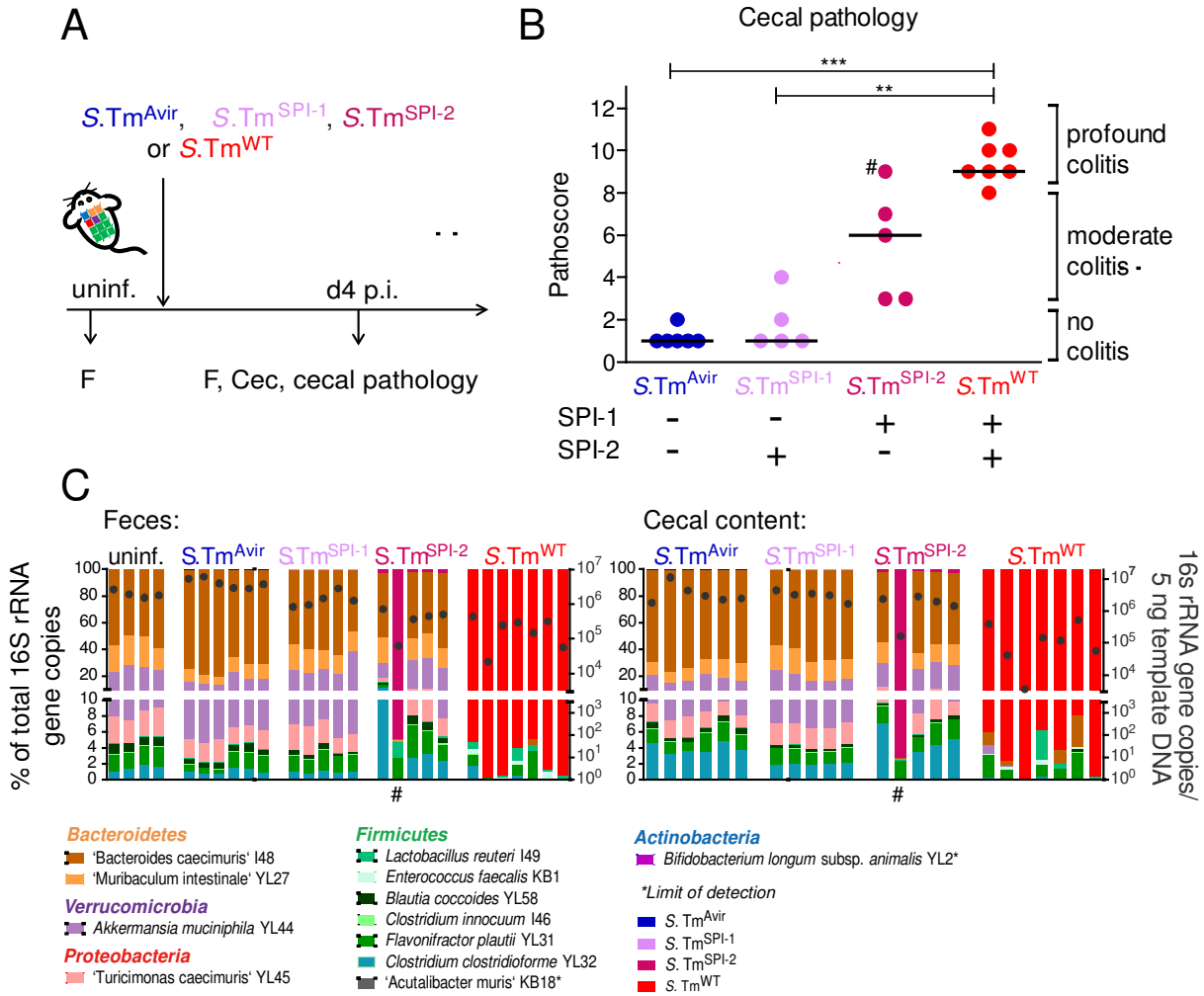


Figure 15: *Salmonella* requires functional T3SS-1 and T3SS-2 to induce dysbiosis at day 4 p.i.. (A) Experimental set-up: Oligo-MM¹² mice were orally infected with 5×10^7 CFUs of either *S. Tm^{Avir}* ($\Delta invG$, *sseD::aphT*), *S. Tm^{SPI-1}* ($\Delta invG$), *S. Tm^{SPI-2}* (*sseD::aphT*) or with *S. Tm^{WT}*. Data from infections with *S. Tm^{Avir}* and *S. Tm^{WT}* originate from the previous experiment (Figure 10). Mice were sacrificed at day 4 p.i. and samples were taken for analysis. There was also a fecal control sample taken before infection. (B) Cecal pathology determined by evaluation of HE stained tissue sections. (C) Analysis of microbiota composition in feces (left) and cecal content (right) at day 4 p.i. with different *Salmonella* mutant strains. Microbiota composition is shown as relative abundance and expressed as % of cumulated 16S rRNA gene copy numbers (% of total 16S rRNA gene copies). The amount of absolute 16S rRNA gene copies (determined by an universal primer / probe combination) is illustrated as black dots (the right y axis). * Limit of detection. Statistical analysis of cecal pathology was performed using Kruskal-Wallis test with Dunn's multiple comparison test (*** $p < 0.001$, ** $p < 0.01$). # Animal that exhibited dysbiotic microbiota after infection with *S. Tm^{SPI-2}*.

Results

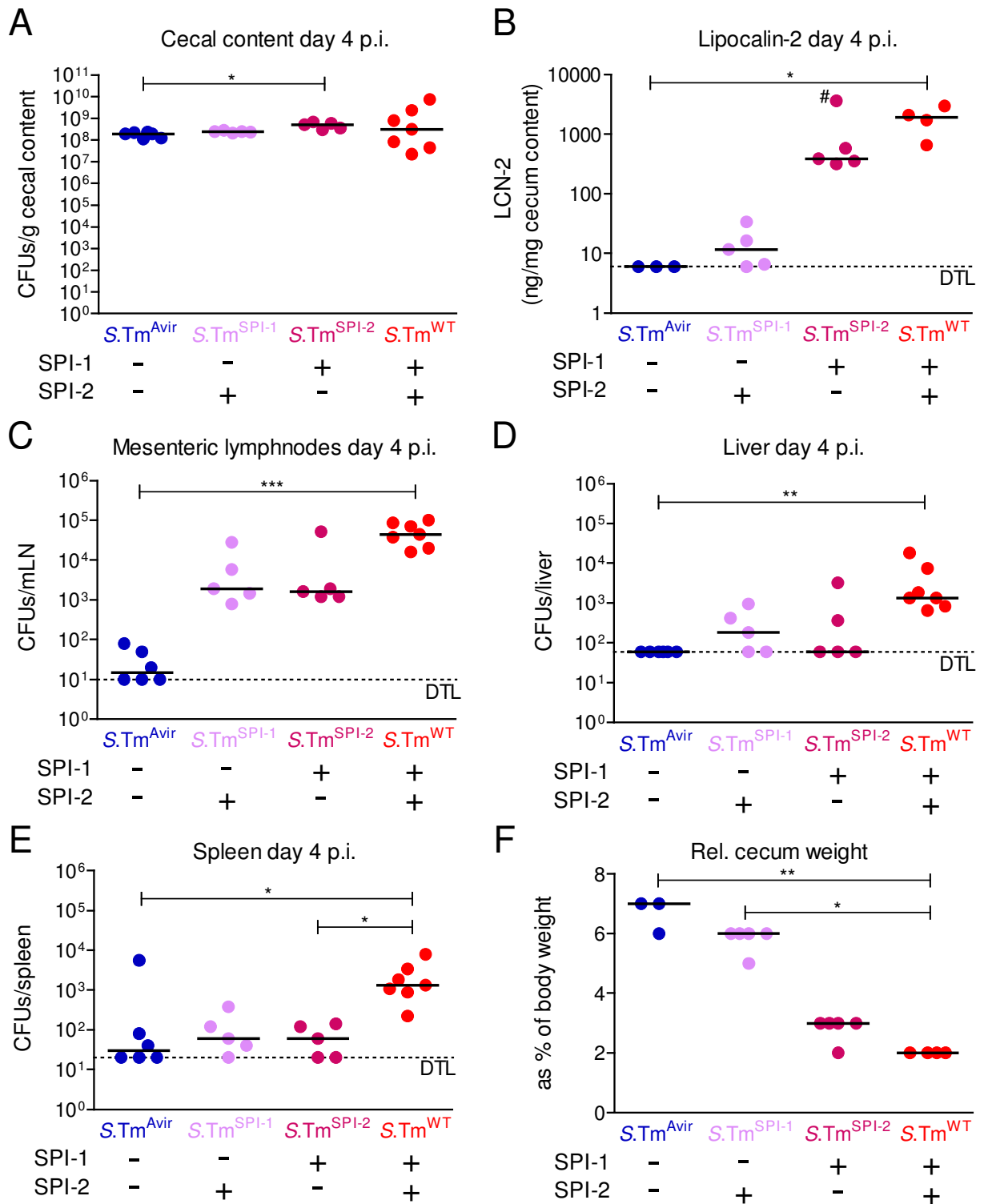


Figure 16: The contribution of SPI-1 and SPI-2 T3SSs to systemic colonization at day 4 p.i.: For experimental set-up refer to Figure 15A. Organs were additionally taken at the indicated time points. **(A)** *Salmonella* loads in cecal content at day 4 p.i. (CFUs *S. Tm* / g content). **(B)** Lipocalin-2 (LCN-2) amount in cecal content at day 4 p.i. measured by ELISA (ng / mg cecal content) **(C) – (E)** Systemic *Salmonella* in mesenteric lymphnodes, liver and spleen (CFUs per organ). **(F)** Relative cecum weight at day 4 p.i. expressed as % of body weight. Statistical analysis between groups was performed using Kruskal-Wallis test with Dunn's multiple comparison test (* $p < 0.05$, ** $p < 0.01$, *** $p < 0.001$). # Animal that exhibited dysbiotic microbiota after infection with *S. Tm*^{SPI-2}. Dashed lines: DTL: limit of detection (mLN: 10 CFUs, liver: 60 CFUs, spleen: 20 CFUs).

Results

In order to correlate shifts in microbiota composition with the presence of a functional T3SS-1 and 2, samples were grouped according to the *S. Tm* mutant strains (uninf., *S. Tm*^{Avir}, *S. Tm*^{SPI-1}, *S. Tm*^{SPI-2} and *S. Tm*^{WT}, Figure 17) and cluster analysis was performed. Grouping of fecal microbiota composition and microbiota composition in cecal content by infection with different *Salmonella* strains was significant, according to Bray Curtis ($p < 0.001$, Adonis) and Pearson ($p < 0.001$, Adonis) distance matrices, with 86% (in feces, Bray Curtis and Pearson) as well as 84% (in cecal content, Bray Curtis) and 85% (in cecal content, Pearson) of variation explained. As already mentioned, the fecal microbiota composition at day 4 p.i. with *S. Tm*^{WT} (functional T3SS-1 + 2) which displayed dysbiosis that was characterized by a domination of *Salmonella* and the presence of some 'intermediate' and 'enriched' Oligo-MM¹² strains (Figures 10; 14) significantly differed compared to the microbiota composition before infection and after infection with *S. Tm*^{Avir} (no functional T3SS-1 and 2, non parametric PERMDISP procedure; Figure 17A,B). Interestingly, microbiota composition in cecal content after infection with *S. Tm*^{SPI-1} (no functional T3SS-1) and *S. Tm*^{Avir} was also significantly different compared to the microbiota composition at day 4 post infection with *S. Tm*^{WT} (non parametric PERMDISP procedure; Figure 17D). 1 out of 5 samples infected with *S. Tm*^{SPI-2} (functional T3SS-1) even clustered together with the dysbiotic microbiota of *S. Tm*^{WT} infected animals (Figure 17C,D). These data indicate that both, T3SS-1 and T3SS-2 synergistically contribute to *Salmonella* induced dysbiosis and that the T3SS-1 might be of more importance.

The mean relative abundance of *S. Tm*^{SPI-1} and *S. Tm*^{Avir} at day 4 p.i. was comparable and less than 1% in feces and cecal content, whereas the relative abundance of *S. Tm*^{SPI-2} was around 20% (Tables 48; 49). This increase was significant compared to the relative abundance of *S. Tm*^{SPI-1} and *S. Tm*^{Avir} (two-way ANOVA with Bonferroni posttest; Tables 48; 49). Besides the increased relative abundance of *S. Tm*^{SPI-2}, the relative abundance of 'Bacteroides caecimuris' I48 was decreased (around -20%) post infection with *S. Tm*^{SPI-2} compared to infection with *S. Tm*^{SPI-1} ($p < 0.001$, two-way ANOVA with Bonferroni posttest; Tables 48; 49). The relative abundance of the residual Oligo-MM¹² strains was comparable at day 4 p.i. with *S. Tm*^{SPI-1} and *S. Tm*^{SPI-2}. Comparing the Oligo-MM¹² composition post infection with *S. Tm*^{SPI-2} and *S. Tm*^{WT}, the relative abundance of 'Bacteroides caecimuris' I48, 'Muribaculum intestinale' YL27 and *Akkermansia muciniphila* YL44 was significantly decreased post infection with *S. Tm*^{WT} (two-way ANOVA with Bonferroni posttest; Tables 48; 49), again underlining a synergistic effect of the both type three secretion systems on the microbiota.

Results

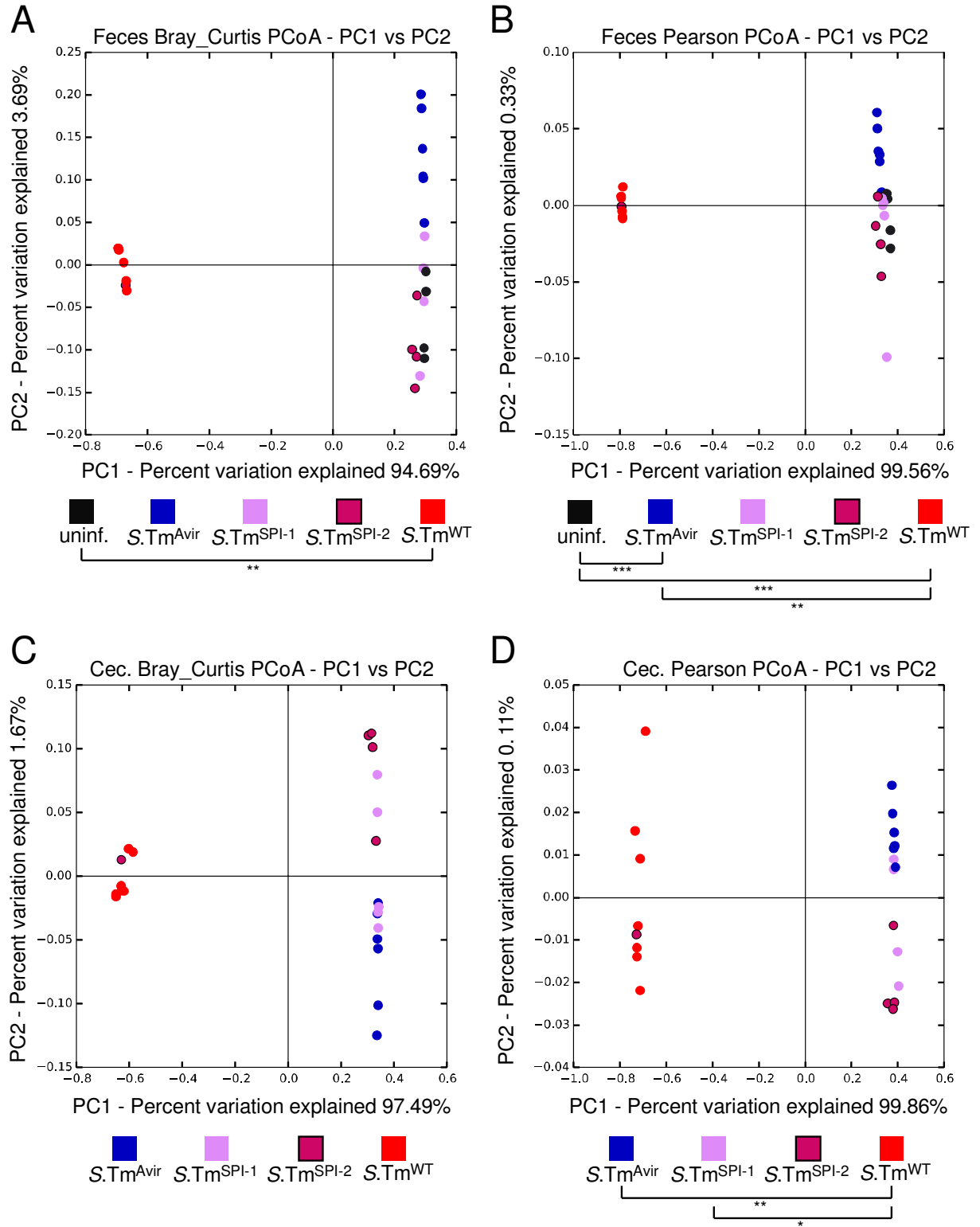


Figure 17: Cluster analysis of Oligo-MM¹² after infection with *S. Tm*^{WT} and *S. Tm* mutant strains deficient in T3SSs. Cluster analysis is based on Bray Curtis or Pearson distance matrices and visualized as PCoA plots. (A) and (B) clustering of fecal Oligo-MM¹² composition after infection with *S. Tm* strains. Fecal microbiota samples were grouped by infection with different *S. Tm* strains. Grouping by infection with different *S. Tm* strains was significant, according to Bray Curtis ($p < 0.001$, Adonis) and Pearson ($p < 0.001$, Adonis) with 86% (Bray Curtis, Pearson) of variation explained. Additional PERMDISP analyses based on Bray Curtis and Pearson distance matrices revealed statistically significant differences in fecal microbiota composition after infection with *S. Tm*^{Avir}, *S. Tm*^{WT} and uninfected samples (** $p < 0.01$, *** $p < 0.001$). (C) and (D) clustering of Oligo-MM¹².

Results

composition after infection with *S. Tm* strains in cecal content. Microbiota samples from cecal content were grouped by infection with different *S. Tm* strains. Grouping was significant, according to Bray Curtis ($p < 0.001$, Adonis) and Pearson ($p < 0.001$, Adonis) with 84% (Bray Curtis) and 85% (Pearson) of variation explained. Additional PERMDISP analyses based on Pearson distance matrix revealed statistically significant differences in microbiota composition in cecal content after infection with *S. Tm*^{Avir}, *S. Tm*^{SPI-1} and *S. Tm*^{WT} (* $p < 0.05$, ** $p < 0.01$).

Table 48: Relative abundance of Oligo-MM¹² strains in feces at day 4 after infection with different *S. Tm* strains deficient in functional T3SSs.

Strain	Mean % of cumulated 16S rRNA gene copy numbers (+/- SD)				
	Day 4 post infection with <i>Salmonella</i> mutants (feces)				
	Uninf.	<i>S. Tm</i> ^{Avir}	<i>S. Tm</i> ^{SPI-1}	<i>S. Tm</i> ^{SPI-2}	<i>S. Tm</i> ^{WT}
'Bacteroides caecimuris' I48	53.96 (4.97)	73.19 ^a (5.43)	57.02 ^d (6.97)	39.80 ^{b,e,g} (22.55)	0.12 ^{c,f,h,i} (0.26)
'Muribaculum intestinale' YL27	20.53 (3.23)	9.36 (2.31)	15.84 (2.21)	14.14 (8.09)	0 ^{c,h,i*}
<i>Akkermansia muciniphila</i> YL44	17.27 (2.85)	11.17 (2.66)	20.00 (7.35)	14.68 (9.37)	0.001 ^{c,f,h,i} (0.004)
'Turicimonas caecimuris' YL45	3.23 (0.35)	2.37 (0.26)	2.76 (0.67)	2.16 (1.27)	DTL
<i>Lactobacillus reuteri</i> I49	0.09 (0.02)	0.12 (0.03)	0.02 (0.02)	0.45 (0.83)	0.59 (0.52)
<i>Enterococcus faecalis</i> KB1	0.002 (0.01)	0.003 (0.01)	0 [*]	0.004 (0.01)	0.37 (0.38)
<i>Blautia coccoides</i> YL58	1.11 (0.14)	0.79 (0.19)	0.48 (0.19)	0.88 (0.59)	DTL
<i>Clostridium innocuum</i> I46	0.10 (0.02)	0.06 (0.02)	0.05 (0.01)	0.12 (0.08)	0.02 (0.05)
<i>Flavonifractor plautii</i> YL31	2.27 (0.24)	1.38 (0.73)	2.17 (0.35)	2.73 (0.79)	0.93 (1.29)
<i>Clostridium clostridioforme</i> YL32	1.44 (0.37)	1.05 (0.32)	0.93 (0.12)	3.92 (4.24)	0.33 (0.66)
'Acutalibacter muris' KB18	DTL	DTL	DTL	DTL	DTL
<i>Bifidobacterium longum</i> subsp. <i>animalis</i> YL2	DTL	DTL	DTL	DTL	DTL
<i>S. Tm</i>	DTL	0.52 (0.11)	0.71 (0.12)	21.12 ^{b,e,g} (41.29)	97.64 ^{c,f,h,i} (2.14)

Significant differences between **a** uninf. vs *S. Tm*^{Avir}, **b** uninf. vs *S. Tm*^{SPI-2}, **c** uninf. vs *S. Tm*^{WT}, **d** *S. Tm*^{Avir} vs *S. Tm*^{SPI-1}, **e** *S. Tm*^{Avir} vs *S. Tm*^{SPI-2}, **f** *S. Tm*^{Avir} vs *S. Tm*^{WT}, **g** *S. Tm*^{SPI-1} vs *S. Tm*^{SPI-2}, **h** *S. Tm*^{SPI-1} vs *S. Tm*^{WT} and **i** *S. Tm*^{SPI-2} vs *S. Tm*^{WT} are indicated; p values were less than 0.001, except: I48 uninf. vs *S. Tm*^{SPI-2} $p < 0.01$, YL44 *S. Tm*^{Avir} vs *S. Tm*^{WT} $p < 0.05$ and YL27 *S. Tm*^{SPI-2} vs *S. Tm*^{WT} $p < 0.01$, two-way ANOVA with Bonferroni posttest. There were no significant differences between uninf. vs *S. Tm*^{SPI-1}. Values are expressed as mean % of cumulated 16S rRNA gene copy number +/- standard deviation (SD). *S. Tm*^{SPI-1}: no functional T3SS-1, *S. Tm*^{SPI-2}: no functional T3SS-2 and *S. Tm*^{Avir}: no functional T3SSs-1 and -2. Uninf.: $n = 4$, *S. Tm*^{Avir}: $n = 6$, *S. Tm*^{SPI-1}: $n = 5$, *S. Tm*^{SPI-2}: $n = 5$, *S. Tm*^{WT}: $n = 7$; Uninf.: uninfected; DTL: limit of detection; * very low abundant.

Results

Table 49: Relative abundance of Oligo-MM¹² strains in cecal content at day 4 after infection with different *S. Tm* strains deficient in functional T3SSs.

Strain	Mean % of cumulated 16S rRNA gene copy numbers (+/- SD)			
	Day 4 post infection with <i>Salmonella</i> mutants			
	<i>S. Tm</i> ^{Avir}	<i>S. Tm</i> ^{SPI-1}	<i>S. Tm</i> ^{SPI-2}	<i>S. Tm</i> ^{WT}
'Bacteroides caecimuris' I48	70.18 (3.97)	63.48 (5.31)	44.14 ^{a,c} (24.94)	1.15 ^{b,d,e} (1.47)
'Muribaculum intestinale' YL27	10.97 (2.35)	16.36 (2.18)	11.27 (6.53)	0.01 ^{b,d,e} (0.01)
<i>Akkermansia muciniphila</i> YL44	9.56 (2.02)	12.50 (3.25)	14.55 (8.15)	0.17 ^{d,e} (0.38)
'Turicimonas caecimuris' YL45	2.05 (0.37)	2.64 (0.11)	1.93 (1.20)	0*
<i>Lactobacillus reuteri</i> I49	0.08 (0.03)	0.01 (0.004)	0.07 (0.07)	0.65 (1.34)
<i>Enterococcus faecalis</i> KB1	0*	0*	0*	0.18 (0.19)
<i>Blautia coccoides</i> YL58	0.60 (0.18)	0.37 (0.07)	0.27 (0.17)	0.07 (0.16)
<i>Clostridium innocuum</i> I46	0.08 (0.02)	0.07 (0.02)	0.07 (0.05)	0.01 (0.02)
<i>Flavonifractor plautii</i> YL31	1.86 (0.51)	1.79 (0.21)	2.27 (0.36)	1.50 (1.28)
<i>Clostridium clostridioforme</i> YL32	3.88 (0.64)	1.94 (0.11)	4.01 (2.58)	0.09 (0.15)
'Acutalibacter muris' KB18	DTL	DTL	DTL	DTL
<i>Bifidobacterium longum</i> subsp. <i>animalis</i> YL2	DTL	DTL	DTL	DTL
<i>S. Tm</i>	0.74 (0.12)	0.83 (0.15)	21.43 ^{a,c} (42.44)	96.18 ^{b,d,e} (3.09)

Significant differences between **a** *S. Tm*^{Avir} vs *S. Tm*^{SPI-2}, **b** *S. Tm*^{Avir} vs *S. Tm*^{WT}, **c** *S. Tm*^{SPI-1} vs *S. Tm*^{SPI-2}, **d** *S. Tm*^{SPI-1} vs *S. Tm*^{WT} and **e** *S. Tm*^{SPI-2} vs *S. Tm*^{WT} are indicated; p values were less than 0.001, except: YL27 *S. Tm*^{Avir} vs *S. Tm*^{WT} p<0.05, YL44 *S. Tm*^{SPI-1} vs *S. Tm*^{WT} p<0.05 as well as *S. Tm*^{SPI-2} vs *S. Tm*^{WT}: YL27 p<0.05 and YL44 p<0.01, two-way ANOVA with Bonferroni posttest. There were no significant differences between *S. Tm*^{Avir} vs *S. Tm*^{SPI-1}. Values are expressed as mean % of total bacteria +/- the standard deviation (SD). *S. Tm*^{SPI-1}: no T3SS-1, *S. Tm*^{SPI-2}: no functional T3SS-2 and *S. Tm*^{Avir}: no functional T3SS-1 and -2. *S. Tm*^{Avir}: n=6, *S. Tm*^{SPI-1}: n=5, *S. Tm*^{SPI-2}: n=5, *S. Tm*^{WT}: n=7; DTL: limit of detection; * very low abundant.

Results

3.4.1.2 The Oligo-MM¹² is resilient to infection with *S. Tm*^{SPI-2}

In order to study the capability of the Oligo-MM¹² to recover from inflammation induced dysbiosis (resilience), Oligo-MM¹² mice were infected with 5×10^7 CFUs of *S. Tm*^{SPI-2} and fecal samples were taken until day 21 p.i. to monitor microbial composition and LCN-2 levels. *S. Tm*^{SPI-2} was chosen because it can induce dysbiosis in a fraction of animals (Figure 15C) and the mice only developed moderate colitis (Figure 15B). It could be additionally show previously that mice do not develop fulminant systemic infection and that the mice survive long-term infection (Endt *et al.* 2010). This is in stark contrast to *S. Tm*^{WT} which induces severe colitis and systemic infection that is life threatening already at day 4 p.i.. As expected, mice did not show signs of disease during the course of infection with *S. Tm*^{SPI-2}. *S. Tm*^{SPI-2} colonized well (10^8 CFUs per g feces) and was not cleared from the gut until day 21 p.i. (Figure 19A). CFUs of *S. Tm*^{SPI-2} in mesenteric lymphnodes were still elevated at day 21 p.i. and comparable to the level observed at day 4 p.i. (Figures 16C; 19B). *S. Tm*^{SPI-2} was additionally still detectable in spleen and liver at day 21 p.i. (Figure 19B) and levels were comparable to day 4 p.i. (Figure 16D,E). This indicates that *S. Tm*^{SPI-2} is not cleared after infection from Oligo-MM¹² mice. For unknown reasons, fecal LCN-2 levels were elevated before infection. LCN-2 levels decreased during the course of infection (Figure 18B). Looking at the microbiota composition, *S. Tm*^{SPI-2} was not able to shift the microbiota composition drastically (Figure 18C). However, according to cluster analyses by days post infection, the microbiota clustered differently at day 4 p.i. (Figure 18D,E) which coincided with a transient increase of *Akkermansia muciniphila* YL44 (Figure 18C). The grouping was significant, according to Bray Curtis ($p < 0.001$, Adonis) and Pearson ($p < 0.007$, Adonis) distance matrices, with 76% (Bray Curtis) as well as 92% (Pearson correlation) of variation explained. Further non parametric PERMDISP analyses revealed significant differences in microbiota composition between days 4 and 5, 5 and 6 as well as between days 14 and 21 (according to Bray Curtis; Figure 18D). According to Pearson, there was also a significant difference in microbial composition between days 5 and 6, 3 and 6 as well as between 14 and 21 (non parametric PERMDISP procedure; Figure 18E). Interestingly, there was no statistical significant difference in microbial composition between day 21 and the Oligo-MM¹² composition before infection. This indicates the potential of the Oligo-MM¹² to fully recover from transient *S. Tm*^{SPI-2} induced dysbiosis.

Results

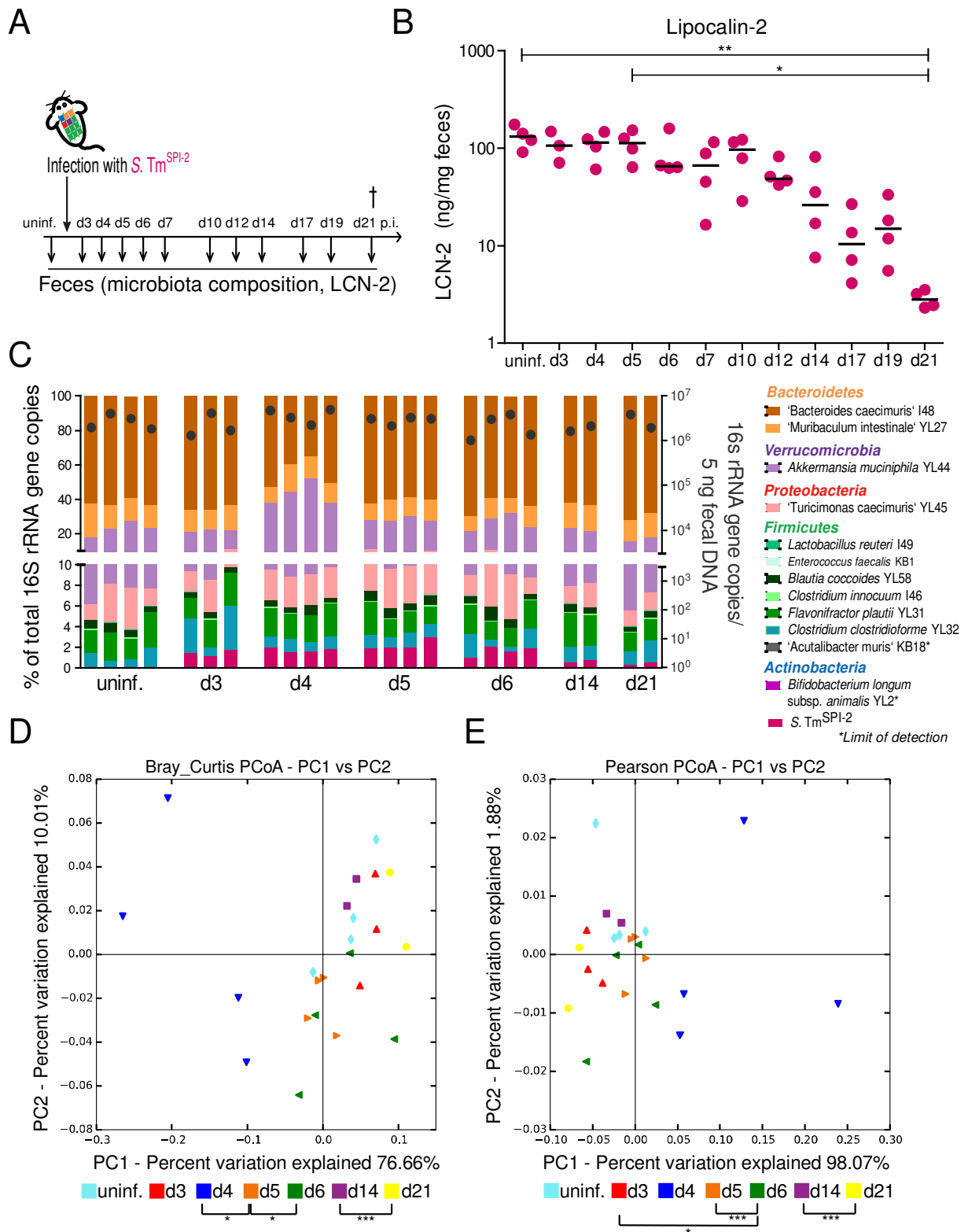


Figure 18: The Oligo-MM¹² is resilient to long-term infection with *S. Tm*^{SPI-2}. (A) Experimental set-up: Oligo-MM¹² mice were infected with 5×10^7 CFUs of *S. Tm*^{SPI-2} (*sseD::aphT*) and housed in gnotocages. During the course of the experiment feces (F) was taken under sterile conditions (for microbiota analysis and Lipocalin-2 ELISA) and mice were finally euthanized at day 21 p.i.. There was also a fecal control sample taken at day 0 before infection (uninf.). (B) Lipocalin-2 (LCN-2) levels in feces measured by ELISA (ng / mg feces). (C) Microbiota composition is shown as relative abundance and expressed as % of cumulated 16S rRNA gene copy numbers (% of total 16S rRNA gene copies). The amount of absolute 16S rRNA gene copies (determined by an universal primers / probe combination) is illustrated as black dots (right y axis). * Limit of detection. Cluster

Results

analysis is based on Bray Curtis **(D)** or Pearson **(E)** distance matrices and visualized as PCoA plots. Fecal microbiota samples were grouped by days post infection with *S. Tm*^{SPI-2} which was significant, according to Bray Curtis ($p < 0.001$, Adonis) and Pearson ($p < 0.007$, Adonis) with 76% (Bray Curtis) and 92% (Pearson) of variation explained. PERMDISP analyses based on Bray Curtis and Pearson distance matrices revealed statistically significant differences in fecal microbiota composition between days post infection with *S. Tm*^{SPI-2} (* $p < 0.05$, ** $p < 0.01$). However, there was no statistically significant difference between day 21 p.i. ($n=2$) and the day before infection ($n=4$).

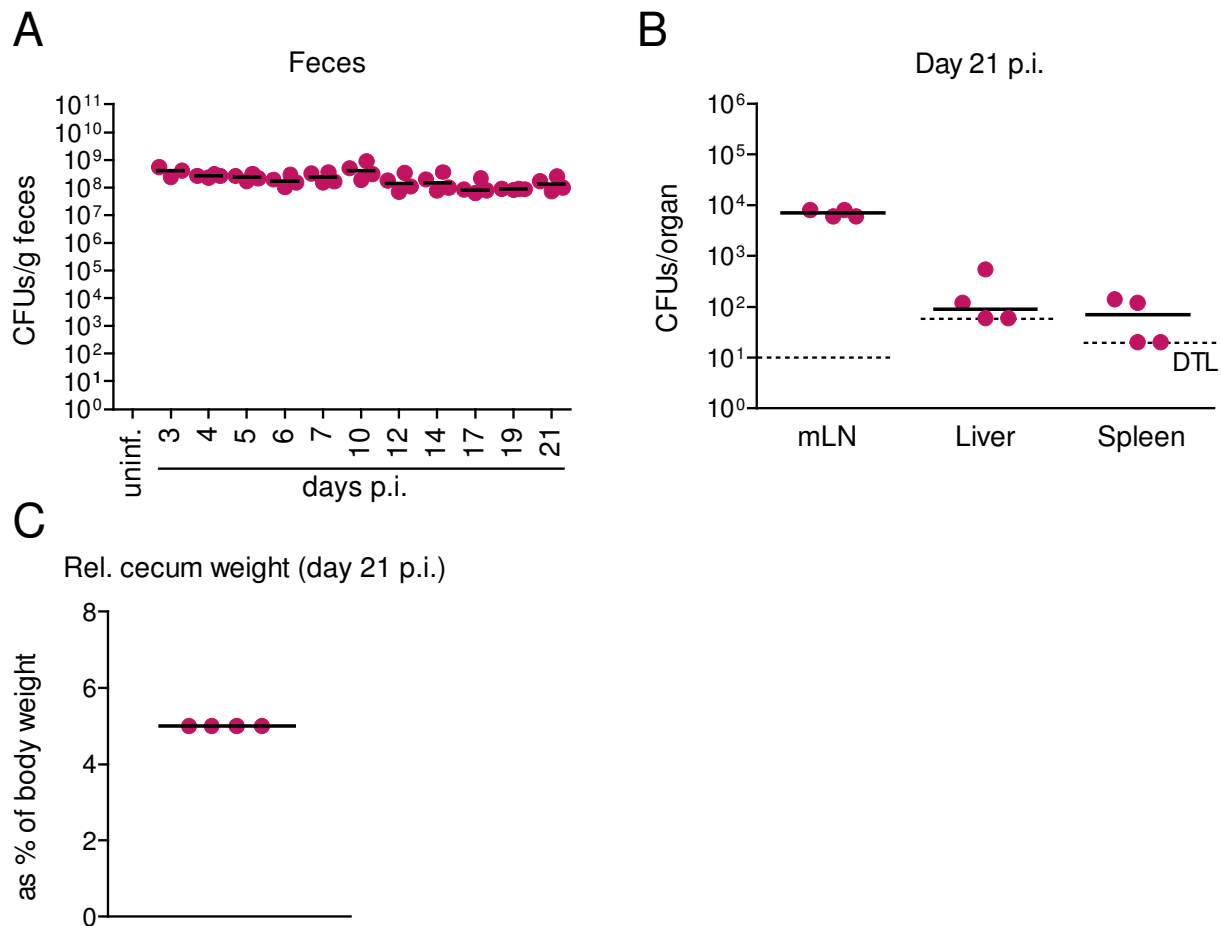


Figure 19: The Oligo-MM¹² do not clear *S. Tm*^{SPI-2} until day 21 post infection. The experimental set-up is detailed in Figure 18A. **(A)** *Salmonella* loads in feces. Feces was sampled at the indicated time points and CFUs / g feces were determined by plating. **(B)** Systemic *Salmonella* in mesenteric lymphnodes (mLN), liver and spleen (CFUs per organ) at day 21 p.i.. **(C)** Relative cecum weight at day 21 p.i. expressed as % of body weight. Dashed lines: DTL: limit of detection (mLN: 10 CFUs, liver: 60 CFUs, spleen: 20 CFUs).

Results

3.4.2 Influence of altered environmental conditions during colitis on the microbiota

3.4.2.1 *In vitro* testing of *Salmonella* strains deficient in anaerobic respiration, siderophore production and ethanolamine utilization

3.4.2.1.1 *S. Tm^{Ni}* ($\Delta narZ$; *narG::cat*; *napA::aphT*) is incapable of nitrate respiration

In order to investigate the importance of nitrate respiration during *Salmonella* 'blooms' in Oligo-MM¹² mice and concomitant microbiota shifts, three genes essential for nitrate respiration *narZ*, *narG* and *napA* (Lopez *et al.* 2012) were deleted in *S. Tm*. *S. Tm* possesses three nitrate reductases encoded by the *narGHI* (nitrated reductase A), *narZYV* (nitrate reductase Z) and *napABC* (periplasmic nitrate reductase) gene clusters. While nitrate reductase Z is constitutively expressed, nitrate reductase A (low affinity) and the periplasmic nitrate reductase (high affinity) are expressed under anaerobic conditions. Especially, the high affinity periplasmic nitrate reductase is important for *Salmonella* during colitis (Vázquez-Torres and Bäumler 2016).

Successful replacement of the genes in *S. Tm^{Ni}* by antibiotic resistance markers was verified by PCR (data not shown) and the phenotype of *S. Tm^{Ni}* was tested *in vitro*. Under aerobic conditions, *S. Tm^{Ni}* in minimal M9 medium showed similar growth compared to *S. Tm^{WT}* (Figure 20A). This was independent of the presence of nitrate (20 mM). None of the two strains reduced nitrate to nitrite when oxygen was present. Remarkably, under anaerobic conditions *S. Tm^{Ni}* showed a growth disadvantage compared to *S. Tm^{WT}* when nitrate was supplemented to the M9 medium (Figure 20B). In contrast to *S. Tm^{WT}*, *S. Tm^{Ni}* failed to reduce nitrate to nitrite under anaerobic conditions (Figure 20B). *S. Tm^{Ni}* was additionally outcompeted by *S. Tm^{WT}* which grew 5 times better in mucin broth supplemented with nitrate (40 mM). There was no competitive advantage in plain mucin broth without nitrate (Figure 20C). This indicates that *S. Tm^{Ni}* is unable to respire nitrate and that the genetic manipulation of the strain just affected nitrate respiration genes since *S. Tm^{Ni}* grew as good as *S. Tm^{WT}* under aerobic conditions.

Results

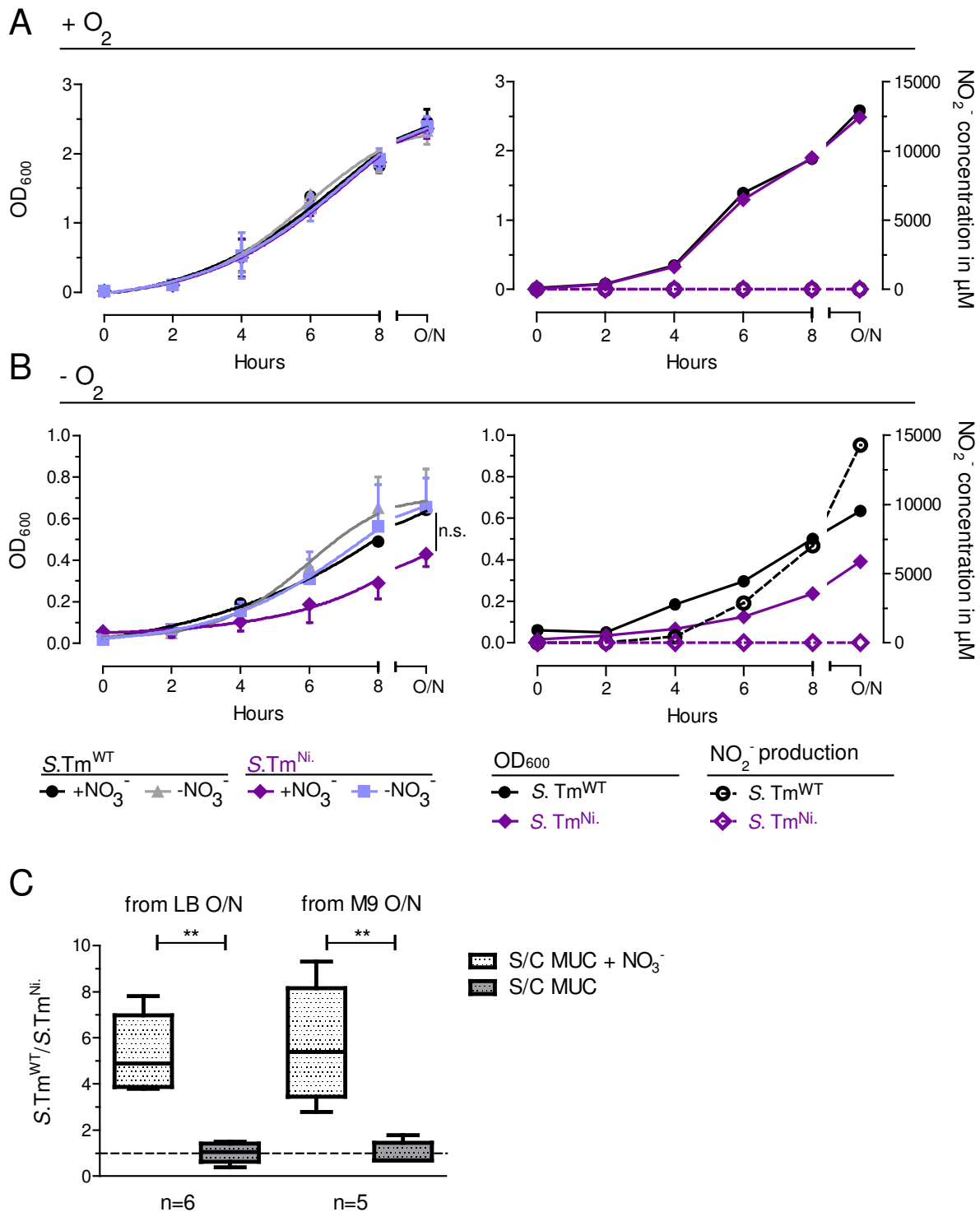


Figure 20: *S. Tm*^{Ni} is unable to respire nitrate and has a growth disadvantage compared to *S. Tm*^{WT} in medium supplemented with nitrate. (A) and (B) growth curves of *S. Tm*^{WT} and *S. Tm*^{Ni} with and without NO₃⁻ (20 mM) under aerobic (+O₂) as well as anaerobic conditions (-O₂; 7% H₂, 10% CO₂, rest N₂) are shown. Bacteria were grown in M9 minimal medium with glucose. Data for growth curves without NO₂⁻ measurement (left curves) originate from 3 independent experiments and are shown as the mean +/- standard deviation of n experiments (n=3 except: t=6, 8 n=2). N.s.: not significant (p>0.05, 1 way ANOVA with Bonferroni's multiple comparison test at the given time point). Growth curves with NO₂⁻ measurement (right curves) show the results of one single experiment that is representative for three independent experiments. Samples were taken after 0, 2, 4, 6 and 8 h as well as over night (o/n). (C) Competitive index: *S. Tm*^{WT} vs *S. Tm*^{Ni}. Bacterial o/n starter cultures in either LB (n=6 from individual colonies) or M9 minimal medium (n=5) were used to inoculate 24 h

Results

co-cultures in mucin broth with (S/C MUC + NO₃⁻ 40 mM) or without NO₃⁻ (S/C MUC) as described (Lopez *et al.* 2012). Box and whiskers blot (whiskers from min to max). ** p<0.01 (Mann-Whitney U test).

3.4.2.1.2 *S. Tm*^{Ni. + Te.} ($\Delta narZ$; *narG*::*cat*; *napA*::*aphT*; *ttrS*::*tet*) shows impaired growth in anaerobic tetrathionate broth

Besides nitrate, tetrathionate is also an anaerobic electron acceptor used by *Salmonella* during inflammation (Winter *et al.* 2010). In order to abolish tetrathionate respiration in addition to nitrate respiration, *ttrS* which is part of a two-component regulatory system essential for expression of tetrathionate reductase (Hensel *et al.* 1999) was replaced by a tetracycline resistance cassette. The genetic modification of *S. Tm*^{Ni. + Te.} was verified by PCR (data not shown) and an *in vitro* competition experiment (*S. Tm*^{Ni.} vs *S. Tm*^{Ni. + Te.}) in mucin broth with or without tetrathionate (40 mM) was performed. In order to enhance the growth of *S. Tm*^{Ni.} and *S. Tm*^{Ni. + Te.} which are both auxotrophic for histidine (SL1344 *Salmonella* background), the mucin broth was additionally supplemented with histidine (500 mg/l). When tetrathionate was added, *S. Tm*^{Ni. + Te.} was outcompeted by trend and *S. Tm*^{Ni.} grew 2.5 times better than *S. Tm*^{Ni. + Te.} as described previously (Winter *et al.* 2010). However when tetrathionate was absent, both strains grew equally well (Figure 21). This indicates that *S. Tm*^{Ni. + Te.} is not able to profit from tetrathionate respiration.

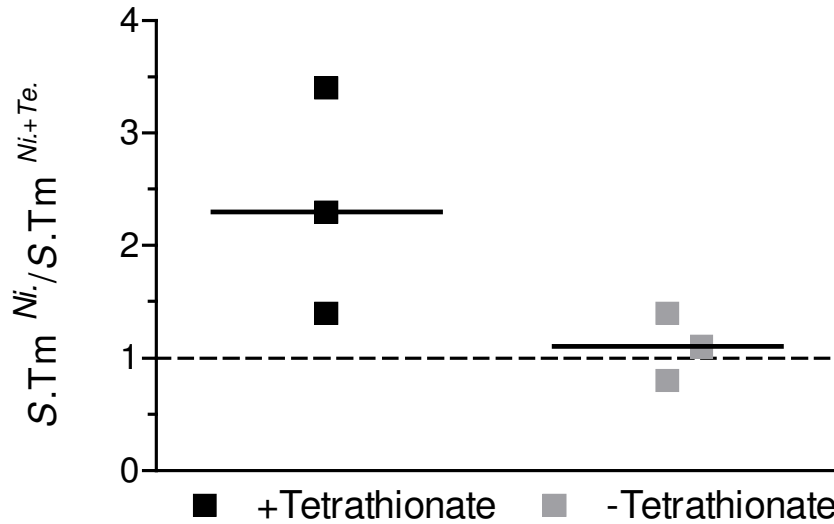


Figure 21: *S. Tm*^{Ni. + Te.} is outcompeted by *S. Tm*^{Ni.} in the presence of tetrathionate under anaerobic conditions. Competitive index: LB starter cultures of *S. Tm*^{Ni.} as well as *S. Tm*^{Ni. + Te.} were used to inoculate 24 h competition cultures in mucin broth supplemented with histidine (500 mg/l) with or without tetrathionate (40 mM). Competitive index with or without tetrathionate was not significantly different (p=0.12, Mann Whitney test). Data are expressed as the median of 3 experiments.

Results

3.4.2.1.3 *S. Tm*^{EntA} (*entA::cat*) is impaired in siderophore secretion

Iron is scarce and even more restricted in the inflamed gut e.g. via host mediated LCN-2 production, which sequesters siderophores such as enterochelin (Raffatellu *et al.* 2009). However, *Salmonella* manages to overcome iron-limitation mediated by LCN-2 secretion using a glycosylated derivative of enterochelin termed salmochelin that cannot be inactivated by LCN-2 (Raffatellu *et al.* 2009). In order to investigate the role of siderophore mediated iron acquisition, *entA* which is a 2,3-dihydroxybenzoic acid (DHB) biosynthetic enzyme involved in the production of salmochelin and enterochelin (Caza *et al.* 2015, Pakarian and Pawelek 2016) was replaced by a chloramphenicol resistance cassette. The knock in of the resistance cassette was confirmed by PCR (data not shown) and the mutant phenotype was characterized *in vitro* using Chromazurol S (CAS) agar plates. CAS together with Hexadecyltrimethylammonium (HDTMA) complexes ferric iron (Fe³⁺) (blue color). In the presence of siderophores, iron can be sequestered from the complex and the agar turns into an orange color. Compared to *S. Tm*^{WT}, *S. Tm*^{EntA} grew equally well in LB starter cultures (Figure 22A) indicating no other genetic alteration than *entA::cat*. When spotted on CAS – agar plates, the halo of *S. Tm*^{EntA} was smaller than *S. Tm*^{WT} (Figure 22B).

Results

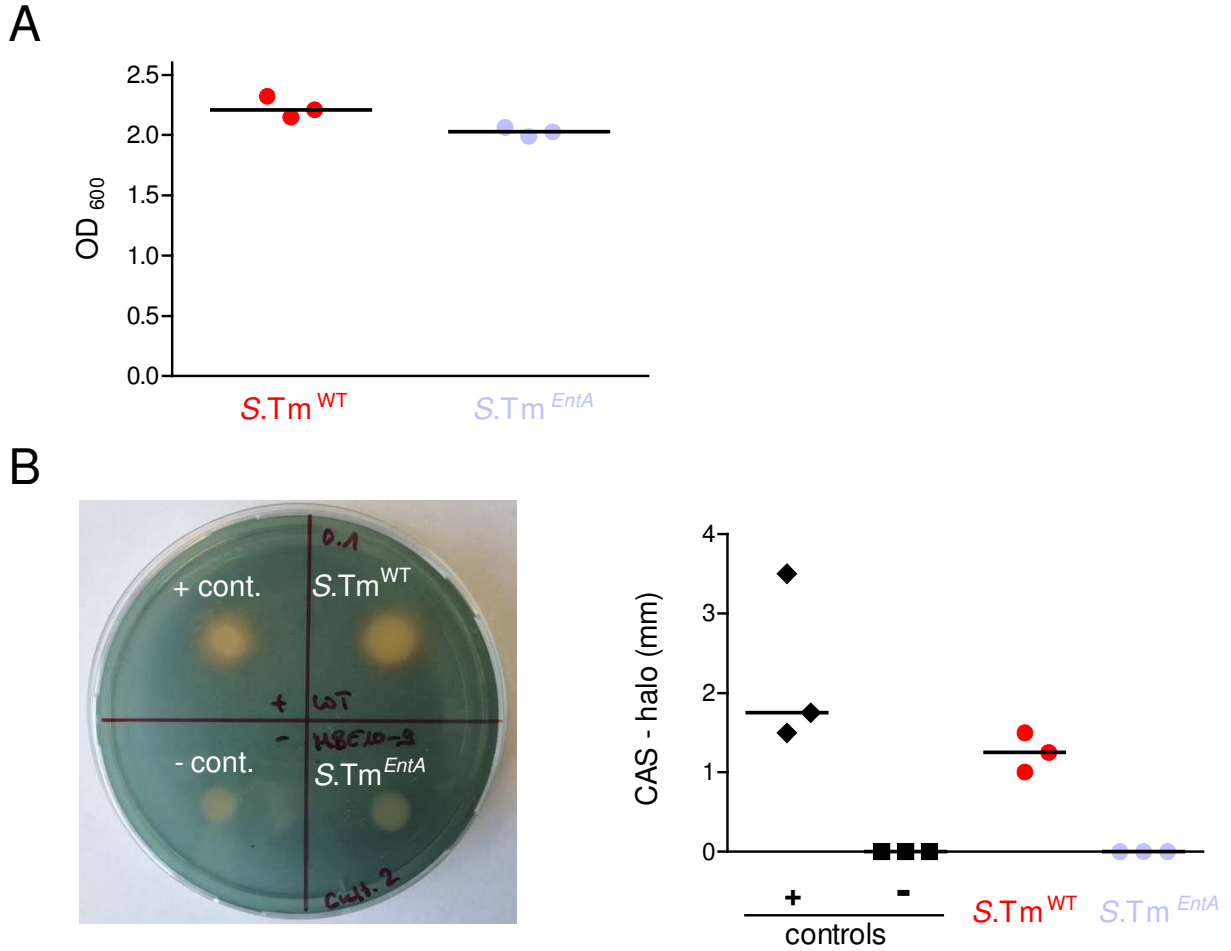


Figure 22: *S. Tm^{EntA}* is unable to acquire iron via siderophore secretion. (A) OD₆₀₀ of 12h LB starter cultures of *S. Tm^{EntA}* as well as *S. Tm^{WT}* used for CAS agar assay (n=3; p=0.1, Mann Whitney test). (B) left, CAS agar plate with bacterial spots: + cont: positive control (HB 1852S WA-CS), - cont: negative control (WA-TS (*ybtA::aphT*)), *S. Tm^{WT}* and *S. Tm^{EntA}*. Right, quantification of orange CAS – halo in mm. Experiments were performed with 3 individual cultures (n=3). Data are shown as the median of 3 experiments.

3.4.2.1.4 *S. Tm^{EA}* (*eutC::aphT*) exhibits reduced growth on ethanolamine under anaerobic conditions in the presence of tetrathionate

Ethanolamine is the preferred energy source of *S. Tm* during tetrathionate respiration (Price-Carter *et al.* 2001). *EutC*, which encodes a subunit of ethanolamine ammonia lyase, an enzyme essential for ethanolamine utilization (Roof and Roth 1988, Roof and Roth 1989, Thiennimitr *et al.* 2011) was replaced by a kanamycin resistance cassette. The genetic modification in *S. Tm^{EA}* was verified by PCR and the mutant phenotype was tested *in vitro*. *S. Tm^{EA}* and *S. Tm^{WT}* showed the same growth kinetics in anaerobic M9 medium containing glucose (Figure 23B). When ethanolamine was the sole electron source (no tetrathionate added), *S. Tm^{EA}* as well as *S. Tm^{WT}* almost showed no growth under anaerobic conditions. Remarkably, when the electron acceptor tetrathionate was added *S. Tm^{WT}* trended to grow better compared to *S. Tm^{EA}* (Figure 23A). This indicates that *S. Tm^{EA}* cannot benefit from ethanolamine as good as *S. Tm^{WT}* does.

Results

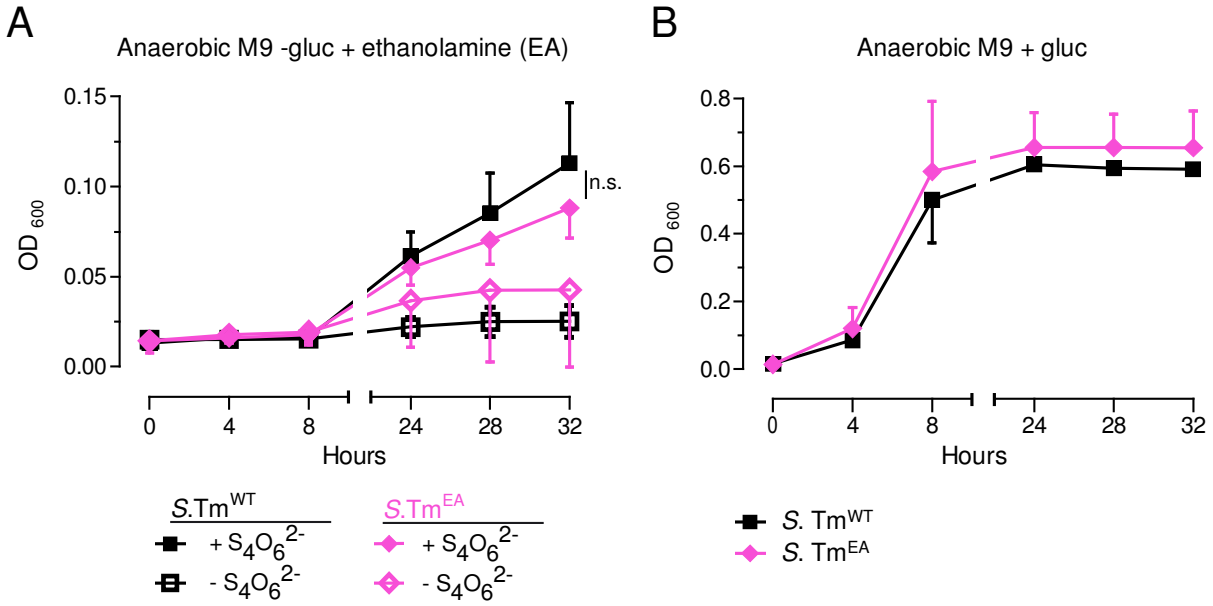


Figure 23: *S. Tm*^{EA} shows reduced growth compared to *S. Tm*^{WT} in M9 + ethanolamine (EA) supplemented with tetrathionate. (A) OD₆₀₀ of *S. Tm*^{EA} and *S. Tm*^{WT} in anaerobic M9 without glucose (- gluc) containing 5 mM ethanolamine with and without tetrathionate (S₄O₆²⁻, 40 mM, n=4). Difference between the growth of *S. Tm*^{EA} and *S. Tm*^{WT} at 32 h in M9 + ethanolamine supplemented with S₄O₆²⁻ was not statistically significant (n.s., p>0.05, 1 way ANOVA with Bonferroni's multiple comparison test). **(B)** OD₆₀₀ of *S. Tm*^{EA} and *S. Tm*^{WT} in anaerobic M9 containing glucose (+ gluc) but no ethanolamine or S₄O₆²⁻ (n=3). Samples were taken after 0, 4, 8, 24, 28, 32 h. Data are expressed as the mean of n experiments +/- standard deviation.

3.4.2.2 Dysbiosis following *Salmonella* 'blooms' is fueled by anaerobic respiration.

So far, the contribution of anaerobic respiration, ethanolamine utilization and iron availability to *Salmonella* 'blooming' has been investigated using the streptomycin pre-treated colitis mouse model (Raffatellu *et al.* 2009, Winter *et al.* 2010, Thiennimitr *et al.* 2011, Lopez *et al.* 2012). In this study, we verify the observed effects using the Oligo-MM¹² that exhibits colitis upon *S. Tm* infection without antibiotic pre-treatment. We further investigate the relative importance of anaerobic respiration, ethanolamine utilization and iron availability during different stage of *Salmonella* ecosystem invasion and 'blooming' and monitor the performance of individual commensal strains during colitis.

Thus, groups of Oligo-MM¹² mice were infected with 5 x 10⁷ CFUs of either *S. Tm*^{EntA} (*entA::cat*; deficient in enterochelin / salmochelin production, n=6), *S. Tm*^{Ni. + Te.} ($\Delta narZ$; *narG::cat*; *napA::aphT*; *ttrS::tet*; deficient in nitrate and tetrathionate respiration, n=6), *S. Tm*^{Ni.} ($\Delta narZ$; *narG::cat*; *napA::aphT*; deficient in nitrate respiration, n=5), *S. Tm*^{EA} (*eutC::aphT*; deficient in ethanolamine utilization, n=6) or *S. Tm*^{WT} (n=7). Feces was taken at different days after infection in order to monitor microbiota composition and determine LCN-2 levels as marker for gut inflammation. Mice were

Results

sacrificed at day 4 p.i., feces and cecal content were harvested for microbiota analysis, cecal pathology was scored and systemic *Salmonella* loads were determined (Figure 24A). All *Salmonella* strains colonized the gut of Oligo-MM¹² mice equally well, only the *S. Tm*^{EA} significantly reduced loads at day 3 p.i. compared to *S. Tm*^{WT} ($p < 0.01$, Kruskal-Wallis test with Dunn's multiple comparison test; Figure 25A). All mutant strains induced severe colitis by day 4 p.i. (Figure 25B) with high and comparable LCN-2 levels (Figure 24B). There was no difference in relative cecum size and systemic *Salmonella* loads at day 4 p.i. (Figure 25C-F) between groups. However, *S. Tm*^{Ni. + Te.} exhibited less cecal pathology compared to *S. Tm*^{WT} ($p < 0.001$, Kruskal-Wallis test with Dunn's multiple comparison test; Figure 25B). Nevertheless, this indicates that all *S. Tm* mutant strains were able to induce colitis at day 4 p.i.. Interestingly, the fecal and cecal microbiota was different after infection with *S. Tm*^{Ni. + Te.}. No domination of *Salmonella* ($\geq 50\%$ of total microbiota composition) after infection with *S. Tm*^{Ni. + Te.} was observed (Figures 24D,E; 26B,C). However, when tetrathionate respiration was still functional, 3 out of 6 samples were dominated by *Salmonella* after infection with *S. Tm*^{Ni.} (Figures 24D,E; 26B,C), indicating an additive effect of both systems. Only 2 of 6 samples were dominated by *S. Tm*^{EA} underlining the importance of ethanolamine for anaerobic respiration (Figures 24D,E; 26B,C). Mice infected with *S. Tm*^{EntA} however showed a similar abundance of samples dominated by *Salmonella* compared to *S. Tm*^{WT} at day 4 p.i. (Figures 24D,E; 26B,C). This demonstrates that iron acquisition via siderophores might play a minor role during late stage of infection, whereas anaerobic respiration was of major importance. In all samples during late stages of infection, domination by *Salmonella* paralleled with decreased total 16S rRNA copies per 5 ng template DNA (Figure 24C-E).

Results

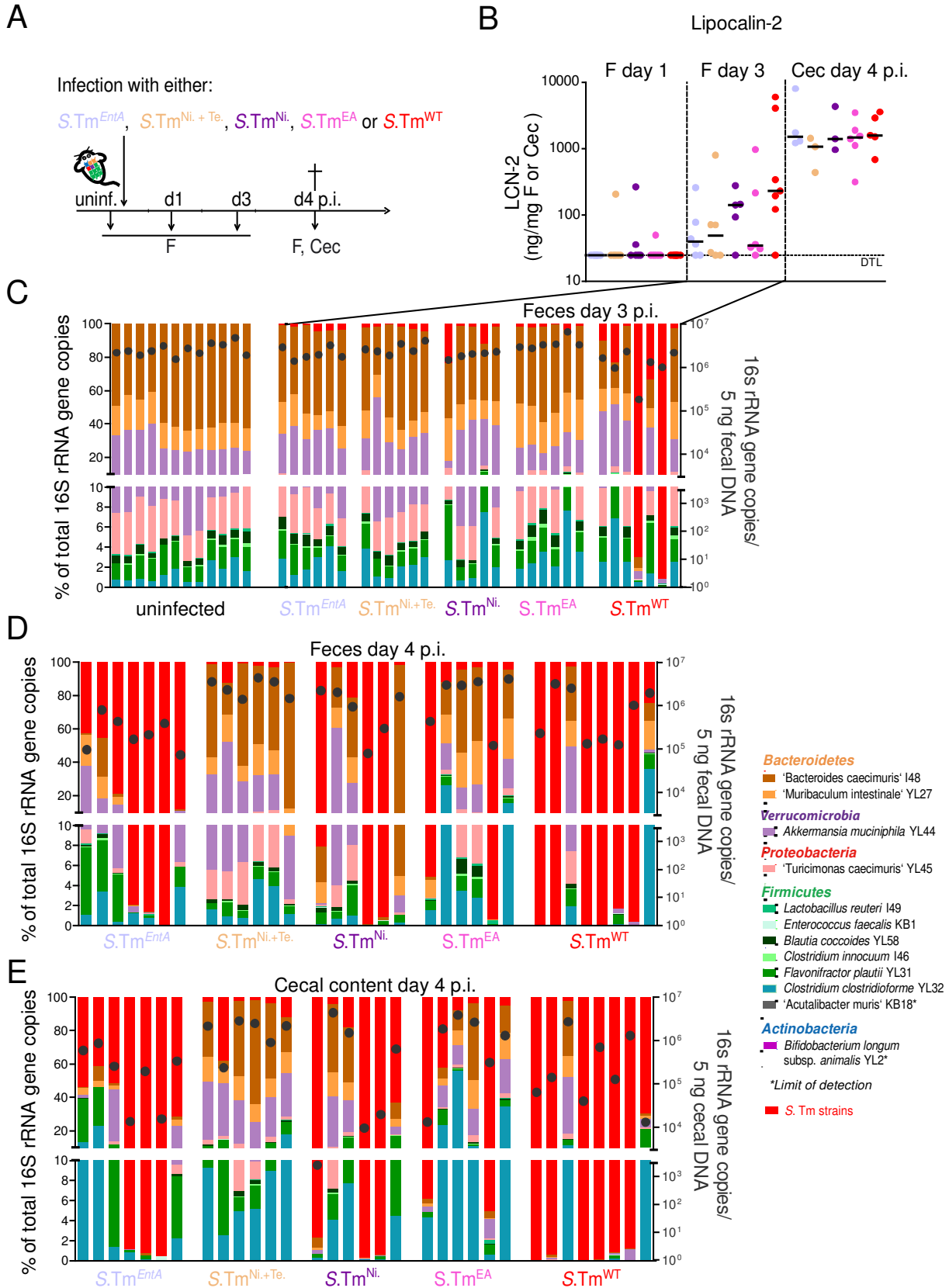


Figure 24: Environmental factors supporting dysbiosis mediated by *Salmonella* 'blooms' during inflammation. (A) Experimental set-up: Oligo-MM¹² were orally infected with 5×10^7 of different *Salmonella* strains: *S. Tm^{EntA}*, *S. Tm^{Ni} + Te*, *S. Tm^{Ni}* or *S. Tm^{WT}*. Feces (F) for microbiota analysis and LCN-2 ELISA was taken before infection and at days 1, 3 and 4 p.i.. Cecal content (Cec) was additionally taken at day 4 p.i.. (B) Lipocalin-2 (LCN-2) levels in feces (days 1 + 3 p.i.) and cecal content (day 4 p.i.) measured by ELISA (ng / mg

Results

content). **(C) – (E)** Analysis of microbiota composition in feces and cecal content at the indicated time points. Microbiota composition is shown as relative abundance and expressed as % of cumulated 16S rRNA gene copy numbers (% of total 16S rRNA gene copies). The amount of absolute 16S rRNA gene copies (determined by an universal primer / probe combination) is illustrated as black dots (right y axis). * Or dashed line: limit of detection (DTL).

In order to further entangle the relative contribution of anaerobic respiration, ethanolamine utilization and iron acquisition via siderophores to *Salmonella* 'blooming', microbiota samples were subsequently clustered by infection with *S. Tm* strains shown in Figure 24A. At early stages of infection (uninfected + day 3 p.i.) grouping of fecal microbiota composition by infection with different *Salmonella* strains was significant, according to Bray Curtis ($p < 0.002$, Adonis) and Pearson ($p < 0.001$, Adonis) distance matrices, with 40% as well as 51% of variation explained. At this early stage, only *S. Tm*^{WT} managed to dominate the 2 out of 7 samples and constitute $\geq 30\%$ of total microbiota composition in 1 sample (Figures 24C; 26A). Non parametric PERMDISP analysis revealed that at day 3 p.i., the microbiota composition after infection with *S. Tm*^{WT} was different compared to uninfected and also different compared to microbiota composition of mice infected with *S. Tm*^{EntA}, *S. Tm*^{Ni. + Te.}, *S. Tm*^{Ni.} and *S. Tm*^{EA} (Figure 26A). At day 3 p.i., there was no significant difference in microbiota composition between uninfected samples and samples infected with *S. Tm*^{EntA}, *S. Tm*^{Ni. + Te.}, *S. Tm*^{Ni.} and *S. Tm*^{EA} (Figure 26A).

During late stages of infection (day 4 p.i.), fecal samples and cecal content were analyzed. Grouping of fecal microbiota composition by infection with different *Salmonella* strains was significant, according to Bray Curtis ($p < 0.003$, Adonis) and Pearson ($p < 0.003$, Adonis) distance matrices, with 39% as well as 48% of variation explained (Figure 26B). Grouping of microbiota composition in cecal content by infection with different *Salmonella* strains was also significant, according to Bray Curtis ($p < 0.004$, Adonis) and Pearson correlation ($p < 0.002$, Adonis), with 41% as well as 45% of variation explained (Figure 26C). Remarkably, the Oligo-MM¹² composition after infection with *S. Tm*^{WT} as well as *S. Tm*^{EntA} clustered separately (Figure 26B,C). Most of the samples were dominated by *S. Tm*^{WT} or *S. Tm*^{EntA}. The percentage of *S. Tm*^{EntA} was $\geq 30\%$ of total microbiota composition at day 4 p.i. for all mice (Figure 26B,C), indicating that iron acquisition via siderophores might be negligible for the induction of dysbiosis during late stages of infection. The following ranking according to mean % of *Salmonella* observed in feces and cecal content underlines the importance of anaerobic respiration and ethanolamine utilization during *Salmonella* 'blooming' and concomitant dysbiosis at day 4 p.i.: *S. Tm*^{WT} (78.10% +/- 40.29% in feces and 83.65% +/- 34.48% in cecal content) > *S. Tm*^{EntA} (78.84% +/- 24.90% in feces and 73.69% +/- 25.50% in cecal content) > *S. Tm*^{Ni.} (52.99% +/- 48.85 in feces and 63.71% +/- 43.29% in cecal content) > *S. Tm*^{EA} (36.42% +/- 47.24% in feces and 41.36% +/- 43.58% in

Results

cecal content) > *S. Tm*^{Ni. + Te.} (3.46% +/- 4.48% in feces and 10.10% +/- 14.35% in cecal content) (Tables 50; 51).

Again, *Salmonella* 'blooming' correlated with decreased relative abundance of 'Bacteroides caecimuris' I48, 'Muribaculum intestinale' YL27 and *Akkermansia muciniphila* YL44 with the lowest relative abundance observed after infection with *S. Tm*^{WT} and *S. Tm*^{EntA} (Tables 50; 51). Remarkably, the relative abundance of *Clostridium clostridioforme* YL32 increased post infection with *S. Tm*^{EA} compared to *S. Tm*^{WT}. This difference was statistically significant in cecal content samples (rel. abundance of YL32: 21.40% +/- 20.91% p.i. with *S. Tm*^{EA} and 2.65% +/- 4.86% p.i. with *S. Tm*^{WT}; $p < 0.05$, two-way ANOVA with Bonferroni posttest; Table 51). Furthermore, according to two-way ANOVA with Bonferroni posttest, there were no statistically significant differences in relative abundance of individual Oligo-MM¹² strains at day 4 p.i. between *S. Tm*^{EntA} vs *S. Tm*^{WT} and *S. Tm*^{Ni.} vs *S. Tm*^{EA} in feces and between *S. Tm*^{EntA} vs *S. Tm*^{Ni.} and *S. Tm*^{EntA} vs *S. Tm*^{WT} in cecal content (Tables 50; 51), again indicating a lower priority of iron acquisition via siderophores and an additive effect of nitrate and tetrathionate respiration at later stages of infection. It is also worth mentioning that in this experiment *S. Tm*^{WT} failed to dominate the Oligo-MM¹² in 2 out of 8 samples (Figure 24D,E). This is in contrast to previous experiments where *S. Tm*^{WT} dominated the Oligo-MM¹² in 7 out of 7 mice at day 4 p.i. (Figure 10C).

Results

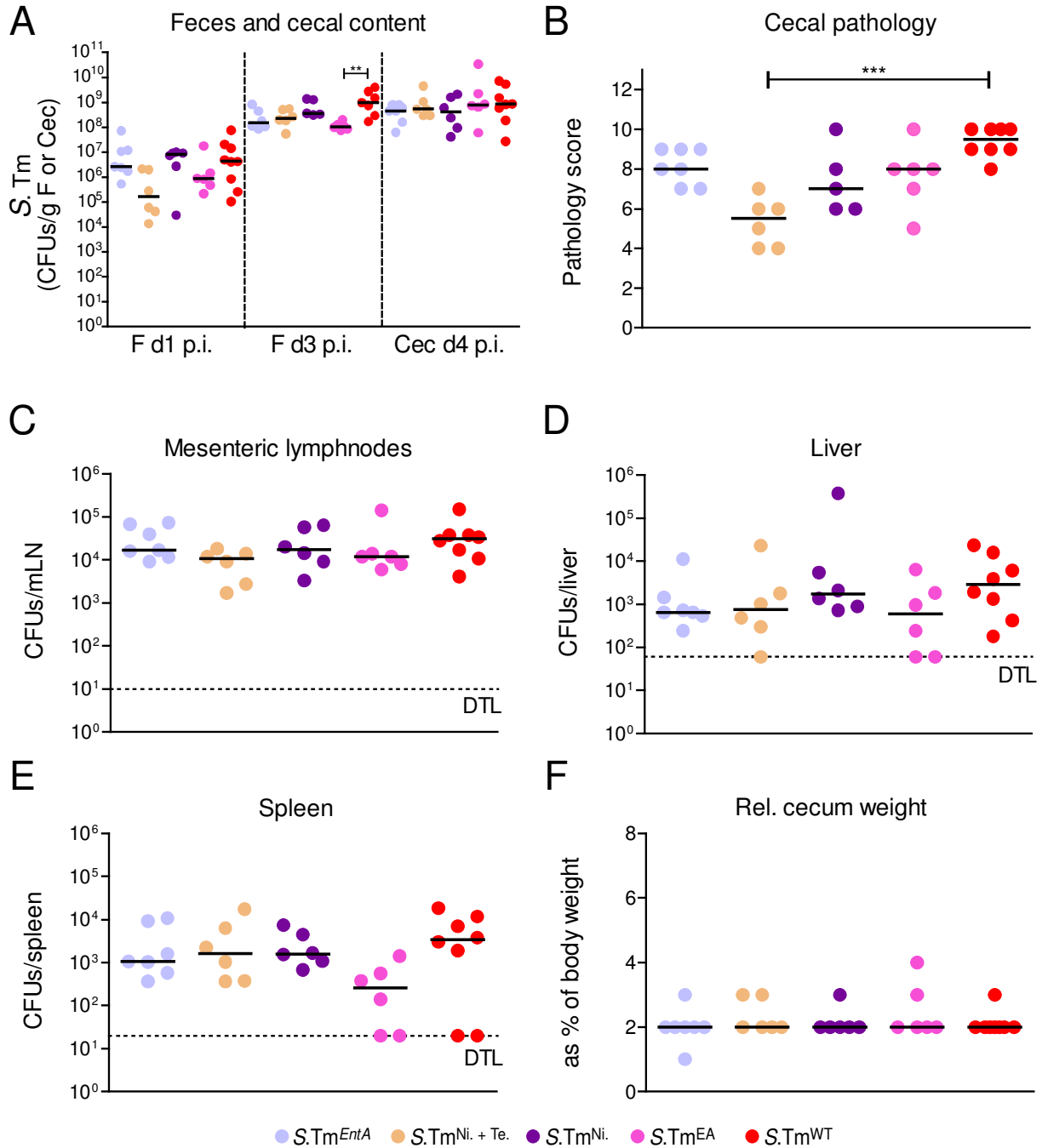
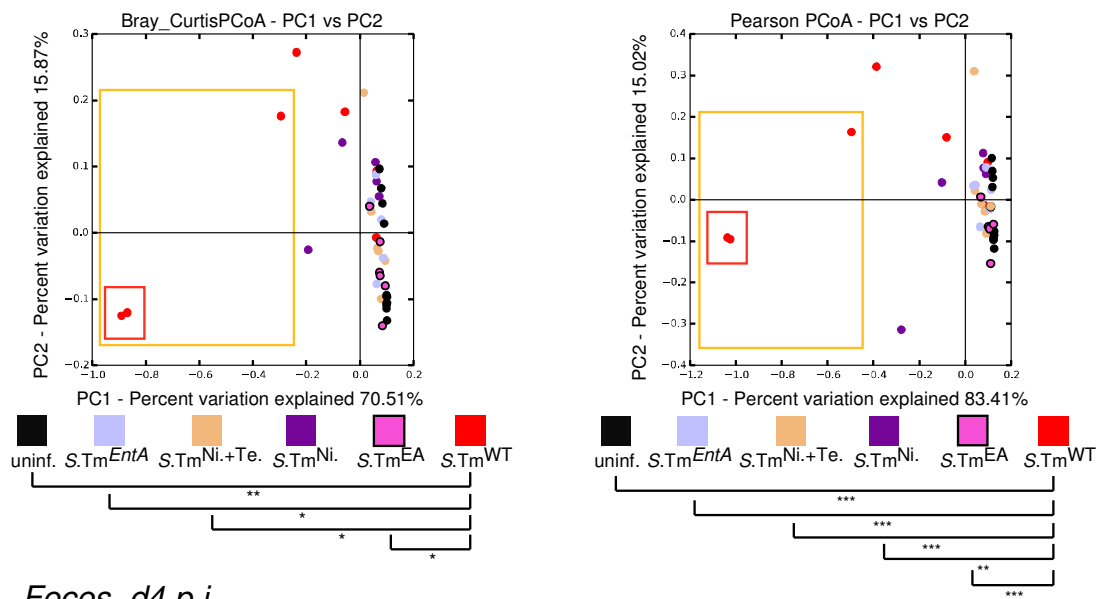


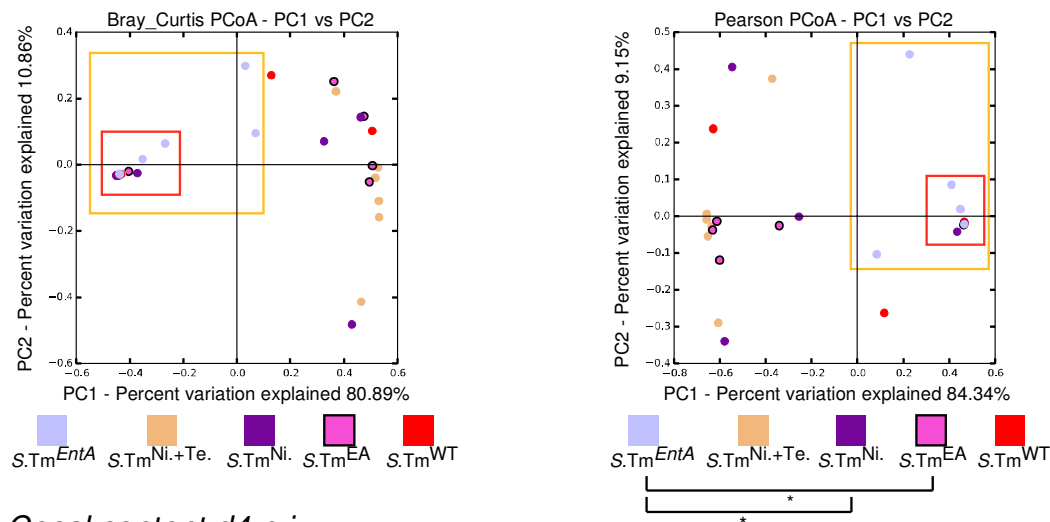
Figure 25: *Salmonella* mutants deficient in siderophore production, anaerobic respiration and ethanolamine utilization show similar colonization kinetics and systemic dissemination compared to *S. Tm*^{WT}. For experimental set-up refer to Figure 24A. Organs were additionally taken at the indicated time points. **(A)** *Salmonella* loads in feces and cecal content at days 1, 3 and 4 p.i. (CFUs *S. Tm* / g content). **(B)** Cecal pathology determined by microscopy of HE stained tissue sections. **(C) – (E)** Systemic *Salmonella* in mesenteric lymphnodes, liver and spleen (CFUs / organ) at day 4 p.i.. **(F)** Relative cecum weight at day 4 p.i. expressed as % of body weight. Values are indicated as median. Statistical analysis between groups was performed using Kruskal-Wallis test with Dunn's multiple comparison test (* $p < 0.05$, ** $p < 0.01$, *** $p < 0.001$). Dashed lines: DTL: limit of detection (mLN: 10 CFUs, liver: 60 CFUs, spleen: 20 CFUs).

Results

A *Feces uninfected + d3 p.i.*



B *Feces d4 p.i.*



C *Cecal content d4 p.i.*

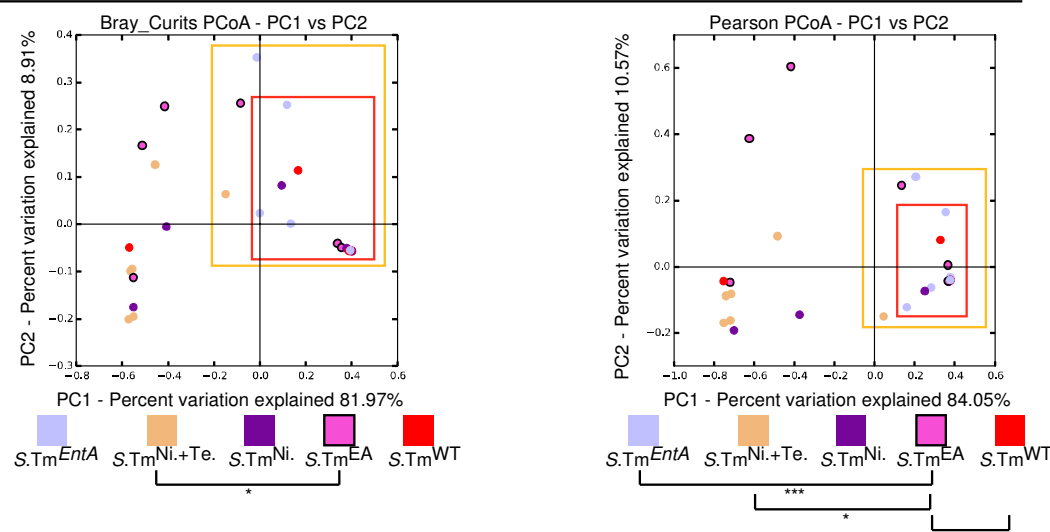


Figure 26: Cluster analysis of Oligo-MM¹² composition after infection with *S. Tm*^{WT} and *Salmonella* strains deficient in siderophore production, anaerobic respiration as well as ethanolamine utilization. Cluster

Results

analysis is based on Bray Curtis or Pearson distance matrices and visualized as PCoA plots. **(A)** Clustering of fecal Oligo-MM¹² composition before infection and day 3 post infection with *S. Tm* strains. Fecal microbiota samples were grouped by infection with different *S. Tm* strains which was significant, according to Bray Curtis ($p < 0.002$, Adonis) and Pearson ($p < 0.001$, Adonis) with 40% (Bray Curtis) and 51% (Pearson) of variation explained. PERMDISP analyses based on Bray Curtis and Pearson distance matrices revealed statistically significant differences in fecal microbiota composition between Oligo-MM¹² infected with *S. Tm*^{WT} and all other *S. Tm* strains (* $p < 0.05$, ** $p < 0.01$, *** $p < 0.001$). **(B)** Clustering of fecal Oligo-MM¹² composition at day 4 post infection with *S. Tm* strains. Fecal microbiota samples were grouped by infection with different *S. Tm* strains which was significant, according to Bray Curtis ($p < 0.003$, Adonis) and Pearson ($p < 0.003$, Adonis) with 39% (Bray Curtis) and 48% (Pearson) of variation explained. PERMDISP analyses based Pearson distance matrix revealed statistically significant differences in fecal microbiota composition between Oligo-MM¹² infected with *S. Tm*^{EntA}, *S. Tm*^{Ni} and *S. Tm*^{EA} (* $p < 0.05$). **(C)** Clustering of Oligo-MM¹² composition in cecal content at day 4 post infection with *S. Tm* strains. Samples from were grouped by infection with different *S. Tm* strains which was significant, according to Bray Curtis ($p < 0.004$, Adonis) and Pearson ($p < 0.002$, Adonis) with 41% (Bray Curtis) and 45% (Pearson) of variation explained. PERMDISP analyses based on Bray Curtis and Pearson distance matrices revealed statistically significant differences in microbiota composition of cecal content between Oligo-MM¹² infected with *S. Tm* strains (* $p < 0.05$, *** $p < 0.001$). Red square: microbiota is dominated by *S. Tm* ($\geq 50\%$); orange square: *S. Tm* accounts for $\geq 30\%$ of total microbiota composition.

Table 50: Relative abundance of Oligo-MM¹² strains after infection with *S. Tm* mutant strains deficient in iron acquisition via siderophores, anaerobic respiration and ethanolamine utilization in feces

Strain	Mean % of cumulated 16S rRNA gene copy numbers (+/- SD)				
	Day 4 post infection with <i>Salmonella</i> mutant strains (feces)				
	<i>S. Tm</i> ^{EntA}	<i>S. Tm</i> ^{Ni + Te.}	<i>S. Tm</i> ^{Ni.}	<i>S. Tm</i> ^{EA}	<i>S. Tm</i> ^{WT}
'Bacteroides caecimuris' I48	3.87 (8.67)	53.37 ^a (22.05)	26.06 ^{b,d} (35.90)	23.85 ^e (21.14)	5.46 ^{f,g} (11.65)
'Muribaculum intestinale' YL27	5.17 (7.61)	11.95 (5.56)	5.29 (6.78)	15.15 (11.45)	4.10 (7.60)
<i>Akkermansia muciniphila</i> YL44	7.37 (10.02)	24.31 (13.17)	12.99 (22.67)	10.35 (8.16)	5.51 (14.66)
'Turicimonas caecimuris' YL45	0.31 (0.48)	3.34 (1.70)	1.04 (1.51)	2.79 (2.26)	0.44 (1.15)
<i>Lactobacillus reuteri</i> I49	0.07 (0.11)	0.01 (0.01)	0.01 (0.02)	0.19 (0.13)	0.01 (0.02)
<i>Enterococcus faecalis</i> KB1	0.01 (0.01)	0.002 (0.004)	0.03 (0.04)	0.003 (0.01)	0.02 (0.01)
<i>Blautia coccoides</i> YL58	0.08 (0.12)	0.31 (0.13)	0.18 (0.19)	0.79 (0.64)	0.13 (0.21)
<i>Clostridium innocuum</i> I46	0.06 (0.10)	0.07 (0.03)	0.06 (0.07)	0.15 (0.12)	0.04 (0.08)
<i>Flavonifractor plautii</i> YL31	2.69 (2.81)	1.05 (0.35)	1.02 (1.05)	2.07 (1.79)	1.50 (3.20)
<i>Clostridium clostridioforme</i> YL32	1.52 (1.48)	2.15 (1.66)	0.34 (0.40)	8.23 (10.37)	4.71 (12.52)
'Acutalibacter muris' KB18	DTL	DTL	DTL	DTL	DTL
<i>Bifidobacterium longum</i> subsp. <i>animalis</i> YL2	DTL	DTL	DTL	DTL	DTL
<i>S. Tm</i>	78.84 (24.90)	3.46 ^a (4.48)	52.99 ^{b,d} (48.85)	36.42 ^{c,e} (47.24)	78.10 ^{f,g,h} (40.29)

Significant differences between **a** *S. Tm*^{EntA} vs *S. Tm*^{Ni + Te.}, **b** *S. Tm*^{EntA} vs *S. Tm*^{Ni.}, **c** *S. Tm*^{EntA} vs *S. Tm*^{EA}, **d** *S. Tm*^{Ni + Te.} vs *S. Tm*^{Ni.}, **e** *S. Tm*^{Ni + Te.} vs *S. Tm*^{EA}, **f** *S. Tm*^{Ni + Te.} vs *S. Tm*^{WT}, **g** *S. Tm*^{Ni.} vs *S. Tm*^{WT} and **h** *S. Tm*^{EA} vs *S. Tm*^{WT} are indicated; p values were less than 0.001, except: *S. Tm*^{EntA} vs *S. Tm*^{Ni.}: I48 $p < 0.05$ and *S. Tm* $p < 0.01$, I48 *S. Tm*^{Ni + Te.}

Results

T_e . vs $S. Tm^{Ni}$ $p < 0.01$, I48 $S. Tm^{Ni + Te}$ vs $S. Tm^{EA}$ $p < 0.01$ and $S. Tm^{Ni}$ vs $S. Tm^{WT}$: I48 $p < 0.05$ and $S. Tm$ $p < 0.01$, two-way ANOVA with Bonferroni posttest. There were no significant differences between $S. Tm^{EntA}$ vs $S. Tm^{WT}$ and $S. Tm^{Ni}$ vs $S. Tm^{EA}$. Values are expressed as mean % of cumulated 16S rRNA gene copy numbers +/- standard deviation (SD). $S. Tm^{EntA}$: no siderophore production (n=7), $S. Tm^{Ni + Te}$: no nitrate and tetrathionate respiration (n=6), $S. Tm^{Ni}$: no nitrate respiration (n=6), $S. Tm^{EA}$: no ethanolamine utilization (n=6), $S. Tm^{WT}$ (n=8). DTL: limit of detection.

Table 51: Relative abundance of Oligo-MM¹² strains after infection with *S. Tm* mutant strains deficient in iron acquisition via siderophores, anaerobic respiration and ethanolamine utilization in cecal content.

Strain	Mean % of cumulated 16S rRNA gene copy numbers (+/- SD)				
	Day 4 post infection with <i>Salmonella</i> mutants (cecum)				
	<i>S. Tm</i> ^{EntA}	<i>S. Tm</i> ^{Ni + Te}	<i>S. Tm</i> ^{Ni}	<i>S. Tm</i> ^{EA}	<i>S. Tm</i> ^{WT}
'Bacteroides caecimuris' I48	1.94 (3.19)	35.23 ^a (20.48)	14.17 ^c (18.27)	13.61 ^d (17.17)	4.41 ^e (11.66)
'Muribaculum intestinale' YL27	1.93 (1.85)	12.02 (2.38)	4.97 (6.24)	7.74 (7.41)	1.79 (4.29)
<i>Akkermansia muciniphila</i> YL44	6.67 (11.83)	26.27 ^a (6.69)	9.06 (12.69)	10.53 (7.85)	5.02 ^e (11.77)
'Turicimonas caecimuris' YL45	0.41 (0.68)	2.91 (1.14)	1.03 (1.43)	1.79 (1.66)	0.54 (1.17)
<i>Lactobacillus reuteri</i> I49	0 (0.07)	0.04 (0.07)	0 (0.07)	0.14 (0.13)	0.01 (0.02)
<i>Enterococcus faecalis</i> KB1	0.07 (0.14)	0.002 (0.004)	0.01 (0.01)	0.02 (0.04)	0.02 (0.03)
<i>Blautia coccoides</i> YL58	0.06 (0.07)	0.53 (0.20)	0.15 (0.18)	0.44 (0.37)	0.05 (0.13)
<i>Clostridium innocuum</i> I46	0.004 (0.01)	0.09 (0.03)	0.05 (0.07)	0.15 (0.20)	0.01 (0.04)
<i>Flavonifractor plautii</i> YL31	9.55 (11.22)	4.74 (4.15)	4.07 (5.25)	2.84 (3.38)	1.86 (3.87)
<i>Clostridium clostridioforme</i> YL32	5.69 (8.67)	8.07 (5.35)	2.79 (3.16)	21.40 (20.91)	2.65 ^h (4.86)
'Acutalibacter muris' KB18	DTL	DTL	DTL	DTL	DTL
<i>Bifidobacterium longum</i> subsp. <i>animalis</i> YL2	DTL	DTL	DTL	DTL	DTL
<i>S. Tm</i>	73.69 (25.50)	10.10 ^a (14.35)	63.71 ^c (43.29)	41.36 ^{b,d,f} (43.58)	83.65 ^{e,g,h} (34.48)

Significant differences between **a** $S. Tm^{EntA}$ vs $S. Tm^{Ni + Te}$, **b** $S. Tm^{EntA}$ vs $S. Tm^{EA}$, **c** $S. Tm^{Ni + Te}$ vs $S. Tm^{Ni}$, **d** $S. Tm^{Ni + Te}$ vs $S. Tm^{EA}$, **e** $S. Tm^{Ni + Te}$ vs $S. Tm^{WT}$, **f** $S. Tm^{Ni}$ vs $S. Tm^{EA}$, **g** $S. Tm^{Ni}$ vs $S. Tm^{WT}$ and **h** $S. Tm^{EA}$ vs $S. Tm^{WT}$ are indicated; p values were less than 0.001, except: YL44 $S. Tm^{EntA}$ vs $S. Tm^{Ni + Te}$ $p < 0.05$, I48 $S. Tm^{Ni + Te}$ vs $S. Tm^{Ni}$ $p < 0.05$, I48 $S. Tm^{Ni + Te}$ vs $S. Tm^{EA}$ $p < 0.05$, YL44 $S. Tm^{Ni + Te}$ vs $S. Tm^{WT}$ $p < 0.01$, $S. Tm$ $S. Tm^{Ni}$ vs $S. Tm^{EA}$ $p < 0.01$, $S. Tm$ $S. Tm^{Ni}$ vs $S. Tm^{WT}$ $p < 0.05$ and YL32 $S. Tm^{EA}$ vs $S. Tm^{WT}$ $p < 0.05$, two-way ANOVA with Bonferroni posttest. There were no significant differences between $S. Tm^{EntA}$ vs $S. Tm^{Ni}$ and $S. Tm^{EntA}$ vs $S. Tm^{WT}$. Values are expressed as mean % of cumulated 16 S rRNA gene copy numbers +/- standard deviation (SD). $S. Tm^{EntA}$: no siderophore production (n=7), $S. Tm^{Ni + Te}$: no nitrate and tetrathionate respiration (n=6), $S. Tm^{Ni}$: no nitrate respiration (n=6), $S. Tm^{EA}$: no ethanolamine utilization (n=6), $S. Tm^{WT}$ (n=8). DTL: limit of detection.

Results

3.4.2.3 The performance of single Oligo-MM¹² strains during inflammation correlates with the presence of fitness genes

Next, fold differences in absolute abundance (fold changes) of each Oligo-MM¹² strain and *Salmonella* between day 0 (uninfected) and day 4 p.i. with *S. Tm*^{WT}, *S. Tm*^{EntA}, *S. Tm*^{Ni. + Te.}, *S. Tm*^{Ni.} and *S. Tm*^{EA} were calculated (Table 53). In this experiment, the Oligo-MM¹² strains could be grouped in strains that are depleted, intermediate or enriched during severe *S. Tm*^{WT} induced colitis (Figure 14; Table 53). In order to obtain more functional information about the performance of individual Oligo-MM¹² strains during *S. Tm* induced inflammation in the gut, RAST (Rapid Annotations using Subsystems Technology) from draft genomes was performed prioritizing the following functional groups (subsystems): nitrogen metabolism / nitrate and nitrite ammonification, ethanolamine (EA) utilization, iron acquisition, siderophore, dormancy and sporulation (Table 52). Genome mining was performed by Debora Garzetti. Remarkably, genomes of the Oligo-MM¹² strains that were depleted during severe *S. Tm*^{WT} induced inflammation, in particular *Akkermansia muciniphila* YL44, 'Bacteroides caecimuris' I48, 'Muribaculum intestinale' YL27 and 'Turicimonas caecimuris' YL45 in general did barely harbor the above mentioned subsystems (Tables 52; 53). 'Turicimonas caecimuris' YL45 harbored putative genes for nitrate respiration and *Akkermansia muciniphila* YL44 harbored genes for siderophores. *Clostridium clostridioforme* YL32 which is also depleted during severe colitis but which was increased upon moderate colitis at day 3 p.i. with *S. Tm*^{WT} (Table 46; Figure 10B,C) harbored genes for ferric iron ABC transporters, nitrite reductase and sporulation genes (Tables 52; 53). In addition, the absolute abundance of *Clostridium clostridioforme* YL32 between day 0 and day 4 p.i. with *S. Tm*^{EntA}, *S. Tm*^{Ni. + Te.} and *S. Tm*^{EA} even increased (Table 53), suggesting that *Clostridium clostridioforme* YL32 might benefit from inflammation. Oligo-MM¹² strains that were assigned to the intermediate group (*Blautia coccoides* YL58, *Flavonifractor plautii* YL31 and *Clostridium innocuum* I46) all harbored sporulation genes (especially *Blautia coccoides* YL58 and *Flavonifractor plautii* YL31) and additionally iron utilization genes (Tables 52; 53). The genome of *Flavonifractor plautii* YL31 contained also ethanolamine utilization genes and *Blautia coccoides* YL58 harbored nitrate respiration genes. Fold changes of *Blautia coccoides* YL58, *Flavonifractor plautii* YL31 and *Clostridium innocuum* I46 between day 0 and day 4 p.i. with *S. Tm*^{WT}, *S. Tm*^{EntA}, *S. Tm*^{Ni. + Te.}, *S. Tm*^{Ni.} and *S. Tm*^{EA} were comparable (Table 53). The two Oligo-MM¹² strains that were enriched during colitis (*Enterococcus faecalis* KB1 and *Lactobacillus reuteri* I49) did almost harbor no sporulation genes. *Enterococcus faecalis* KB1 harbored genes for ethanolamine utilization and siderophores, whereas *Lactobacillus reuteri* I49 harbored genes for nitrate respiration (Tables 52; 53). The absolute abundance of *Lactobacillus reuteri* I49 between day 0 and day 4 p.i. increased slightly p.i. with *S. Tm*^{EntA} and *S. Tm*^{EA} and the absolute abundance of *Enterococcus faecalis* KB1 was increased after infections with *S. Tm*^{WT}, *S. Tm*^{EntA}, *S. Tm*^{Ni.} and *S. Tm*^{EA} (Table 53).

Results

Taken together, Oligo-MM¹² strains that were depleted during severe colitis in general harbored no or few genes involved in sporulation, ethanolamine utilization, iron uptake or nitrate respiration. Strains that persisted during severe inflammation or decreased moderately (intermediate group) especially harbored sporulation genes. There were additionally genes for iron uptake, ethanolamine utilization and nitrate respiration in this group. Strains that were enriched during severe colitis mostly harbored genes for nitrate respiration, ethanolamine utilization and iron uptake. There were almost no genes related to dormancy or sporulation present in this enriched group.

Table 52: Functional groups (subsystems) of the Oligo-MM¹² determined by RAST automated annotation.

Subsystem	Putative gene	Oligo-MM ¹² strains											
		Depleted					Intermediate			Enriched		DTL	
		YL 44	I 48	YL 27	YL 45	YL 32	YL 58	YL 31	I 46	KB 1	I 49	KB 18	YL 2
Nitrogen metabolism nitrate and nitrite ammonific.	Nitrite reductase probable [NAD(P)H] subunit (EC 1.7.1.4)					+	+						
	Nitrate/nitrite transporter				+						+		
	Respiratory nitrate reductase alpha chain (EC 1.7.99.4)				+						+		
	Respiratory nitrate reductase gamma chain (EC 1.7.99.4)				+						+		
	Respiratory nitrate reductase delta chain (EC 1.7.99.4)				+						+		
	Respiratory nitrate reductase beta chain (EC 1.7.99.4)				+						+		
	Cytochrome c552 precursor (EC 1.7.2.2)				+								
	Cytochrome c-type heme lyase subunit nrff, nitrite reductase complex assembly				+								
	Cytochrome c-type heme lyase subunit nrfG, nitrite reductase complex assembly				+								
	Ferredoxin-type protein NapF (periplasmic nitrate reductase)				+								
	Ferredoxin-type protein NapG (periplasmic nitrate reductase)				+								
	Nitrate ABC transporter, ATP-binding protein				+								
	Nitrate/nitrite response regulator protein				+								
	Nitrate/nitrite sensor protein (EC 2.7.3.-)				+								
	NrfC protein				+								
	NrfD protein				+								
	Periplasmic nitrate reductase precursor (EC 1.7.99.4)				+								
	Polyferredoxin NapH (periplasmic nitrate reductase)				+								
EA utilization	Ethanolamine utilization polyhedral-body-like protein EutN							+		+			
	Ethanolamine sensory transduction histidine kinase							+		+			
	Ethanolamine permease							+		+			

Results

Subsystem	Putative gene	Oligo-MM ¹² strains											
		Depleted					Intermediate			Enriched		DTL	
		YL 44	I 48	YL 27	YL 45	YL 32	YL 58	YL 31	I 46	KB 1	I 49	KB 18	YL 2
	Ethanolamine two-component response regulator							+		+			
	Ethanolamine utilization protein similar to PduL							+		+			
	ATP:Cob(I)alamin adenosyltransferase (EC 2.5.1.17)							+					
	Ethanolamine utilization protein similar to PduA/PduJ							+		+			
	Ethanolamine utilization protein EutA							+		+			
	Ethanolamine utilization protein similar to PduV							+		+			
	Ethanolamine utilization protein EutJ							+					
	Acetate kinase (EC 2.7.2.1)							+		+			
	Ethanolamine ammonia-lyase light chain (EC 4.3.1.7)							+		+			
	Ethanolamine utilization protein similar to PduT							+					
	Ethanolamine ammonia-lyase heavy chain (EC 4.3.1.7)							+		+			
	Ethanolamine utilization polyhedral-body-like protein EutL							+		+			
	Ethanolamine utilization polyhedral-body-like protein EutM									+			
	Protein clustered with ethanolamine utilization									+			
Iron acquisition	Ferric iron ABC transporter, ATP-binding protein					+	+		+				
	Two-component sensor kinase, associated with ferric iron transporter					+							
	Two-component response regulator, associated with ferric iron transporter,					+							
	Ferric iron ABC transporter, iron-binding protein					+	+		+				
	Ferric iron ABC transporter, permease protein					+	+		+				
Siderophore	Uncharacterized iron compound ABC uptake transporter, permease protein							+					
	Iron compound ABC uptake transporter substrate-binding protein	+						+		+			
	Iron compound ABC uptake transporter ATP-binding protein	+						+		+			
	Iron compound ABC uptake transporter permease protein	+						+		+			
Dormancy and sporul.	FIG006789: Stage V sporulation protein									+		+	
	Protein of unknown function identified by role in sporulation (SpoVG)					+	+	+					
	RNA polymerase sporulation specific sigma factor SigE					+	+	+					
	RNA polymerase sporulation specific sigma factor SigF					+	+	+					
	RNA polymerase sporulation specific sigma factor SigG					+	+	+					
	RNA polymerase sporulation specific sigma factor SigH						+						

Results

Subsystem	Putative gene	Oligo-MM ¹² strains											
		Depleted					Intermediate			Enriched		DTL	
		YL 44	I 48	YL 27	YL 45	YL 32	YL 58	YL 31	I 46	KB 1	I 49	KB 18	YL 2
	RNA polymerase sporulation specific sigma factor SigK					+	+	+					
	Spore cortex-lytic enzyme precursor											+	
	Spore cortex-lytic enzyme, lytic transglycosylase SleB							+				+	
	Spore cortex-lytic enzyme, N-acetylglucosaminidase SleL (EC 3.2.1.-)							+				+	
	Spore germination protein GerKA							+				+	
	Spore germination protein GerKB											+	
	Spore germination protein GerKC							+				+	
	Spore germination protein YpeB							+				+	
	Spore maturation protein A					+	+	+	+			+	
	Spore maturation protein B					+	+	+	+			+	
	Sporulation sigma-E factor processing peptidase (SpoII GA)					+	+	+					
	Stage 0 sporulation two-component response regulator (Spo0A)					+	+	+				+	
	Stage II sporulation protein D (SpoIID)					+	+	+					
	Stage II sporulation protein P					+	+	+					
	Stage II sporulation protein related to metalloproteases (SpoIIQ)					+	+						
	Stage II sporulation protein required for processing of pro-sigma-E (SpoIIR)					+	+	+					
	Stage II sporulation serine phosphatase for sigma-F activation (SpoIIE)						+	+					
	Stage III sporulation protein AA					+	+	+					
	Stage III sporulation protein AB					+	+	+					
	Stage III sporulation protein AC					+	+	+					
	Stage III sporulation protein AD					+	+	+					
	Stage III sporulation protein AE					+	+	+				+	
	Stage III sporulation protein AF					+							
	Stage III sporulation protein AG					+	+	+					
	Stage III sporulation protein AH					+	+	+					
	Stage III sporulation protein D					+	+	+					
	Stage IV sporulation pro-sigma-K processing enzyme (SpoIVFB)							+					
	Stage IV sporulation protein A					+	+	+					
	Stage IV sporulation protein B					+	+	+					
	Stage V sporulation protein AA (SpoVAA)						+						
	Stage V sporulation protein AB (SpoVAB)						+						
	Stage V sporulation protein AC (SpoVAC)					+	+	+					
	Stage V sporulation protein AD (SpoVAD)					+	+	+					

Results

Subsystem	Putative gene	Oligo-MM ¹² strains											
		Depleted					Intermediate			Enriched		DTL	
		YL 44	I 48	YL 27	YL 45	YL 32	YL 58	YL 31	I 46	KB 1	I 49	KB 18	YL 2
	Stage V sporulation protein AE (SpoVAE)					+	+	+					
	Stage V sporulation protein AF (SpoVAF)					+							
	Stage V sporulation protein B					+	+	+				+	
	Stage V sporulation protein T, AbrB family transcriptional regulator (SpoVT)					+	+	+					

Table 53: Fold difference in absolute abundance (fold change) of Oligo-MM¹² strains between d0 (uninfected) vs d4 p.i. with different *Salmonella* strains

Strain	Fold change d0 vs d4 p.i.					Putative genes for:			
	<i>S. Tm</i> ^{WT}	<i>S. Tm</i> ^{EntA}	<i>S. Tm</i> ^{Ni.+Te.}	<i>S. Tm</i> ^{Ni.}	<i>S. Tm</i> ^{EA}	Iron AC	Nitrate	EA	Spor.
YL44	-76	-2	2	-2	-3	+	-	-	-
I48	-943	-40	1	-3	-5	-	-	-	-
YL27	-2043	-43	1	-2	-2	-	-	-	-
YL45	-1398	-121	-1	-3	-2	-	+++	-	-
YL32	-245	2	3	-3	3	++	+	-	+++
YL58	-11	-6	-2	-2	-2	+	+	-	+++
YL31	-37	2	-1	-1	-1	++	-	+++	+++
I46	-3	-1	-1	-1	-2	+	-	-	+
KB1	18	14	-1	14	2	+	-	+++	+
I49	-1	2	-5	-2	2	-	++	-	-
KB18	DTL	DTL	DTL	DTL	DTL	-	-	-	+++
YL2	DTL	DTL	DTL	DTL	DTL	-	-	-	-
<i>S. Tm</i>	208,819	190,248	3,065	96,323	4,727				

Fold changes between day 0 (uninfected) and day 4 p.i. were calculated with absolute 16S rRNA gene copy numbers per 5 ng template DNA determined by qPCR that were normalized to a million gene copies determined by universal probe. Oligo-MM¹² strains were group as in Figure 14 in depleted, intermediate and enriched after infection with *S. Tm*^{WT}. + ≤ 3 putative genes (Table 52), ++ 4 - 5 putative genes (Table 52) and +++ more than 5 putative genes (Table 52). Iron AC: iron acquisition, Nitrate: nitrate respiration, EA: ethanolamine utilization, Spor.: sporulation, DTL: limit of detection.

Results

3.4.3 Influence of innate immune system on microbiota composition during colitis

3.4.3.1 Depletion of neutrophils does not prevent dysbiosis and *Salmonella* 'blooming'

Neutrophil infiltration is a hallmark of *Salmonella*-induced colitis (Loetscher *et al.* 2012). In order to assess whether neutrophils are involved in dysbiosis upon *Salmonella*-induced colitis, neutrophils were depleted using α -Ly6G and α -G-CSF antibodies and mice were infected with *S. Tm*^{WT} (Figure 29A). Antibody mediated depletion was confirmed by FACS analysis gating on CD45⁺, SYTOX⁻, CD3⁻, CD11b⁺, Ly-6G⁺, Ly-6C-intermediate cells (Figure 27) and immuno-fluorescence microscopy (Figure 28). Besides the control mice (treated with isotype control), only mice with confirmed neutrophil depletion were included in the analysis (46% of mice in depleted group).

Before infection as well as at day 3 p.i. with *S. Tm*^{WT}, Oligo-MM¹² compositions were comparable between mice that had received isotype or depletion antibodies (Figure 29C,D,E). Remarkably, depletion of neutrophils favored *Salmonella* 'blooming' at day 4 p.i.. 4 out of 6 samples were dominated by *Salmonella* and inflammation was also increased (Figure 29B,C), whereas the Oligo-MM¹² from mice that had received isotype antibodies (neutrophils still present) were protected. Domination of *Salmonella* coincided with decreased amounts of overall bacteria (Figure 29C). Dysbiosis observed at day 4 p.i. correlated well with cluster analysis where fecal microbiota of antibody-depleted mice clustered separately (Figure 29D,E). Grouping of fecal microbiota composition by treatment with different antibodies and days post infection was significant, according to Bray Curtis ($p < 0.002$, Adonis) and Pearson ($p < 0.001$, Adonis) distance matrices, with 63% (Bray Curtis) as well as 70% (Pearson) of variation explained. LCN-2 levels were highly elevated at day 4 p.i. in mice that had received either isotype or depletion antibodies. Interestingly, depletion of neutrophils increased LCN-2 levels compared to control at day 4 p.i. by trend (Figure 29B). This trend was also observed in CD18^{-/-} mice (deficient in extravasation of neutrophils) associated with a SPF microbiota that were infected with *S. Tm*^{WT} (day 1 p.i.) after streptomycin treatment (Figure 31B).

Antibody mediated depletion of neutrophils did not change the abundance of *S. Tm*^{WT} in feces and cecal content during the course of infection (Figure 30A). However, CD18^{-/-} mice showed significantly more *Salmonella* in cecal content compared to CD18^{+/-} mice at day 1 p.i. with *S. Tm*^{WT} ($p < 0.05$, Kruskal-Wallis test with Dunn's multiple comparison test; Figure 31A). Systemic *Salmonella* loads in mesenteric lymphnodes were higher after antibody mediated depletion of neutrophils at day 4 p.i. ($p < 0.01$, Kruskal-Wallis test with Dunn's multiple comparison test; Figure 30B). However, systemic *Salmonella* loads in liver and spleen in antibody depleted and CD18^{-/-} mice were not significantly different. There was a tendency that the absence of neutrophils favors *Salmonella* expansion in these organs (Figures 30; 31). Taken together, this data suggest that neutrophils play a protective role

Results

against systemic *Salmonella* infection and do not contribute to *Salmonella*-induced dysbiosis and 'blooming'.

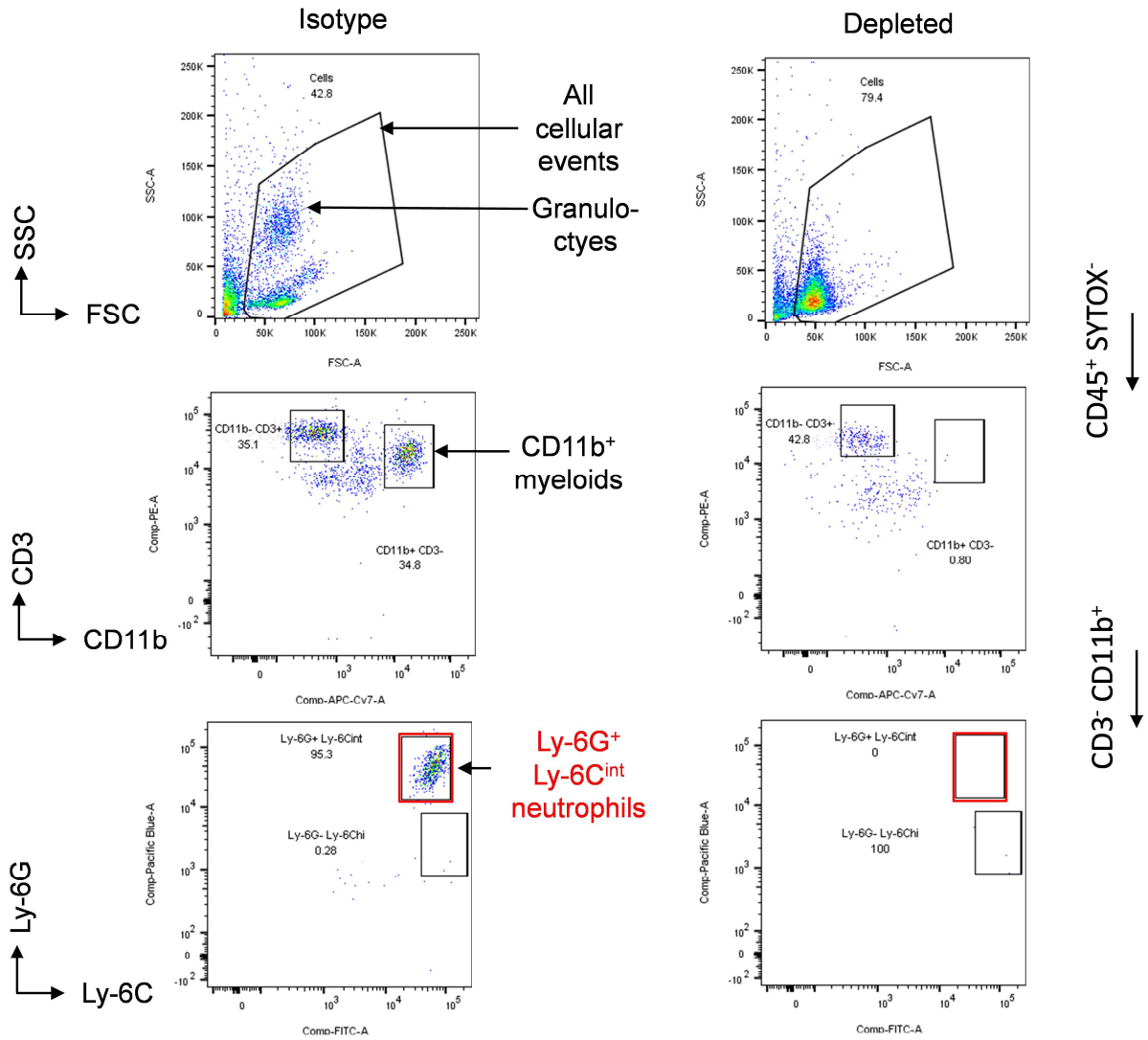


Figure 27: Confirmation of neutrophil depletion by FACS. Successful depletion of neutrophils was confirmed by FACS gating on CD45⁺, SYTOX⁻, CD3⁻, CD11b⁺, Ly-6G⁺, Ly-6C-intermediate (Ly-6G^{int}) cells. Left, example for isotype control; right, example for successful neutrophil depletion.

Results

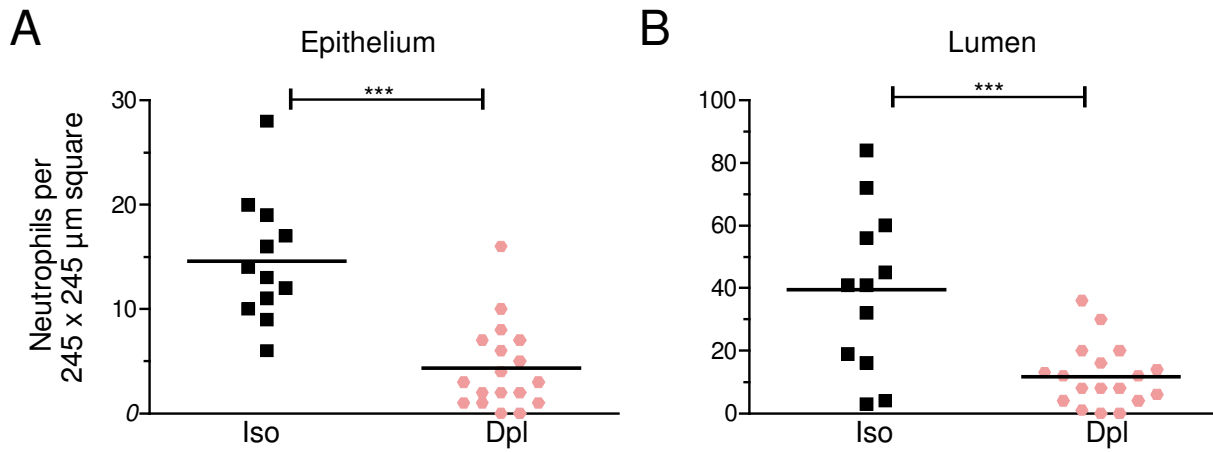


Figure 28: Quantification of neutrophils at the epithelium and in the gut lumen by immuno-fluorescence microscopy. CD18-positive neutrophils at the epithelium (A) and in the lumen (B) were antibody-stained and quantified by counting neutrophils present in 245 x 245 μm squares. Data are expressed as the mean. Statistical analysis was performed using unpaired t test (***) $p < 0.001$. Iso.: isotype control group; Dpl.: neutrophil-depleted group.

Results

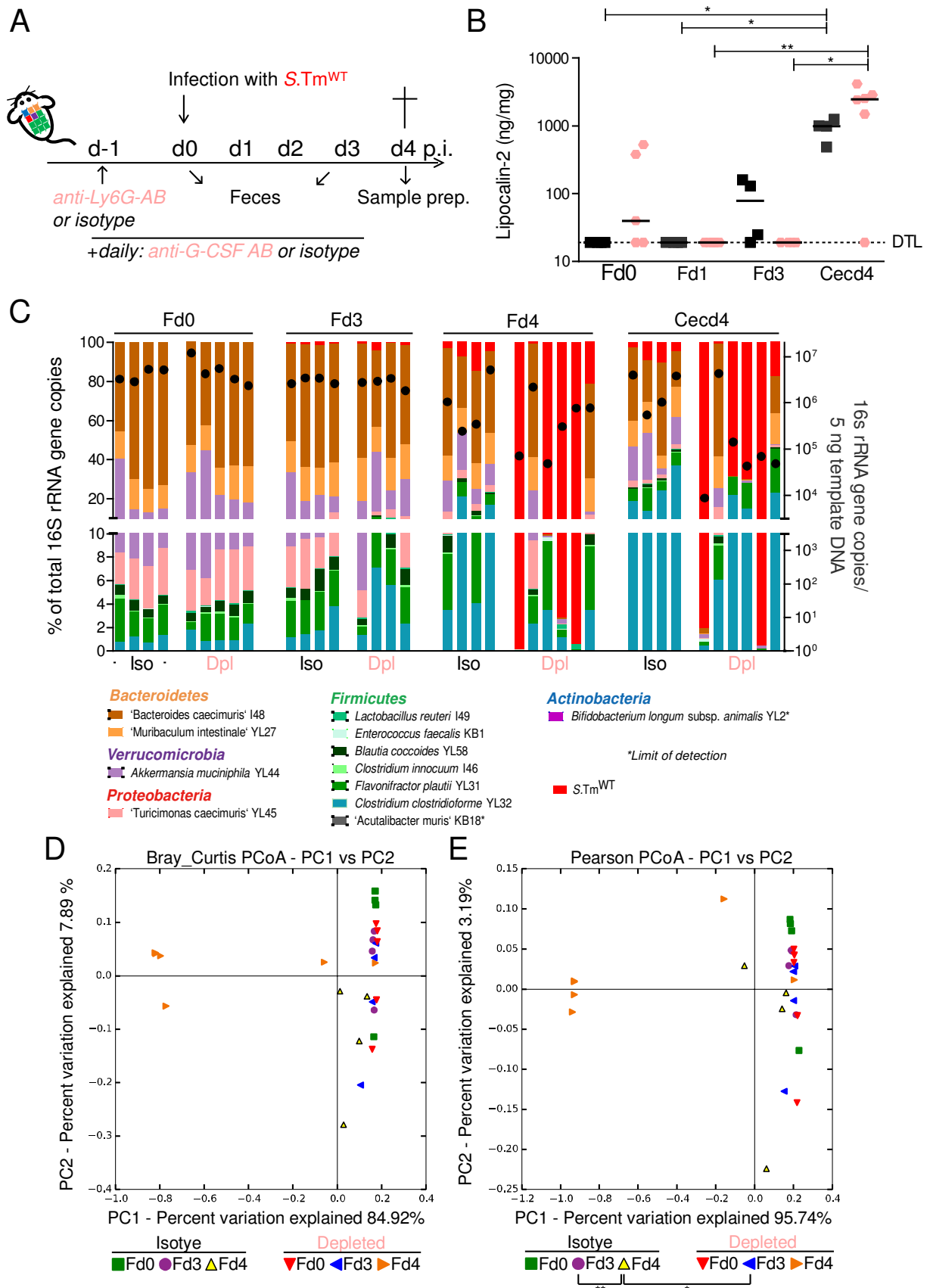


Figure 29: Neutrophils protect Oligo-MM¹² from *S. Tm* induced dysbiosis. (A) Experimental set-up: Oligo-MM¹² were treated with one dose of α -Ly6G antibody (150 μ g) or isotype control one day before infection with *S. Tm*^{WT} (5 x 10⁷ CFUs). In addition, α -G-CSF antibody (10 μ g) or isotype control were daily administered starting from day -1 until day 3 p.i. with *S. Tm*^{WT}. All antibodies were given via the intraperitoneal route. **(B)** Lipocalin-2

Results

levels in feces and cecal content (ng / mg content; * $p < 0.05$, ** $p < 0.01$, Kruskal-Wallis test with Dunn's multiple comparison test). **(C)** Analysis of microbiota composition in feces. Microbiota composition is shown as relative abundance and expressed as % of cumulated 16S rRNA gene copy numbers (% of total 16S rRNA gene copies). The amount of absolute 16S rRNA gene copies (determined by an universal primer / probe combination) is illustrated as black dots (right y axis). Cluster analysis is based on Bray Curtis **(D)** or Pearson **(E)** distance matrices and visualized as PCoA plots. Fecal microbiota samples were grouped by infection with *S. Tm*^{WT} and antibody mediated depletion of neutrophils (or isotype control) which was significant, according to Bray Curtis ($p < 0.002$, Adonis,) and Pearson ($p < 0.001$, Adonis,) with 63% (Bray Curtis) and 70% (Pearson) of variation explained. PERMDISP analyses based on Pearson distance matrices revealed statistically significant differences in fecal microbiota composition between day 3 and day 4 p.i. in the control group and there was also a difference between day 4 p.i. control group and day 3 p.i. depleted group (* $p < 0.05$, ** $p < 0.01$).

Results

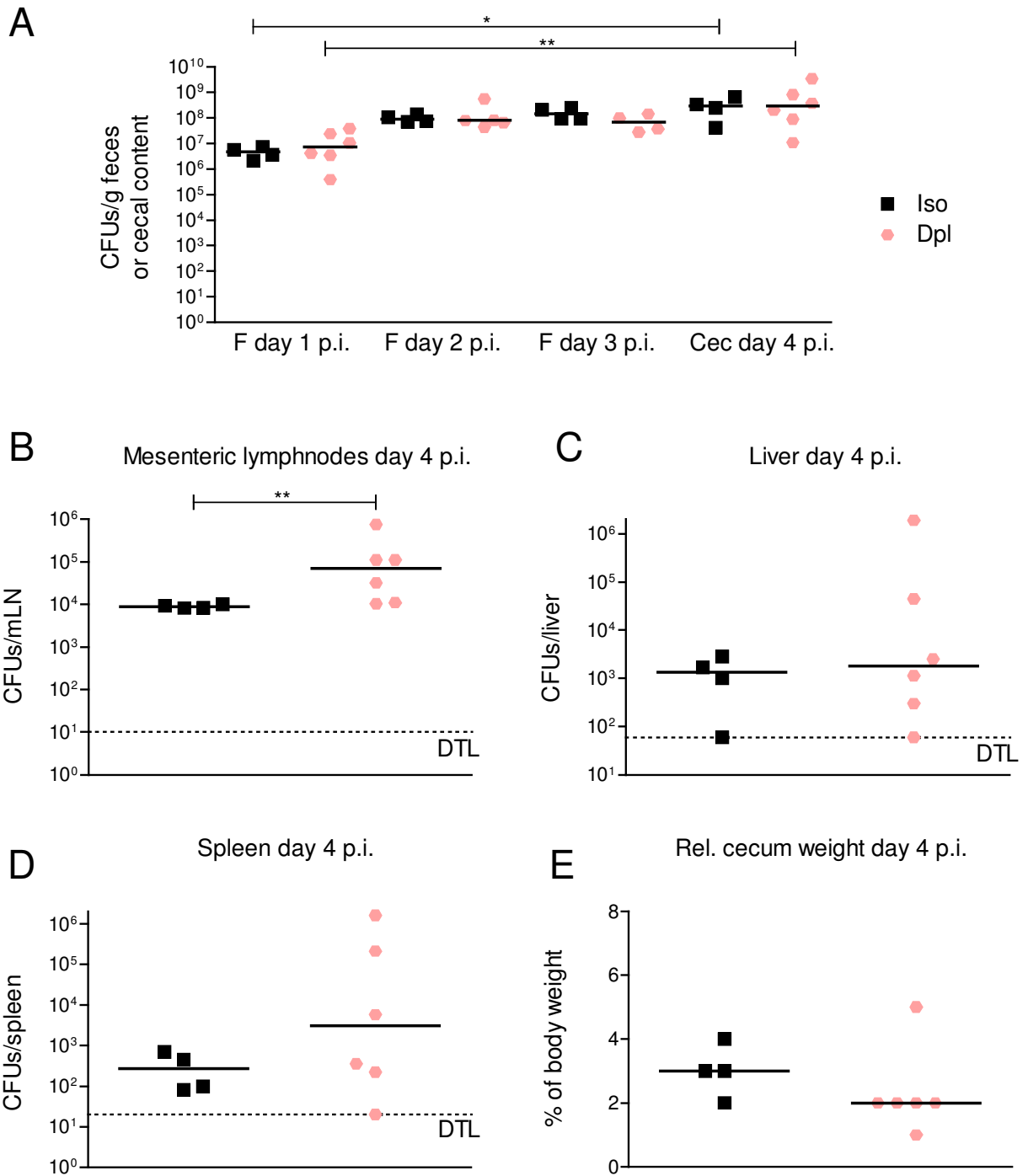


Figure 30: Influence of neutrophil depletion on the course of *Salmonella* infection and pathogenesis. For experimental set-up refer to (Figure 29A). **(A)** *Salmonella* loads in feces (F) and cecal content (cec) at days 1, 2, 3 and 4 p.i. (CFUs *S. Tm* / g content). Statistical analysis between multiple groups was performed using Kruskal-Wallis test with Dunn's multiple comparison test (* $p < 0.05$, ** $p < 0.01$). **(B) – (D)** Systemic *Salmonella* loads in mesenteric lymphnodes, liver and spleen at day 4 p.i. (CFUs / organ). **(F)** Relative cecum weight at day 4 p.i. expressed as % of body weight. Statistical analysis between two groups was performed using Mann Whitney test (* $p < 0.05$, ** $p < 0.01$). Dashed lines: DTL: limit of detection (mLN: 10 CFUs, liver: 60 CFUs, spleen: 20 CFUs).

Results

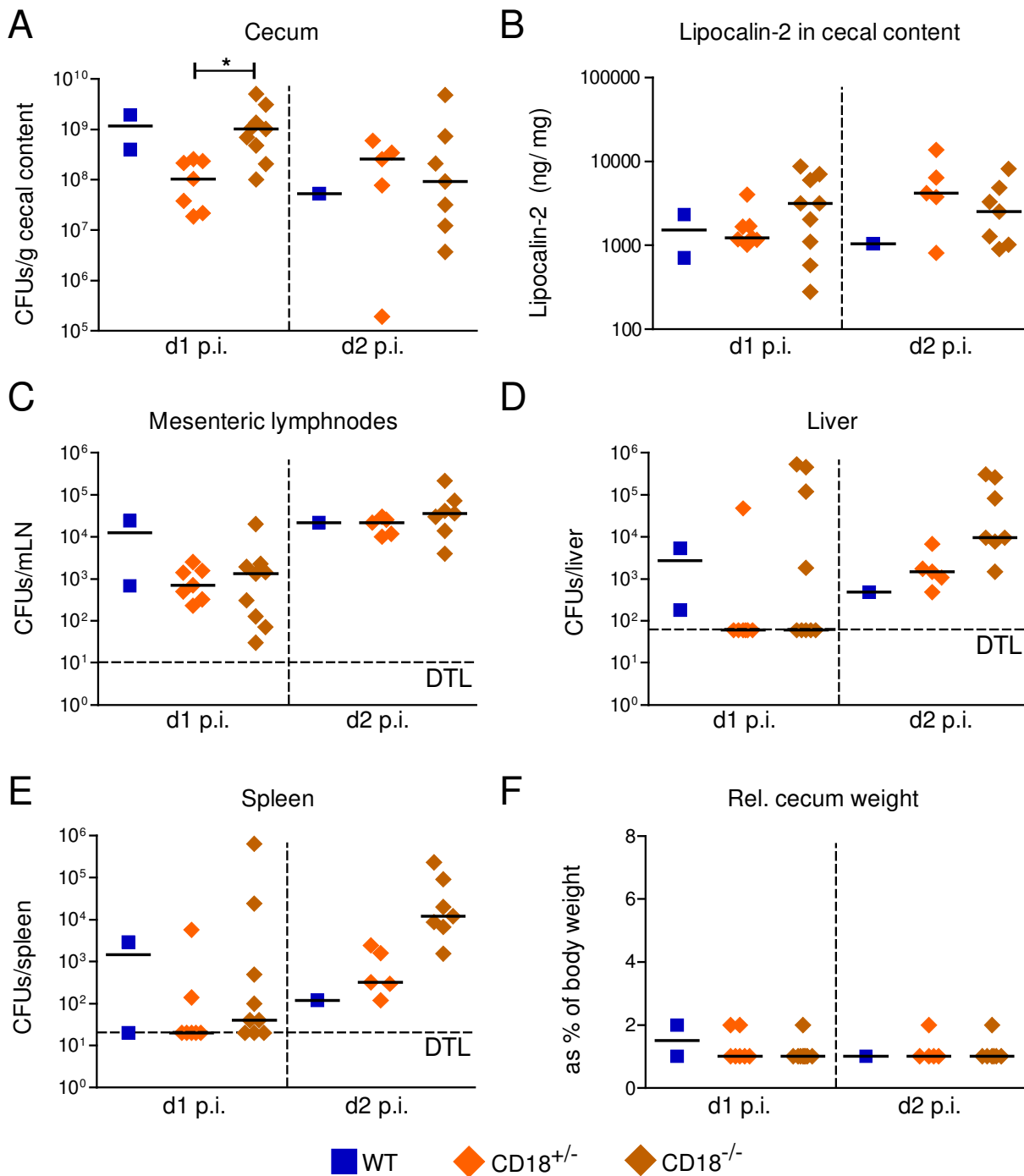


Figure 31: CD18^{-/-} mice display elevated *Salmonella* loads in the cecum at day 1 post infection with *S. Tm*. C57BL/6J WT (blue), C57BL/6J CD18^{+/-} (orange) and C57BL/6J CD18^{-/-} (brown) mice were pre-treated with one single dose of streptomycin (50 μ l of 0.5 g/ml stock by oral gavage) and were infected one day later with 5×10^7 CFUs of *S. Tm*^{WT}. At day 1 and day 2 post infection (p.i.) mice were euthanized and samples were prepared. **(A)** *S. Tm*^{WT} loads in the cecum (CFUs / g content). **(B)** Lipocalin-2 levels (ng / mg cecal content). **(C) – (E)** Transmigration of *S. Tm*^{WT} into mesenteric lymphnodes, liver and spleen (CFUs / organ). **(F)** Relative cecum weight at day 4 p.i. expressed as % of body weight. * $p < 0.05$, Kruskal-Wallis test with Dunn's multiple comparison test. Dashed lines: DTL: limit of detection (mLN: 10 CFUs, liver: 60 CFUs, spleen: 20 CFUs).

Results

3.5 Comparing the influence of infections with other enteric pathogens and T-cell-induced colitis on Oligo-MM¹² composition.

In order to compare dysbiosis and the performance of individual commensal strains upon infection with *S. Tm*, *Citrobacter rodentium* and *Clostridium difficile* as well as T-cell-induced colitis, we used gnotobiotic C57BL/6J mice associated with the Oligo-MM¹² and aimed to identify unbiased and general aspects of dysbiosis induced by gut inflammation.

3.5.1 *Citrobacter rodentium* infection does not lead to dysbiosis in Oligo-MM¹² mice

For infection, 8 Oligo-MM¹² mice were distributed in 3 gnotocages (2 x n=3 and 1 x n=2) and orally infected with 1 x 10⁸ CFUs of *Citrobacter rodentium* DBS100 (*C. rodentium*) in a one day interval. This procedure was performed, in order to avoid daily opening of gnotocages for sampling of feces. Feces was taken at the indicated time points for microbiota analysis, determination of *C. rodentium* CFUs and for LCN-2 quantification until mice were sacrificed at day 42 p.i.. *C. rodentium* colonized efficiently already at day 1 p.i. with 3.14 x 10⁷ CFUs peaking at day 11 p.i. with 1.26 x 10⁸ CFUs in feces. After day 11 p.i., *C. rodentium* loads started to decline until plateauing from day 19 p.i. on with 8.15 x 10⁶ CFUs, where they remained until day 42 p.i. (Figure 32A). The colonization with *C. rodentium* correlated with increased fecal LCN-2 levels starting from day 7 p.i. on. LCN-2 levels peaked around day 15 and day 16 p.i. and decreased afterwards. This is in line with a previous study showing highest colitis at day 14 p.i. (Gustafsson *et al.* 2013). From day 23 p.i. on, LCN-2 levels were below or close to the detection limit, indicating resolution of intestinal inflammation (Figure 32B). *C. rodentium* induced around 4 times less LCN-2 at day 15 p.i. (around 500 ng/mg feces) compared to *S. Tm*^{WT} at day 4 p.i. (Figure 11B). Moreover, *C. rodentium* infection failed to induce dysbiosis during the course of the experiment. *C. rodentium* levels were less than 1% of total microbiota (Figure 32C). The relative cecum weight at day 42 post infection with *C. rodentium* was comparable to the relative cecum weight at day 4 p.i. with *S. Tm*^{Avir} (Figure 16F), indicating no pathological changes (Figure 33D). There were low levels of *C. rodentium* found in mesenteric lymph nodes, liver or spleen tissues at day 42 p.i. (Figure 33A-C).

Results

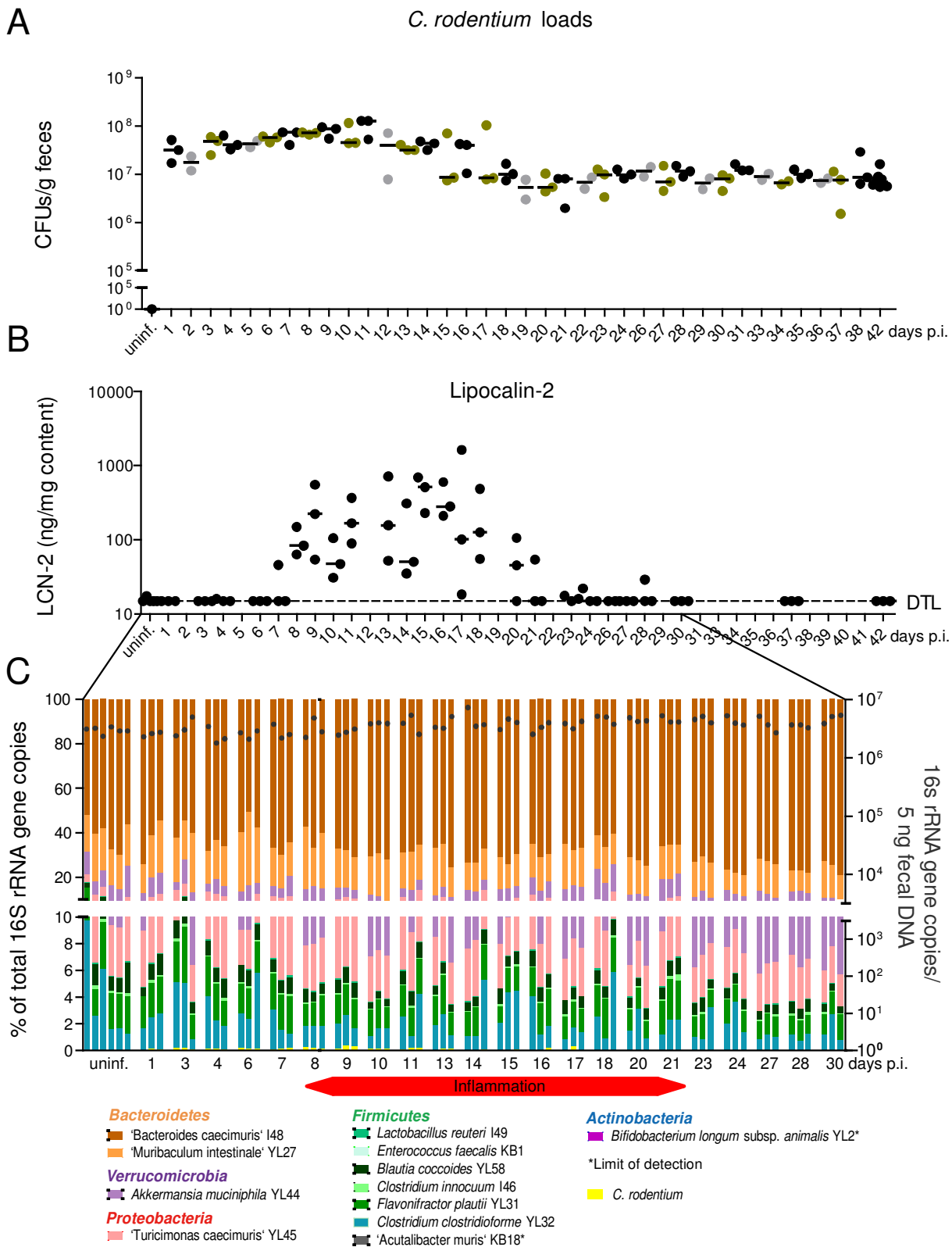


Figure 32: Course of *Citrobacter rodentium* infection in Oligo-MM¹² mice. 8 Oligo-MM¹² mice were distributed in 3 sterile gnotocages (2 x n=3, 1 x n=2) and infected with 1 x 10⁸ CFUs of *C. rodentium* (DBS 100) in a 1 day interval. Feces was sampled at the indicated time point in order to determine *C. rodentium* loads, to analyze microbiota composition and to determine LCN-2 levels. **(A)** *C. rodentium* loads in feces day 0 – day 38 p.i. and cecal content day 42 p.i. (CFUs S. Tm / g content). Mice from different gnotocages are colored differently. **(B)** Lipocalin-2 (LCN-2) amount in feces day 0 - day 37 p.i. and cecal content day 42 p.i. measured by ELISA (ng / mg content). **(C)** Analysis of fecal microbiota composition. Microbiota composition is shown as relative abundance and expressed as % of cumulated 16S rRNA gene copy numbers (% of total 16S rRNA gene copies). The amount

Results

of absolute 16S rRNA gene copies (determined by an universal primer / probe combination) is illustrated as black dots (right y axis). * Limit of detection (DTL).

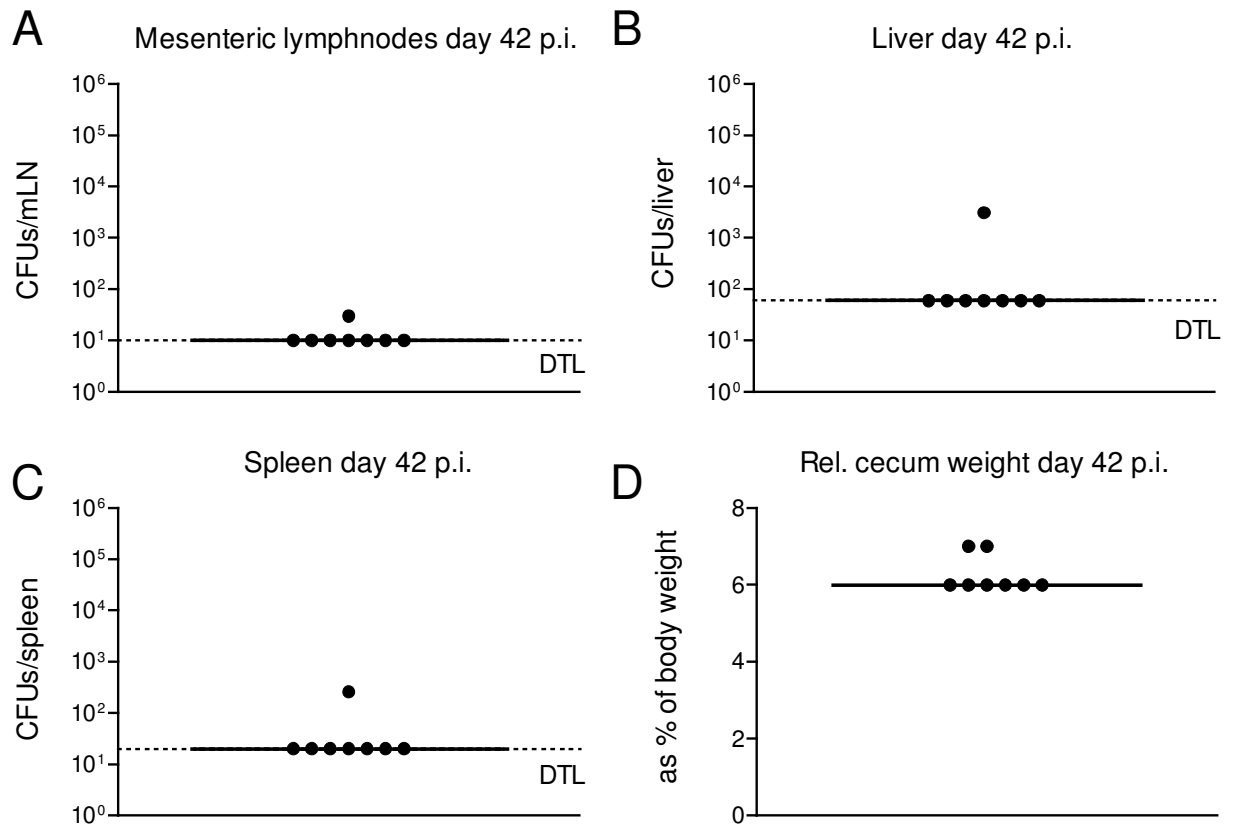


Figure 33: Systemic *Citrobacter rodentium* loads at day 42 p.i.. (A) – (C) Systemic *C. rodentium* loads in mesenteric lymphnodes, liver and spleen (CFUs / organ) determined at day 42 p.i.. (D) Relative cecum weight at day 42 p.i. expressed as % of body weight. Dashed lines: DTL: limit of detection (mLN: 10 CFUs, liver: 60 CFUs, spleen: 20 CFUs).

Results

3.5.2 *Clostridium difficile* infection shifts Oligo-MM¹² composition at day 3 p.i.

All infections with *Clostridium difficile* DH196 (*C. difficile*) were performed by Nicolas Studer of Prof. Hapfelmeier's group (University of Bern). Feces or cecal content were taken at the indicated time points (Figure 34) and DNA was extracted by Nicolas Studer using the modified stool kit from Qiagen. Plating of intestinal contents as well as LCN-2 ELISA was also performed by Nicolas Studer. The extracted intestinal DNA was subsequently sent to Munich and the microbiota was analyzed by qPCR.

Briefly, Oligo-MM¹² mice were orally infected with 10^3 of *C. difficile* DH196 spores in 100 µl of sterile PBS and samples were taken at the indicated time points (Figure 35). *C. difficile* colonized Oligo-MM¹² mice starting from day 1 p.i. (1.61×10^5 CFUs) on with 4.29×10^7 CFUs at day 3 p.i. (Figure 34A). Colonization with *C. difficile* also paralleled with elevated LCN-2 levels (Figure 34B). Looking at the microbiota composition, *C. difficile* shifted the Oligo-MM¹² composition at day 3 p.i. and dominated 2 out of 5 samples (Figure 35A). Shifts were mainly characterized by decreased relative abundance of 'Bacteroides caecimuris' I48 and 'Muribaculum intestinale' YL27 and increased relative abundance of Firmicutes strains especially *Clostridium innocuum* I46 and *Akkermansia muciniphila* YL44 (Figure 35A). Cluster analysis was additionally performed. Grouping of microbiota composition by days and infection was significant, according to Bray Curtis ($p < 0.001$, Adonis) and Pearson ($p < 0.001$, Adonis) distance matrices, with 66% as well as 76% of variation explained. The Oligo-MM¹² composition of samples from uninfected mice as well as infected mice clustered together until day 1 p.i. (Figure 35B,C). At day 3 p.i. with *C. difficile*, the Oligo-MM¹² composition clustered significantly different (Non parametric PERMDISP procedure; Figure 35B,C). Further details of microbiota composition are shown in section 3.5.4.

Results

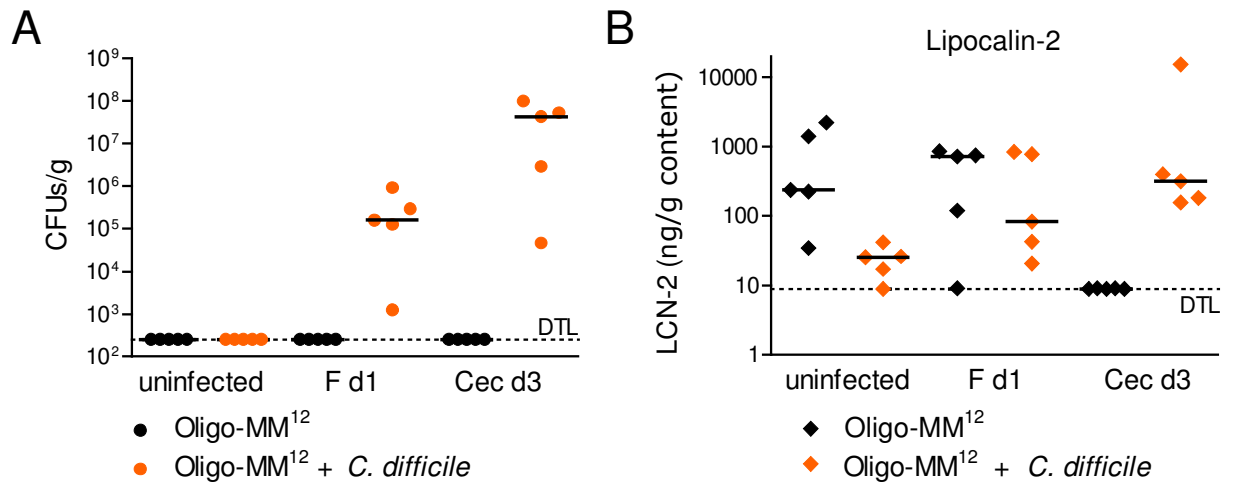


Figure 34: *Clostridium difficile* loads and Lipocalin-2 levels in Oligo-MM¹² mice. (A) *C. difficile* loads in feces (uninfected and day 1 p.i.) and in cecal content (day 3 p.i.; CFUs / g content). (B) Lipocalin-2 (LCN-2) amount in feces (uninfected and day 1 p.i.) and in cecal content (day 3 p.i.) measured by ELISA (ng / g content). DTL: limit of detection.

Results

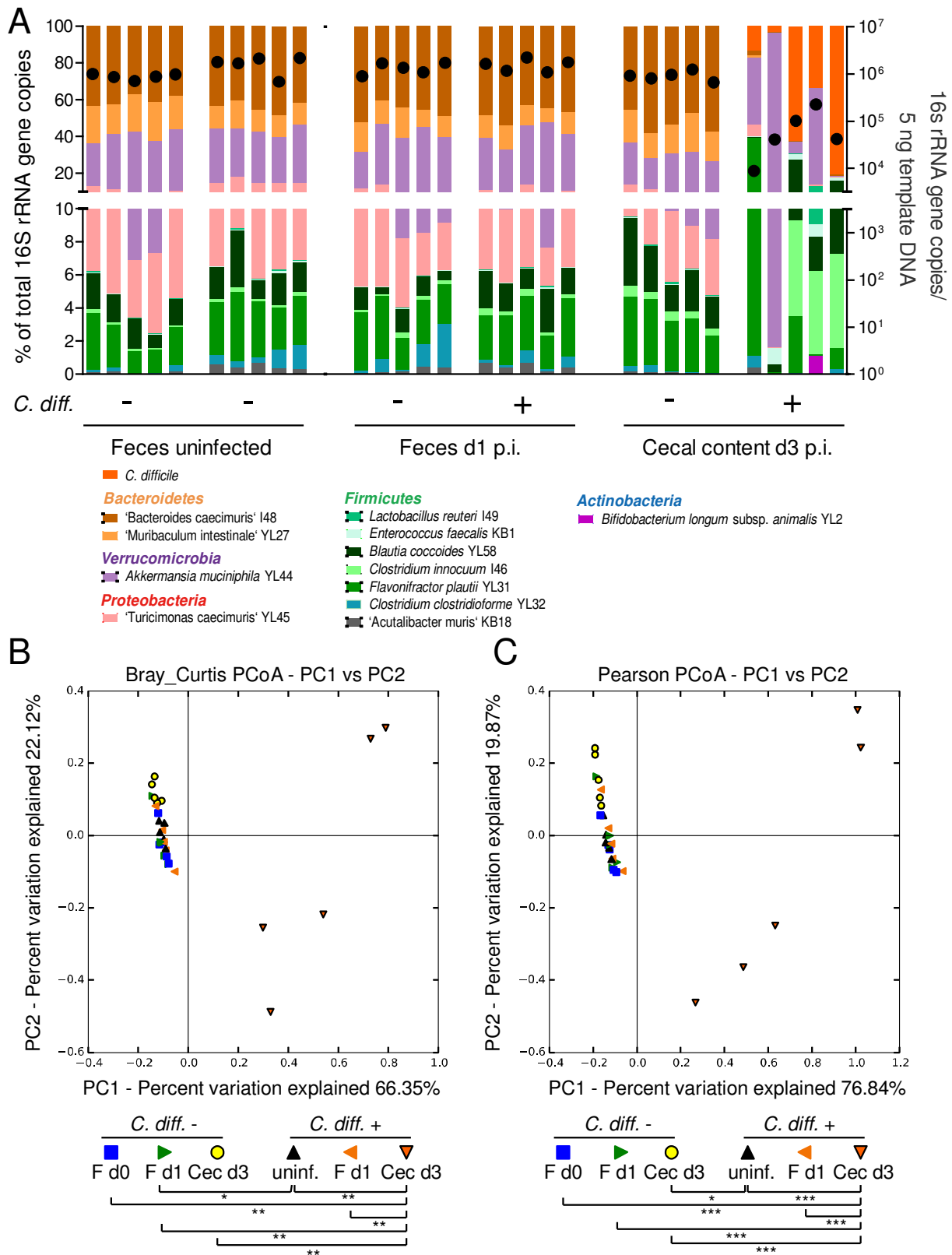


Figure 35: *Clostridium difficile* shifts Oligo-MM¹² composition at day 3 p.i.: Oligo-MM¹² mice were infected with 1×10^3 spores of *C. difficile* DH196 and kept in individually ventilated cages during the course of the experiment. In order to analyze microbiota composition, feces was taken before infection as well as at day 1 p.i.. Cecal content was additionally harvested at day 3 p.i.. **(A)** Analysis of microbiota composition in feces and cecal content. Microbiota composition is shown as relative abundance and expressed as % of cumulated 16S rRNA gene copy numbers (% of total 16S rRNA gene copies). The amount of absolute 16S rRNA gene copies (determined by an universal primer / probe combination) is illustrated as black dots (right y axis). Clustering of

Results

Oligo-MM¹² composition in feces and cecal content after oral infection with 1×10^3 CFUs of *C. difficile* DH196 spores is based on Bray Curtis (**B**) or Pearson (**C**) distance matrices and visualized as PCoA plots. Microbiota samples were grouped by infection with *C. difficile* or uninfected and days p.i. which was significant, according to Bray Curtis ($p < 0.001$, Adonis) and Pearson ($p < 0.001$, Adonis) with 66% (Bray Curtis) and 76% (Pearson) of variation explained. PERMDISP analyses based on Bray Curtis and Pearson distance matrices revealed statistically significant differences in fecal microbiota composition especially between day 3 p.i. with *C. difficile* and earlier time points (* $p < 0.05$, ** $p < 0.01$, *** $p < 0.001$).

3.5.3 Reversible, T-cell-induced colitis in RAG1^{-/-} mice associated with the Oligo-MM¹² and *Helicobacter typhlonius* induced mild microbiota shifts

The reversible colitis model (Brasseit *et al.* 2016) was established in the laboratory of Prof. Mueller (University of Bern) and all mouse experiments shown here were conducted by Martin Faderl. Briefly, RAG1^{-/-} Oligo-MM¹² mice that were either generated by cohousing germfree RAG1^{-/-} with Oligo-MM¹² donor mice or by direct association of germfree RAG1^{-/-} with the Oligo-MM¹² consortium were gavaged with 2×10^8 CFUs of *Helicobacter typhlonius* CCUG48335T (*H. typhlonius*). 14 days later colitogenic CD45RB^{hi} T-cells or PBS were adoptively transferred. In order to induce remission of colitis, mice were treated with α -CD4 antibodies (or isotype control) in 3 days intervals starting from day 24 post t-cell transfer. Mice were euthanized at day 34 post T-cell transfer and samples were prepared (Figure 36). Fecal DNA was extracted by Martin Faderl using the modified stool kit (Qiagen) and samples were sent to Munich for microbiota analysis by qPCR. LCN-2 levels were also determined in Bern.

At day 34 post T-cell transfer, RAG1^{-/-} Oligo-MM¹² mice associated with *H. typhlonius* showed elevated LCN-2 levels after treatment with α -CD4 antibodies or isotype, whereas mice which were only associated with *H. typhlonius* missing CD45RB^{hi} T-cells (PBS group) were uninfamed (Figure 37). Antibody mediated CD4⁺ T-cell depletion had no significant effect on LCN-2 levels and Inflammation. Inflammation correlated with moderate shifts in Oligo-MM¹² composition observed in the CD45RB^{hi} + α -CD4 antibody or isotype control groups. However, shifts were very mild and characterized by increasing relative abundance of *Clostridium innocuum* I46 and *Enterococcus faecalis* KB1 (Figure 38A). Grouping of microbiota composition by treatment (PBS, CD45RB^{hi} + α -CD4 antibody, CD45RB^{hi} + isotype) was not significant, according to both Bray Curtis ($p = 0.091$, Adonis) and Pearson correlation ($p = 0.201$, Adonis), with only 12% as well as 14% of variation explained. There was no statistically significant difference between groups ($p > 0.05$, Non parametric PERMDISP procedure; Figure 38B,C). This further indicates that microbiota shifts observed in this model were rather subtle.

Results

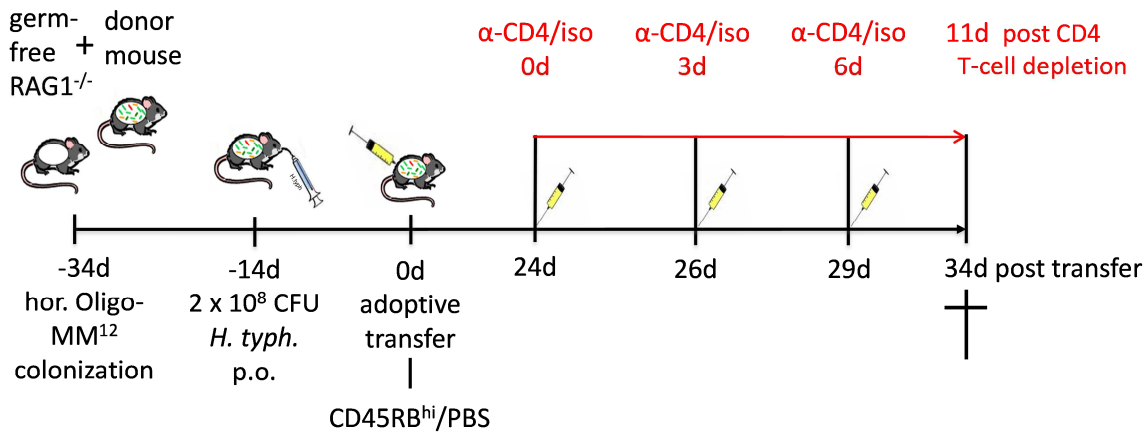


Figure 36: Reversible colitis model: germfree RAG1^{-/-} mice were either cohoused with C57BL/6J Oligo-MM¹² mice for 20 days in order to allow vertical bacterial transmission or were directly associated with the Oligo-MM¹² (not shown in scheme). 14 days prior to the adoptive transfer of colitogenic CD45RB^{hi} T-cells or PBS (control), mice were orally (p.o.) inoculated with 2 x 10⁸ CFUs of *H. typhlonius* CCUG48335T (*H. typh.*). In order to induce remission of colitis, mice were treated with α-CD4 antibody (or isotype control) in 3 days intervals starting from day 24 post T-cell transfer. Mice were euthanized at day 34 post T-cell transfer and intestinal content was collected.

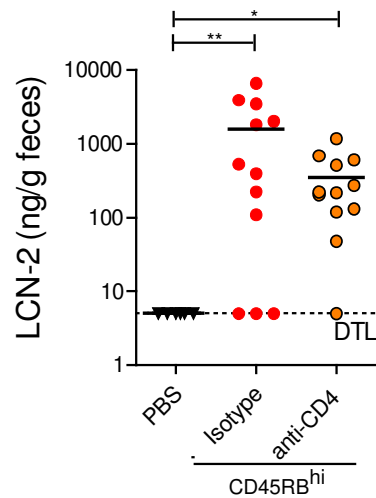


Figure 37: Lipocalin-2 amounts in RAG^{-/-} Oligo-MM¹² mice transferred with CD45RB^{hi} T-cells or PBS control with α-CD4 antibody or isotype treatment. Lipocalin-2 (LCN-2) levels in feces at day 34 post T-cell transfer measured by ELISA (ng / g feces). DTL: limit of detection. Statistical analysis between groups was performed using Kruskal-Wallis test with Dunn's multiple comparison test (* p < 0.05, ** p < 0.01).

Results

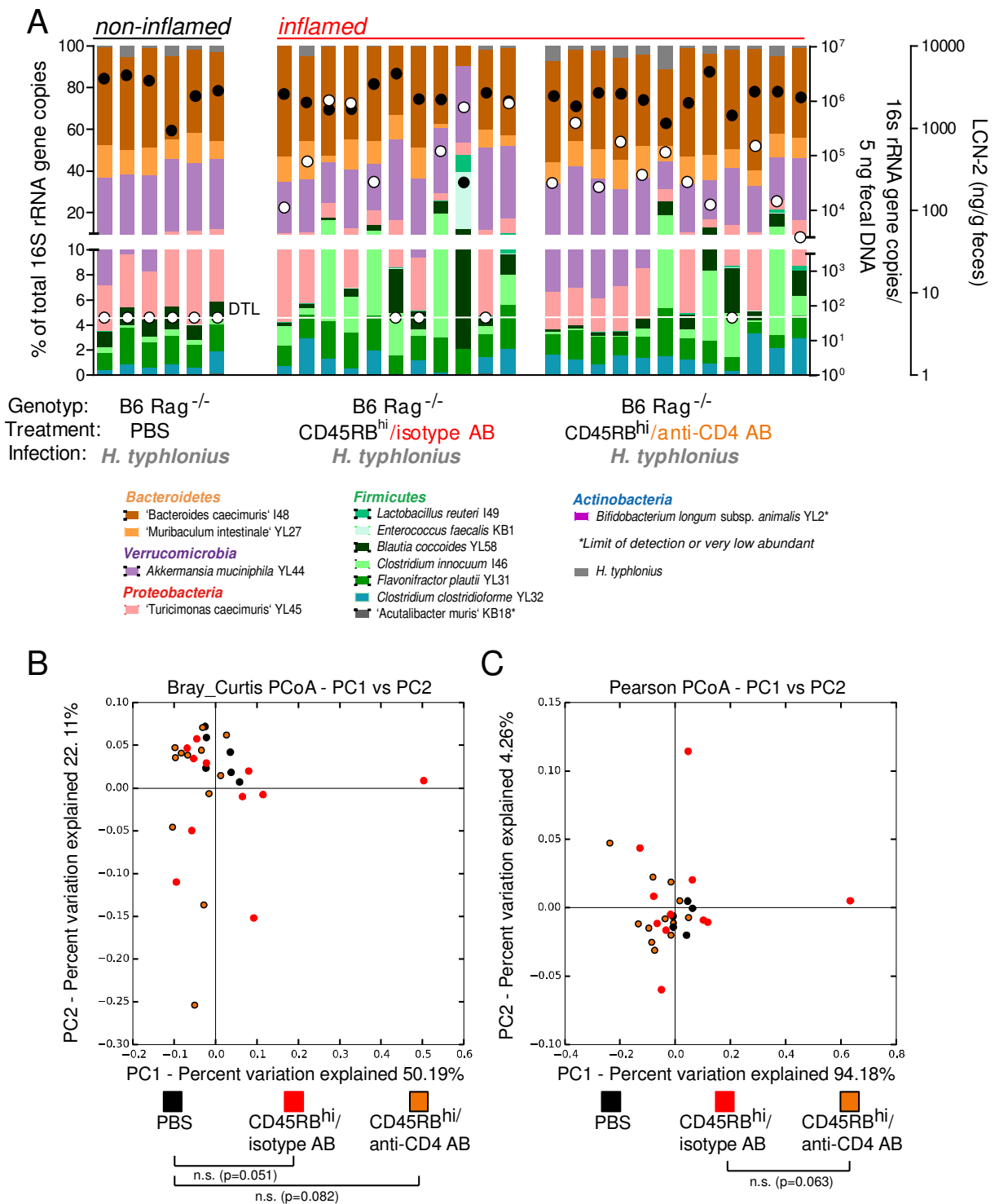


Figure 38: Oligo-MM¹² composition slightly shifts during colitis in RAG1^{-/-} Oligo-MM¹² mice associated with *Helicobacter typhlonius* and colitogenic T-cells. For experimental set-up refer to Figure 36. **(A)** Analysis of fecal microbiota composition at day 34 post T-cell transfer. Microbiota composition is shown as relative abundance and expressed as % of cumulated 16S rRNA gene copy numbers (% of total 16S rRNA gene copies). The amount of absolute 16S rRNA gene copies (determined by an universal primer / probe combination) is illustrated as black dots (right y axis). LCN-2 levels are indicated as white dots (ng / g feces, 2nd right y-axis). The limit of detection (DTL) of the LCN-2 ELISA is marked as white line. Cluster analysis of Oligo-MM¹² composition in intestinal content after infection with *H. typhlonius* and transfer of colitogenic T-cell as well as α -CD4 antibody (or isotype control) is based on Bray Curtis **(B)** or Pearson **(C)** distance matrices and visualized as PCoA plots. Microbiota samples were grouped by treatment (PBS, CD45RB^{hi} + α -CD4 antibody, CD45RB^{hi} + isotype) which was not significant, according to both Bray Curtis (p=0.091, Adonis) and Pearson (p=0.201, Adonis) distance matrices, with only 12% as well as 14% of variation explained. PERMDISP analyses based on Bray Curtis and

Results

Pearson distance matrices revealed no statistically significant differences in Oligo-MM¹² composition after different treatments ($p>0.05$).

3.5.4 Comparison of the impact of infections with *S. Tm*, *C. rodentium* and *C. difficile* as well as T-cell-induced colitis on the Oligo-MM¹² composition

Next, the impact of infections with different enteric pathogens and T-cell-induced colitis on Oligo-MM¹² composition was compared. All laboratories used C57BL/6J mice stably associated with the Oligo-MM¹² consortium. Baseline compositions of uninfected mice between labs slightly differed (non parametric PERMDISP procedure; Figure 39B,C). At baseline, there was already *H. typhlonius* present in Oligo-MM¹² mice used for the reversible colitis model. However, Oligo-MM¹² composition was similar between laboratories, since the Oligo-MM¹² composition grouped by infection and days post infection clustered together. Only the Oligo-MM¹² composition of mice housed in the MvP (Munich) clustered separately (Figure 39B,C). Grouping of microbiota composition by infection with different pathogens and days post infection was significant, according to both Bray Curtis ($p<0.001$, Adonis) and Pearson ($p<0.001$, Adonis) distance matrices, with 84% as well as 89% of variation explained. Oligo-MM¹² composition after infections with *C. rodentium* at day 15 and day 16 p.i., *S. Tm*^{WT} at day 3 p.i. as well as after *H. typhlonius* infection with consecutive CD45RB^{hi} T-cell transfer plus α -CD4 or isotype antibody were still comparable to their respective baseline microbiota composition. Interestingly, only *S. Tm* and *C. difficile* were able to 'bloom' and dominate the microbiota at day 4 and day 3 p.i., respectively (Figure 39). Oligo-MM¹² composition at day 4 p.i. with *S. Tm*^{WT} as well as at day 3 p.i. with *C. difficile* clustered apart from each other and differed also significantly compared to baseline microbiota and Oligo-MM¹² compositions after infection with *C. rodentium* and after T-cell-induced colitis (non parametric PERMDISP procedure; Figure 39B,C).

Domination of *Salmonella* with 97.64% \pm 2.14% (mean % \pm SD) and *C. difficile* with 38.77% \pm 32.58% of total microbiota was accompanied by drastically decreased fold changes in absolute abundance as well as relative abundance of 'Bacteroides caecimuris' I48 and 'Muribaculum intestinale' YL27 between non-inflamed (baseline) and inflamed (Tables 54; 55). On the Contrary, both strains were still at the baseline level post infection with *C. rodentium* or *H. typhlonius* together with CD45RB^{hi} T-cell transfer (Table 54). *C. rodentium* only constituted 0.05% \pm 0.09% and *H. typhlonius* 0.87% \pm 1.56% of total microbiota (Table 55). In contrast to infection with *S. Tm*^{WT} at day 4 p.i., *Akkermansia muciniphila* YL44 was not decreased and seemed even to profit from infection with *C. difficile* at day 3 p.i. (Figure 39A). The abundance of 'Turicimonas caecimuris' YL45 and *Clostridium clostridioforme* YL32 was decreased after infection with *S. Tm*^{WT} and *C. difficile* but remained unchanged after infection with *C. rodentium* and slightly increased after *H. typhlonius*

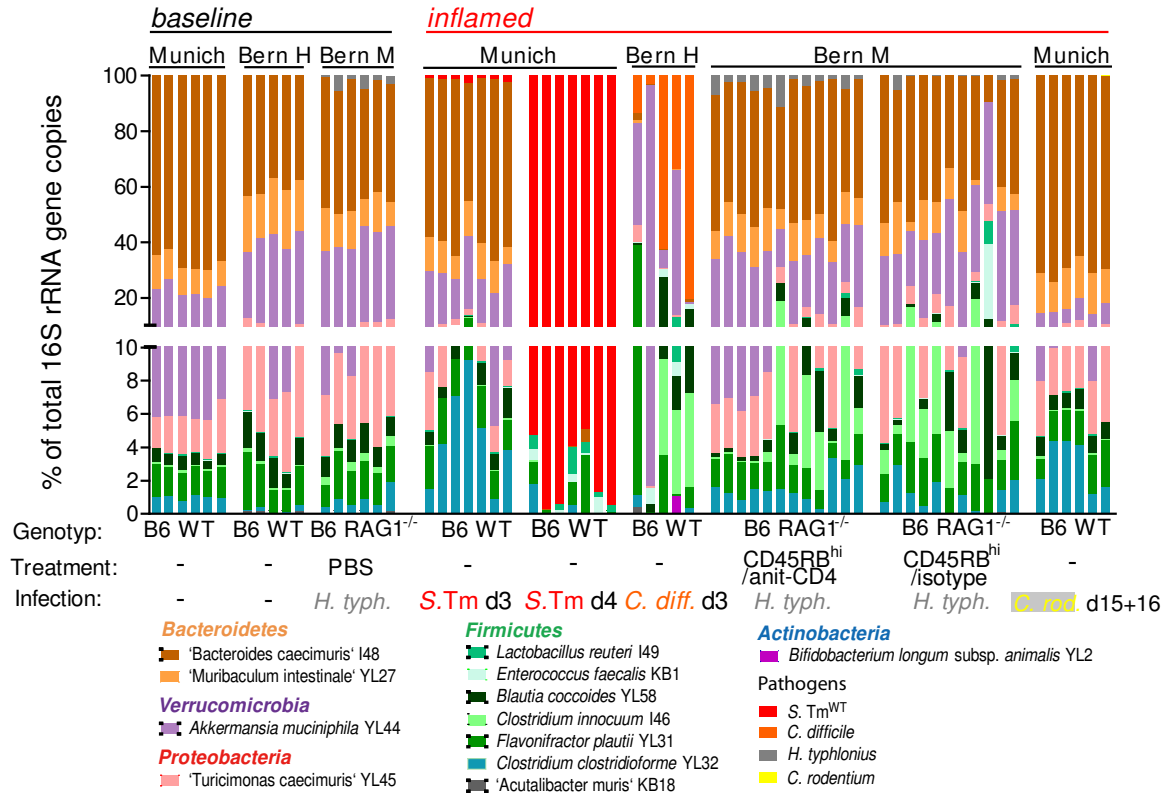
Results

infection together with CD45RB^{hi} T-cell transfer (Table 54). The abundance of *Blautia coccoides* YL58 and *Flavonifractor plautii* YL31, strains that stay constant during inflammation (Figure 14) was rather unchanged after infection with *C. difficile*, *C. rodentium* or *H. typhlonius* together with CD45RB^{hi} T-cell transfer (Table 54). Remarkably, compared to baseline the abundance of *Clostridium innocuum* I46 was increased after infection with *C. difficile* and *H. typhlonius* together with CD45RB^{hi} T-cell transfer representing 3.30% +/- 3.03% as well as 4.29% +/- 5.38% of total microbiota composition (Tables 54; 55; Figure 39A). This increase was absent after infection with *Salmonella* or *C. rodentium*. *Enterococcus faecalis* KB1 and *Lactobacillus reuteri* I49, also increased after *Salmonella* induced inflammation (Figure 14) and benefited from infection with *C. difficile* and *H. typhlonius* together with CD45RB^{hi} T-cell transfer (KB1: both, I49 only *C. difficile*; Table 54; Figure 39A). Additionally, 'Acutalibacter muris' KB18 was detected in samples from Prof. Hapfelmeier's (Bern H) and Prof. Mueller's (Bern M) laboratories. The abundance of KB18 was decreased after infection with *C. difficile* and *H. typhlonius* together with CD45RB^{hi} T-cell transfer (Table 54).

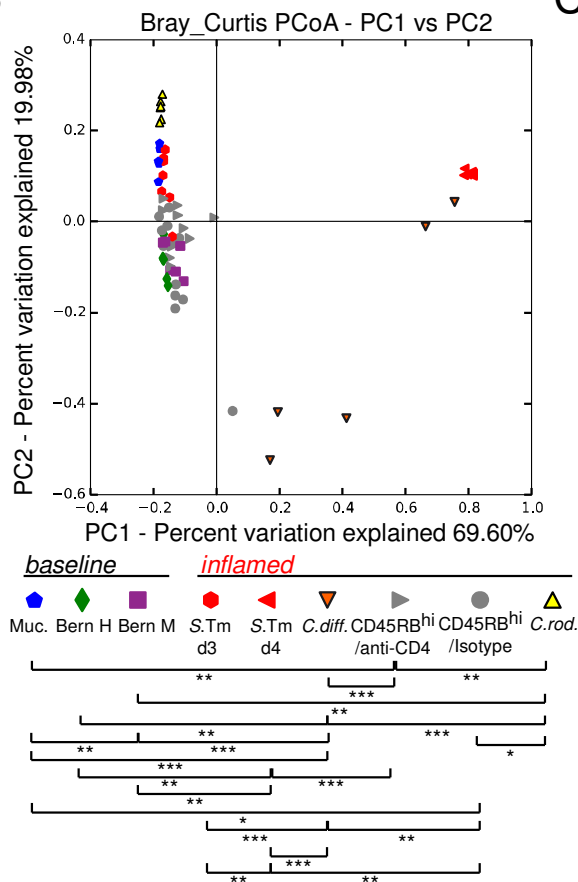
Taken together, *S. Tm* and *C. difficile* were able to induce severe dysbiosis characterized by decreasing abundance of Gram-negatives and an expansion of *Enterococcus faecalis* KB1 and *Lactobacillus reuteri* I49. *S. Tm* even dominated the microbiota with 97.64% of total microbiota composition. In stark contrast, *C. rodentium* failed to shift the Oligo-MM¹² composition and *H. typhlonius* together with CD45RB^{hi} T-cell transfer induced moderate microbiota shifts. *C. difficile* as well as *H. typhlonius* together with CD45RB^{hi} T-cell transfer facilitated the growth of *Clostridium innocuum* I46. In addition, *C. difficile* infection might also be important for the expansion of *Akkermansia muciniphila* YL44.

Results

A



B



C

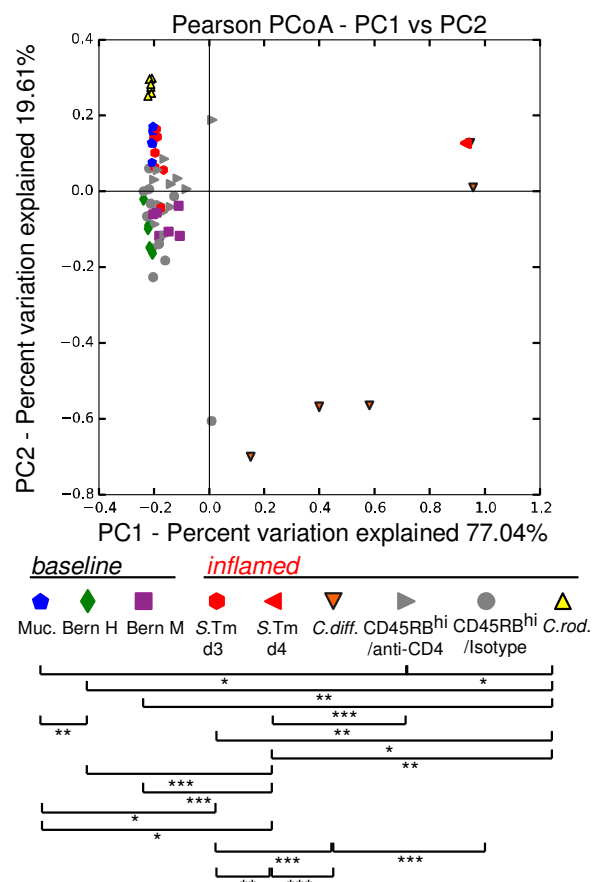


Figure 39: Comparison of the impact of infections with *S. Tm*, *C. difficile* and *C. rodentium* as well as colitis induced by colitogenic T-cells on the Oligo-MM¹² composition. (A) Analysis of microbiota composition in

Results

intestinal content (feces: Munich, Bern M, Bern H baseline; cecal content: Bern H day 3 p.i.). Microbiota composition is shown as relative abundance and expressed as % of cumulated 16S rRNA gene copy numbers (% of total 16S rRNA gene copies). Baseline Oligo-MM¹² compositions in the laboratories of Prof. Stecher (MvP, Munich), Prof. Hapfelmeier (Bern H) and Prof. Mueller (Bern M) before CD45RB^{hi} T-cell transfer were compared to the Oligo-MM¹² composition after infection with different enteric pathogens or CD45RB^{hi} T-cell transfer as indicated. Cluster analysis of Oligo-MM¹² composition in intestinal content after infection with different pathogens is based on Bray Curtis (**B**) or Pearson (**C**) distance matrices and visualized as PCoA plots. Microbiota samples were grouped by infection with different pathogens and days post infection which was significant, according to both Bray Curtis ($p < 0.001$, Adonis) and Pearson ($p < 0.001$, Adonis) distance matrices, with 84% as well as 89% of variation explained. PERMDISP analyses based on Bray Curtis and Pearson distance matrices revealed statistically significant differences in Oligo-MM¹² composition especially after infection with *S. Tm*^{WT} (day 4 p.i.), *C. difficile* (*C. diff.*, day 3p.i.) and other pathogens and time points (* $p < 0.05$, ** $p < 0.01$, *** $p < 0.001$).

Table 54: Fold difference in absolute abundance (fold change) of individual Oligo-MM¹² strains observed after infection with different enteric pathogens and T-cell-induced colitis

Strain	Infection			
	<i>S. Tm</i> ^{WT}	<i>C. difficile</i>	<i>H. typh.</i> +CD45RB ^{hi}	<i>C. rodentium</i>
	(F d1 vs F d4)	(F d1 vs Cec d3)	(uninfl. vs infl.)	(F d1 vs Fd 15+16)
<i>Akkermansia muciniphila</i> YL44	-6,945	1	-1	-1
' <i>Bacteroides caecimuris</i> ' I48	-5,811	-154	1	1
' <i>Muribaculum intestinale</i> ' YL27	-5,799	-168	-1	-2
' <i>Turicimonas caecimuris</i> ' YL45	-4,105	-49	-1	-1
<i>Clostridium clostridioforme</i> YL32	-317	-14	2	1
<i>Blautia coccoides</i> YL58	-44	1	-1	-1
<i>Flavonifractor plautii</i> YL31	-10	-4	-1	-2
<i>Clostridium innocuum</i> I46	-2	13	3	-1
<i>Enterococcus faecalis</i> KB1	13	25	5	1
<i>Lactobacillus reuteri</i> I49	14	4	1	1
' <i>Acutalibacter muris</i> ' KB18	DTL	-474	-172	DTL
<i>Bifidobacterium longum</i> subsp. <i>animalis</i> YL2	DTL	19	DTL	DTL
<i>S. Tm</i> ^{WT}	9,032	-	-	-
<i>C. difficile</i>	-	41,783	-	-
<i>H. typhlonius</i>	-	-	-1	-
<i>C. rodentium</i>	-	-	-	-1

Fold changes between different time points post infection as indicated in brackets were calculated with absolute values that were normalized to a million gene copies determined by universal probe. Bacteria were grouped in categories as in Figure 14: bacteria that were depleted by pathogen induced inflammation (YL44, I48, YL27, YL45 and YL32); Oligo-MM¹² strains that coped better with colitis (YL58, YL31 and I46); strains that were enriched during inflammation (KB1 and I49); strains that were hardly detected by qPCR (KB18 and YL2) and pathogens. DTL: limit of detection.

Results

Table 55: Relative abundance of Oligo-MM¹² strains in intestinal content after infection with different enteric pathogens and T-cell-induced colitis

Strain	mean % of cumulated 16 S rRNA gene copy numbers (+/- SD)			
	Inflammation induced by infection with			
	<i>S. Tm</i>	<i>C. difficile</i>	<i>H. typh.</i> + CD45RB ^{hi} /Iso	<i>C. rodentium</i>
'Bacteroides caecimuris' I48	0.12 (0.26)	0.81 (1.05)	40.44 ^{b,d} (11.95)	70.11 ^{c,e,f} (2.98)
'Muribaculum intestinale' YL27	0*	0.26 (0.40)	9.29 (5.91)	13.68 ^e (1.65)
<i>Akkermansia muciniphila</i> YL44	0.001 (0.004)	38.15 ^a (38.15)	29.73 ^b (6.83)	6.29 ^{e,f} (1.24)
'Turicimonas caecimuris' YL45	DTL	1.45 (2.70)	5.96 (1.40)	3.71 (0.84)
<i>Lactobacillus reuteri</i> I49	0.59 (0.52)	0.85 (1.70)	0.88 (2.50)	0.06 (0.03)
<i>Enterococcus faecalis</i> KB1	0.37 (0.38)	1.39 (0.96)	2.51 (8.18)	0*
<i>Blautia coccoides</i> YL58	DTL	5.94 (7.52)	2.58 (3.01)	1.02 (0.15)
<i>Clostridium innocuum</i> I46	0.02 (0.05)	3.30 (3.03)	4.29 (5.38)	0.12 (0.04)
<i>Flavonifractor plautii</i> YL31	0.93 (1.29)	8.55 (16.46)	2.34 (0.67)	2.01 (0.54)
<i>Clostridium clostridioforme</i> YL32	0.33 (0.66)	0.21 (0.32)	1.10 (0.94)	2.95 (1.49)
'Acutalibacter muris' KB18	DTL	0.08 (0.17)	0.01 (0.04)	DTL
<i>Bifidobacterium longum</i> subsp. <i>animalis</i> YL2	DTL	0.23 (0.48)	DTL	DTL
Pathogen	97.64 (2.14)	38.77 ^a (32.58)	0.87 ^{b,d} (1.56)	0.05 ^{c,e} (0.09)

Oligo-MM¹² after infections with *S. Tm*^{WT}, *H. typhlonius* (*H. typh.*) + CD45RB^{hi} + isotype antibody and *C. rodentium* (*C. rod.*) was analyzed using fecal DNA. DNA from cecal content was used to determine the Oligo-MM¹² composition after infection with *C. difficile* (*C. diff.*). Significant differences between **a** *S. Tm* vs *C. diff.*, **b** *S. Tm* vs *H. typh.*, **c** *S. Tm* vs *C. rod.*, **d** *C. diff.* vs *H. typh.*, **e** *C. diff.* vs *C. rod.* and **f** *H. typh.* vs *C. rod.* are indicated; p values were less than 0.001, except: YL27 *S. Tm* vs *C. rod.* p<0.01 and YL27 *C. diff.* vs *C. rod.* p<0.05, two-way ANOVA with Bonferroni posttest. Values are expressed as mean % of cumulated 16 S rRNA gene copy numbers +/- standard deviation (SD). The microbiota was analyzed at the following days post infection: *S. Tm*: day 4 p.i. (n=7), *C. difficile* day 3 p.i. (n=5), *H. typhlonius* + CD45RB^{hi} + isotype control antibody: day 34 p.i. (n=11) and *C. rodentium*: days 15 + 16 p.i. (n=6). * Very low abundant. DTL: limit of detection.

4. Discussion

4.1 The Oligo-MM¹², a novel consortium of gut commensals applicable for studies of host-microbe interactions

Since the gut microbiota is highly complex, different gnotobiotic animal models have been developed in the past years ranging from low complexity with only one or two gut commensals to more complex communities (Freter and Abrams 1972, Klaasen *et al.* 1991, Bry *et al.* 1996, Dewhirst *et al.* 1999, Mahowald *et al.* 2009, Becker *et al.* 2011, McNulty *et al.* 2011) which enabled host-microbe interaction studies. These models microbiota were either collections of bacterial isolates from humans or were based on murine bacterial isolates, like the Altered Schaedler Flora (ASF). One has to take into account that phenotypes observed in animals associated with human bacteria (humanized animal models) might be biased because mutualistic microbiota-host effects mediated by long-term co-evolution between host-specific bacteria and host are missing and that different genetic backgrounds between humans and mice might additionally impact on bacterial colonization (Wos-Oxley *et al.* 2012). Therefore, gnotobiotic mice associated with murine bacterial isolates, like the ASF would be more suitable for host-microbe interaction studies. However, the ASF is currently not available in public strain collections due to intellectual property rights.

To this end, we have established a novel and highly defined model microbiota that consists of 12 murine bacterial isolates, termed the Oligo-Mouse-Microbiota (Oligo-MM¹²) which can be easily applied to germfree mice and stably colonizes over filial generations. Remarkably, the bacterial consortium covers representatives of 5 eubacterial phyla including a novel family ('Muribaculaceae'), genera ('Acutalibacter muris' and 'Turicimonas muris') and species ('Bacteroides caecimuris' I48). Since the Oligo-MM¹² strains grow reliably after freezing, the microbiota can be shipped and shared between different research facilities and can be therefore used as platform for comparable host-microbe interaction studies. Moreover, the Oligo-MM¹² strains are also included in the Mouse Intestinal Bacterial Collection (miBC) and are available to the research community (Lagkouvardos *et al.* 2016). Strain-specific FISH was additionally established. Moreover, the genome of each Oligo-MM¹² strain has been sequenced which enables correlations of phenotypes with gene functions. In addition, I have established strain-specific qPCR assays for quantification of individual Oligo-MM¹² strains making the Oligo-MM¹² a valuable and versatile research tool for fast and affordable investigations.

Discussion

4.1.1 Strain-specific quantitative real-time PCR enables reliable, fast and affordable quantification of individual Oligo-MM¹² strains

Strain-specific qPCR assays targeting hypervariable regions of the 16S rRNA gene (Figures 42) are now available for all Oligo-MM¹² strains and enable fast microbiota analyses. In the past years, strain identification based on hypervariable regions of the 16S rRNA gene has become a method of choice since culturing of anaerobic gut commensals is challenging (Brown *et al.* 2013) and not suitable for determination of relative microbiota composition. In addition, powerful next generation 16S rRNA gene amplicon sequencing (NGAS) techniques were developed which enable strain identification in samples of unknown constitution. However, NGAS are biased by PCR errors, variable regions targeted, analysis pipelines used and depend on quality as well as completeness of reference databases such as SILVA or greengenes (Hiergeist *et al.* 2015), <http://greengenes.lbl.gov/>, <https://www.arb-silva.de/>). Therefore, novel species which are not yet included in a reference data base might not be detected or mistakenly attributed to wrong taxa. Thus, the novel Oligo-MM¹² strains 'Acutalibacter muris' KB18, 'Muribaculum intestinale' YL27 and 'Bacteroides caecimuris' I48 were assigned to Ruminococcaceae; *Incertae Sedis* (KB18), Bacteroidales; *Incertae Sedis* (YL27) and *Bacteroides* (I48) using SILVA data base (PhD thesis of Sandrine Brugiroux). In addition, the sensitivity of NGAS is relatively low. We obtained 10,000 sequencing reads per gram of intestinal content (10¹¹ bacteria per gram intestinal content) which translates into a detection limits of 10⁷ CFUs per gram of intestinal content.

Therefore, highly strain-specific, hydrolysis probe based qPCR assays were designed in this study which enable quantification of individual community members. Initial attempts to establish a SYBR green based qPCR protocol operating with only two specific primers were not successful because qPCR specificity and efficiency were not acceptable. The major problem was the design of strain-specific primer sets that target a short hypervariable region of the 16S rRNA gene and perform efficiently. Nevertheless, SYBR green based qPCR was used previously in other models (Barman *et al.* 2008, Ganesh *et al.* 2013). A third oligonucleotide, the hydrolysis probe together with new primers designed using the software Primer Express 3 (Applied Bio), finally increased strain-specificity and improved qPCR efficiency. Compared to NGAS, qPCR is affordable, faster, doesn't depend on bioinformatical analysis tools and detects bacterial strains down to an abundance of 10⁴ – 10⁵ CFUs / g intestinal content (Brugiroux *et al.* 2016) which is 100 – 1,000 times more sensitive compared to NGAS. However, like NGAS, qPCR is biased by the DNA extraction method which can yield different Gram-negative / Gram-positive ratios according to the lysis efficiency of the DNA extraction method (data not shown) and doesn't allow to detect contaminations because it enables only detection of specifically targeted bacteria. One has to take into account that both methods,

Discussion

NGAS and qPCR, are biased concerning the 16S rRNA gene copy number per genome. Since bacteria have different copy numbers of 16S rRNA gene operons, the actual abundance of individual commensals might be miss-calculated. For this reasons, one should consider normalizing the 16S rRNA gene copy numbers per amount of 16S rRNA operon numbers present in the genome or additionally using DNA and 16S rRNA gene independent methods, in order to verify NGAS or qPCR results. Strain-specific FISH that targets ribosomal rRNA would be an option. Nevertheless, strain-specific qPCR is a valuable method for studying changes in bacterial composition upon different treatments or disturbances.

4.1.2 The Oligo-MM¹² as a tool to study kinetics of microbiota maturation as well as shifts in microbial composition and phenotypes upon changes in diet

We studied colonization kinetics of the Oligo-MM¹² once administered orally in germfree mice (Figure 6). Interestingly, we observed 3 maturation stages (early, intermediate and stable). The microbiota adopted a stable composition after 7 days post inoculation. At the early stage (day 1 post inoculation), the microbiota was dominated by *Akkermansia muciniphila* YL44, 'Bacteroides caecimuris' I48 and *Bifidobacterium longum* subsp. *animalis* YL2 and relative abundance of *Enterococcus faecalis* KB1 was also elevated (Figure 6; Table 40). At this stage, these specific Oligo-MM¹² strains might profit from direct access to the host mucus which might be especially metabolized by *Akkermansia muciniphila* YL44 (Derrien *et al.* 2004). In addition, oxygen that might be present in the gut of germfree mice lacking microbiota derived butyrate which renders the epithelium hypoxic (Rivera-Chávez *et al.* 2016) might promote growth of *Enterococcus faecalis* KB1. *Enterococcus faecalis* KB1 has been shown to expand in aerobic liquid culture (data shown in MD thesis of Patrick Schiller). Oxygen might be additionally tolerated by *Bifidobacterium longum* subsp. *animalis* YL2 (Andriantsoanirina *et al.* 2013). Along this line, Martin and co-workers also identified *Bifidobacterium* species as early colonizers of the infant gut (Martin *et al.* 2016). Obligate anaerobic members, e.g. 'Bacteroides caecimuris' I48 might thrive later when oxygen is consumed. During early colonization, accessibility of dietary nutrients plays a role during microbiota maturation. It could be shown that the abundance of Bacteroidetes and *Bifidobacterium* was predominant in infants after weaning and transition to table foods (Fallani *et al.* 2011, Koenig *et al.* 2011) and later also abundance of Firmicutes such as *Clostridium* spp. increased (Bergström *et al.* 2014). Thus, the maturation of the Oligo-MM¹² partially resembles the maturation of the human microbiota.

During the intermediate stage (days 2 - 4 post inoculation), there was a peak in relative abundance of 'Bacteroides caecimuris' I48 and also relative abundance of 'Turicimonas caecimuris' YL45, 'Muribaculum intestinale' YL27 and *Flavonifractor plautii* YL31 increased by trend. The relative abundance of *Akkermansia muciniphila* YL44 and *Bifidobacterium longum* subsp. *animalis* YL2

Discussion

dropped compared to the early stage (Figure 6; Table 40). A further decrease in oxygen concentration and altered mucus structure and composition upon bacterial colonization might be the reasons for this microbiota shift. The mucus layer is divided in a tight inner layer which serves a barrier and a loose outer layer which is colonized by bacteria (Johansson *et al.* 2008). Interestingly, Johansson and colleagues further observed that colonization of germfree mice with conventional microbiota led to the development of a tight inner and a loose outer mucus layer which coincided with increased abundance of Bacteroidetes and decreased abundance of Firmicutes in the distal colon during early colonization (Johansson *et al.* 2015), suggesting that new niches for intestinal commensals become available during the maturation of the mucus layer.

From day 7 post inoculation on, the Oligo-MM¹² composition stabilized. At this stage, *Bifidobacterium longum* subsp. *animalis* YL2 and *Enterococcus faecalis* KB1 were hardly detectable (limit of detection: 13 and 25 16S rRNA gene copy number per 5 ng template DNA, respectively). 'Muribaculum intestinale' YL27 and *Akkermansia muciniphila* YL44 expanded and the relative abundance of 'Bacteroides caecimuris' I48 was reduced, but 'Bacteroides caecimuris' I48 was still the dominating species. The relative abundance of other Firmicutes and 'Turicimonas caecimuris' YL45 was comparable to intermediate stage (Figure 6; Table 40). Remarkably, 'Acutalibacter muris' KB18 was only detected in the inoculum indicating that this strain was outcompeted by the residual Oligo-MM¹² commensals at least under housing conditions in our facility. According to qPCR based microbiota analyses, 10 out of 12 Oligo-MM¹² strains were detected when the microbiota has fully matured. *Bifidobacterium longum* subsp. *animalis* YL2 and 'Acutalibacter muris' KB18 (limit of detection: 1 16S rRNA gene copy number per 5 ng template DNA) were below the limit of detection of the respective qPCR assay during the stable stage.

Since this characteristic maturation kinetic of the microbiota was observed after colonizing germfree mice with the Oligo-MM¹² consortium, this model could be further used to conduct mechanistic studies of microbe-host or microbe-microbe interactions during early colonization of a germfree host. On the one hand the structure and composition of the mucus layer (Johansson *et al.* 2015), direct microbe-microbe interactions and increased oxygenation (Rivera-Chávez *et al.* 2016) might shape microbial composition during early colonization. On the other hand also the maturation of the host immune system during colonization including secretion of antimicrobial peptides and IgA, cytokine production as well as induction of certain T- and B-cells might be involved in shaping the microbiota composition (Macpherson and Uhr 2004, Cash *et al.* 2006, Atarashi *et al.* 2008, Vaishnav *et al.* 2008, Sonnenberg *et al.* 2012, Atarashi *et al.* 2013). Transcriptomics of the host epithelium and RNAseq of the Oligo-MM¹² during early colonization could shed more light on host-microbe interaction during early colonization.

Discussion

Moreover, we switched standard diet to high-fat (HF) diet and supplemented oleic acid (OA) and monitored to Oligo-MM¹² composition at 6, 12, 24 h post diet change. HF and OA increased relative abundance of *Akkermansia muciniphila* YL44 and lowered abundance of 'Bacteroides caecimuris' I48 compared to standard diet (Figure 9; Table 43). This is in line with a previous study in mice where HF and high sugar (HS) diet also increased relative abundance of Firmicutes and Verrucomicrobia as well as decreased abundance of Bacteroidetes (Carmody *et al.* 2015). A study conducted with malnourished and healthy children revealed that HF diet caused also a decrease in Bacteroidetes and an increase in Proteobacteria (*E. coli* and *Klebsiella* spp.) in human infants (Monira *et al.* 2011). In addition, Microbiome analysis of obese individuals revealed decreased abundance of Bacteroidetes, *Bifidobacterium* and butyrate producing Firmicutes as well as higher abundance of Actinobacteria and *Lactobacillus* spp. (Duncan *et al.* 2008, Armougom *et al.* 2009, Turnbaugh *et al.* 2009, Million *et al.* 2012). This change in microbiota composition might be attributed to a lower content of non-digestible carbohydrate (fiber) in HF / HS diet, which is usually fermented by commensals in the lower gastro-intestinal tract (Walker *et al.* 2011).

Interestingly, the presence of *Akkermansia* renders the host more susceptible to infection with *S. Tm* (Ganesh *et al.* 2013). However, parallels between different diets, changes in microbiota composition and susceptibility to enteric infection need to be studied elsewhere in more detail.

4.1.3 The Oligo-MM¹² that is stable over several generations and between animal facilities is a robust model microbiota for the research community

By breeding mice associated with the Oligo-MM¹² under germfree conditions, we showed that the microbiota is vertically transmitted from parental (P) to filial (F) generations. Remarkably, the Oligo-MM¹² composition was stable over at least 6 generations (Figure 7). *Bifidobacterium longum* subsp. *animalis* YL2 was not detected in any generation and 'Acutalibacter muris' KB18 could be only detected at low levels in fecal samples from the P and F1 generation (Table 41). According to cluster analysis, especially the Oligo-MM¹² composition of the P generation was different compared to that of the F generations (Figure 7B,C). Here, it is worth mentioning that the Oligo-MM¹² mice were generated at the CMF in Bern (generations P and F1) and later distributed to the MvP in Munich (generations F2 – F6) and also to the ETHZ. Thus, different housing conditions and chow might be the reason for the slight differences in overall microbiota composition observed between the parental and filial generations as described previously (Rausch *et al.* 2016). There were additional fluctuations of relative abundance of 'Bacteroides caecimuris' I48 and *Akkermansia muciniphila* YL44 between the generations F1 – F4 (Table 41). However, these differences in microbial composition were subtle and thus the overall Oligo-MM¹² composition was considered as robust over 6 generations.

Discussion

The Oligo-MM¹² was designed as a reductionist model for host-microbe interaction studies that is available to a broad research community. So far, the Oligo-MM¹² is already established at different animal facilities. Therefore, we next wanted to investigate the influence of different housing conditions on the overall Oligo-MM¹² composition, because a similar microbiota composition between animal facilities is a prerequisite for comparability of data. Thus, microbiota composition of Oligo-MM¹² mice housed at the CMF in Bern (either in isolators or in individually ventilated cages (IVC)), in the ETHZ and the MvP in Munich were compared in this study (Figure 8). All qPCR based microbiota analyses were conducted by one person in order to minimize variability and to attribute subtle changes in microbial composition to different housing conditions. There were only minor differences in relative abundance of individual Oligo-MM¹² strains of mice housed at the CMF and ETHZ (Table 42) and overall, β -analysis revealed that samples from different facilities were in one cluster (Figure 8C). In contrast, the overall Oligo-MM¹² composition of mice housed at the MvP clustered slightly apart from samples of mice housed at the CMF and ETHZ (Figure 8D,C). Interestingly, 'Acutalibacter muris' KB18 was only detected in mice housed at the CMF and ETHZ. These differences might be attributed to differences in chow used in the different housing facilities (MvP: ssniff; CMF and ETHZ: KLIBA NAFAG). Nevertheless, since overall Oligo-MM¹² composition was highly similar between housing facilities, we conclude that the Oligo-MM¹² is a highly defined and stable model microbiota that can be used to obtain reproducible analyses between different research facilities.

4.2 The influence of *Salmonella*-induced gut inflammation on the indigenous microbiota in the Oligo-MM¹² model

S. Tm invades the gut ecosystem in a stepwise manner. It has been postulated that there are several stages of gut ecosystem invasion until *S. Tm* induces full blown disease (Figure 2) (Ferreyra *et al.* 2014): first *S. Tm* has to break CR that is conferred by the indigenous microbiota. This initial step can be facilitated by antibiotic intake (Barthel *et al.* 2003, Ng *et al.* 2013, Rivera-Chávez *et al.* 2016). Once CR is broken the pathogen expands in the gut, it induces inflammation and outcompetes the resident microbiota by profiting from the nutritional environment of an inflammatory gut milieu and escapes host defense mechanisms (Raffatellu *et al.* 2009, Winter *et al.* 2010, Thiennimitr *et al.* 2011, Lopez *et al.* 2012). However, until now it is unclear which mechanisms underlying ecosystem invasion and *Salmonella* 'blooming' is the most important and how gut inflammation impacts on individual commensal species of a healthy gut microbiota.

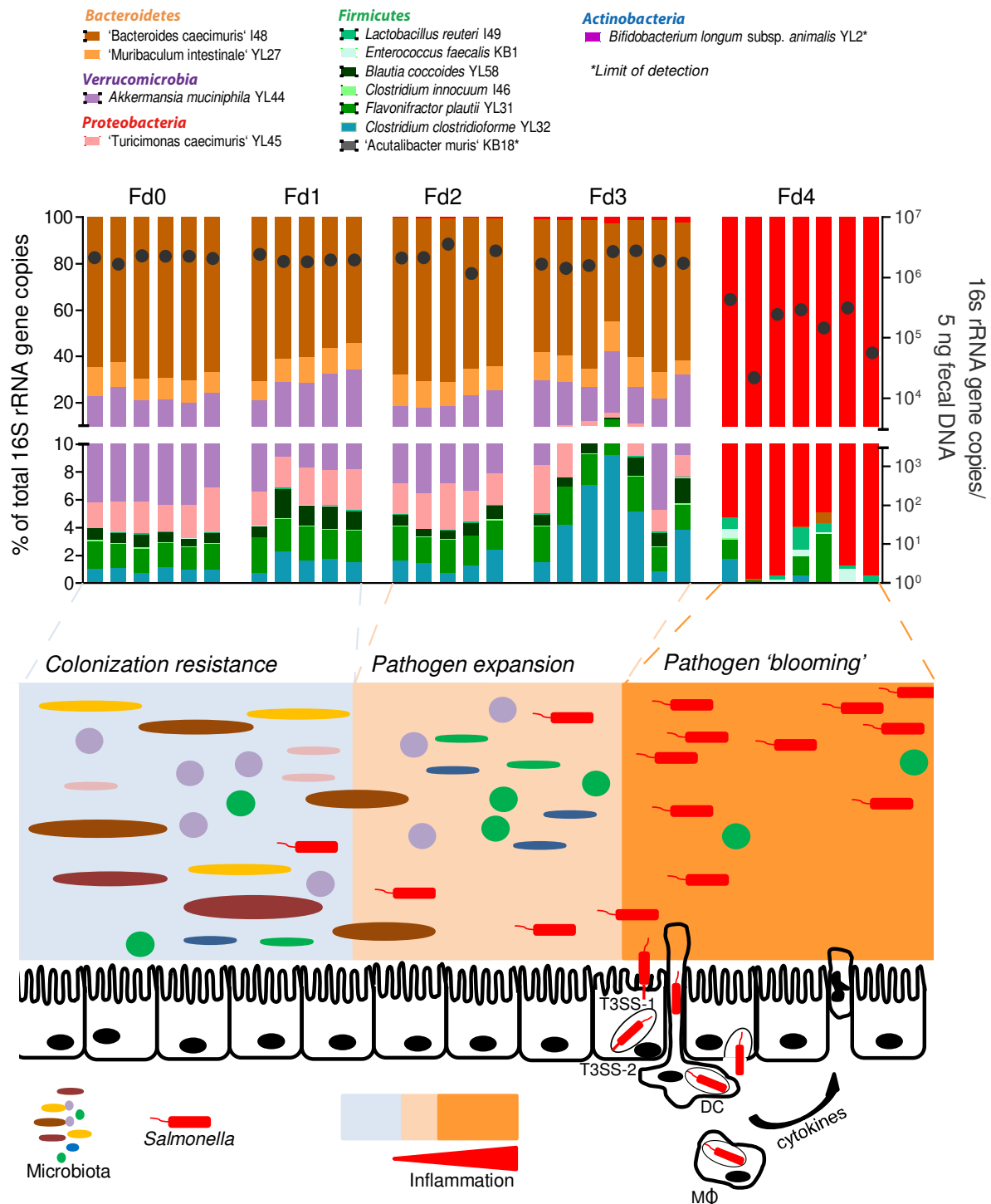
Here, mechanisms underlying *Salmonella*-induced 'blooming' and the impact of inflammation on individual commensal bacteria were investigated using the novel Oligo-MM¹² consortium. To our

Discussion

knowledge this is the first study that prioritizes the importance of anaerobic respiration, iron acquisition via siderophores and ethanolamine utilization by *S. Tm* during 'blooms' and concomitant dysbiosis using a defined gnotobiotic mouse model. Until now, it remains further elusive how infiltrating neutrophils, which might directly kill commensals and *S. Tm*, impact on the microbiota during *Salmonella*-induced colitis. Therefore, we compared the contribution of an altered nutritional environment of an inflammatory gut milieu and potential neutrophil-mediated killing of commensals to *Salmonella*-'blooms' and concomitant microbiota shifts. Furthermore, data how gut inflammation impacts on individual bacterial species are scarce. Here we performed detailed analyses how single Oligo-MM¹² commensals 'perform' during severe *Salmonella*-induced colitis and correlate survival with putative fitness genes of the commensals including sporulation, iron acquisition, anaerobic respiration and ethanolamine utilization.

We show that the Oligo-MM¹² serve as excellent tool to study this questions. *S. Tm* expands in Oligo-MM¹² mice and induces severe colitis accompanied by systemic infection and drastic microbiota shifts by days 3 - 4 p.i. without antibiotic pre-treatment (Figures 10; 11). Interestingly, the Oligo-MM¹² mediates CR during early stages of infection (day 1 p.i.). However, after 2 days, *S. Tm* can further expand and finally 'blooms' at day 4 p.i.. Because of this step-wise infection process, Oligo-MM¹² mice manifest as ideal model to mechanistically study different stages of pathogen-mediated ecosystem invasion (Figure 40). The Oligo-MM¹² is composed of defined murine isolates which guarantees long-term co-evolution between mouse commensals and the murine host. Other *Salmonella* colitis models rely on antibiotic pre-treatment prior to infection which breaks CR mediated by the microbiota (Barthel *et al.* 2003), are not well defined (Barman *et al.* 2008) or are based on a humanized microbiota (Ganesh *et al.* 2013). These model might be excellent for studying the impact of *Salmonella* infection on the host, however since the Oligo-MM¹² is not antibiotic pre-treated and well defined our model might be more suitable for studying microbe-pathogen and microbe-microbe interaction during *S. Tm* induced colitis.

Discussion



Discussion

4.2.1 Profiling the performance of Oligo-MM¹² strains in the presence of *Salmonella*-induced gut inflammation during ecosystem invasion

To our knowledge, this is the first study that shows the impact of gradual *Salmonella*-ecosystem invasion that is accompanied by inflammation on individual species of a normal gut microbiota using a gnotobiotic mouse model based on a highly defined consortium consisting of mouse-adapted bacterial strains.

Upon infection with *S. Tm*^{WT}, Oligo-MM¹² mice exhibited severe colitis at day 4 p.i.. Inflammation onset was already observed at day 3 p.i. (Figures 10; 11). Induction of colitis was dependent on functional Type 3 secretion systems (T3SS) because infection with an avirulent *Salmonella* strain *S. Tm*^{Avir} which is deficient in functional T3SS-1 and 2 failed to induce colitis in this model (Figures 10B; 11B). Although T3SS-1 and 2 synergistically contribute to inflammation and *Salmonella* 'bloating', T3SS-1 seems to be of major importance (Figures 15; 16; 17). This observation is in line with previous *S. Tm* infection experiments conducted with streptomycin pre-treated C57BL/6J mice (Hapfelmeier *et al.* 2005) and FvB mice (Barman *et al.* 2008). Exacerbating inflammation was categorized in 3 stages according to inflammation grade and cecal pathology: non-inflamed (no colitis, pathoscore: 0 - 3, uninfected - day 2 p.i.), intermediate (moderate colitis, pathoscore: 3 - 9; day 3 p.i.) and inflamed (profound colitis, pathoscore: > 9; day 4 p.i.) (Figure 10B). Cluster analyses revealed that the Oligo-MM¹² composition in feces and cecal content differed at all stages of infection with *S. Tm*^{WT} (Figures 12C,D; 13C,D).

S. Tm^{WT} started to expand at day 3 p.i. (Figure 10C; Tables 44; 46). Since no antibiotics were applied prior to infection, this pathogen expansion might be fueled by microbiota derived hydrogen as shown previously (Maier *et al.* 2013). This hypothesis could be investigated by infecting Oligo-MM¹² mice with *Salmonella* strains deficient in hydrogenases and additional monitoring of *S. Tm*^{WT} expansion at day 3 p.i. Co-infection experiments with a hydrogenase mutant *S. Tm* strain and *S. Tm*^{WT} could additionally be performed. Pathogen expansion was accompanied by increased cecal pathology (Figure 10B) and moderate changes in microbiota composition (Figures 10C; 12C,D; 13C,D). This change was characterized by decreased relative abundance of 'Bacteroides caecimuris' I48 as well as increased relative abundance of *Akkermansia muciniphila* YL44 and *Clostridium clostridioforme* YL32 (Tables 44; 46). One could hypothesize that reduced amounts of 'Bacteroides caecimuris' I48 could increase the accessibility to host mucus structures which might favor growth of *Akkermansia muciniphila* YL44 (Derrien *et al.* 2004).

Interestingly, *Akkermansia muciniphila* has been shown to further promote *Salmonella* pathology by affecting the mucosal barrier disturbing host-mucus homeostasis (Ganesh *et al.* 2013) which might

Discussion

be an additional early microbiota dependent mechanism (besides microbiota derived hydrogen) that primes *Salmonella* 'blooming'. Additional *S. Tm* infection experiments with Oligo-MM¹¹ mice lacking *Akkermansia muciniphila* YL44 could strengthen this hypothesis. Remarkably, compared to standard diet, HF diet and OA supplementation increased relative abundance of *Akkermansia muciniphila* YL44 whereas relative abundance of 'Bacteroides caecimuris' I48 was decreased (Figure 9). Therefore, these changes in nutrition might render to host more susceptible to *Salmonella* infection. This hypothesis is currently further investigated in the laboratory of Prof. Hardt (ETH, Zurich). The relative abundance of *Clostridium clostridioforme* YL32 in feces was also increased at day 3 p.i. with *S. Tm*^{WT} (Table 46). It could be demonstrated that a *Clostridium clostridioforme* strain was able to attach to and invade colonic epithelium cells which was followed by the induction of pro-inflammatory cytokines (Ohkusa *et al.* 2009). This induction of pro-inflammatory cytokines may further promote inflammation and thereby fuel *Salmonella* growth. This data suggest that during early stages of infection, *S. Tm* induces an inflammatory tone in the gut by favoring the growth of potentially colitogenic members of the indigenous microbiota. This increased inflammatory tone precedes pathogen 'blooming' and concomitant collateral damage of the microbiota.

At day 4 p.i. with *S. Tm*^{WT}, full blown colitis and *Salmonella* 'blooms' were apparent (Figure 10). Absolute abundance of *Salmonella* increased around 8,000 – 9,000 fold in feces and cecal content (Figure 14). *S. Tm*^{WT} dominated the microbiota during this late stage of infection (more than 96% of total bacteria in feces and cecal content) which correlated with severe dysbiosis and decreased abundance of bacteria in the gut measured as total 16S rRNA gene copy numbers (Figure 10; Table 44; 46). This decrease in overall bacteria upon *S. Tm* induced inflammation was also observed previously (Stecher *et al.* 2007). It has to be mentioned here, that the number of total bacteria was determined using an universal primer / probe combination targeting all Oligo-MM¹² strains and *Salmonella*. Besides bacterial DNA, DNA recovered from the inflamed gut contains variable fractions of eukaryotic DNA extracted from shed epithelial cells (Sellin *et al.* 2014) and infiltrating neutrophils (Loetscher *et al.* 2012). Eukaryotic DNA cannot be distinguished from bacterial DNA. Therefore, less bacterial template DNA is applied for the qPCR assay which might mistakenly lead to underestimation of bacterial 16S rRNA gene copy numbers. Nevertheless, individual members of the Oligo-MM¹² performed differently in the presence of *S. Tm*^{WT}-induced gut inflammation. Oligo-MM¹² strains were subsequently grouped in 3 categories, according to their increasing or decreasing abundance during *Salmonella*-induced colitis: depleted, intermediate and enriched (Figure 14). Especially absolute and relative abundance of Gram-negative strains belonging to the phyla Bacteroidetes, Proteobacteria and Verrucomicrobia: 'Bacteroides caecimuris' I48, 'Muribaculum intestinale' YL27, 'Turicimonas caecimuris' YL45 and *Akkermansia muciniphila* YL44 as well as of the Gram-variable Firmicute *Clostridium clostridioforme* YL32 were highly reduced during full blown

Discussion

S. Tm-induced colitis (Figure 14; Tables 44; 46). The strains that were assigned to the intermediate group: *Blautia coccoides* YL58, *Flavonifractor plautii* YL31 and *Clostridium innocuum* I46 belonged to the phylum Firmicutes and stained Gram-positive or Gram-variable. These strains could be more resistant to inflammation as relative and absolute abundance were less reduced during colitis (Figure 14; Tables 44; 46). Remarkably, absolute abundance of *Lactobacillus reuteri* I49 and *Enterococcus faecalis* KB1, both Gram-positive Firmicutes increased during *S. Tm*-induced gut inflammation (Figure 14). *Bifidobacterium longum* subsp. *animalis* YL2 and 'Acetivibrio muris' KB18 were below limit of detection of the respective qPCR assay even before onset of colitis. These strains might therefore be outcompeted by the residual Oligo-MM¹² strains under MvP housing conditions.

Interestingly, most observations are in line with previous studies based on streptomycin pre-treated mice, 129/SVJ mice, humanized C3H mice or FvB mice (Table 1) showing decreased abundance of *Bacteroides* spp., Verrucomicrobia (*Akkermansia muciniphila*), Firmicutes, *Barnesiella* spp. and *Clostridium* spp. as well as increased abundance of *Salmonella* and *Enterococcus* spp. (Stecher *et al.* 2007, Barman *et al.* 2008, Ganesh *et al.* 2013, Kaiser *et al.* 2013) during *Salmonella*-induced colitis. However, in contrast to studies based on streptomycin pre-treated C57BL/6J mice performing competition experiments with *Lactobacillus reuteri* (*L. reuteri* RR^{Rif}) and wildtype *Salmonella* (Stecher *et al.* 2007) and on FvB mice (Barman *et al.* 2008) which report decreased abundance of *Lactobacillus* spp. upon *Salmonella* infection, the Oligo-MM¹² strain *Lactobacillus reuteri* I49 increased during *S. Tm*-induced colitis.

Lactobacillus reuteri strains can exert immune modulatory properties which contribute to suppression of inflammation. Therefore, *L. reuteri* is used as probiotic for treating inflammatory diseases (Thomas *et al.* 2016). Our observation that *Lactobacillus reuteri* I49 expands during pathogen induced inflammation further supports the applicability of *L. reuteri* as probiotic strain during inflammatory disease since this bacterium seems to withstand harsh inflammatory conditions. However, how *Lactobacillus reuteri* I49 exactly impacts on *S. Tm*-induced gut inflammation needs to be assessed experimentally. In addition to the Oligo-MM¹², Oligo-MM¹¹ mice lacking *Lactobacillus reuteri* I49 should be infected with *S. Tm*^{WT} and pro-inflammatory cytokine and LCN-2 levels as well as colitis scores should be compared between groups. These experiments might reveal possible immune modulatory effects of this strain.

Enterococcus faecalis which, also seems to be adapted to inflammation, is on the one hand able to stimulate local mucosal immunity (Castro *et al.* 2016). On the other hand, *Enterococcus faecalis* is associated with disease, induction of pro-inflammatory cytokines (Diederich *et al.* 2016) and with the development of chronic intestinal inflammation which is accompanied by tissue damage caused by metalloprotease activity (Steck *et al.* 2011). Moreover, *Enterococcus faecalis* is able to form biofilms

Discussion

which might render this strain more resistant to inflammation (Fabretti *et al.* 2006). *Enterococcus faecalis* can also be an opportunistic pathogen (Pham *et al.* 2014). Upon enteric infection with *C. rodentium* of *Il22ra1^{tm1a/tm1a}* mice, commensal *Enterococcus faecalis* aggravated disease and caused systemic infection. This was dependent on fucosylation and on the diversity of anaerobic commensal symbionts that protected from *Enterococcus faecalis* out-growth, underlining the importance of a well-balanced microbiota which keeps opportunistic pathogens in check. Likewise, *Enterococcus faecalis* KB1 could also boost *Salmonella* pathology in the Oligo-MM¹² model. This hypothesis could be tested with *S. Tm* infection of Oligo-MM¹¹ mice lacking *Enterococcus faecalis*. Possible systemic *Enterococcus faecalis* levels as well as inflammation induced pathology should be compared between Oligo-MM¹² and Oligo-MM¹¹.

Blautia coccooides YL58, *Flavonifractor plautii* YL31 and *Clostridium innocuum* I46 didn't seem to benefit from severe colitis observed at day 4 p.i. with *S. Tm*^{WT} but decreased moderately in absolute and relative abundance. Interestingly, a previous study conducted by Tuovinen and colleagues showed that *Blautia coccooides* was able to induce TNF-alpha and IL-10 expression (Tuovinen *et al.* 2013), indicating both an inflammatory and anti-inflammatory potential of this strain. *Flavonifractor plautii* has been shown to be involved in conversion of catechins a flavonoid subclass which is (together with its metabolites) beneficial for healthy (Kutschera *et al.* 2011). *Clostridium innocuum* is resistant to bile acids and was associated with the microbiota of an chronically inflamed gut (Wohlgemuth *et al.* 2011). This indicates that *Blautia coccooides* YL58 and *Clostridium innocuum* I46 might contribute to inflammation.

Absolute and relative abundance of 'Bacteroides caecimuris' I48, 'Muribaculum intestinale' YL27, 'Turicimonas caecimuris' YL45, *Akkermansia muciniphila* YL44 and *Clostridium clostridioforme* YL32 decreased tremendously during full blown *Salmonella*-induced colitis. Since 'Bacteroides caecimuris' I48, 'Muribaculum intestinale' YL27 and 'Turicimonas caecimuris' YL45 are novel species, so far knowledge about these bacterial strains is scarce. However, Ubeda and co-workers identified a protective effect of species belonging to the *Barnesiella* genus against vancomycin resistant *Enterococcus* infection (Ubeda *et al.* 2013). Since 'Muribaculum intestinale' YL27 highly resembles *Barnesiella*, this Oligo-MM¹² strain might be engaged in suppressing enterococcal 'blooms' during homeostasis. Interestingly, *Akkermansia muciniphila* YL44 and *Clostridium clostridioforme* YL32 which might have prepared the way for *Salmonella*-ecosystem invasion on earlier time points of infection were massively reduced during severe colitis at day 4 p.i..

In contrast, a *Salmonella* strain lacking functional T3SS-1 and 2 (*S. Tm*^{Avir}) was unable to induce colitis and concomitant dysbiosis during the course of infection in Oligo-MM¹² mice (Figures 10; 11). This is in line with previous observations (Stecher *et al.* 2007). According to cluster analyses, there was no

Discussion

difference in overall Oligo-MM¹² composition in feces and cecal content at different days post infection with *S. Tm*^{Avir} (Figures 12A,B; 13A,B). However, there were minor but significant changes in relative abundance of *Akkermansia muciniphila* YL44 and 'Bacteroides caecimuris' I48 in feces and cecal content. Especially, *Akkermansia muciniphila* YL44 was increased in cecal content at day 3 p.i. with *S. Tm*^{Avir}, whereas relative abundance of 'Bacteroides caecimuris' I48 decreased (Tables 45; 47). This could be an effect mediated by the presence of *Salmonella* or could just simply be microbiota variations observed between different experiments since fluctuations in relative abundance of *Akkermansia muciniphila* YL44 and 'Bacteroides caecimuris' I48 were also observed in studies of Oligo-MM¹² stability over generations (Figure 7; Table 41).

4.2.2 Performance of Oligo-MM¹² strains in a colitic environment correlates with the presence fitness genes

We hypothesized that the performance of individual Oligo-MM¹² strains is dependent on certain fitness genes that were previously shown to enable survival or even provide *Salmonella* a benefit during colitis. Therefore, we mined annotated draft genomes of the Oligo-MM¹² strains (Table 52). The analysis focused on putative genes that encompass anaerobic respiration (nitrogen metabolism / nitrate, nitrite ammonification), ethanolamine utilization, iron acquisition and siderophore production. These factors are important for pathogen expansion in an inflammatory milieu (Raffatellu *et al.* 2009, Winter *et al.* 2010, Thiennimitr *et al.* 2011, Lopez *et al.* 2012) and might therefore also contribute to survival of certain gut commensals. The presence of dormancy and sporulation genes was also investigated.

Indeed, the performance of individual microbiota members in a colitic environment correlates with the presence of fitness genes, since Oligo-MM¹² strains which were depleted during colitis hardly harbor any of the above motioned putative fitness genes and strains that seemed to benefit from colitis are potentially able to acquire iron via siderophores, utilize ethanolamine and respire anaerobically (Tables 52; 53). Previous studies showing 'blooms' of Enterobacteriaceae and *Enterococcus* species during gut inflammation or antibiotic induced perturbation of the microbiota are in line with our data (Stecher *et al.* 2010, Ubeda *et al.* 2010, Taur *et al.* 2012). We further extend these studies by confirming the presence of putative fitness genes in commensal bacteria other than Enterobacteriaceae which were already shown to be able to perform nitrate respiration and utilize ethanolamine (Bertin *et al.* 2011, Rendon *et al.* 2015).

Moreover, we correlated the presence of sporulation genes with increased capability of resistance and therefore hypothesized that the potential of undergoing sporulation is an essential mechanism for the recovery from dysbiosis (resilience), since sporulation increases tolerance against stress such

Discussion

as heat and hydrogen peroxide (Moeller *et al.* 2012). We therefore investigated the potential of the Oligo-MM¹² to recover from *Salmonella*-induced dysbiosis using a *Salmonella* strain deficient in a functional T3SS-2 (*S. Tm*^{SPI-2}, Figure 18). In contrast to *S. Tm*^{WT}, *S. Tm*^{SPI-2} doesn't induce life threatening systemic infection (Endt *et al.* 2010). In addition, a previous experiment showed that in contrast to a *Salmonella* strain lacking functional T3SS-1 (*S. Tm*^{SPI-1}), *S. Tm*^{SPI-2} is able to induce dysbiosis (Figures 15; 17) and that *S. Tm*^{SPI-2} induced inflammation is milder compared to inflammation induced by *S. Tm*^{WT} (Figures 15B; 16B). Therefore, *S. Tm*^{SPI-2} was used for a long-term infection of Oligo-MM¹² mice. One has to mention that for unknown reasons LCN-2 levels were already elevated before infection with *S. Tm*^{SPI-2} in this long-term experiment. Elevated LCN-2 levels could be attributed to increased stress which mice might suffer during export from the isolator and handling before infection. However, this could not be confirmed by respective control experiments (data not shown). Nevertheless, *S. Tm*^{SPI-2} colonized Oligo-MM¹² mice and was not outcompeted by the microbiota until day 21 p.i. (Figure 19A). According to cluster analyses, the Oligo-MM¹² composition was changed at day 4 p.i. (Figure 18D,E). Differences were mainly characterized by increased relative abundance of *Salmonella* and *Akkermansia muciniphila* YL44 (Figure 18C). However, major shifts in β -diversity were not observed. The minor shift in microbial composition was reverted back to that before infection (resilience). Unfortunately, the Oligo-MM¹² shifts were only mild and the effect of spore forming and germination on resilience could not be further investigated using *S. Tm*^{SPI-2}. However, this experiment underlined the emergence of *Akkermansia muciniphila* YL44 in *Salmonella*-induced dysbiosis.

Next, we wanted to experimentally test that whether commensal bacteria profit from nitrate and iron limitation. Since we were not able to genetically modify any of the Oligo-MM¹² strains, we performed an *in vitro* batch cultures in rich anaerobic medium without mucin using Oligo-MM¹² bacteria recovered from cecal content. We simulated iron starvation during anti-microbial immune response by adding different concentrations of either dipyrpyridyl or diethylenetriaminepentaacetic acid (DTPA). Anaerobic batch cultures supplemented with 10 mM of nitrate were additionally performed. Interestingly, iron starvation mediated by the application of 300 μ M of dipyrpyridyl which binds Fe²⁺ promoted outgrowth of *Enterococcus faecalis* KB1 and inhibited the growth of the residual Oligo-MM¹² strains at time point 8h post inoculation. In the presence of 100 μ M of DTPA which sequesters Fe³⁺, *Enterococcus faecalis* KB1 growth was also promoted and additionally *Clostridium innocuum* I46 and 'Turicimonas caecimuris' YL45 were more abundant under this condition. In contrast to iron starvation, additional nitrate had no obvious effect on the Oligo-MM¹² composition after 8h (data shown in MD thesis of Patrick Schiller), indicating that the Oligo-MM¹² strains might be unable to respire nitrate during *Salmonella*-induced colitis. However, iron limitation might confer an additional fitness advantage especially to *Enterococcus faecalis* KB1 (likewise *Salmonella*) over the residual

Discussion

microbiota. The importance of ethanolamine utilization and anaerobic tetrathionate respiration were not yet investigated using *in vitro* cultures.

4.2.3 Investigating the contribution of anaerobic respiration, ethanolamine utilization and iron acquisition via siderophores to *Salmonella* 'bloating' and concomitant dysbiosis

In order to investigate and to prioritize the effects of iron acquisition via siderophores, nitrate and tetrathionate respiration as well as ethanolamine utilization on *Salmonella* 'blooms' and concomitant dysbiosis, single infections of Oligo-MM¹² mice with either *S. Tm*^{WT}, *S. Tm*^{EntA}, *S. Tm*^{Ni. + Te.}, *S. Tm*^{Ni.} or *S. Tm*^{EA} were performed (Figure 24). To our knowledge, this is the first study that investigates the contribution of nutritional factors present in an inflammatory milieu to pathogen outgrowth and displacement of the indigenous microbiota during early *Salmonella* expansion phase and later pathogen 'blooming' using one defined gnotobiotic mouse model with mouse adapted strains. Interestingly, none of the *Salmonella* mutant strains induced dysbiosis at day 3 p.i., whereas *S. Tm*^{WT} already dominated 29% of the samples ($\geq 50\%$ of total microbiota composition, Figure 24C). This indicates that during early time points of infection anaerobic respiration, ethanolamine utilization and iron acquisition via siderophores synergistically contribute to early *Salmonella* 'blooming'. Especially, ethanolamine might be important for early gut colonization since *S. Tm*^{EA} shows less CFUs at day 3 p.i. in feces compared to *S. Tm*^{WT} (Figure 25A). However, at day 4 p.i., nitrate and tetrathionate additively contribute the most to *Salmonella* blooms and concomitant dysbiosis. Ethanolamine utilization is also important during late stages of infection. However, iron acquisition via siderophores seems to be negligible for the induction of dysbiosis in this model (Figure 24D,E; Tables 50; 51). To this end, the importance of nutritional factors during severe *Salmonella*-induced colitis can be ranked as follows: nitrate and tetrathionate respiration > ethanolamine utilization > iron acquisition via siderophores.

Ethanolamine is generated by breaking down phosphatidylethanolamine which is part of the mammalian as well as the bacterial cell membrane engaging phosphodiesterases (Proulx and Fung 1969, Randle *et al.* 1969, Ansell *et al.* 1973, Larson *et al.* 1983). Thus, ethanolamine is an abundant nutrient in the gut that can serve as carbon and nitrogen source (Roof and Roth 1988). However, ethanolamine utilization is quite costly, since a micro-compartment containing toxic by-products and enzymes needed for ethanolamine utilization such as ethanolamine ammonia lyase encoded by *eutBC* (big and small subunits) which converts ethanolamine into acetaldehyde and ammonia (nitrogen source) in the presence of cobalamin, alcohol dehydrogenase encoded by *eutG* which converts acetaldehyde to ethanol (carbon source) or aldehyde oxidoreductase encoded by *eutE* which converts acetaldehyde to acetyl-CoA (Krebs cycle) is established (Roof and Roth 1988, Roof and Roth 1989, Stojiljkovic *et al.* 1995, Garsin 2010). Thus, we believe that ethanolamine utilization is

Discussion

only available for a subset of gut bacteria. Previous investigations showed the presence of genes needed for ethanolamine utilization in Actinobacteria spp., Proteobacteria, Enterobacteriaceae and Firmicutes like *Enterococcus faecalis* (Del Papa and Perego 2008, Fox *et al.* 2009, Tsoy *et al.* 2009), which is in line with our observation that *Enterococcus faecalis* KB1 and *Flavonifractor plautii* YL31 are the only Oligo-MM¹² strains which harbor genes for ethanolamine utilization (Tables 52; 53). Thus, this nutrient might selectively be consumed by *Salmonella* and possibly also by *Enterococcus faecalis* KB1 and *Flavonifractor plautii* YL31 during pathogen expansion when inflammation is not yet full blown and anaerobic electron acceptors might not yet be available. Interestingly, compared to *S. Tm*^{WT}, the relative abundance of *Clostridium clostridioforme* YL32 was increased in cecal content after infection with *S. Tm*^{EA} (Table 51). This observation is interesting, since relative abundance of *Clostridium clostridioforme* YL32 was also elevated at day 3 p.i. with *S. Tm*^{WT} (Table 46). *Clostridium clostridioforme* YL32 might benefit from ethanolamine during pathogen expansion and during late stages of infection with *S. Tm*^{EA} since unconsumed ethanolamine might still be available. However, we could not find putative functional genes for ethanolamine utilization by RAST automated genome annotation. An Additional *in vitro* culture assay could provide further evidence whether *Clostridium clostridioforme* YL32 is able to use ethanolamine.

As a consequence of the antimicrobial immune response during *Salmonella*-induced colitis, nitrate and tetrathionate become available (Levitt *et al.* 1999, Furne *et al.* 2001, Szabó *et al.* 2007, Winter *et al.* 2010, Winter *et al.* 2013) and now further promote pathogen ‘blooming’ and dysbiosis at late stages of infection. The contribution of both anaerobic electron acceptors to *Salmonella*-induced disease was so important that a *Salmonella* strain lacking nitrate and tetrathionate respiration exhibited less cecal pathology compared to wildtype (Figure 25B).

Iron is an essential micronutrient and important for replication of pathogens. Thus, the iron availability is tightly regulated by the host and free iron is scarce because it is bound to heme, or iron binding proteins such as transferrin, ferritin and lactoferrin (Birgegård and Caro 1984, Andrews 2000, Diaz-Ochoa *et al.* 2014). Therefore, bacteria evolved siderophores which have a high affinity to ferric iron (Fe³⁺) sequestering iron from host iron binding proteins (Neilands 1995, Griffiths 1999). Upon infection, the host can additionally limit iron availability by up regulation of the iron regulating hormone hepcidin which inactivates the iron exporter ferroportin and by secretion of the siderophore sequestering antimicrobial protein LCN-2 (Goetz *et al.* 2002, Flo *et al.* 2004, Nemeth *et al.* 2004, Armitage *et al.* 2011, Correnti and Strong 2012). In this study we investigated the contribution of siderophore production on *Salmonella* ‘blooming’ and the induction of dysbiosis. Interestingly, impaired acquisition of ferric iron via siderophores (enterochelin and salmochelin which is resistant to LCN-2 sequestration (Raffatellu *et al.* 2009)) did not obviously contribute to

Discussion

Salmonella 'blooms' and dysbiosis (Figures 24; 26). However, other iron uptake mechanisms might be important. Thus, Bacteria could directly uptake ferrous iron (Fe^{2+}) via Feo proteins. This mechanism might be important during early *Salmonella* ecosystem invasion when oxygenation is low and unbound iron can be found in contrast to the inflamed gut (Andrews *et al.* 2003, Diaz-Ochoa *et al.* 2014). In addition, since *Salmonella*-induced colitis coincides with tissue damage (Figure 25B), *Salmonella* might also acquire iron from heme (Braun and Hantke 2011).

It also needs to be mentioned here that in this set of experiment *S. Tm*^{WT} failed to dominate the microbiota in 2 out of 8 samples (Figure 24D,E) which is in contrast to previous experiments where *S. Tm*^{WT} was the dominating species in 100% of the samples (Figure 10C). Possible reasons for this effect could be that the Oligo-MM¹² strains somehow evolved to a consortium that provides enhanced CR against *S. Tm*^{WT} infection or mice diversified despite germfree housing by accumulating environmental bacteria which might contribute to this increased CR. 16S rRNA gene amplicon sequencing using broad-range primers could give a hint for the presence of possible contaminants in the Oligo-MM¹² consortium. New bacterial strains might be discovered which can protect from *Salmonella*-induced dysbiosis.

4.2.4 'Nutrient-' versus 'killing-hypothesis', the role of infiltrating neutrophils for *Salmonella* 'blooming' and dysbiosis

So far, it is not understood whether pathogen-induced dysbiosis is caused indirectly by commensals being outcompeted by a pathogen which profits from the nutritional environment of an inflammatory milieu ('nutrient-hypothesis') or directly by host immune response mediated killing ('killing-hypothesis').

Neutrophil infiltration in the inflamed gut lumen is a hallmark of *Salmonella*-induced colitis (Loetscher *et al.* 2012). It was hypothesized that neutrophils directly mediate killing of commensal gut microbes and thereby promote *Salmonella* 'blooming' and dysbiosis. In order to investigate this, neutrophils of Oligo-MM¹² mice were directly depleted using antibodies against a neutrophil epitope (α -Ly6G) as well as antibodies against granulocyte-colony stimulating factor (α -G-CSF) (Trautwein-Weidner *et al.* 2014) and additionally infected with *S. Tm*^{WT} (Figure 29A). It was quite surprising that the control mice exhibited by trend less LCN-2 levels compared to neutrophil-depleted mice. However, LCN-2 levels were elevated in both groups (Figure 29B). *Salmonella* loads in spleen and liver were increased by trend after antibody mediated depletion of neutrophils and also after *S. Tm*^{WT} infection of streptomycin pre-treated CD18^{-/-} mice which are deficient in extravasation of neutrophils (Figures 30C,D; 31D,E). There were significantly higher *Salmonella* loads in mesenteric lymphnodes after antibody mediated depletion of neutrophils and *S. Tm*^{WT} additionally better colonized the guts

Discussion

of streptomycin pre-treated CD18^{-/-} mice (Figures 30B; 31A). The protective effect conferred by neutrophils is in line with a study previously conducted by Maier and co-workers which shows that neutrophils impose a tight bottle neck on *Salmonella* by NADPH-oxidase mediated killing of invading *Salmonella* (Maier *et al.* 2014).

Interestingly, none of the microbiota samples from the isotype control group was dominated by *Salmonella*, whereas *Salmonella* 'blooming' was apparent in 4 out of 6 samples in neutrophil depleted Oligo-MM¹² mice (Figure 29C). This indicates that, at least in this experimental setting, neutrophil depletion did not protect from *Salmonella*-induced dysbiosis and 'blooms'. This is in stark contrast to our assumption that neutrophils might pave the way for *Salmonella* by directly killing other commensals or facilitating the production of anaerobic electron acceptors. To our knowledge, this study provides first evidence that neutrophils protect commensal gut microbes from pathogen 'blooming' and dysbiosis and other mechanisms such as the altered nutritional environment or possible also increased oxygenation (Rivera-Chávez *et al.* 2016) are more important. This data strengthen the 'nutrient-hypothesis' rather than the 'killing-hypothesis'.

However, the absence of *Salmonella* 'blooms' and dysbiosis in isotype control (Figure 29C) mice was unexpected and in stark contrast to previous experiments where *Salmonella* dominated the microbiota (Figure 10C). Interestingly, such *Salmonella* 'blooms' were already absent in some mice infected with *S. Tm*^{WT} that served as controls for infection experiment with *Salmonella* mutant strains (Figure 24D,E). As consequence, we are setting up new Oligo-MM¹² mice and are planning to repeat the neutrophil depletion experiment using this new Oligo-MM¹² generation. Nevertheless, these experiments demonstrate that upon depletion of neutrophils a microbiota loses its ability to protect from *Salmonella* 'blooms' and concomitant dysbiosis. In other words, *Salmonella* 'bloating' and concomitant shifts in microbial composition might not be mediated by neutrophil-mediated killing of competing gut commensals. In fact, *Salmonella* benefits even more from an inflammatory milieu by selectively using anaerobic electron acceptors as well as ethanolamine and thereby outcompetes the indigenous microbiota during colitis (Figure 41).

Discussion

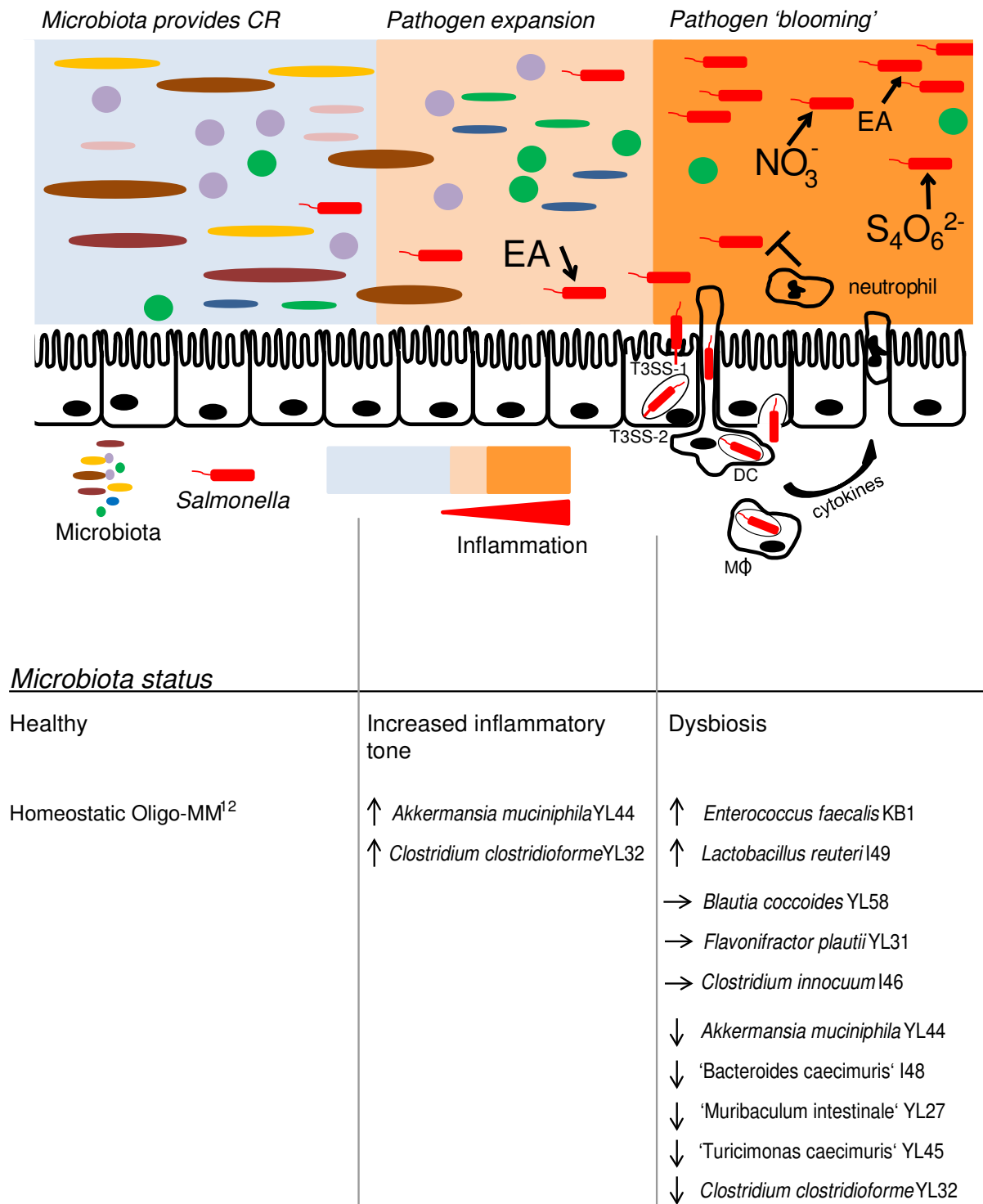


Figure 41: Performance of single Oligo-MM¹² strains during *S. Tm* induced colitis as well as known mechanisms underlining *S. Tm* 'blooms' and dysbiosis. A homeostatic Oligo-MM¹² provides colonization resistance (CR) against *S. Tm* until day 1 p.i.. However, *S. Tm* already starts to expand at day 2 p.i. which increases the inflammatory tone at day 3 p.i.. This increased inflammatory tone coincides with increased relative abundance of *Akkermansia muciniphila* YL44 and *Clostridium clostridioforme* YL32. During pathogen expansion *S. Tm* might especially benefit from ethanolamine (EA) utilization. At later stages of infection (day 4 p.i.), *S. Tm* induces severe gut inflammation and 'blooms'. This was mainly powered by nitrate (NO_3^-) and tetrathionate ($\text{S}_4\text{O}_6^{2-}$) respiration as well as EA utilization. Interestingly, infiltrating neutrophils counteract *Salmonella* 'blooming' and seem to protect the microbiota from dysbiosis. When neutrophils fail to keep *S. Tm* in check, *Salmonella* 'blooming' and dysbiosis is apparent during late stages of infection. *S. Tm* induced dysbiosis of the Oligo-MM¹² is characterized by an increased relative abundance of *Enterococcus faecalis* KB1

Discussion

and *Lactobacillus reuteri* I49; stable or moderately decreased relative abundance of *Blautia coccoides* YL58, *Flavonifractor plautii* YL31 and *Clostridium innocuum* I46 as well as massively decreased relative abundance of 'Bacteroides caecimuris' I48, 'Muribaculum intestinale' YL27, 'Turicimonas caecimuris' YL45, *Akkermansia muciniphila* YL44 and *Clostridium clostridioforme* YL32. *Bifidobacterium longum* subsp. *animalis* YL2 and 'Acutalibacter muris' KB18 were already below the limit of detection of the specific qPCR assay in healthy Oligo-MM¹².

4.3 Parallels between dysbiosis induced by enteric pathogens and chronic gut inflammation

In this thesis, dysbiosis induced by infections with *S. Tm*, *C. rodentium* and *C. difficile* was compared to colitis induced by infection with *H. typhlonius* in a colitogenic CD45RB^{hi} T-cell transfer model using the Oligo-MM¹² as model for all experiments. These sets of experiments were conducted in collaboration with Prof. Hapfelmeier and Nicolas Studer (University of Bern) who performed infection experiments with *C. difficile* (Studer *et al.* 2016) as well as Prof. Mueller and Martin Faderl (University of Bern) who established the T-cell dependent colitis model that is based on the Oligo-MM¹² (Brasseit *et al.* 2016).

S. Tm and *C. difficile* were able to thrive in the inflamed gut and induced dysbiosis which was mainly characterized by decreased abundance of Gram-negative bacteria like 'Bacteroides caecimuris' I48 and 'Muribaculum intestinale' YL27. Interestingly, the expansion of *Enterococcus faecalis* KB1 and *Lactobacillus reuteri* I49 was observed after infection with both enteric pathogens (Figure 39A). The inflammatory milieu created by infection with *S. Tm* and *C. difficile* might enhance growth of these Oligo-MM¹² strains. *Enterococcus faecalis* was previously shown to harbor genes for ethanolamine utilization (Del Papa and Perego 2008) and might additionally acquire iron (Table 52). Besides *Enterococcus faecalis* KB1, *Lactobacillus reuteri* I49 might also withstand increased oxygenation during inflammation (Ianniello *et al.* 2015, Rivera-Chávez *et al.* 2016). Our data additionally suggest that *Lactobacillus reuteri* I49 might profit from nitrate respiration (Table 52). Inflammation induced by *S. Tm* and *C. difficile* coincided with reduced absolute abundance of total 16S rRNA gene copy numbers, indicating decreased abundance of gut microbes possibly mediated by outcompeting of commensals by the pathogens as observed previously (Stecher *et al.* 2007). Interestingly, infection with *C. difficile* led to increased relative abundance of *Akkermansia muciniphila* YL44 at day 3 p.i. which has been also observed at day 3 p.i. with *S. Tm* (Figures 10C; 35A; Table 46). *Akkermansia muciniphila* was previously shown to aggravate *Salmonella* infection by interfering with the mucus barrier and might benefit from mucin which might be more accessible during inflammation (Derrien *et al.* 2004, Ganesh *et al.* 2013).

Discussion

Shifts in microbiota composition after *C. difficile* infection are in line with studies based on microbiota samples from human patient which observed increased abundance of Verrucomicrobia, *Lactobacillus* spp. and *Enterococcus* spp. as well as decreased abundance of *Bacteroides* spp. (Table 1) (Manges *et al.* 2010, Seekatz and Young 2014), underlining the translational potential of Oligo-MM¹² derived data. Pathogenesis and out-growth of *C. difficile* in Oligo-MM¹² mice might depend on bile acid metabolism, since secondary bile acids were able to inhibit spore germination (Theriot *et al.* 2016). An unpublished investigation conducted by Studer and co-workers showed that mice colonized with Oligo-MM¹² almost completely lack secondary bile acids. By adding *Clostridium scindens*, a secondary bile acid producer, to the Oligo-MM¹² consortium, concentrations of secondary bile acids increased which paralleled with increased resistance against *C. difficile* induced disease (Studer *et al.* 2016). This in line with a previous study showing the protective effect of *C. scindens* by secondary bile acid production (Buffie *et al.* 2015).

H. typhlonius infection of Rag^{-/-} mice, associated with the Oligo-MM¹², together with transfer of colitogenic CD45RB^{hi} T-cells induced inflammation (Figure 37; 38A). Remission of colitis was additionally mediated by the application of α -CD4 antibodies targeting colitogenic T-cells (Figure 36). However, colitis only induced slight shifts in Oligo-MM¹² composition and the absolute abundance of gut bacteria was unchanged (Figure 38A). Especially, relative abundance of *Clostridium innocuum* I46 and *Enterococcus faecalis* KB1 was increased after T-cell-induced colitis (Figure 38A; Table 55). Increased abundance of *Clostridium innocuum* I46 was also observed after infection with *C. difficile* (Figure 35A). *Clostridium innocuum* I46 which has been previously shown to be associated with an inflamed gut (Wohlgemuth *et al.* 2011) was additionally more resistant to *S. Tm* induced colitis and might play a central role in the pathogenesis of *C. difficile*, *Salmonella* and CD45RB^{hi} T-cell-induced colitis by enhancing the inflammatory tone in the gut. Infection experiments with Oligo-MM¹¹ mice without *Clostridium innocuum* I46 might shed more light on the importance of this commensal for pathogenesis. Spore formation might be a mechanism for sustained viability of *Clostridium innocuum* I46 during inflammation (Table 52). Microbiota changes during IBD have been characterized by decreased abundance of butyrate producing bacteria (Table 1) (Rajilic-Stojanovic *et al.* 2013, Takahashi *et al.* 2016). It might therefore be interesting to measure concentrations of short chain fatty (SCFA) like butyrate after onset of colitis in Oligo-MM¹² mice. Decreased butyrate concentrations might lead to increased epithelial oxygenation (Rivera-Chávez *et al.* 2016) and favor not only pathogen growth but might also sustain expansion of aerotolerant commensals and inhibit obligate anaerobes. Therefore, aerotolerant Oligo-MM¹² strains need to be identified and correlated with concentrations of butyrate during colitis and depletion in *S. Tm*-induced colitis. So far, aerobic batch cultures revealed that especially *Enterococcus faecalis* KB1 is able to grow in the presence of oxygen and outcompetes the residual Oligo-MM¹² strains (data shown in MD thesis of Patrick

Discussion

Schiller). The determination of SCFA concentrations might be also relevant in mice infected with other enteric pathogens.

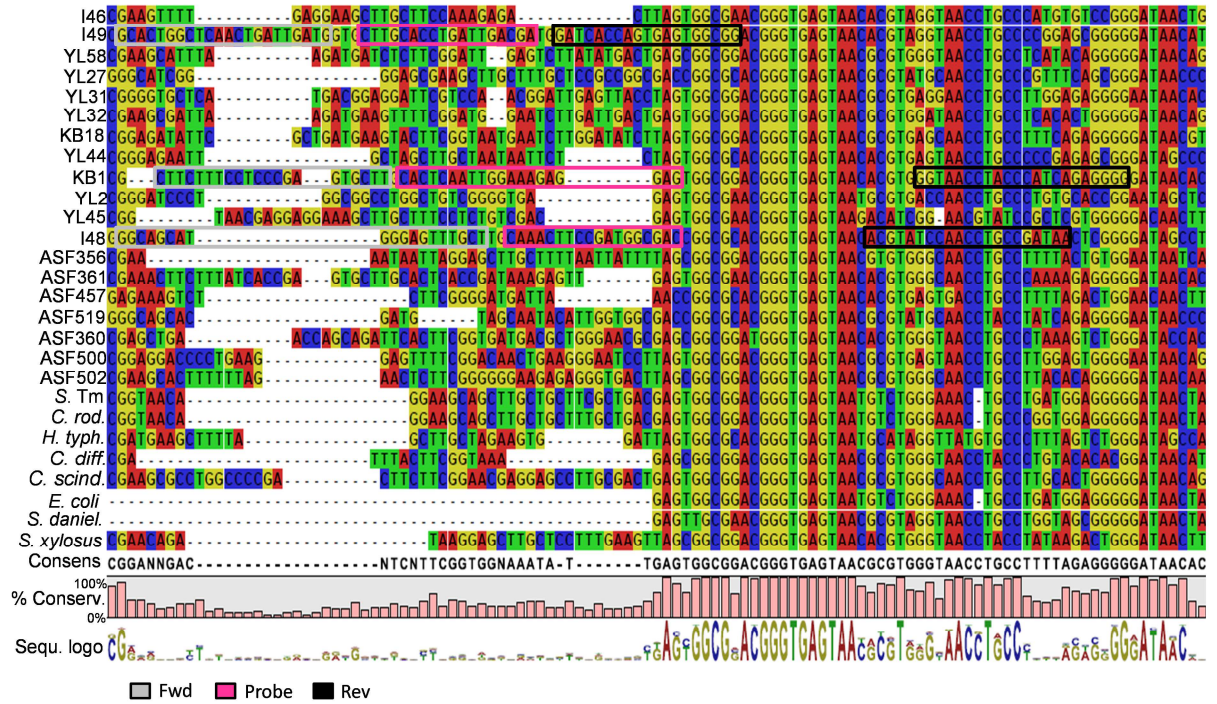
Infection of Oligo-MM¹² mice with *C. rodentium* did not induce shifts in microbial composition, despite, *C. rodentium* infection induced inflammation, measured by LCN-2 levels (4 times less as after infection with *S. Tm*) between days 7 and 23 p.i. (Figure 32). LCN-2 levels declined after 23 days p.i. and *C. rodentium* was not outcompeted by the Oligo-MM¹². It seems that *C. rodentium* can be controlled by the Oligo-MM¹² and possibly also by the immune response. Indeed, the microbiota has been previously shown to clear *C. rodentium* (Kamada *et al.* 2012). In this study *C. rodentium* was cleared in mice associated with a normal SPF microbiota by 21 p.i., whereas infection persisted in germfree mice. In addition, secretory IgA might be also involved in keeping *C. rodentium* in check (Endt *et al.* 2010). It would be interesting to investigate if single Oligo-MM¹² strains alone or special consortia contribute to CR against *C. rodentium*. Moreover, it could be assessed whether CR is mediated by direct microbiota-pathogen interactions or indirectly by competition for nutrients or secretion of antimicrobial substances. According to Vong and colleagues, *Lactobacilli* confer protection against *C. rodentium* (Vong *et al.* 2015). Thus, *Lactobacillus reuteri* I49 might be involved in providing CR against this enteric pathogen. *C. rodentium* induces EPEC like pathology in mice (Luperchio and Schauer 2001). However, since dysbiosis was not observed, correlations of *C. rodentium* / EPEC gut ecosystem invasion and microbiota shifts could not be performed.

Collectively, this data suggest that key species among the Oligo-MM¹² are positively or negatively correlated with inflammation caused by infection with different enteric pathogens and CD45RB^{hi} T-cell-induced colitis. Especially, 'Bacteroides caecimuris' I48 and 'Muribaculum intestinale' YL27, both belonging to the phylum Bacteroidetes, decreased during *S. Tm* and *C. difficile*-induced inflammation. In contrast, *Enterococcus faecalis* KB1 and *Lactobacillus reuteri* I49 benefited from colitis in all colitis models. Moreover, *Akkermansia muciniphila* YL44 expanded after early infection with *S. Tm* and infection with *C. difficile*. Relative abundance of *Clostridium innocuum* I46 was additionally increased after infection with *C. difficile* or T-cell-induced colitis. This increased abundance of key species might serve as future biomarker for inflammatory diseases. Furthermore, anti-inflammatory commensals can be explored and extended to potential therapeutics. Further investigations are needed if and how these increased key species impact on pathogenesis of enteric pathogens and chronic gut inflammation.

5. Appendix

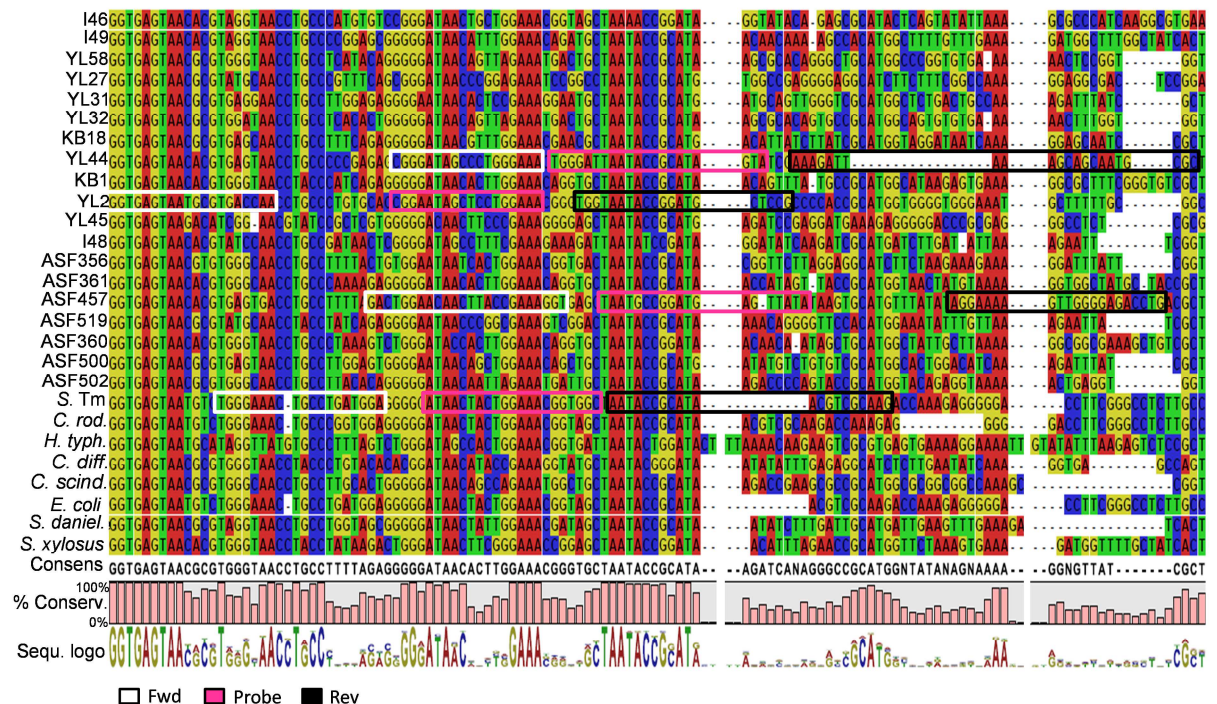
A

V1



B

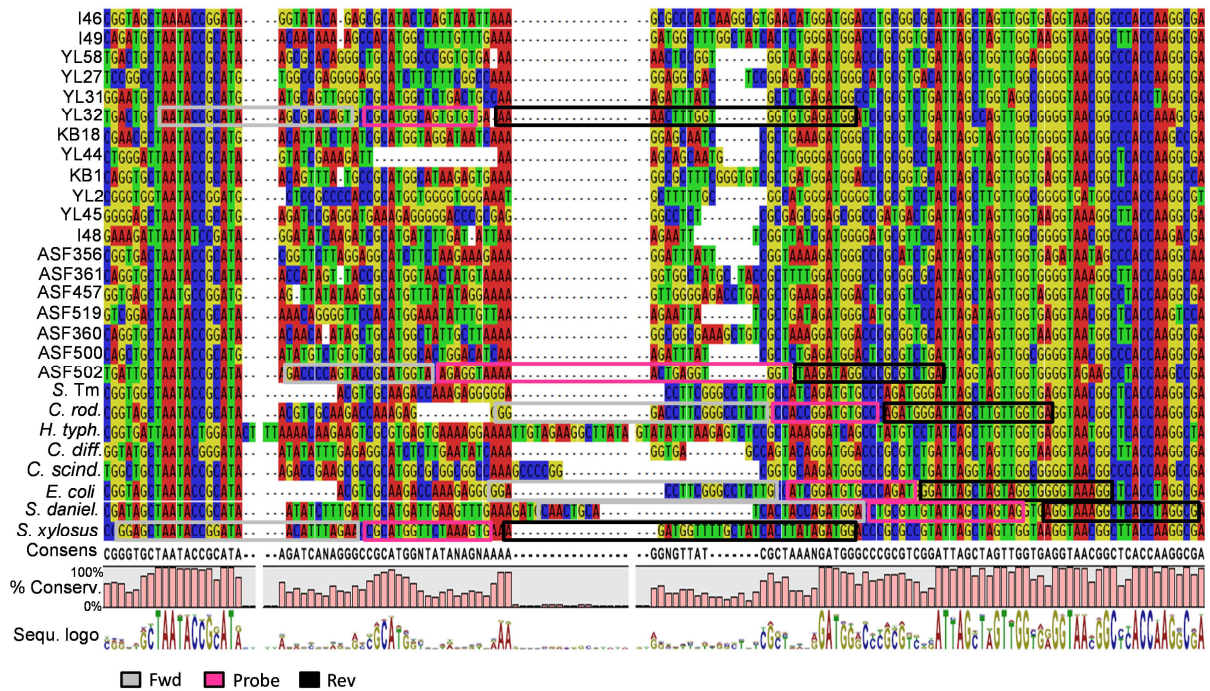
V2



Appendix

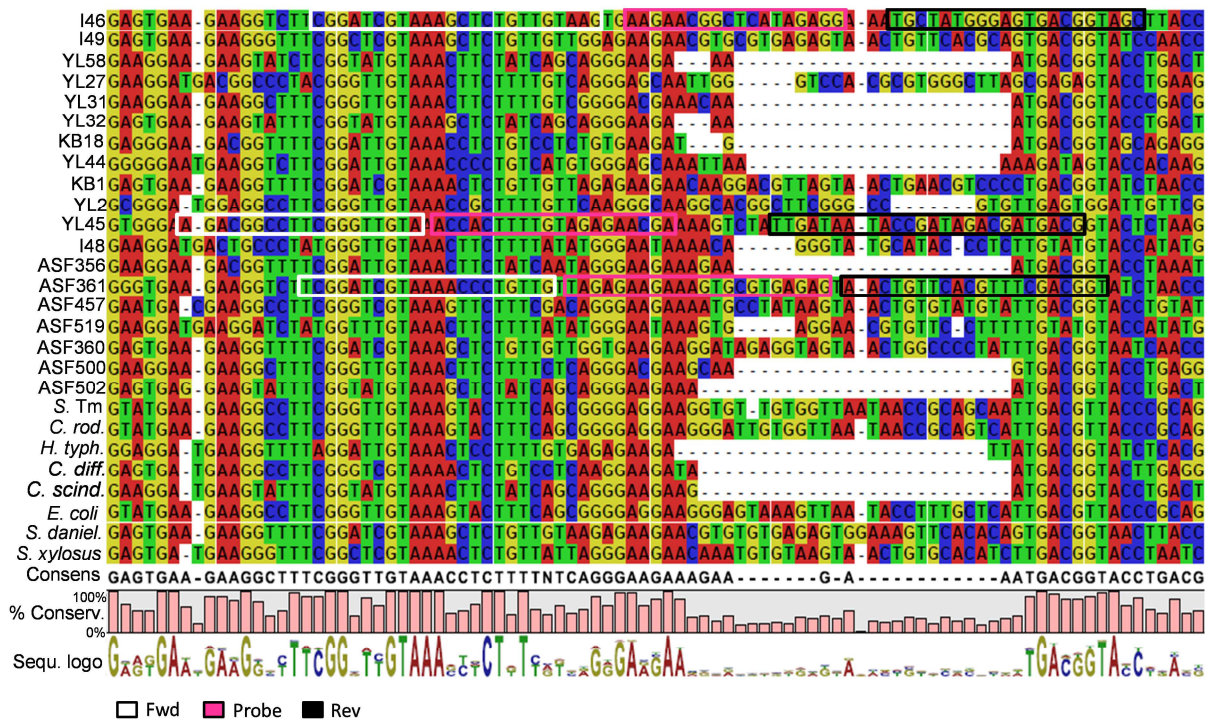
C

V2



D

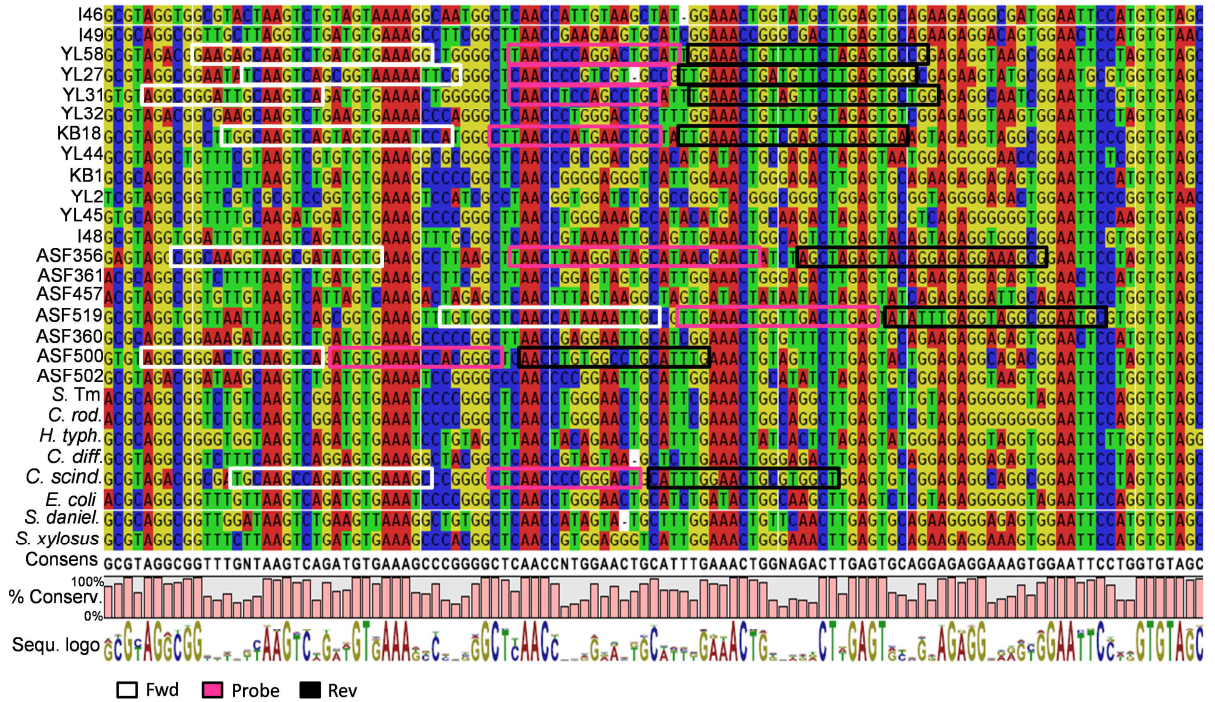
V3



Appendix

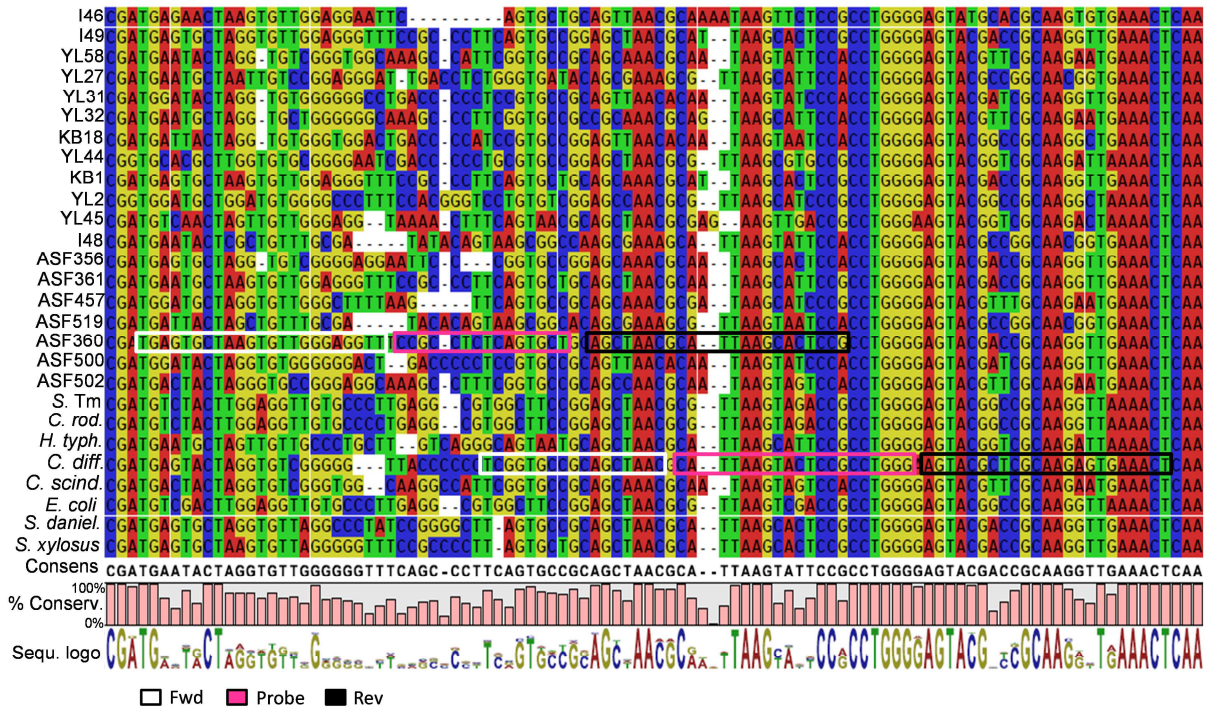
E

V4



F

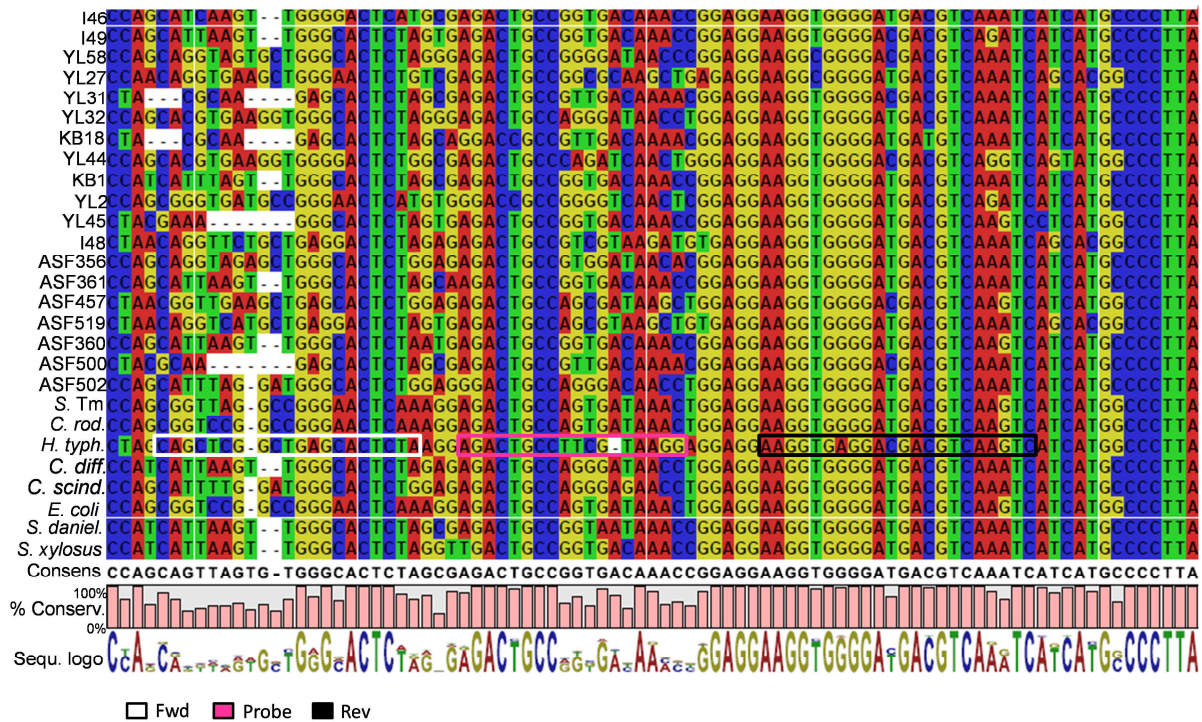
V5



Appendix

G

V7



H

V7

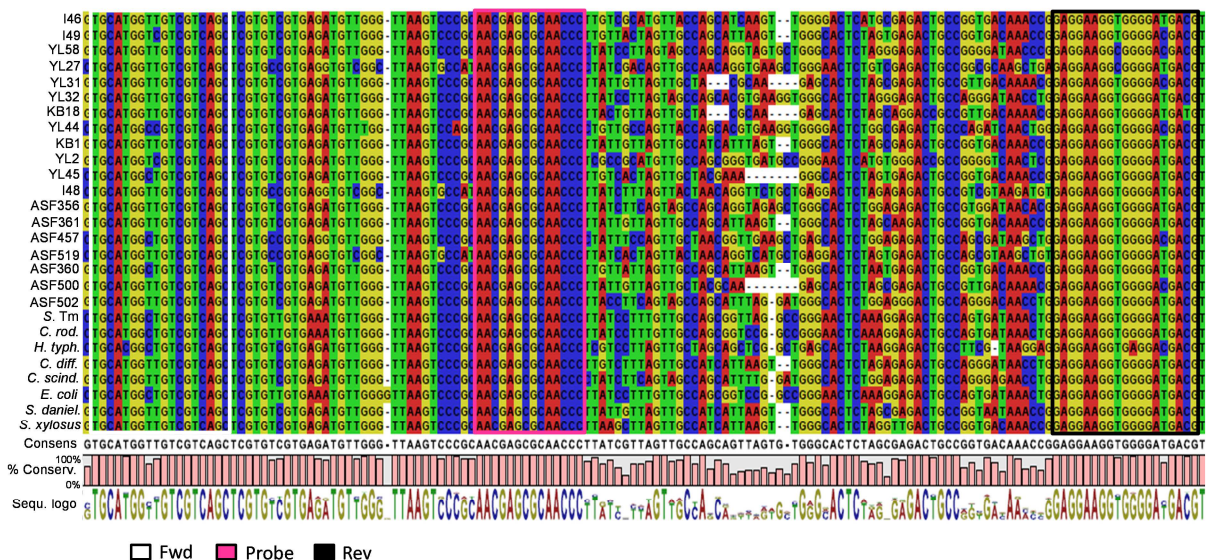


Figure 42: Strain-specific primer and hydrolysis probes targeting hypervariable regions of the 16S rRNA gene. 27 16S rRNA gene sequences were aligned using the software CLC DNA Workbench 6.0.2 (CLC bio, Denmark) and hypervariable (V) regions were identified according to (Chakravorty *et al.* 2007). (A) V1 nucleotides: 69 – 99, (B) and (C) V2 nucleotides: 137 – 242, (D) V3 nucleotides: 433 – 497, (E) V4 nucleotides: 576 – 682, (F) V5 nucleotides: 822 – 879, (G) V7 nucleotides: 1117 – 1173, (H) homologous regions around V7. Primers and hydrolysis probes were designed to match strain-specific sequences with high variability and low consensus

Appendix

between strains. For designing the universal primer / probe combination, a region with maximum homology was chosen. The binding sites of forward and reverse primers are marked in gray or white and black, respectively. The binding site of the hydrolysis probes is highlighted in pink.

Literature

Agus, A., J. Denizot, J. Thévenot, M. Martinez-Medina, S. Massier, P. Sauvanet, A. Bernalier-Donadille, S. Denis, P. Hofman and R. Bonnet (2016). "Western diet induces a shift in microbiota composition enhancing susceptibility to Adherent-Invasive E. coli infection and intestinal inflammation." Scientific reports **6**.

Aitken, S. L., M. J. Alam, M. Khaleduzzuman, S. T. Walk, W. L. Musick, V. P. Pham, J. L. Christensen, R. L. Atmar, Y. Xie and K. W. Garey (2015). "In the endemic setting, Clostridium difficile ribotype 027 is virulent but not hypervirulent." Infection Control & Hospital Epidemiology **36**(11): 1318-1323.

Ananthakrishnan, A. N. (2011). "Clostridium difficile infection: epidemiology, risk factors and management." Nature Reviews Gastroenterology and Hepatology **8**(1): 17-26.

Andrews, N. C. (2000). "Iron homeostasis: insights from genetics and animal models." Nature Reviews Genetics **1**(3): 208-217.

Andrews, S. C., A. K. Robinson and F. Rodríguez-Quinones (2003). "Bacterial iron homeostasis." FEMS microbiology reviews **27**(2-3): 215-237.

Andriantsoanirina, V., S. Allano, M. J. Butel and J. Aires (2013). "Tolerance of Bifidobacterium human isolates to bile, acid and oxygen." Anaerobe **21**: 39-42.

Ansell, G. B., J. N. Hawthorne and R. M. C. Dawson (1973). Form and function of phospholipids, Elsevier Scientific Publishing Co.

Antharam, V. C., E. C. Li, A. Ishmael, A. Sharma, V. Mai, K. H. Rand and G. P. Wang (2013). "Intestinal dysbiosis and depletion of butyrogenic bacteria in Clostridium difficile infection and nosocomial diarrhea." Journal of clinical microbiology **51**(9): 2884-2892.

Armitage, A. E., L. A. Eddowes, U. Gileadi, S. Cole, N. Spottiswoode, T. A. Selvakumar, L.-P. Ho, A. R. Townsend and H. Drakesmith (2011). "Hepcidin regulation by innate immune and infectious stimuli." Blood **118**(15): 4129-4139.

Armougom, F., M. Henry, B. Vialettes, D. Raccach and D. Raoult (2009). "Monitoring bacterial community of human gut microbiota reveals an increase in Lactobacillus in obese patients and Methanogens in anorexic patients." PloS one **4**(9): e7125.

Atarashi, K., J. Nishimura, T. Shima, Y. Umesaki, M. Yamamoto, M. Onoue, H. Yagita, N. Ishii, R. Evans and K. Honda (2008). "ATP drives lamina propria TH17 cell differentiation." Nature **455**(7214): 808-812.

Literature

Atarashi, K., T. Tanoue, K. Oshima, W. Suda, Y. Nagano, H. Nishikawa, S. Fukuda, T. Saito, S. Narushima and K. Hase (2013). "Treg induction by a rationally selected mixture of Clostridia strains from the human microbiota." Nature **500**(7461): 232-236.

Aziz, R. K., D. Bartels, A. A. Best, M. DeJongh, T. Disz, R. A. Edwards, K. Formsma, S. Gerdes, E. M. Glass and M. Kubal (2008). "The RAST Server: rapid annotations using subsystems technology." BMC genomics **9**(1): 1.

Baothman, O. A., M. A. Zamzami, I. Taher, J. Abubaker and M. Abu-Farha (2016). "The role of Gut Microbiota in the development of obesity and Diabetes." Lipids in Health and Disease **15**(1): 1.

Barbut, F., D. Decre, V. Lalande, B. Burghoffer, L. Noussair, A. Gigandon, F. Espinasse, L. Raskine, J. Robert and A. Mangeol (2005). "Clinical features of Clostridium difficile-associated diarrhoea due to binary toxin (actin-specific ADP-ribosyltransferase)-producing strains." Journal of medical microbiology **54**(2): 181-185.

Barman, M., D. Unold, K. Shifley, E. Amir, K. Hung, N. Bos and N. Salzman (2008). "Enteric salmonellosis disrupts the microbial ecology of the murine gastrointestinal tract." Infection and immunity **76**(3): 907-915.

Barthel, M., S. Hapfelmeier, L. Quintanilla-Martínez, M. Kremer, M. Rohde, M. Hogardt, K. Pfeffer, H. Rüssmann and W.-D. Hardt (2003). "Pretreatment of mice with streptomycin provides a Salmonella enterica serovar Typhimurium colitis model that allows analysis of both pathogen and host." Infection and immunity **71**(5): 2839-2858.

Baumgart, M., B. Dogan, M. Rishniw, G. Weitzman, B. Bosworth, R. Yantiss, R. H. Orsi, M. Wiedmann, P. McDonough and S. G. Kim (2007). "Culture independent analysis of ileal mucosa reveals a selective increase in invasive Escherichia coli of novel phylogeny relative to depletion of Clostridiales in Crohn's disease involving the ileum." The ISME journal **1**(5): 403-418.

Bearson, S. M., H. K. Allen, B. L. Bearson, T. Looft, B. W. Brunelle, J. D. Kich, C. K. Tuggle, D. O. Bayles, D. Alt and U. Y. Levine (2013). "Profiling the gastrointestinal microbiota in response to Salmonella: low versus high Salmonella shedding in the natural porcine host." Infection, Genetics and Evolution **16**: 330-340.

Becker, N., J. Kunath, G. Loh and M. Blaut (2011). "Human intestinal microbiota: Characterization of a simplified and stable gnotobiotic rat model." Gut microbes **2**(1): 25-33.

Berger, T., A. Togawa, G. S. Duncan, A. J. Elia, A. You-Ten, A. Wakeham, H. E. Fong, C. C. Cheung and T. W. Mak (2006). "Lipocalin 2-deficient mice exhibit increased sensitivity to Escherichia coli infection but not to ischemia-reperfusion injury." Proceedings of the National Academy of Sciences of the United States of America **103**(6): 1834-1839.

Bergström, A., T. H. Skov, M. I. Bahl, H. M. Roager, L. B. Christensen, K. T. Ejlerskov, C. Mølgaard, K. F. Michaelsen and T. R. Licht (2014). "Establishment of intestinal microbiota during early life: a

Literature

longitudinal, explorative study of a large cohort of Danish infants." Applied and environmental microbiology **80**(9): 2889-2900.

Bergström, J. H., K. A. Berg, A. M. Rodríguez-Piñeiro, B. Stecher, M. E. Johansson and G. C. Hansson (2014). "AGR2, an endoplasmic reticulum protein, is secreted into the gastrointestinal mucus." PloS one **9**(8): e104186.

Bertin, Y., J. Girardeau, F. Chaucheyras-Durand, B. Lyan, E. Pujos-Guillot, J. Harel and C. Martin (2011). "Enterohaemorrhagic Escherichia coli gains a competitive advantage by using ethanolamine as a nitrogen source in the bovine intestinal content." Environmental microbiology **13**(2): 365-377.

Birgegård, G. and J. Caro (1984). "Increased ferritin synthesis and iron uptake in inflammatory mouse macrophages." Scandinavian journal of haematology **33**(1): 43-48.

Brasseit, J., E. Althaus-Steiner, M. Faderl, N. Dickgreber, L. Saurer, V. Genitsch, T. Dolowschiak, H. Li, D. Finke and W. Hardt (2016). "CD4 T cells are required for both development and maintenance of disease in a new mouse model of reversible colitis." Mucosal immunology **9**(3): 689-701.

Braun, V. and K. Hantke (2011). "Recent insights into iron import by bacteria." Current opinion in chemical biology **15**(2): 328-334.

Britton, R. A. and V. B. Young (2014). "Role of the intestinal microbiota in resistance to colonization by Clostridium difficile." Gastroenterology **146**(6): 1547-1553.

Brosius, J., M. L. Palmer, P. J. Kennedy and H. F. Noller (1978). "Complete nucleotide sequence of a 16S ribosomal RNA gene from Escherichia coli." Proceedings of the National Academy of Sciences **75**(10): 4801-4805.

Brown, J., W. M. De Vos, P. S. DiStefano, J. Doré, C. Huttenhower, R. Knight, T. D. Lawley, J. Raes and P. Turnbaugh (2013). "Translating the human microbiome." Nat Biotechnol **31**(4): 304-308.

Brugiroux, S., M. Beutler, C. Pfann, D. Garzetti, H.-J. Ruscheweyh, D. Ring, M. Diehl, S. Herp, Y. Lötscher and S. Hussain (2016). "Genome-guided design of a defined mouse microbiota that confers colonization resistance against Salmonella enterica serovar Typhimurium." Nature Microbiology **2**: 16215.

Bry, L., P. G. Falk, T. Midtvedt and J. I. Gordon (1996). "A model of host-microbial interactions in an open mammalian ecosystem." Science **273**(5280): 1380.

Buffie, C. G., V. Bucci, R. R. Stein, P. T. McKenney, L. Ling, A. Gobourne, D. No, H. Liu, M. Kinnebrew and A. Viale (2015). "Precision microbiome reconstitution restores bile acid mediated resistance to Clostridium difficile." Nature **517**(7533): 205-208.

Literature

Buffie, C. G. and E. G. Pamer (2013). "Microbiota-mediated colonization resistance against intestinal pathogens." Nature Reviews Immunology **13**(11): 790-801.

Buttó, L. F. and D. Haller (2016). "Dysbiosis in intestinal inflammation: Cause or consequence." International Journal of Medical Microbiology.

Caporaso, J. G., J. Kuczynski, J. Stombaugh, K. Bittinger, F. D. Bushman, E. K. Costello, N. Fierer, A. G. Pena, J. K. Goodrich and J. I. Gordon (2010). "QIIME allows analysis of high-throughput community sequencing data." Nature methods **7**(5): 335-336.

Carmody, R. N., G. K. Gerber, J. M. Luevano, D. M. Gatti, L. Somes, K. L. Svenson and P. J. Turnbaugh (2015). "Diet dominates host genotype in shaping the murine gut microbiota." Cell Host & Microbe **17**(1): 72-84.

Carroll, I. M., T. Ringel-Kulka, J. P. Siddle and Y. Ringel (2012). "Alterations in composition and diversity of the intestinal microbiota in patients with diarrhea-predominant irritable bowel syndrome." Neurogastroenterology & Motility **24**(6): 521-e248.

Cash, H. L., C. V. Whitham, C. L. Behrendt and L. V. Hooper (2006). "Symbiotic bacteria direct expression of an intestinal bactericidal lectin." Science **313**(5790): 1126-1130.

Caspari, D. and J. M. Macy (1983). "The role of carbon dioxide in glucose metabolism of *Bacteroides fragilis*." Archives of microbiology **135**(1): 16-24.

Castro, M. S., M. A. Molina, M. B. Azpiroz, A. M. Díaz, R. Ponzio, M. D. Sparo, M. A. Manghi and A. M. Canellada (2016). "Probiotic activity of *Enterococcus faecalis* CECT7121: effects on mucosal immunity and intestinal epithelial cells." Journal of Applied Microbiology.

Caza, M., A. Garénaux, F. Lépine and C. M. Dozois (2015). "Catecholate siderophore esterases Fes, IroD and IroE are required for salmochelins secretion following utilization, but only IroD contributes to virulence of extra-intestinal pathogenic *Escherichia coli*." Molecular microbiology **97**(4): 717-732.

Chakravorty, S., D. Helb, M. Burday, N. Connell and D. Alland (2007). "A detailed analysis of 16S ribosomal RNA gene segments for the diagnosis of pathogenic bacteria." Journal of microbiological methods **69**(2): 330-339.

Cherepanov, P. P. and W. Wackernagel (1995). "Gene disruption in *Escherichia coli*: Tc R and Km R cassettes with the option of Flp-catalyzed excision of the antibiotic-resistance determinant." Gene **158**(1): 9-14.

Chu, H., A. Khosravi, I. P. Kusumawardhani, A. H. Kwon, A. C. Vasconcelos, L. D. Cunha, A. E. Mayer, Y. Shen, W.-L. Wu and A. Kambal (2016). "Gene-microbiota interactions contribute to the pathogenesis of inflammatory bowel disease." Science **352**(6289): 1116-1120.

Literature

Chung, H., S. J. Pamp, J. A. Hill, N. K. Surana, S. M. Edelman, E. B. Troy, N. C. Reading, E. J. Villablanca, S. Wang and J. R. Mora (2012). "Gut immune maturation depends on colonization with a host-specific microbiota." Cell **149**(7): 1578-1593.

Clavel, T., I. Lagkouvardos, M. Blaut and B. Stecher (2016). "The mouse gut microbiome revisited: From complex diversity to model ecosystems." International Journal of Medical Microbiology.

Cleary, J., L.-C. Lai, R. K. Shaw, A. Straatman-Iwanowska, M. S. Sonnenberg, G. Frankel and S. Knutton (2004). "Enteropathogenic Escherichia coli (EPEC) adhesion to intestinal epithelial cells: role of bundle-forming pili (BFP), EspA filaments and intimin." Microbiology **150**(3): 527-538.

Collins, J., R. Borojevic, E. Verdu, J. Huizinga and E. Ratcliffe (2014). "Intestinal microbiota influence the early postnatal development of the enteric nervous system." Neurogastroenterology & Motility **26**(1): 98-107.

Collins, J. W., C. Chervaux, B. Raymond, M. Derrien, R. Brazeilles, A. Kosta, I. Chambaud, V. F. Crepin and G. Frankel (2014). "Fermented dairy products modulate C. rodentium induced colonic hyperplasia." Journal of Infectious Diseases: jiu205.

Correnti, C. and R. K. Strong (2012). "Mammalian siderophores, siderophore-binding lipocalins, and the labile iron pool." Journal of Biological Chemistry **287**(17): 13524-13531.

Datsenko, K. A. and B. L. Wanner (2000). "One-step inactivation of chromosomal genes in Escherichia coli K-12 using PCR products." Proceedings of the National Academy of Sciences **97**(12): 6640-6645.

Del Papa, M. F. and M. Perego (2008). "Ethanolamine activates a sensor histidine kinase regulating its utilization in Enterococcus faecalis." Journal of bacteriology **190**(21): 7147-7156.

Derrien, M., E. E. Vaughan, C. M. Plugge and W. M. de Vos (2004). "Akkermansia muciniphila gen. nov., sp. nov., a human intestinal mucin-degrading bacterium." International journal of systematic and evolutionary microbiology **54**(5): 1469-1476.

Dethlefsen, L., S. Huse, M. L. Sogin and D. A. Relman (2008). "The pervasive effects of an antibiotic on the human gut microbiota, as revealed by deep 16S rRNA sequencing." PLoS Biol **6**(11): e280.

Dewhirst, F. E., C.-C. Chien, B. J. Paster, R. L. Ericson, R. P. Orcutt, D. B. Schauer and J. G. Fox (1999). "Phylogeny of the defined murine microbiota: altered Schaedler flora." Applied and environmental microbiology **65**(8): 3287-3292.

Dewhirst, F. E., C. C. Chien, B. J. Paster, R. L. Ericson, R. P. Orcutt, D. B. Schauer and J. G. Fox (1999). "Phylogeny of the defined murine microbiota: altered Schaedler flora." Appl Environ Microbiol **65**(8): 3287-3292.

Literature

Diaz-Ochoa, V. E., S. Jellbauer, S. Klaus and M. Raffatellu (2014). "Transition metal ions at the crossroads of mucosal immunity and microbial pathogenesis." Frontiers in Cellular and Infection Microbiology **4**.

Diederich, A.-K., K. A. Duda, F. Romero-Saavedra, R. Engel, O. Holst and J. Huebner (2016). "Deletion of fabN in *Enterococcus faecalis* results in unsaturated fatty acid auxotrophy and decreased release of inflammatory cytokines." Innate immunity: 1753425916639669.

Donohoe, D. R., L. B. Collins, A. Wali, R. Bigler, W. Sun and S. J. Bultman (2012). "The Warburg effect dictates the mechanism of butyrate-mediated histone acetylation and cell proliferation." Molecular cell **48**(4): 612-626.

Donohoe, D. R., D. Holley, L. B. Collins, S. A. Montgomery, A. C. Whitmore, A. Hillhouse, K. P. Curry, S. W. Renner, A. Greenwalt and E. P. Ryan (2014). "A gnotobiotic mouse model demonstrates that dietary fiber protects against colorectal tumorigenesis in a microbiota-and butyrate-dependent manner." Cancer discovery **4**(12): 1387-1397.

Duncan, S. H., G. Loble, G. Holtrop, J. Ince, A. Johnstone, P. Louis and H. Flint (2008). "Human colonic microbiota associated with diet, obesity and weight loss." International journal of obesity **32**(11): 1720-1724.

Eckburg, P. B., E. M. Bik, C. N. Bernstein, E. Purdom, L. Dethlefsen, M. Sargent, S. R. Gill, K. E. Nelson and D. A. Relman (2005). "Diversity of the human intestinal microbial flora." Science **308**(5728): 1635-1638.

Endt, K., B. Stecher, S. Chaffron, E. Slack, N. Tchitchek, A. Benecke, L. Van Maele, J.-C. Sirard, A. J. Mueller and M. Heikenwalder (2010). "The microbiota mediates pathogen clearance from the gut lumen after non-typhoidal *Salmonella* diarrhea." PLoS pathogens **6**(9): e1001097.

Faber, F., L. Tran, M. X. Byndloss, C. A. Lopez, E. M. Velazquez, T. Kerrinnes, S.-P. Nuccio, T. Wangdi, O. Fiehn and R. M. Tsolis (2016). "Host-mediated sugar oxidation promotes post-antibiotic pathogen expansion." Nature.

Fabretti, F., C. Theilacker, L. Baldassarri, Z. Kaczynski, A. Kropec, O. Holst and J. Huebner (2006). "Alanine esters of enterococcal lipoteichoic acid play a role in biofilm formation and resistance to antimicrobial peptides." Infection and immunity **74**(7): 4164-4171.

Faith, J. J., P. P. Ahern, V. K. Ridaura, J. Cheng and J. I. Gordon (2014). "Identifying gut microbe–host phenotype relationships using combinatorial communities in gnotobiotic mice." Science translational medicine **6**(220): 220ra211-220ra211.

Faith, J. J., N. P. McNulty, F. E. Rey and J. I. Gordon (2011). "Predicting a human gut microbiota's response to diet in gnotobiotic mice." Science **333**(6038): 101-104.

Literature

Faith, J. J., F. E. Rey, D. O'Donnell, M. Karlsson, N. P. McNulty, G. Kallstrom, A. L. Goodman and J. I. Gordon (2010). "Creating and characterizing communities of human gut microbes in gnotobiotic mice." The ISME journal **4**(9): 1094-1098.

Falk, P. G., L. V. Hooper, T. Midtvedt and J. I. Gordon (1998). "Creating and maintaining the gastrointestinal ecosystem: what we know and need to know from gnotobiology." Microbiology and Molecular Biology Reviews **62**(4): 1157-1170.

Fallani, M., S. Amarri, A. Uusijarvi, R. Adam, S. Khanna, M. Aguilera, A. Gil, J. M. Vieites, E. Norin and D. Young (2011). "Determinants of the human infant intestinal microbiota after the introduction of first complementary foods in infant samples from five European centres." Microbiology **157**(5): 1385-1392.

Ferreyra, J. A., K. M. Ng and J. L. Sonnenburg (2014). "The Enteric Two-Step: nutritional strategies of bacterial pathogens within the gut." Cellular microbiology **16**(7): 993-1003.

Flint, H. J., K. P. Scott, S. H. Duncan, P. Louis and E. Forano (2012). "Microbial degradation of complex carbohydrates in the gut." Gut microbes **3**(4): 289-306.

Flo, T. H., K. D. Smith, S. Sato, D. J. Rodriguez, M. A. Holmes, R. K. Strong, S. Akira and A. Aderem (2004). "Lipocalin 2 mediates an innate immune response to bacterial infection by sequestering iron." Nature **432**(7019): 917-921.

Flockhart, L., K. Pintar, A. Cook, S. McEwen, R. Friendship, D. Kelton and F. Pollari (2016). "Distribution of Salmonella in Humans, Production Animal Operations and a Watershed in a FoodNet Canada Sentinel Site." Zoonoses and Public Health.

Forbes, J. D., G. Van Domselaar and C. N. Bernstein (2016). "Microbiome Survey of the Inflamed and Noninflamed Gut at Different Compartments Within the Gastrointestinal Tract of Inflammatory Bowel Disease Patients." Inflammatory bowel diseases **22**(4): 817-825.

Fox, K. A., A. Ramesh, J. E. Stearns, A. Bourgoigne, A. Reyes-Jara, W. C. Winkler and D. A. Garsin (2009). "Multiple posttranscriptional regulatory mechanisms partner to control ethanolamine utilization in *Enterococcus faecalis*." Proceedings of the National Academy of Sciences **106**(11): 4435-4440.

Frank, D. N., A. L. S. Amand, R. A. Feldman, E. C. Boedeker, N. Harpaz and N. R. Pace (2007). "Molecular-phylogenetic characterization of microbial community imbalances in human inflammatory bowel diseases." Proceedings of the National Academy of Sciences **104**(34): 13780-13785.

Freter, R. and G. D. Abrams (1972). "Function of various intestinal bacteria in converting germfree mice to the normal state." Infection and immunity **6**(2): 119-126.

Literature

Furne, J., J. Springfield, T. Koenig, E. DeMaster and M. D. Levitt (2001). "Oxidation of hydrogen sulfide and methanethiol to thiosulfate by rat tissues: a specialized function of the colonic mucosa." Biochemical pharmacology **62**(2): 255-259.

Ganesh, B. P., R. Klopfeisch, G. Loh and M. Blaut (2013). "Commensal Akkermansia muciniphila Exacerbates Gut Inflammation in Salmonella Typhimurium-Infected Gnotobiotic Mice." PloS one **8**(9): e74963.

Garsin, D. A. (2010). "Ethanolamine utilization in bacterial pathogens: roles and regulation." Nature Reviews Microbiology **8**(4): 290-295.

Gerlach, R. G., D. Jäckel, N. Geymeier and M. Hensel (2007). "Salmonella pathogenicity island 4-mediated adhesion is coregulated with invasion genes in Salmonella enterica." Infection and immunity **75**(10): 4697-4709.

Geuking, M. B., J. Cahenzli, M. A. Lawson, D. C. Ng, E. Slack, S. Hapfelmeier, K. D. McCoy and A. J. Macpherson (2011). "Intestinal bacterial colonization induces mutualistic regulatory T cell responses." Immunity **34**(5): 794-806.

Godinez, I., T. Haneda, M. Raffatellu, M. D. George, T. A. Paixão, H. G. Rolán, R. L. Santos, S. Dandekar, R. M. Tsolis and A. J. Bäumler (2008). "T cells help to amplify inflammatory responses induced by Salmonella enterica serotype Typhimurium in the intestinal mucosa." Infection and immunity **76**(5).

Godinez, I., M. Raffatellu, H. Chu, T. A. Paixao, T. Haneda, R. L. Santos, C. L. Bevins, R. M. Tsolis and A. J. Bäumler (2009). "Interleukin-23 orchestrates mucosal responses to Salmonella enterica serotype Typhimurium in the intestine." Infection and immunity **77**(1): 387-398.

Goetz, D. H., M. A. Holmes, N. Borregaard, M. E. Bluhm, K. N. Raymond and R. K. Strong (2002). "The neutrophil lipocalin NGAL is a bacteriostatic agent that interferes with siderophore-mediated iron acquisition." Molecular cell **10**(5): 1033-1043.

Goodman, A. L., G. Kallstrom, J. J. Faith, A. Reyes, A. Moore, G. Dantas and J. I. Gordon (2011). "Extensive personal human gut microbiota culture collections characterized and manipulated in gnotobiotic mice." Proceedings of the National Academy of Sciences: 201102938.

Griffiths, E. (1999). "Iron in biological systems." Iron and infection. Wiley, Chichester, United Kingdom: 1-26.

Gustafsson, J. K., N. Navabi, A. M. Rodriguez-Piñeiro, A. H. Alomran, P. Premaratne, H. R. Fernandez, D. Banerjee, H. Sjövall, G. C. Hansson and S. K. Lindén (2013). "Dynamic changes in mucus thickness and ion secretion during Citrobacter rodentium infection and clearance."

Literature

Hapfelmeier, S., K. Ehrbar, B. Stecher, M. Barthel, M. Kremer and W.-D. Hardt (2004). "Role of the Salmonella pathogenicity island 1 effector proteins SipA, SopB, SopE, and SopE2 in Salmonella enterica subspecies 1 serovar Typhimurium colitis in streptomycin-pretreated mice." Infection and immunity **72**(2): 795-809.

Hapfelmeier, S. and W.-D. Hardt (2005). "A mouse model for S. typhimurium-induced enterocolitis." Trends in microbiology **13**(10): 497-503.

Hapfelmeier, S., B. Stecher, M. Barthel, M. Kremer, A. J. Müller, M. Heikenwalder, T. Stallmach, M. Hensel, K. Pfeffer and S. Akira (2005). "The Salmonella pathogenicity island (SPI)-2 and SPI-1 type III secretion systems allow Salmonella serovar typhimurium to trigger colitis via MyD88-dependent and MyD88-independent mechanisms." The Journal of Immunology **174**(3): 1675-1685.

Helaine, S., A. M. Cheverton, K. G. Watson, L. M. Faure, S. A. Matthews and D. W. Holden (2014). "Internalization of Salmonella by macrophages induces formation of nonreplicating persisters." Science **343**(6167): 204-208.

Hensel, M., A. P. Hinsley, T. Nikolaus, G. Sawers and B. C. Berks (1999). "The genetic basis of tetrathionate respiration in Salmonella typhimurium." Molecular microbiology **32**(2): 275-287.

Hiergeist, A., J. Gläsner, U. Reischl and A. Gessner (2015). "Analyses of intestinal microbiota: Culture versus Sequencing." ILAR Journal **56**(2): 228-240.

Hoffmann, C., D. A. Hill, N. Minkah, T. Kirn, A. Troy, D. Artis and F. Bushman (2009). "Community-wide response of the gut microbiota to enteropathogenic Citrobacter rodentium infection revealed by deep sequencing." Infection and immunity **77**(10): 4668-4678.

Hoffmann, T. W., H.-P. Pham, C. Bridonneau, C. Aubry, B. Lamas, C. Martin-Gallausiaux, M. Moroldo, D. Rainteau, N. Lapaque and A. Six (2015). "Microorganisms linked to inflammatory bowel disease-associated dysbiosis differentially impact host physiology in gnotobiotic mice." The ISME journal.

Hoiseth, S. K. and B. Stocker (1981). "Aromatic-dependent Salmonella typhimurium are non-virulent and effective as live vaccines."

Hooper, L. V., D. R. Littman and A. J. Macpherson (2012). "Interactions between the microbiota and the immune system." Science **336**(6086): 1268-1273.

Hooper, L. V. and A. J. Macpherson (2010). "Immune adaptations that maintain homeostasis with the intestinal microbiota." Nature Reviews Immunology **10**(3): 159-169.

Huang, Y.-L., C. Chassard, M. Hausmann, M. von Itzstein and T. Hennot (2015). "Sialic acid catabolism drives intestinal inflammation and microbial dysbiosis in mice." Nature communications **6**.

Literature

Ianniello, R., J. Zheng, T. Zotta, A. Ricciardi and M. Gänzle (2015). "Biochemical analysis of respiratory metabolism in the heterofermentative *Lactobacillus spicheri* and *Lactobacillus reuteri*." Journal of Applied Microbiology **119**(3): 763-775.

Johansson, M. E., H. E. Jakobsson, J. Holmén-Larsson, A. Schütte, A. Ermund, A. M. Rodríguez-Piñeiro, L. Arike, C. Wising, F. Svensson and F. Bäckhed (2015). "Normalization of host intestinal mucus layers requires long-term microbial colonization." Cell Host & Microbe **18**(5): 582-592.

Johansson, M. E., M. Phillipson, J. Petersson, A. Velcich, L. Holm and G. C. Hansson (2008). "The inner of the two Muc2 mucin-dependent mucus layers in colon is devoid of bacteria." Proceedings of the National Academy of Sciences **105**(39): 15064-15069.

Kaiser, B. L. D., J. Li, J. A. Sanford, Y.-M. Kim, S. R. Kronewitter, M. B. Jones, C. T. Peterson, S. N. Peterson, B. C. Frank and S. O. Purvine (2013). "A multi-omic view of host-pathogen-commensal interplay in *Salmonella*-mediated intestinal infection." PloS one **8**(6): e67155.

Kaiser, P., M. Diard, B. Stecher and W. D. Hardt (2012). "The streptomycin mouse model for *Salmonella* diarrhea: functional analysis of the microbiota, the pathogen's virulence factors, and the host's mucosal immune response." Immunological reviews **245**(1): 56-83.

Kamada, N., Y.-G. Kim, H. P. Sham, B. A. Vallance, J. L. Puente, E. C. Martens and G. Núñez (2012). "Regulated virulence controls the ability of a pathogen to compete with the gut microbiota." Science **336**(6086): 1325-1329.

Kaniga, K., J. C. Bossio and J. E. Galán (1994). "The *Salmonella typhimurium* invasion genes *invF* and *invG* encode homologues of the AraC and PulD family of proteins." Molecular microbiology **13**(4): 555-568.

Kelly, C. J., L. Zheng, E. L. Campbell, B. Saeedi, C. C. Scholz, A. J. Bayless, K. E. Wilson, L. E. Glover, D. J. Kominsky and A. Magnuson (2015). "Crosstalk between microbiota-derived short-chain fatty acids and intestinal epithelial HIF augments tissue barrier function." Cell Host & Microbe **17**(5): 662-671.

Kenny, B., R. DeVinney, M. Stein, D. J. Reinscheid, E. A. Frey and B. B. Finlay (1997). "Enteropathogenic *E. coli* (EPEC) transfers its receptor for intimate adherence into mammalian cells." Cell **91**(4): 511-520.

Kerckhoffs, A. P., K. Ben-Amor, M. Samsom, M. E. van der Rest, J. de Vogel, J. Knol and L. M. Akkermans (2011). "Molecular analysis of faecal and duodenal samples reveals significantly higher prevalence and numbers of *Pseudomonas aeruginosa* in irritable bowel syndrome." Journal of medical microbiology **60**(2): 236-245.

Klaasen, H., J. Koopman, M. Van den Brink, H. Van Wezel and A. Beynen (1991). "Mono-association of mice with non-cultivable, intestinal, segmented, filamentous bacteria." Archives of microbiology **156**(2): 148-151.

Literature

Koenig, J. E., A. Spor, N. Scalfone, A. D. Fricker, J. Stombaugh, R. Knight, L. T. Angenent and R. E. Ley (2011). "Succession of microbial consortia in the developing infant gut microbiome." Proceedings of the National Academy of Sciences **108**(Supplement 1): 4578-4585.

Kortman, G. A., M. L. Mulder, T. J. Richters, N. K. Shanmugam, E. Trebicka, J. Boekhorst, H. M. Timmerman, R. Roelofs, E. T. Wiegierinck and C. M. Laarakkers (2015). "Low dietary iron intake restrains the intestinal inflammatory response and pathology of enteric infection by food-borne bacterial pathogens." European journal of immunology **45**(9): 2553-2567.

Kotloff, K. L., J. P. Nataro, W. C. Blackwelder, D. Nasrin, T. H. Farag, S. Panchalingam, Y. Wu, S. O. Sow, D. Sur and R. F. Breiman (2013). "Burden and aetiology of diarrhoeal disease in infants and young children in developing countries (the Global Enteric Multicenter Study, GEMS): a prospective, case-control study." The Lancet **382**(9888): 209-222.

Krych, L., C. H. Hansen, A. K. Hansen, F. W. van den Berg and D. S. Nielsen (2013). "Quantitatively different, yet qualitatively alike: a meta-analysis of the mouse core gut microbiome with a view towards the human gut microbiome." PloS one **8**(5): e62578.

Kutschera, M., W. Engst, M. Blaut and A. Braune (2011). "Isolation of catechin-converting human intestinal bacteria." Journal of Applied Microbiology **111**(1): 165-175.

Lagkouvardos, I., R. Pukall, B. Abt, B. U. Foesel, J. P. Meier-Kolthoff, N. Kumar, A. Bresciani, I. Martínez, S. Just and C. Ziegler (2016). "The Mouse Intestinal Bacterial Collection (miBC) provides host-specific insight into cultured diversity and functional potential of the gut microbiota." Nature Microbiology **1**: 16131.

Larson, T., M. Ehrmann and W. Boos (1983). "Periplasmic glycerophosphodiester phosphodiesterase of *Escherichia coli*, a new enzyme of the *glp* regulon." Journal of Biological Chemistry **258**(9): 5428-5432.

Lawley, T. D., D. M. Bouley, Y. E. Hoy, C. Gerke, D. A. Relman and D. M. Monack (2008). "Host transmission of *Salmonella enterica* serovar Typhimurium is controlled by virulence factors and indigenous intestinal microbiota." Infection and immunity **76**(1): 403-416.

Lawley, T. D., K. Chan, L. J. Thompson, C. C. Kim, G. R. Govoni and D. M. Monack (2006). "Genome-wide screen for *Salmonella* genes required for long-term systemic infection of the mouse." PLoS Pathog **2**(2): e11.

Lawley, T. D., N. J. Croucher, L. Yu, S. Clare, M. Sebaihia, D. Goulding, D. J. Pickard, J. Parkhill, J. Choudhary and G. Dougan (2009). "Proteomic and genomic characterization of highly infectious *Clostridium difficile* 630 spores." Journal of bacteriology **191**(17): 5377-5386.

Literature

- Levitt, M. D., J. Furne, J. Springfield, F. Suarez and E. DeMaster (1999). "Detoxification of hydrogen sulfide and methanethiol in the cecal mucosa." The Journal of clinical investigation **104**(8): 1107-1114.
- Ley, R. E., F. Bäckhed, P. Turnbaugh, C. A. Lozupone, R. D. Knight and J. I. Gordon (2005). "Obesity alters gut microbial ecology." Proceedings of the National Academy of Sciences of the United States of America **102**(31): 11070-11075.
- Linnenbrink, M., J. Wang, E. A. Hardouin, S. Künzel, D. Metzler and J. F. Baines (2013). "The role of biogeography in shaping diversity of the intestinal microbiota in house mice." Molecular ecology **22**(7): 1904-1916.
- Liu, J. Z., S. Jellbauer, A. J. Poe, V. Ton, M. Pesciaroli, T. E. Kehl-Fie, N. A. Restrepo, M. P. Hosking, R. A. Edwards and A. Battistoni (2012). "Zinc sequestration by the neutrophil protein calprotectin enhances Salmonella growth in the inflamed gut." Cell Host & Microbe **11**(3): 227-239.
- Loetscher, Y., A. Wieser, J. Lengefeld, P. Kaiser, S. Schubert, M. Heikenwalder, W.-D. Hardt and B. Stecher (2012). "Salmonella transiently reside in luminal neutrophils in the inflamed gut." PloS one **7**(4): e34812.
- Lopez, C. A., S. E. Winter, F. Rivera-Chávez, M. N. Xavier, V. Poon, S.-P. Nuccio, R. M. Tsolis and A. J. Bäumlér (2012). "Phage-mediated acquisition of a type III secreted effector protein boosts growth of salmonella by nitrate respiration." MBio **3**(3): e00143-00112.
- Luperchio, S. A. and D. B. Schauer (2001). "Molecular pathogenesis of Citrobacter rodentium and transmissible murine colonic hyperplasia." Microbes and Infection **3**(4): 333-340.
- Lupp, C., M. L. Robertson, M. E. Wickham, I. Sekirov, O. L. Champion, E. C. Gaynor and B. B. Finlay (2007). "Host-mediated inflammation disrupts the intestinal microbiota and promotes the overgrowth of Enterobacteriaceae." Cell Host & Microbe **2**(2): 119-129.
- Macpherson, A. J. and T. Uhr (2004). "Induction of protective IgA by intestinal dendritic cells carrying commensal bacteria." Science **303**(5664): 1662-1665.
- Mahowald, M. A., F. E. Rey, H. Seedorf, P. J. Turnbaugh, R. S. Fulton, A. Wollam, N. Shah, C. Wang, V. Magrini and R. K. Wilson (2009). "Characterizing a model human gut microbiota composed of members of its two dominant bacterial phyla." Proceedings of the National Academy of Sciences **106**(14): 5859-5864.
- Maier, L., M. Diard, M. E. Sellin, E.-S. Chouffane, K. Trautwein-Weidner, B. Periaswamy, E. Slack, T. Dolowschiak, B. Stecher and C. Loverdo (2014). "Granulocytes Impose a Tight Bottleneck upon the Gut Luminal Pathogen Population during Salmonella Typhimurium Colitis." PLoS pathogens **10**(12): e1004557.

Literature

Maier, L., R. Vyas, C. D. Cordova, H. Lindsay, T. S. B. Schmidt, S. Brugiroux, B. Periaswamy, R. Bauer, A. Sturm and F. Schreiber (2013). "Microbiota-derived hydrogen fuels Salmonella typhimurium invasion of the gut ecosystem." Cell Host & Microbe **14**(6): 641-651.

Mallick, E. M., M. E. McBee, V. K. Vanguri, A. R. Melton-Celsa, K. Schlieper, B. J. Karalius, A. D. O'Brien, J. R. Butterton, J. M. Leong and D. B. Schauer (2012). "A novel murine infection model for Shiga toxin-producing Escherichia coli." The Journal of clinical investigation **122**(11): 4012-4024.

Manges, A. R., A. Labbe, V. G. Loo, J. K. Atherton, M. A. Behr, L. Masson, P. A. Tellis and R. Brousseau (2010). "Comparative metagenomic study of alterations to the intestinal microbiota and risk of nosocomial Clostridium difficile-associated disease." Journal of Infectious Diseases **202**(12): 1877-1884.

Marchesi, J. and F. Shanahan (2007). "The normal intestinal microbiota." Curr Opin Infect Dis **20**(5): 508-513.

Martin, R., H. Makino, A. C. Yavuz, K. Ben-Amor, M. Roelofs, E. Ishikawa, H. Kubota, S. Swinkels, T. Sakai and K. Oishi (2016). "Early-Life Events, Including Mode of Delivery and Type of Feeding, Siblings and Gender, Shape the Developing Gut Microbiota." PloS one **11**(6): e0158498.

Maurice, C. F., H. J. Haiser and P. J. Turnbaugh (2013). "Xenobiotics shape the physiology and gene expression of the active human gut microbiome." Cell **152**(1): 39-50.

McEllistrem, M. C., R. J. Carman, D. N. Gerding, C. Genheimer and L. Zheng (2005). "A hospital outbreak of Clostridium difficile disease associated with isolates carrying binary toxin genes." Clinical infectious diseases **40**(2): 265-272.

McNulty, N. P., T. Yatsunenko, A. Hsiao, J. J. Faith, B. D. Muegge, A. L. Goodman, B. Henrissat, R. Oozeer, S. Cools-Portier and G. Gobert (2011). "The impact of a consortium of fermented milk strains on the gut microbiome of gnotobiotic mice and monozygotic twins." Science translational medicine **3**(106): 106ra106-106ra106.

Mead, P. S., L. Slutsker, V. Dietz, L. F. McCaig, J. S. Bresee, C. Shapiro, P. M. Griffin and R. V. Tauxe (1999). "Food-related illness and death in the United States." Emerging infectious diseases **5**(5): 607.

Million, M., M. Maraninchi, M. Henry, F. Armougom, H. Richet, P. Carrieri, R. Valero, D. Raccach, B. Vialettes and D. Raoult (2012). "Obesity-associated gut microbiota is enriched in Lactobacillus reuteri and depleted in Bifidobacterium animalis and Methanobrevibacter smithii." International journal of obesity **36**(6): 817-825.

Miranda, K. M., M. G. Espey and D. A. Wink (2001). "A rapid, simple spectrophotometric method for simultaneous detection of nitrate and nitrite." Nitric oxide **5**(1): 62-71.

Literature

- Moeller, R., I. Vlašić, G. Reitz and W. L. Nicholson (2012). "Role of altered rpoB alleles in *Bacillus subtilis* sporulation and spore resistance to heat, hydrogen peroxide, formaldehyde, and glutaraldehyde." Archives of microbiology **194**(9): 759-767.
- Monira, S., S. Nakamura, K. Gotoh, K. Izutsu, H. Watanabe, N. H. Alam, H. P. Endtz, A. Cravioto, S. Ali and T. Nakaya (2011). "Gut microbiota of healthy and malnourished children in Bangladesh." Frontiers in microbiology **2**: 228.
- Narushima, S., K. Itoh, Y. Miyamoto, S.-H. Park, K. Nagata, K. Kuruma and K. Uchida (2006). "Deoxycholic acid formation in gnotobiotic mice associated with human intestinal bacteria." Lipids **41**(9): 835-843.
- Nataro, J. P. and J. B. Kaper (1998). "Diarrheagenic *Escherichia coli*." Clinical microbiology reviews **11**(1): 142-201.
- Natividad, J. M., C. L. Hayes, J.-P. Motta, J. Jury, H. J. Galipeau, V. Philip, C. L. Garcia-Rodenas, H. Kiyama, P. Bercik and E. F. Verdu (2013). "Differential induction of antimicrobial REGIII by the intestinal microbiota and *Bifidobacterium breve* NCC2950." Applied and environmental microbiology **79**(24): 7745-7754.
- Neilands, J. (1995). "Siderophores: structure and function of microbial iron transport compounds." Journal of Biological Chemistry **270**(45): 26723-26726.
- Nemeth, E., M. S. Tuttle, J. Powelson, M. B. Vaughn, A. Donovan, D. M. Ward, T. Ganz and J. Kaplan (2004). "Hepcidin regulates cellular iron efflux by binding to ferroportin and inducing its internalization." Science **306**(5704): 2090-2093.
- Ng, K. M., J. A. Ferreyra, S. K. Higginbottom, J. B. Lynch, P. C. Kashyap, S. Gopinath, N. Naidu, B. Choudhury, B. C. Weimer and D. M. Monack (2013). "Microbiota-liberated host sugars facilitate post-antibiotic expansion of enteric pathogens." Nature **502**(7469): 96-99.
- Nguyen, T. L. A., S. Vieira-Silva, A. Liston and J. Raes (2015). "How informative is the mouse for human gut microbiota research?" Disease Models and Mechanisms **8**(1): 1-16.
- Nicholson, J. K., E. Holmes, J. Kinross, R. Burcelin, G. Gibson, W. Jia and S. Pettersson (2012). "Host-gut microbiota metabolic interactions." Science **336**(6086): 1262-1267.
- Oh, P. L., A. K. Benson, D. A. Peterson, P. B. Patil, E. N. Moriyama, S. Roos and J. Walter (2010). "Diversification of the gut symbiont *Lactobacillus reuteri* as a result of host-driven evolution." The ISME journal **4**(3): 377-387.
- Ohkusa, T., T. Yoshida, N. Sato, S. Watanabe, H. Tajiri and I. Okayasu (2009). "Commensal bacteria can enter colonic epithelial cells and induce proinflammatory cytokine secretion: a possible pathogenic mechanism of ulcerative colitis." Journal of medical microbiology **58**(5): 535-545.

Literature

Pakarian, P. and P. D. Pawelek (2016). "Intracellular co-localization of the Escherichia coli enterobactin biosynthetic enzymes EntA, EntB, and EntE." Biochemical and Biophysical Research Communications.

Patel, J. C. and J. E. Galán (2005). "Manipulation of the host actin cytoskeleton by Salmonella—all in the name of entry." Current opinion in microbiology **8**(1): 10-15.

Pelludat, C. (1999). Molekulare Charakterisierung der Pathogenitätsinsel von Yersinia enterocolitica und ihr Einfluss auf die aktive Eisenaufnahme.

Pham, T. A. N., S. Clare, D. Goulding, J. M. Arasteh, M. D. Stares, H. P. Browne, J. A. Keane, A. J. Page, N. Kumasaka and L. Kane (2014). "Epithelial IL-22RA1-mediated fucosylation promotes intestinal colonization resistance to an opportunistic pathogen." Cell Host & Microbe **16**(4): 504-516.

Portillo, F., J. W. Foster, M. E. Maguire and B. B. Finlay (1992). "Characterization of the micro-environment of Salmonella typhimurium-containing vacuoles within MDCK epithelial cells." Molecular microbiology **6**(22): 3289-3297.

Price-Carter, M., J. Tingey, T. A. Bobik and J. R. Roth (2001). "The Alternative Electron Acceptor Tetrathionate Supports B12-Dependent Anaerobic Growth of Salmonella enterica Serovar Typhimurium on Ethanolamine or 1, 2-Propanediol." Journal of bacteriology **183**(8): 2463-2475.

Price, M. N., P. S. Dehal and A. P. Arkin (2009). "FastTree: computing large minimum evolution trees with profiles instead of a distance matrix." Mol Biol Evol **26**(7): 1641-1650.

Proulx, P. and C. Fung (1969). "Metabolism of phosphoglycerides in E. coli IV. The positional specificity and properties of phospholipase A." Canadian journal of biochemistry **47**(12): 1125-1128.

Quast, C., E. Pruesse, P. Yilmaz, J. Gerken, T. Schweer, P. Yarza, J. Peplies and F. O. Glöckner (2013). "The SILVA ribosomal RNA gene database project: improved data processing and web-based tools." Nucleic acids research **41**(D1): D590-D596.

Raffatellu, M., M. D. George, Y. Akiyama, M. J. Hornsby, S.-P. Nuccio, T. A. Paixao, B. P. Butler, H. Chu, R. L. Santos and T. Berger (2009). "Lipocalin-2 Resistance Confers an Advantage to Salmonella enterica Serotype Typhimurium for Growth and Survival in the Inflamed Intestine." Cell Host & Microbe **5**(5): 476-486.

Rajilic-Stojanovic, M., F. Shanahan, F. Guarner and W. M. de Vos (2013). "Phylogenetic analysis of dysbiosis in ulcerative colitis during remission." Inflammatory bowel diseases **19**(3): 481-488.

Randle, C. L., P. W. Albro and J. C. Dittmer (1969). "The phosphoglyceride composition of Gram-negative bacteria and the changes in composition during growth." Biochimica et Biophysica Acta (BBA)-Lipids and Lipid Metabolism **187**(2): 214-220.

Literature

Rausch, P., M. Basic, A. Batra, S. C. Bischoff, M. Blaut, T. Clavel, J. Gläsner, S. Gopalakrishnan, G. A. Grassl and C. Günther (2016). "Analysis of factors contributing to variation in the C57BL/6J fecal microbiota across German animal facilities." International Journal of Medical Microbiology.

Rendon, J., E. Pilet, Z. Fahs, F. Seduk, L. Sylvi, M. H. Chehade, F. Pierrel, B. Guigliarelli, A. Magalon and S. Grimaldi (2015). "Demethylmenaquinol is a substrate of Escherichia coli nitrate reductase A (NarGHI) and forms a stable semiquinone intermediate at the NarGHI quinol oxidation site." Biochimica et Biophysica Acta (BBA)-Bioenergetics **1847**(8): 739-747.

Rescigno, M., G. Rotta, B. Valzasina and P. Ricciardi-Castagnoli (2001). "Dendritic cells shuttle microbes across gut epithelial monolayers." Immunobiology **204**(5): 572-581.

Ridler, C. (2016). "IBD: Dysbiosis underlies CARD9 risk alleles in colitis." Nature Reviews Gastroenterology & Hepatology **13**(6): 316-316.

Ridlon, J. M., D.-J. Kang and P. B. Hylemon (2006). "Bile salt biotransformations by human intestinal bacteria." Journal of lipid research **47**(2): 241-259.

Rivera-Chávez, F., S. E. Winter, C. A. Lopez, M. N. Xavier, M. G. Winter, S.-P. Nuccio, J. M. Russell, R. C. Laughlin, S. D. Lawhon and T. Sterzenbach (2013). "Salmonella uses energy taxis to benefit from intestinal inflammation." PLoS Pathog **9**(4): e1003267.

Rivera-Chávez, F., L. F. Zhang, F. Faber, C. A. Lopez, M. X. Byndloss, E. E. Olsan, G. Xu, E. M. Velazquez, C. B. Lebrilla and S. E. Winter (2016). "Depletion of Butyrate-Producing Clostridia from the Gut Microbiota Drives an Aerobic Luminal Expansion of Salmonella." Cell Host & Microbe **19**(4): 443-454.

Roof, D. M. and J. R. Roth (1988). "Ethanolamine utilization in Salmonella typhimurium." Journal of bacteriology **170**(9): 3855-3863.

Roof, D. M. and J. R. Roth (1989). "Functions required for vitamin B12-dependent ethanolamine utilization in Salmonella typhimurium." Journal of bacteriology **171**(6): 3316-3323.

Rousseau, C., F. Levenez, C. Fouqueray, J. Doré, A. Collignon and P. Lepage (2011). "Clostridium difficile colonization in early infancy is accompanied by changes in intestinal microbiota composition." Journal of clinical microbiology **49**(3): 858-865.

Rupnik, M., M. H. Wilcox and D. N. Gerding (2009). "Clostridium difficile infection: new developments in epidemiology and pathogenesis." Nature Reviews Microbiology **7**(7): 526-536.

Russell, A. B., A. G. Wexler, B. N. Harding, J. C. Whitney, A. J. Bohn, Y. A. Goo, B. Q. Tran, N. A. Barry, H. Zheng and S. B. Peterson (2014). "A type VI secretion-related pathway in Bacteroidetes mediates interbacterial antagonism." Cell Host & Microbe **16**(2): 227-236.

Literature

Said, H. M. (2011). "Intestinal absorption of water-soluble vitamins in health and disease." Biochemical Journal **437**(3): 357-372.

Scharffetter-Kochanek, K., H. Lu, K. Norman, N. Van Nood, F. Munoz, S. Grabbe, M. McArthur, I. Lorenzo, S. Kaplan and K. Ley (1998). "Spontaneous skin ulceration and defective T cell function in CD18 null mice." The Journal of experimental medicine **188**(1): 119-131.

Schauer, D. and S. Falkow (1993). "Attaching and effacing locus of a *Citrobacter freundii* biotype that causes transmissible murine colonic hyperplasia." Infection and immunity **61**(6): 2486-2492.

Schauer, D. B., B. A. Zabel, I. F. Pedraza, C. M. O'Hara, A. G. Steigerwalt and D. J. Brenner (1995). "Genetic and biochemical characterization of *Citrobacter rodentium* sp. nov." Journal of clinical microbiology **33**(8): 2064-2068.

Schmieger, H. (1972). "Phage P22-mutants with increased or decreased transduction abilities." Molecular and General Genetics MGG **119**(1): 75-88.

Schulte, M. and M. Hensel (2016). "Models of intestinal infection by *Salmonella enterica*: introduction of a new neonate mouse model." F1000Research **5**.

Seekatz, A. M. and V. B. Young (2014). "*Clostridium difficile* and the microbiota." The Journal of clinical investigation **124**(10): 4182-4189.

Sellin, M. E., A. A. Müller, B. Felmy, T. Dolowschiak, M. Diard, A. Tardivel, K. M. Maslowski and W.-D. Hardt (2014). "Epithelium-Intrinsic NAIP/NLRC4 Inflammasome Drives Infected Enterocyte Expulsion to Restrict *Salmonella* Replication in the Intestinal Mucosa." Cell Host & Microbe **16**(2): 237-248.

Simonyte, S. K., L. Vidman, P. Rydén and C. E. West (2016). "Emerging evidence of the role of gut microbiota in the development of allergic diseases." Current opinion in allergy and clinical immunology.

Sokol, H., B. Pigneur, L. Watterlot, O. Lakhdari, L. G. Bermúdez-Humarán, J.-J. Gratadoux, S. Blugeon, C. Bridonneau, J.-P. Furet and G. Corthier (2008). "*Faecalibacterium prausnitzii* is an anti-inflammatory commensal bacterium identified by gut microbiota analysis of Crohn disease patients." Proceedings of the National Academy of Sciences **105**(43): 16731-16736.

Sonnenberg, G. F., L. A. Monticelli, T. Alenghat, T. C. Fung, N. A. Hutnick, J. Kunisawa, N. Shibata, S. Grunberg, R. Sinha and A. M. Zahm (2012). "Innate lymphoid cells promote anatomical containment of lymphoid-resident commensal bacteria." Science **336**(6086): 1321-1325.

Literature

- Sorg, J. A. and A. L. Sonenshein (2010). "Inhibiting the initiation of *Clostridium difficile* spore germination using analogs of chenodeoxycholic acid, a bile acid." Journal of bacteriology **192**(19): 4983-4990.
- Spees, A. M., T. Wangdi, C. A. Lopez, D. D. Kingsbury, M. N. Xavier, S. E. Winter, R. M. Tsolis and A. J. Bäumlér (2013). "Streptomycin-induced inflammation enhances *Escherichia coli* gut colonization through nitrate respiration." MBio **4**(4): e00430-00413.
- Stecher, B., M. Barthel, M. C. Schlumberger, L. Haberli, W. Rabsch, M. Kremer and W. D. Hardt (2008). "Motility allows *S. Typhimurium* to benefit from the mucosal defence." Cellular microbiology **10**(5): 1166-1180.
- Stecher, B., D. Berry and A. Loy (2013). "Colonization resistance and microbial ecophysiology: using gnotobiotic mouse models and single-cell technology to explore the intestinal jungle." FEMS microbiology reviews **37**(5): 793-829.
- Stecher, B., S. Chaffron, R. Käppeli, S. Hapfelmeier, S. Friedrich, T. C. Weber, J. Kirundi, M. Suar, K. D. McCoy and C. von Mering (2010). "Like will to like: abundances of closely related species can predict susceptibility to intestinal colonization by pathogenic and commensal bacteria." PLoS Pathog **6**(1): e1000711.
- Stecher, B., R. Denzler, L. Maier, F. Bernet, M. J. Sanders, D. J. Pickard, M. Barthel, A. M. Westendorf, K. A. Krogfelt and A. W. Walker (2012). "Gut inflammation can boost horizontal gene transfer between pathogenic and commensal Enterobacteriaceae." Proceedings of the National Academy of Sciences **109**(4): 1269-1274.
- Stecher, B., S. Hapfelmeier, C. Müller, M. Kremer, T. Stallmach and W.-D. Hardt (2004). "Flagella and chemotaxis are required for efficient induction of *Salmonella enterica* serovar Typhimurium colitis in streptomycin-pretreated mice." Infection and immunity **72**(7): 4138-4150.
- Stecher, B., R. Robbiani, A. W. Walker, A. M. Westendorf, M. Barthel, M. Kremer, S. Chaffron, A. J. Macpherson, J. Buer and J. Parkhill (2007). "*Salmonella enterica* serovar typhimurium exploits inflammation to compete with the intestinal microbiota." PLoS biology **5**(10): e244.
- Stecher, B., R. Robbiani, A. W. Walker, A. M. Westendorf, M. Barthel, M. Kremer, S. Chaffron, A. J. Macpherson, J. Buer and J. Parkhill (2007). "*Salmonella enterica* serovar typhimurium exploits inflammation to compete with the intestinal microbiota." PLoS Biol **5**(10): e244.
- Stecher, B., R. Robbiani, A. W. Walker, A. M. Westendorf, M. Barthel, M. Kremer, S. Chaffron, A. J. Macpherson, J. Buer, J. Parkhill, G. Dougan, C. von Mering and W. D. Hardt (2007). "*Salmonella enterica* Serovar Typhimurium Exploits Inflammation to Compete with the Intestinal Microbiota." PLoS Biol **5**(10): e244.

Literature

Steck, N., M. Hoffmann, I. G. Sava, S. C. Kim, H. Hahne, S. L. Tonkonogy, K. Mair, D. Krueger, M. Pruteanu and F. Shanahan (2011). "Enterococcus faecalis metalloprotease compromises epithelial barrier and contributes to intestinal inflammation." Gastroenterology **141**(3): 959-971.

Stefka, A. T., T. Feehley, P. Tripathi, J. Qiu, K. McCoy, S. K. Mazmanian, M. Y. Tjota, G.-Y. Seo, S. Cao and B. R. Theriault (2014). "Commensal bacteria protect against food allergen sensitization." Proceedings of the National Academy of Sciences **111**(36): 13145-13150.

Stelter, C., R. Käppeli, C. König, A. Krah, W.-D. Hardt, B. Stecher and D. Bumann (2011). "Salmonella-induced mucosal lectin RegIII β kills competing gut microbiota." PloS one **6**(6): e20749.

Stojiljkovic, I., A. J. Bäumler and F. Heffron (1995). "Ethanolamine utilization in Salmonella typhimurium: nucleotide sequence, protein expression, and mutational analysis of the cchA cchB eutE eutJ eutG eutH gene cluster." Journal of bacteriology **177**(5): 1357-1366.

Stojiljkovic, I., V. Kumar and N. Srinivasan (1999). "Non-iron metalloporphyrins: potent antibacterial compounds that exploit haem/Hb uptake systems of pathogenic bacteria." Molecular microbiology **31**(2): 429-442.

Stubbs, S., M. Rupnik, M. Gibert, J. Brazier, B. Duerden and M. Popoff (2000). "Production of actin-specific ADP-ribosyltransferase (binary toxin) by strains of Clostridium difficile." FEMS Microbiology Letters **186**(2): 307-312.

Studer, N., L. Desharnais, M. Beutler, S. Brugiroux, M. A. Terrazos, L. Menin, C. M. Schürch, K. D. McCoy, S. A. Kuehne and N. P. Minton (2016). "Functional Intestinal Bile Acid 7 α -Dehydroxylation by Clostridium scindens Associated with Protection from Clostridium difficile Infection in a Gnotobiotic Mouse Model." Frontiers in Cellular and Infection Microbiology **6**.

Szabó, C., H. Ischiropoulos and R. Radi (2007). "Peroxynitrite: biochemistry, pathophysiology and development of therapeutics." Nature reviews Drug discovery **6**(8): 662-680.

Takahashi, K., A. Nishida, T. Fujimoto, M. Fujii, M. Shioya, H. Imaeda, O. Inatomi, S. Bamba, A. Andoh and M. Sugimoto (2016). "Reduced Abundance of Butyrate-Producing Bacteria Species in the Fecal Microbial Community in Crohn's Disease." Digestion **93**(1): 59-65.

Taur, Y., J. B. Xavier, L. Lipuma, C. Ubeda, J. Goldberg, A. Gobourne, Y. J. Lee, K. A. Dubin, N. D. Socci and A. Viale (2012). "Intestinal domination and the risk of bacteremia in patients undergoing allogeneic hematopoietic stem cell transplantation." Clinical infectious diseases **55**(7): 905-914.

Theriot, C. M., A. A. Bowman and V. B. Young (2016). "Antibiotic-induced alterations of the gut microbiota alter secondary bile acid production and allow for Clostridium difficile spore germination and outgrowth in the large intestine." MSphere **1**(1): e00045-00015.

Literature

Thiennimitr, P., S. E. Winter, M. G. Winter, M. N. Xavier, V. Tolstikov, D. L. Huseby, T. Sterzenbach, R. M. Tsois, J. R. Roth and A. J. Bäuml (2011). "Intestinal inflammation allows *Salmonella* to use ethanolamine to compete with the microbiota." Proceedings of the National Academy of Sciences **108**(42): 17480-17485.

Thomas, C. M., D. Saulnier, J. K. Spinler, P. Hemarajata, C. Gao, S. E. Jones, A. Grimm, M. A. Balderas, M. D. Burstein and C. Morra (2016). "FolC2-mediated folate metabolism contributes to suppression of inflammation by probiotic *Lactobacillus reuteri*." Microbiologyopen.

Trautwein-Weidner, K., A. Gladiator, S. Nur, P. Diethelm and S. LeibundGut-Landmann (2014). "IL-17-mediated antifungal defense in the oral mucosa is independent of neutrophils." Mucosal immunology.

Tsoy, O., D. Ravcheev and A. Mushegian (2009). "Comparative genomics of ethanolamine utilization." Journal of bacteriology **191**(23): 7157-7164.

Tuovinen, E., J. Keto, J. Nikkilä, J. Mättö and K. Lähdenmäki (2013). "Cytokine response of human mononuclear cells induced by intestinal *Clostridium* species." Anaerobe **19**: 70-76.

Turnbaugh, P. J., M. Hamady, T. Yatsunenkov, B. L. Cantarel, A. Duncan, R. E. Ley, M. L. Sogin, W. J. Jones, B. A. Roe and J. P. Affourtit (2009). "A core gut microbiome in obese and lean twins." Nature **457**(7228): 480-484.

Turnbaugh, P. J., V. K. Ridaura, J. J. Faith, F. E. Rey, R. Knight and J. I. Gordon (2009). "The effect of diet on the human gut microbiome: a metagenomic analysis in humanized gnotobiotic mice." Science translational medicine **1**(6): 6ra14-16ra14.

Ubeda, C., V. Bucci, S. Caballero, A. Djukovic, N. C. Toussaint, M. Equinda, L. Lipuma, L. Ling, A. Gobourne and D. No (2013). "Intestinal microbiota containing *Barnesiella* species cures vancomycin-resistant *Enterococcus faecium* colonization." Infection and immunity **81**(3): 965-973.

Ubeda, C., L. Lipuma, A. Gobourne, A. Viale, I. Leiner, M. Equinda, R. Khanin and E. G. Pamer (2012). "Familial transmission rather than defective innate immunity shapes the distinct intestinal microbiota of TLR-deficient mice." The Journal of experimental medicine **209**(8): 1445-1456.

Ubeda, C. and E. G. Pamer (2012). "Antibiotics, microbiota, and immune defense." Trends in immunology **33**(9): 459-466.

Ubeda, C., Y. Taur, R. R. Jenq, M. J. Equinda, T. Son, M. Samstein, A. Viale, N. D. Socci, M. R. van den Brink and M. Kamboj (2010). "Vancomycin-resistant *Enterococcus* domination of intestinal microbiota is enabled by antibiotic treatment in mice and precedes bloodstream invasion in humans." The Journal of clinical investigation **120**(12): 4332-4341.

Literature

Uchiya, K. i., M. A. Barbieri, K. Funato, A. H. Shah, P. D. Stahl and E. A. Groisman (1999). "A Salmonella virulence protein that inhibits cellular trafficking." The EMBO Journal **18**(14): 3924-3933.

Vaishnava, S., C. L. Behrendt, A. S. Ismail, L. Eckmann and L. V. Hooper (2008). "Paneth cells directly sense gut commensals and maintain homeostasis at the intestinal host-microbial interface." Proceedings of the National Academy of Sciences **105**(52): 20858-20863.

Valiente, E., M. Cairns and B. Wren (2014). "The Clostridium difficile PCR ribotype 027 lineage: a pathogen on the move." Clinical Microbiology and Infection **20**(5): 396-404.

van Nood, E., A. Vrieze, M. Nieuwdorp, S. Fuentes, E. G. Zoetendal, W. M. de Vos, C. E. Visser, E. J. Kuijper, J. F. Bartelsman and J. G. Tijssen (2013). "Duodenal infusion of donor feces for recurrent Clostridium difficile." New England Journal of Medicine **368**(5): 407-415.

Vázquez-Torres, A. and A. J. Bäumler (2016). "Nitrate, nitrite and nitric oxide reductases: from the last universal common ancestor to modern bacterial pathogens." Current opinion in microbiology **29**: 1-8.

Vivinus-Nébot, M., G. Frin-Mathy, H. Bziouche, R. Dainese, G. Bernard, R. Anty, J. Filippi, M.-C. Saint-Paul, M. K. Tulic and V. Verhasselt (2014). "Functional bowel symptoms in quiescent inflammatory bowel diseases: role of epithelial barrier disruption and low-grade inflammation." Gut **63**(5): 744-752.

Vong, L., L. J. Pinnell, P. Määtänen, C. W. Yeung, E. Lurz and P. M. Sherman (2015). "Selective enrichment of commensal gut bacteria protects against Citrobacter rodentium-induced colitis." American Journal of Physiology-Gastrointestinal and Liver Physiology **309**(3): G181-G192.

Voth, D. E. and J. D. Ballard (2005). "Clostridium difficile toxins: mechanism of action and role in disease." Clinical microbiology reviews **18**(2): 247-263.

Walker, A. W., J. Ince, S. H. Duncan, L. M. Webster, G. Holtrop, X. Ze, D. Brown, M. D. Stares, P. Scott and A. Bergerat (2011). "Dominant and diet-responsive groups of bacteria within the human colonic microbiota." The ISME journal **5**(2): 220-230.

Warny, M., J. Pepin, A. Fang, G. Killgore, A. Thompson, J. Brazier, E. Frost and L. C. McDonald (2005). "Toxin production by an emerging strain of Clostridium difficile associated with outbreaks of severe disease in North America and Europe." The Lancet **366**(9491): 1079-1084.

Weisburg, W. G., S. M. Barns, D. A. Pelletier and D. J. Lane (1991). "16S ribosomal DNA amplification for phylogenetic study." Journal of bacteriology **173**(2): 697-703.

Willing, B. P., V. P. Singh and S. Proctor (2016). "Koch's postulates, microbial dysbiosis and inflammatory bowel disease." Clinical Microbiology and Infection.

Literature

Winter, S. E. and A. J. Bäumlér (2014). "Why related bacterial species bloom simultaneously in the gut: principles underlying the 'Like will to like' concept." Cellular microbiology **16**(2): 179-184.

Winter, S. E., C. A. Lopez and A. J. Bäumlér (2013). "The dynamics of gut-associated microbial communities during inflammation." EMBO reports **14**(4): 319-327.

Winter, S. E., P. Thiennimitr, M. G. Winter, B. P. Butler, D. L. Huseby, R. W. Crawford, J. M. Russell, C. L. Bevins, L. G. Adams and R. M. Tsois (2010). "Gut inflammation provides a respiratory electron acceptor for Salmonella." Nature **467**(7314): 426-429.

Wohlgemuth, S., S. Keller, R. Kertscher, M. Stadion, D. Haller, S. Kisling, G. Jahreis, M. Blaut and G. Loh (2011). "Intestinal steroid profiles and microbiota composition in colitic mice." Gut microbes **2**(3): 159-166.

Wos-Oxley, M. L., A. Bleich, A. P. Oxley, S. Kahl, L. M. Janus, A. Smoczek, H. Nahrstedt, M. C. Pils, S. Taudien and M. Platzer (2012). "Comparative evaluation of establishing a human gut microbial community within rodent models." Gut microbes **3**(3): 234-249.

Xavier, R. and D. Podolsky (2007). "Unravelling the pathogenesis of inflammatory bowel disease." Nature **448**(7152): 427-434.

Xiao, L., Q. Feng, S. Liang, S. B. Sonne, Z. Xia, X. Qiu, X. Li, H. Long, J. Zhang and D. Zhang (2015). "A catalog of the mouse gut metagenome." Nature biotechnology **33**(10): 1103-1108.

Yi, P. and L. Li (2012). "The germfree murine animal: an important animal model for research on the relationship between gut microbiota and the host." Veterinary microbiology **157**(1): 1-7.

Zheng, X., G. Xie, A. Zhao, L. Zhao, C. Yao, N. H. Chiu, Z. Zhou, Y. Bao, W. Jia and J. K. Nicholson (2011). "The footprints of gut microbial–mammalian co-metabolism." Journal of proteome research **10**(12): 5512-5522.

Danksagung

Danksagung

An dieser Stelle möchte ich mich besonders bei Prof. Dr. Bärbel Stecher bedanken, die mich exzellent während meiner Doktorarbeit betreut hat. Danke, dass man sich immer mit jeglichen Belangen an sie wenden konnte und stets Rat und konstruktive Kritik bekommen hat. Besonders möchte ich mich auch für das mir entgegengebrachte Vertrauen bedanken, welches ein freies und kreatives Arbeiten in einer sehr angenehmen Arbeitsatmosphäre ermöglichte. Auch möchte ich Dr. Hans Nitschko und Helga Mairhofer für ihren Ratschlag bezüglich quantitativer PCR, sowie Dr. Ombeline Rossier und Prof. Dr. Dr. Jürgen Heesemann für wertvolle Diskussionen danken.

Des Weiteren möchte ich mich bei allen aktuellen und ehemaligen Mitarbeitern der AG Stecher bedanken: Lubov Nedialkova, Sandrine Brugiroux, Manuel Diehl, Diana Ring, Dr. Martin Köppel, Stefanie Spriewald, Simone Herp, Jana Glaser, Maja Sidstedt, Saib Hussain, Dr. Debora Garzetti, Tobias Baumgartner, Patrick Schiller, Philipp Münch, Artur Kibler, Claudia Eberl und Nancy Obeng. Ihr wart immer hilfsbereit und tolle Kollegen! Mein besonderer Dank geht dabei an Sandrine Brugiroux für die Heranführung an mein Thema, Diana Ring und Simone Herp für die gemeinsame Durchführung von Experimenten mit gnotobiotischen Mäusen, Dr. Debora Garzetti für alle bioinformatischen Belange, Patrick Schiller für *in vitro* Kulturdaten und Saib Hussain für die Zucht gnotobiotischer Mauslinien.

Ich möchte mich zudem bei unseren Kollaborationspartnern: Prof. Christoph Mueller, Martin Faderl, Prof. Siegfried Hapfelmeier, Nicolas Studer, Prof. Wolf-Dietrich Hardt und Sandra Wotzka für die gute Zusammenarbeit bedanken.

Mein besonderer Dank geht auch an meine Freunde und Familie, sowie an Marianne, die mich nicht nur kulinarisch während meiner Doktorarbeit unterstützt hat.

Curriculum Vitae

Curriculum Vitae

Personal data

Name:	Markus Beutler
Date of birth:	10.11.1985
Place of birth:	Kelheim
Nationality:	German

Formation

Since 10/2012	PhD student in the group 'microbiota and infection' of Prof. Barbara Stecher-Letsch, Ludwig-Maximilians-University, Munich, Germany
10/2010 – 09/2012	<p>Postgraduate studies: Master of Science in 'Molecular Medicine' (M.Sc.), Georg-August-University Göttingen, Germany</p> <p>Thesis: 'The <i>in vitro</i> cardiovascular pharmacology of the Papuan small-eyed snake (<i>Micropechis ikaheka</i>) and the taipan (<i>Oxyuranus scutellatus canni</i>).'</p> <p>Thesis was conducted in the Cardiovascular Therapeutics Unit and the Australian Venom Research Unit, Department of Pharmacology, University of Melbourne, Australia</p>
10/2007 – 09/2010	<p>Undergraduate studies: Bachelor of Science in 'Biology' (B.Sc.), University of Regensburg, Germany</p> <p>Thesis: 'Störungen des RPE/EZM Komplexes bei Mäusen mit Mutationen im TIMP3 Gen.'</p>
09/2006 – 05/2007	Civilian service: Retex (social facility), Regensburg, Germany
09/1997 – 06/2006	Secondary school: Johannes- Nepomuk- Gymnasium, Rohr in NdB, Germany

Curriculum Vitae

Publications

- 2016 Studer, N., L. Desharnais, **M. Beutler**, S. Brugiroux, M. A. Terrazos, L. Menin, C. M. Schürch, K. D. McCoy, S. A. Kuehne and N. P. Minton (2016). "Functional Intestinal Bile Acid 7 α -Dehydroxylation by *Clostridium scindens* Associated with Protection from *Clostridium difficile* Infection in a Gnotobiotic Mouse Model." Frontiers in Cellular and Infection Microbiology **6**.
- Brugiroux, S., **M. Beutler**, C. Pfann, D. Garzetti, H. Ruscheweyh, M. Diehl, D. Ring, Y. Lötscher, S. Hussain, R. Pukall, D. H. Huson, P. C. Münch, A. C. McHardy, K. D. McCoy, A. J. Macpherson, A. Loy, T. Clavel, D. Berry and B. Stecher. "Genome-guided modular design of a novel defined mouse microbiota that confers colonization resistance against *Salmonella enterica* serovar Typhimurium." Nature Microbiology **2**: 16215.
- 2015 Spriewald, S., J. Glaser, **M. Beutler**, M. B. Koeppel and B. Stecher (2015). "Reporters for Single-Cell Analysis of Colicin Ib Expression in *Salmonella enterica* Seroovar Typhimurium." PloS one **10**(12): e0144647.
- 2014 Pla, D., O. K. Paiva, L. Sanz, **M. Beutler**, C. E. Wright, J. J. Calvete, D. J. Williams and J. M. Gutiérrez (2014). "Preclinical efficacy of Australian antivenoms against the venom of the small-eyed snake, *Micropechis ikaheka*, from Papua New Guinea: An antivenomics and neutralization study." Journal of proteomics **110**: 198-208.
- Paiva, O., D. Pla, C. E. Wright, **M. Beutler**, L. Sanz, J. M. Gutiérrez, D. J. Williams and J. J. Calvete (2014). "Combined venom gland cDNA sequencing and venomomics of the New Guinea small-eyed snake, *Micropechis ikaheka*." Journal of proteomics **110**: 209-229.
- 2013 Hupfeld, T., B. Chapuy, V. Schrader, **M. Beutler**, C. Veltkamp, R. Koch, S. Cameron, T. Aung, D. Haase and P. LaRosee (2013). "Tyrosinekinase inhibition facilitates cooperation of transcription factor SALL4 and ABC transporter A3 towards intrinsic CML cell drug resistance." British journal of haematology **161**(2): 204-213.

Conference presentations

- 2015 **Beutler, M.**, S. Brugiroux, S. Herp, D. Garzetti, P. Schiller, S. Hussain, D. Ring, K. D. McCoy, A. J. Macpherson and B. Stecher. "Investigating the mechanisms of *Salmonella*-induced dysbiosis using the Oligo-Mouse-Microbiota model." 8th Seeon Conference "Microbiota, Probiota and Host", Seeon, Germany. **Talk**
- 2014 **Beutler, M.**, S. Brugiroux, S. Herp, S. Hussain, D. Ring, K. D. McCoy, A. J. Macpherson and B. Stecher. "Addressing the influence of *S. Typhimurium* induced gut inflammation on the Oligo-Mouse-Microbiota". Gemeinsame Jahrestagung der Deutschen Gesellschaft für Hygiene und Mikrobiologie (DGHM) und der Vereinigung für Allgemeine und Angewandte Mikrobiologie (VAAM), Dresden, Germany. **Poster**

Curriculum Vitae

2013

Beutler, M., S. Brugiroux, S. Herp, S. Hussain, D. Ring, K. D. McCoy, A. J. Macpherson and B. Stecher. "Addressing the influence of *S. Typhimurium* induced gut inflammation on the Oligo-Mouse-Microbiota". 7th Seeon Conference "Microbiota, Probiota and Host", Seeon, Germany. **Talk**

Beutler, M., S. Brugiroux, M. Diehl, K. D. McCoy and B. Stecher. "Establishment of a specific hydrolysis probe quantification method for the Oligo-Mouse Microbiota model". FEMS - 5th Congress of European Microbiologists, Leipzig, Germany. **Poster**

Beutler, M., S. Brugiroux, M. Diehl and B. Stecher. "Establishment of a specific hydrolysis probe quantification method for the Oligo-Mouse Microbiota model". 6th Seeon Conference "Microbiota, Probiota and Host", Seeon, Germany. **Poster**